



HAL
open science

Identification et caractérisation d'un nouvel inhibiteur de Rac1 à visée thérapeutique : implication en physiopathologies bronchiques et oncologie

Lindsay Rose

► **To cite this version:**

Lindsay Rose. Identification et caractérisation d'un nouvel inhibiteur de Rac1 à visée thérapeutique : implication en physiopathologies bronchiques et oncologie. Médecine humaine et pathologie. Nantes Université, 2022. Français. NNT : 2022NANU1034 . tel-04317029

HAL Id: tel-04317029

<https://theses.hal.science/tel-04317029>

Submitted on 1 Dec 2023

HAL is a multi-disciplinary open access archive for the deposit and dissemination of scientific research documents, whether they are published or not. The documents may come from teaching and research institutions in France or abroad, or from public or private research centers.

L'archive ouverte pluridisciplinaire **HAL**, est destinée au dépôt et à la diffusion de documents scientifiques de niveau recherche, publiés ou non, émanant des établissements d'enseignement et de recherche français ou étrangers, des laboratoires publics ou privés.

THESE DE DOCTORAT DE

NANTES UNIVERSITE

ECOLE DOCTORALE N° 605

Biologie Santé

Spécialité : *Physiologie, Physiopathologie, Biologie Systémique Médicale*

Par

Lindsay ROSE

Identification et caractérisation d'un nouvel inhibiteur de Rac1 à visée thérapeutique

Implication en physiopathologies bronchiques et oncologie

Thèse présentée et soutenue à Nantes, le 30 Novembre 2022

Unité de recherche : L'Institut du Thorax, INSERM UMR1087 – CNRS UMR 6291

Rapporteurs avant soutenance :

Anne BLANGY

Stéphanie CABANTOUS

Directrice de recherche CNRS, Université de Montpellier

Chargée de recherche INSERM, Université de Toulouse

Composition du Jury :

Président : Laurent BOYER

Examineurs : Anne BLANGY

Stéphanie CABANTOUS

Laurent BOYER

Dir. de thèse : Vincent SAUZEAU

Directeur de recherche INSERM, Université Côte d'Azur, Nice

Directrice de recherche CNRS, Université de Montpellier

Chargée de recherche INSERM, Université de Toulouse

Directeur de recherche INSERM, Université Côte d'Azur, Nice

Chargé de recherche INSERM, Nantes Université

Invité(s)

Gervaise LOIRAND

Stéphane TELETCHÉA

Directrice de recherche INSERM, Nantes Université

Maître de conférences, Nantes Université

Remerciements

Je tiens tout d'abord à remercier Dr. Anne Blangy et Dr. Stéphanie Cabantous pour avoir accepté de prendre le temps d'étudier mon travail de thèse en qualité de rapportrices. Je remercie également Dr. Laurent Boyer examinateur de cette thèse et Dr. Stéphane Téletchéa invité à participer à mon jury de thèse pour le temps consacré à l'évaluation de mon travail.

Je remercie l'Institut du Thorax et Richard Redon pour leur accueil au sein du laboratoire depuis mon stage de Master 1.

Merci à Gervaise Loirand pour votre accueil dans l'équipe III et vos différents conseils au cours de ces années passées au laboratoire.

Vincent, merci d'avoir encadré mon travail durant ces 3 années de thèse et aussi lors de mes stages de master 1 et master 2. Je te remercie pour ta patience, tes différents conseils, ton implication et ton aide au cours de ces années au laboratoire. Ta passion pour la science, la recherche et tes idées à profusion sont un réel exemple malgré que tout ne se passe pas toujours comme prévu, après tout c'est ça la science! Ce fut un réel plaisir d'être ton troisième (ou quatrième, on ne sait plus trop comment compter) Padawan.

Florian, merci de m'avoir encadré durant mon stage de master 1 et mon arrivée au laboratoire. Tu m'as fait découvrir la vie de stagiaire et doctorant de l'équipe III à l'Institut du Thorax, le monde fanstatique des Western-Blot et des cellules musculaires lisses. Merci pour ta patience, tes conseils et ton encadrement.

Morgane, merci d'avoir été là à chaque moment pendant ma thèse, ce n'était pas toujours facile mais avoir une collègue comme toi ça aide. Merci pour ta gentillesse, ton écoute, tes conseils, de m'avoir appris la culture cellulaire, de prendre soin de nous tous, de nous nourrir (miam les bons cookies, roses des sables et aux réjouissances), de veiller au recyclage et au bon rangement des paillasses. Merci pour tous ces moments partagés au cours de ces 5 années et merci pour ton amitié!

Milène, on est arrivé en même temps au laboratoire pour nos stages de master 1 puis en master 2 et l'on s'est retrouvé pour cette folle aventure qu'est la thèse. Merci pour ton soutien au cours de ces années, entre doctorantes on se sert les coudes. Merci pour ton aide, tes conseils et tous ces moments partagés. Courage pour l'écriture de ta thèse, tu verras ça va bien se passer, on est là pour te soutenir dans cette étape et après on pourra fêter ça!

Marc, également appelé Marco Le Bricolo ou Le Rigolo selon la situation. Merci pour tous tes conseils, ton aide pour la biologie moléculaire et la biochimie. Je voulais aussi (et surtout) te remercier pour tous ces fous rires, tes blagues et tes spectacles que ce soit les chansons (surtout une « Elle, tu l'aimes ... » qui reste bien en tête, je compte sur toi pour apprendre la suite des paroles pour ta prochaine représentation), les mimes ou autres mises en scènes.

Anne-Clémence merci pour tes conseils et ton énergie. Céline merci pour ta gentillesse, ta bienveillance et ta patience. Tu te soucies toujours de notre bien-être, de notre état. Corentin merci pour tous les moments partagés et fais attention à toi à la salle. Dorian merci pour tes conseils avisés, ton regard clinique sur le projet et de m'avoir fait découvrir le FACS.

J'ai également une pensée pour les nouveaux arrivants dans l'équipe, Thibaud, Laurent, Sarah, Tom, Marie, Nathan, Hugo et Mary Adel et également tous les collègues de l'Institut avec lesquels j'ai eu la chance d'échanger pendant ces années passées au laboratoire.

Maman, Papa, merci d'avoir toujours cru en moi et de m'avoir toujours encouragé à faire ce que je voulais et ce qui me plaisait. Kenny merci à toi de m'avoir toujours encouragé, poussé à me dépasser et donné le meilleur de moi-même. Merci de m'avoir toujours poussé à aiguïser ma curiosité, à comprendre comment les choses fonctionnent pour répondre à toutes mes questions « mais pourquoi ? ».

Merci aussi à mes amis Kitty, Anaïs, Fabien, Thibault, Audrey de m'avoir soutenu, encouragé, supporté et d'avoir tenté de comprendre ce que je faisais pendant ces années de thèse bien que ce ne soit pas du tout votre domaine.

Julien, mon pilier, merci n'est pas suffisant pour tout ce que tu mérites. Ce qui est sûr c'est que sans toi, je n'aurai jamais fait tout ça. Merci de m'avoir toujours encouragé, soutenu et d'avoir tellement cru en moi, sans tes encouragements et ton soutien je ne sais pas si j'aurai pu vivre cette aventure de thèse. Merci d'avoir supporté et écouté toutes mes présentations au cours de cette thèse, tout ce que je pouvais faire au labo alors que tu n'y comprenais pas toujours quelque chose. Merci pour tout ce que tu as fait au quotidien pour moi pendant cette aventure de thèse et ce que tu feras pour toutes les autres qui nous restent à vivre.

Table des matières

Liste des abréviations	i
Table des figures.....	iii
Table des tableaux	iv
INTRODUCTION	1
I- Les protéines G monomériques de la famille Rho :	1
I.1- Présentation générale des Rho GTPases :	1
I.2- Structure des Rho GTPases :	2
I.3- Régulation de l'activité des Rho GTPases :	5
I.3.1- Les facteurs d'échange de nucléotides guanyliques (GEFs) :	6
I.3.2- Les protéines activatrices de l'activité GTPasique (GAPs) :	11
I.3.3. Les protéines inhibitrices de la dissociation guanylique (GDIs) :	13
II- Rôles physiologiques de la GTPase Rac1 :	15
II.1- Organisation du cytosquelette d'actine et migration cellulaire :	15
II.2- Régulation du cycle cellulaire et de la prolifération :	18
II.3- Régulation des NADPH oxydases :	18
II.4- Régulation de la contraction des cellules musculaires lisses :	19
III- Rôles physiopathologiques de Rac1 :	21
III.1- Rac1 dans la physiopathologie des CMLs :	22
III.1.1- La contractilité des CMLs :	22
III.1.2- Le remodelage des CMLs :	22
III.2- Rac1 en oncologie :	23
III.2.1- La prolifération des cellules tumorales :	24
III.2.2- La formation de métastases :	26
IV- Stratégies thérapeutiques régulant l'activité de la GTPase Rac1 :	27
V.1- Utilisation de toxines inhibant Rac1 :	28
V.2- Inhibiteurs des modifications post-traductionnelles de Rac1 :	29
V.3- Inhibiteurs de la formation du complexe Rac1-GEF :	30
V.4- Inhibiteurs de l'échange nucléotidique :	32
V.5- Inhibiteurs des interactions entre Rac1 et ses effecteurs :	34

OBJECTIFS DE THESE	37
RESULTATS	38
Première partie : Rôle de Rac1 dans les cellules musculaires lisses bronchiques et le remodelage des voies aériennes associés à l’asthme allergique sévère	38
Article 1: Essential role of smooth muscle Rac1 in severe asthma associated-airway remodeling.....	41
Article 2: Bronchial smooth muscle cell in asthma: where does it fit?	57
Deuxième partie : Identification et caractérisation d’un nouvel inhibiteur pharmacologique de Rac1	73
Article 3: A Rac GTPase-Specific Small Molecule Inhibitor targets metastasis in triple negative breast cancer	75
DISCUSSION.....	165
BIBLIOGRAPHIE	172
ANNEXES	185
Annexe 1: Smooth muscle Rac1 contributes to pulmonary hypertension.....	185

Liste des abréviations

ADN : acide désoxyribonucléique
ATP : adénosine triphosphate
bFGF : facteur de croissance basique des fibroblastes
Cdk : kinases dépendantes de la cycline
cGMP : guanosine monophosphate cyclique
CML : cellule musculaire lisse
CMLb : cellule musculaire lisse bronchique
CMLv : cellule musculaire lisse vasculaire
DAG : diacylglycérol
DH : domaine homologue à Dbl
DHR : région homologue aux DOCK
EMT : transition épithélio-mésenchymateuse
eNOS : NO synthase endothéliale
EGF : facteur de croissance épidermique
ExoS : exoenzyme S de *Pseudomonas aeruginosa*
GAP : protéine activatrice de l'activité GTPasique
GDI : protéine inhibitrice de la dissociation guanylique
GDP : guanosine diphosphate
GEF : facteur d'échange guanylique
GGTase-I : géranylgeranyltransférase de type 1
GTP : guanosine triphosphate
HTAP : hypertension artérielle pulmonaire
HRB : hyperréactivité bronchique
HRG : héguiline/neureguiline-1
HT : toxine hémorragique
IL : interleukine
IP3 : inositol 1,4,5-trisphosphate
LCC : large clostridial cytotoxins
LIMK : LIM-kinase

LT : toxine létale
MLC : chaîne légère de la myosine
MLCK : kinase de la chaîne légère de la myosine
MLCP : phosphatase de chaîne légère de la myosine
NADPH : nicotinamide adénine dinucléotide phosphatase
NLS : signal de localisation nucléaire
NO : monoxyde d'azote
NOX : NADPH oxydase
PAK : p-21 activated kinase
PDE5 : phosphodiesterase 5
PDGF-BB : facteur de croissance dérivé des plaquettes BB
PH : domaine homologue à la pleckstrine
PKC : protéine kinase C
PLC : phospholipase C
Rac1 : Ras-related C3 botulinum toxin substrate 1
Rho : Ras homologue
ROCK : Rho kinase
ROS : espèces réactives de l'oxygène
RyR : récepteurs à la ryanodine
SptP : protéine tyrosine phosphatase de *Salmonella typhimurium*
YopE : protéine externe E de *Yersinia pseudotuberculosis*

Table des figures

Figure 1 : Dendrogramme des membres de la famille des Rho GTPases (Bustelo, Sauzeau, et Berenjano 2007)	1
Figure 2 : Séquences primaires des Rho GTPases et structure cristallographique de Rac1	4
Figure 3 : Cycle d'activation des GTPases de la famille Rho (d'après Loirand, Sauzeau, et Pacaud 2013)	5
Figure 4 : Les GEFs à domaine DH (Cook, Rossman, et Der 2014)	7
Figure 5 : Structure cristallographique du complexe Rac1/Tiam1 (d'après Worthylake, Rossman, et Sondek 2000)	9
Figure 6 : Structure des GEFs de la famille DOCK (Laurin et Côté 2014)	11
Figure 7 : Structure des protéines de la famille RhoGAP (Ligeti, Welti, et Scheffzek 2012).....	12
Figure 8 : Structure cristallographique du complexe Rac1/GAP (PDB : 1HE1)	13
Figure 9 : Structure cristallographique du complexe Rac/GDI (PDB : 1DS6)	15
Figure 10 : Régulation de la migration cellulaire mésenchymateuse par les GTPases de la famille Rho	17
Figure 11 : Schéma d'assemblage et d'activation des NOXs (Panday et al. 2015)	19
Figure 12 : Régulation de la contraction des CMLv	21
Figure 13 : Fréquence des modifications de séquence ou d'expression de Rac1 observées dans différents types de cancer (d'après cBioPortal)	24
Figure 14 : Voies de signalisations moléculaires impliquant Rac1 dans la prolifération et la survie des cellules tumorales	26
Figure 15 : Les différentes stratégies thérapeutiques ciblant Rac1	28
Figure 16 : Modèle de docking du NSC23766 sur la GTPase Rac1 (Sauzeau, Beignet, et Bailly 2022).....	31
Figure 17 : Prévalence du cancer à travers le monde en 2020 (GLOBOCAN 2020) ..	73

Table des tableaux

Tableau I : Les différents inhibiteurs de Rac1.....	36
---	----

INTRODUCTION

I- Les protéines G monomériques de la famille Rho :

I.1- Présentation générale des Rho GTPases :

La famille des protéines Rho (Ras homologous) fait partie de la superfamille Ras et se compose de 20 petites GTPases ayant un poids moléculaire de 20 à 30 kDa (Figure 1). Ces protéines sont exprimées par l'ensemble des organismes eucaryotes et se caractérisent par leur capacité à se lier au nucléotide GTP (guanosine triphosphate). Il existe d'une part les Rho GTPases dites « classiques » telles que RhoA, Rac, Cdc42, RhoD et RhoF présentes sous forme active liée au GTP ou inactive liée au GDP (guanosine diphosphate). D'autre part les Rho GTPases « atypiques » telles que RHO-BTB, RND, RHOV, RHOH et RHOH sont liées exclusivement au GTP. Leur activité peut être régulée par différents mécanismes tels que leur niveau d'expression ou de phosphorylation. Les GTPases monomériques de la famille Rho les plus étudiées et les mieux caractérisées sont les protéines RhoA, Rac et Cdc42.

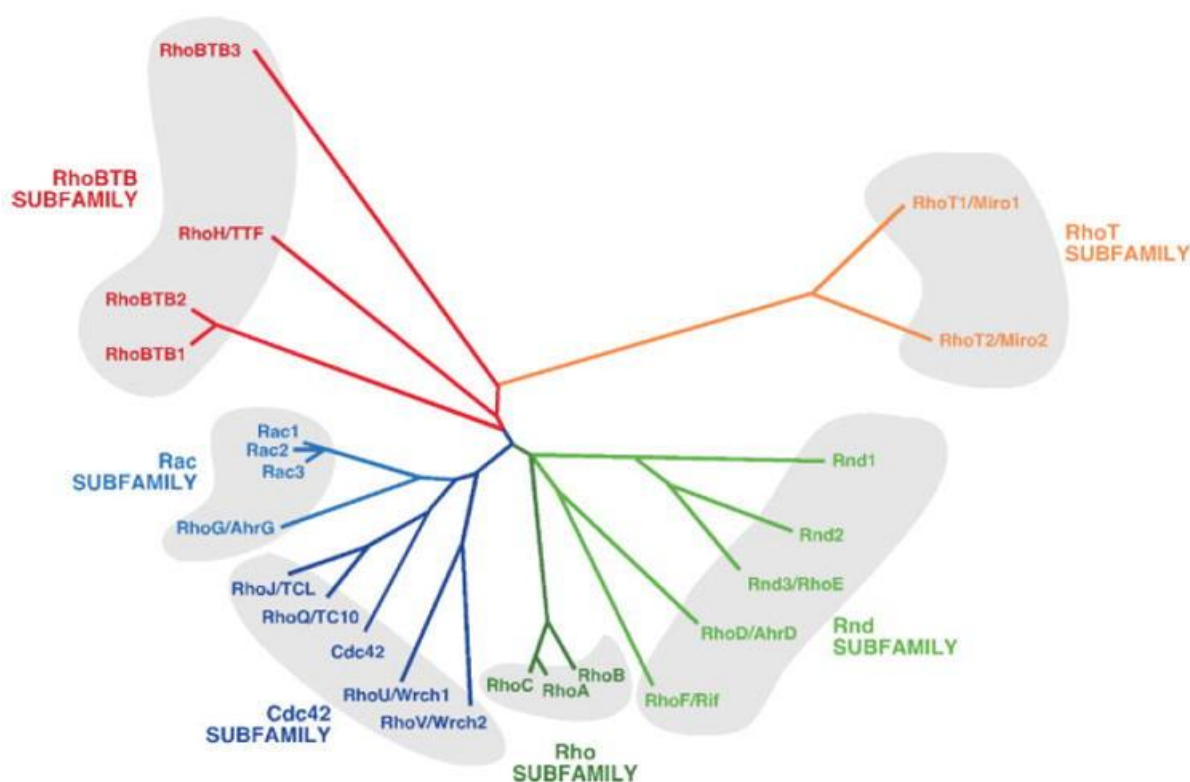


Figure 1 : Dendrogramme des membres de la famille des Rho GTPases
(Bustelo, Sauzeau, et Berenjeno 2007)

La fonction principale de ces protéines est de contrôler l'organisation du cytosquelette d'actine. L'activation de RhoA entraîne la formation de fibres de stress constituées de filaments d'actine alignés en faisceaux denses ainsi que de points d'adhésions focales. L'activation de Cdc42 induit la formation de longs filaments d'actine droits appelés filopodes. L'activation de Rac1, quant à elle, conduit à la polymérisation de l'actine à la périphérie de la cellule, à la formation de lamellipodes et de protrusions membranaires. Ces protéines sont donc des acteurs clés de la régulation de l'organisation du cytosquelette d'actine et participent de ce fait à la morphologie, la polarité, la migration, la prolifération et l'adhésion cellulaire (Etienne-Manneville et Hall 2002).

Au cours de ma thèse, je me suis intéressée plus particulièrement à la protéine Rac. Il existe 4 homologues de la protéine Rac, Rac1/2/3 et RhoG. Rac1 (Ras-related C3 botulinum toxin substrate 1) est une protéine ubiquitaire codée par un gène présent sur le chromosome 7 (7p22) chez l'Homme et est composé de 7 exons (Matos et al. 2000). La protéine Rac2 est codée par le gène situé sur le chromosome 22 (22q13.1) et est exprimée exclusivement dans les cellules hématopoïétiques. Le gène codant pour la protéine Rac3 se situe sur le chromosome 17 (17q25.3) et cette forme de Rac est exprimée majoritairement au niveau cérébral (Courjal et al. 1997). Concernant la protéine RhoG, elle est codée par le gène situé sur le chromosome 11 (11p15.4) et est exprimée dans les fibroblastes, les leucocytes, les cellules neuronales et endothéliales. Ces protéines présentent une forte homologie de séquence avec 88% d'homologie entre Rac1 et Rac2, 77% entre Rac1 et Rac3 et 72% entre Rac1 et RhoG (Vincent, Jeanteur, et Fort 1992; Wertheimer et al. 2012).

I.2- Structure des Rho GTPases :

Les Rho GTPases sont des protéines monomériques composées d'un domaine G central, d'une région d'insertion et d'une extrémité C-terminale hypervariable selon les membres de la famille (Figure 2).

Le domaine G est constitué d'un feuillet- β à 6 brins antiparallèles entouré par 5 hélices- α . Ce domaine se caractérise par 5 boucles polypeptidiques G1 à G5 qui forment la poche nucléotidique permettant la fixation du GDP ou du GTP (Sprang 1997). Le motif G1 contient la séquence consensus GXXXXGK(S/T) qui réalise la liaison entre le feuillet β 1 et l'hélice α 1 de la GTPase et se lie également aux α - et β -phosphates du nucléotide grâce à la Lys16 conservée entre les GTPases Rac, RhoA et Cdc42. La boucle G1 est également impliquée dans la coordination de l'ion Mg^{2+} par le biais de la Thr17 pour Rac, RhoA et Cdc42. Le Mg^{2+}

participe au maintien de la structure tridimensionnelle de la protéine ainsi qu'à la stabilisation de la liaison entre la protéine et le nucléotide. La boucle G2 assure la liaison entre l'hélice $\alpha 1$ et le brin $\beta 2$. Cette boucle participe à la coordination du Mg^{2+} grâce à la Thr35 conservée entre les différentes GTPases et fait partie intégrante de la région Switch I. Le motif G3 situé entre le brin $\beta 3$ et l'hélice $\alpha 2$ se lie au γ -phosphate du nucléotide et également au Mg^{2+} . La boucle G3 fait partie de la région Switch II et de l'hélice $\alpha 2$. La boucle G4 relie le brin $\beta 5$ et l'hélice $\alpha 4$ pour participer à la reconnaissance de la base guanidine. Le motif G5 participe également à la reconnaissance de la guanine et se situe entre le brin $\beta 6$ et l'hélice $\alpha 5$ (Itzen et Goody 2011).

La région d'insertion unique, de 10 à 15 acides aminés, se trouve entre l'hélice $\alpha 4$ et le brin $\beta 5$. Cette séquence peptidique est impliquée dans l'interaction entre la GTPase et les facteurs d'échange de nucléotides guanyliques (GEFs) ainsi qu'entre la GTPase et ses effecteurs (Lam et Hordijk 2013). Ce domaine permet l'activation des effecteurs et des cascades de signalisation qui en découlent.

L'extrémité C-terminale des RhoGTPases contient un motif CAAX qui participe à la localisation des GTPases. Ce motif subit une modification post-traductionnelle qui consiste en l'ajout d'un motif prényle sur la cystéine par les farnésyl- ou géranyl-géranyl-transférases. L'ajout de ce motif lipidique permet un adressage de la GTPase à la membrane plasmique. L'extrémité C-terminale des GTPases contient également une région hypervariable qui participe également à la localisation de ces protéines. Dans le cas de Rac1, cette région contient une séquence polybasique correspondant au signal de localisation nucléaire (NLS) (Lam et Hordijk 2013).

Les régions Switch I et II sont essentielles pour le passage des protéines de leur état inactif à un état actif. Ces régions vont subir des modifications structurelles permettant le remplacement du GDP par le GTP. Pour Rac1, la région Switch I correspond aux résidus 26 à 36 et la région Switch II correspond aux résidus 59 à 76. Les différentes études structurales des GTPases ont mis en évidence les différentes interactions existant entre le nucléotide et les GTPases. Lorsque la protéine est sous forme active (liée au GTP), deux liaisons hydrogène sont établies entre le phosphate γ du nucléotide et la Thr35 au niveau du Switch I et la Gly60 de la région Switch II de Rac1. Lors de l'hydrolyse du GTP en GDP, il y a libération du phosphate γ et les liaisons établies entre celui-ci et les régions Switch sont donc perdues entraînant un relâchement de la conformation de la protéine (Schaefer, Reinhard, et Hordijk 2014).

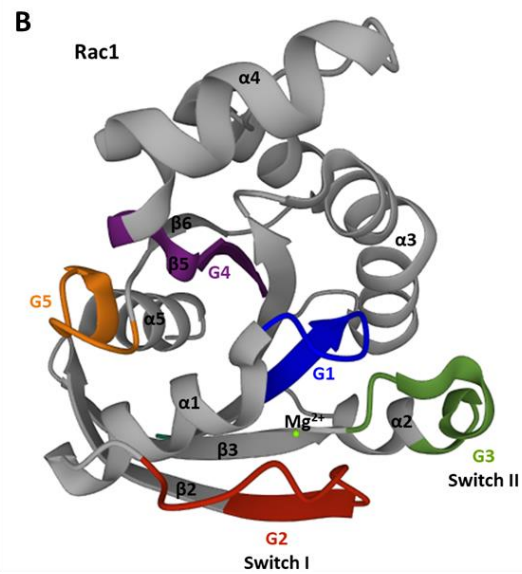
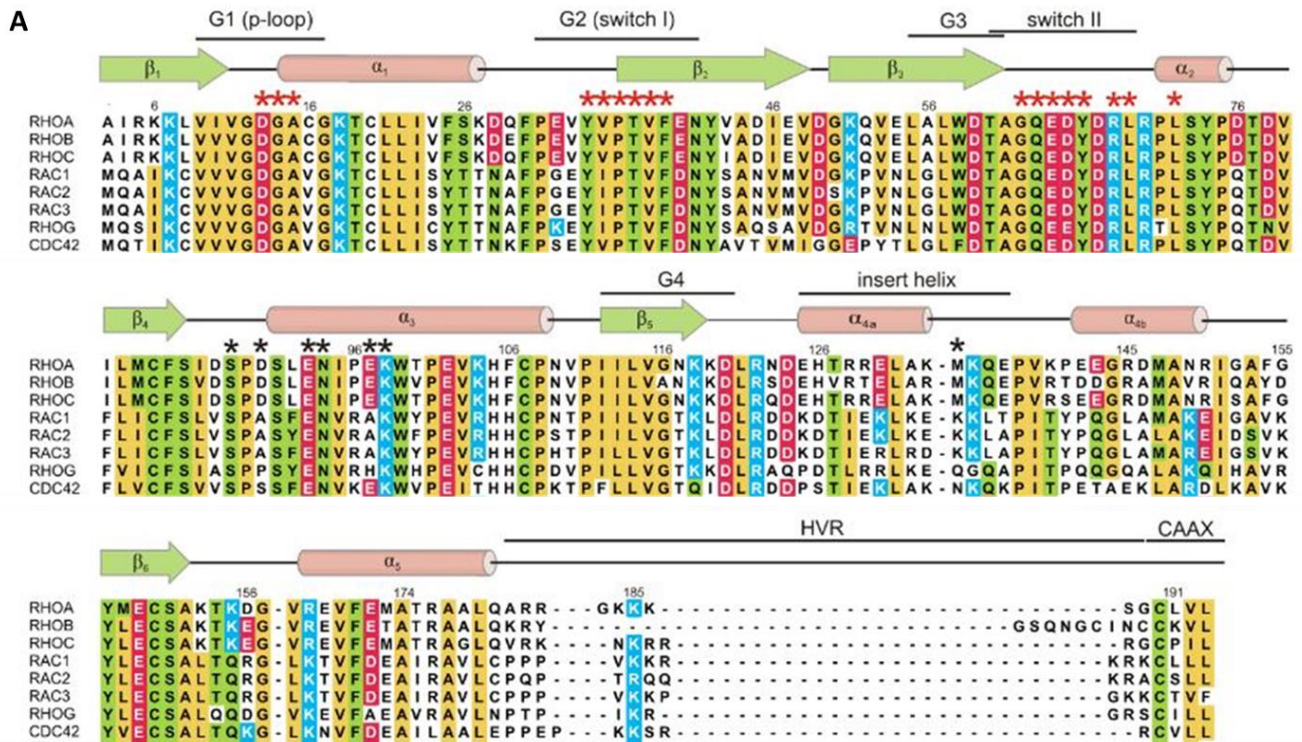


Figure 2 : Séquences primaires des Rho GTPases et structure cristallographique de Rac1

(A) Alignement des séquences des GTPases de la famille Rho. Les domaines et les principaux motifs structuraux sont annotés. Les acides aminés en jaune sont de type hydrophobes, en vert hydrophyles, en rouge chargés négativement, en bleu chargés positivement (Amin et al. 2016). (B) Structure cristallographique de Rac1 (PDB : 3TH5). Les différents domaines G1 à G5 et les motifs structuraux hélices α et brins β sont symbolisés.

I.3- Régulation de l'activité des Rho GTPases :

Les GTPases agissent comme des commutateurs moléculaires en passant d'un état inactif lié au GDP dans le cytosol à un état actif lié au GTP et ancré à la membrane plasmique (Figure 3). Ce cycle d'activation/inactivation des Rho GTPases est finement régulé par différentes familles de protéines. Les GEFs sont activés en réponse à différents stimuli externes et catalysent l'échange du GDP par le GTP. Une fois liées au GTP, les GTPases peuvent interagir avec leurs effecteurs spécifiques et initier différentes cascades de signalisation régulant de nombreux processus cellulaires. Les GTPases possèdent une activité GTPasique intrinsèque permettant l'hydrolyse du GTP en GDP. Cette activité intrinsèque étant faible, les protéines activatrices de l'activité GTPasique (GAPs) agissent comme des catalyseurs en accélérant la réaction d'hydrolyse du GTP et favorisent donc le retour de la protéine à un état inactif. Les GTPases sous forme inactive sont séquestrées dans le cytosol par les GDIs.

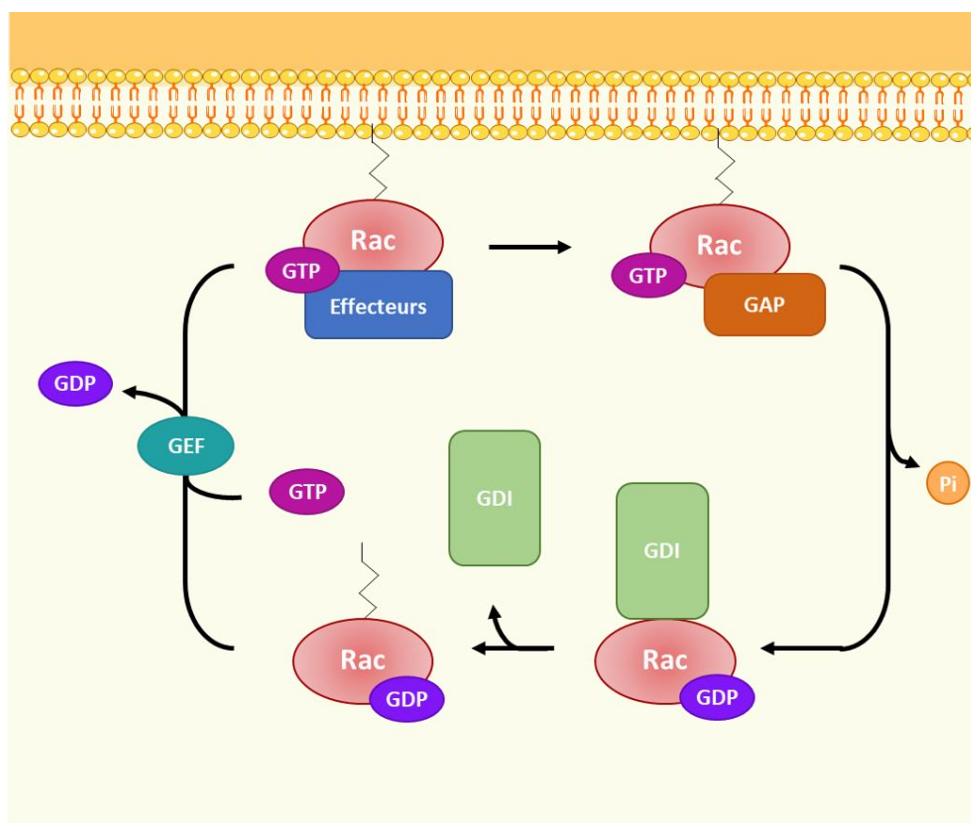


Figure 3 : Cycle d'activation des GTPases de la famille Rho (d'après Loirand, Sauzeau, et Pacaud 2013)

Rac1 cycle entre un état inactif lié au GDP et un état actif lié au GTP. Ce cycle d'activation est régulé par les GEFs responsables de l'échange du GDP par le GTP ; les GAPs favorisent l'hydrolyse du GTP et le retour de la GTPase à un état inactif ; les GDIs séquestrent Rac1 sous forme inactive dans le cytosol.

I.3.1- Les facteurs d'échange de nucléotides guanyliques (GEFs) :

Il existe plus de 80 GEFs régulant l'activité des Rho GTPases qui se répartissent en deux familles : les GEFs à domaine DH (Dbl-Homology) et les GEFs à domaine DHR (Dock Homology Region). Les GEFs peuvent activer différentes GTPases monomériques, être spécifiques d'une sous-famille ou spécifique d'une seule GTPase monomérique (Snyder et al. 2002).

La plus grande famille de GEFs, les GEFs à domaine DH, regroupe 71 membres qui sont tous constitués d'un domaine DH en tandem avec un domaine PH (Pleckstrin Homology) (Fort et Blangy 2017) (Figure 4). Les domaines DH-PH forment souvent la structure minimale nécessaire à l'activité des GEFs. Les domaines DH se composent d'un assemblage d'hélices α et de 3 régions CR1 à CR3 hautement conservées. Ces régions forment chacune une hélice α et s'assemblent pour former le cœur du domaine DH. Les domaines CR1 et CR3 constituent une partie du site de fixation des GEFs sur les GTPases et sont en interaction direct avec les domaines Switch I et Switch II des Rho GTPases. Le domaine PH, quant à lui, interagit avec les phospholipides et participe à la localisation membranaire des Rho GTPases (Zheng 2001; Hakoshima 2003; Hoffman et Cerione 2002).

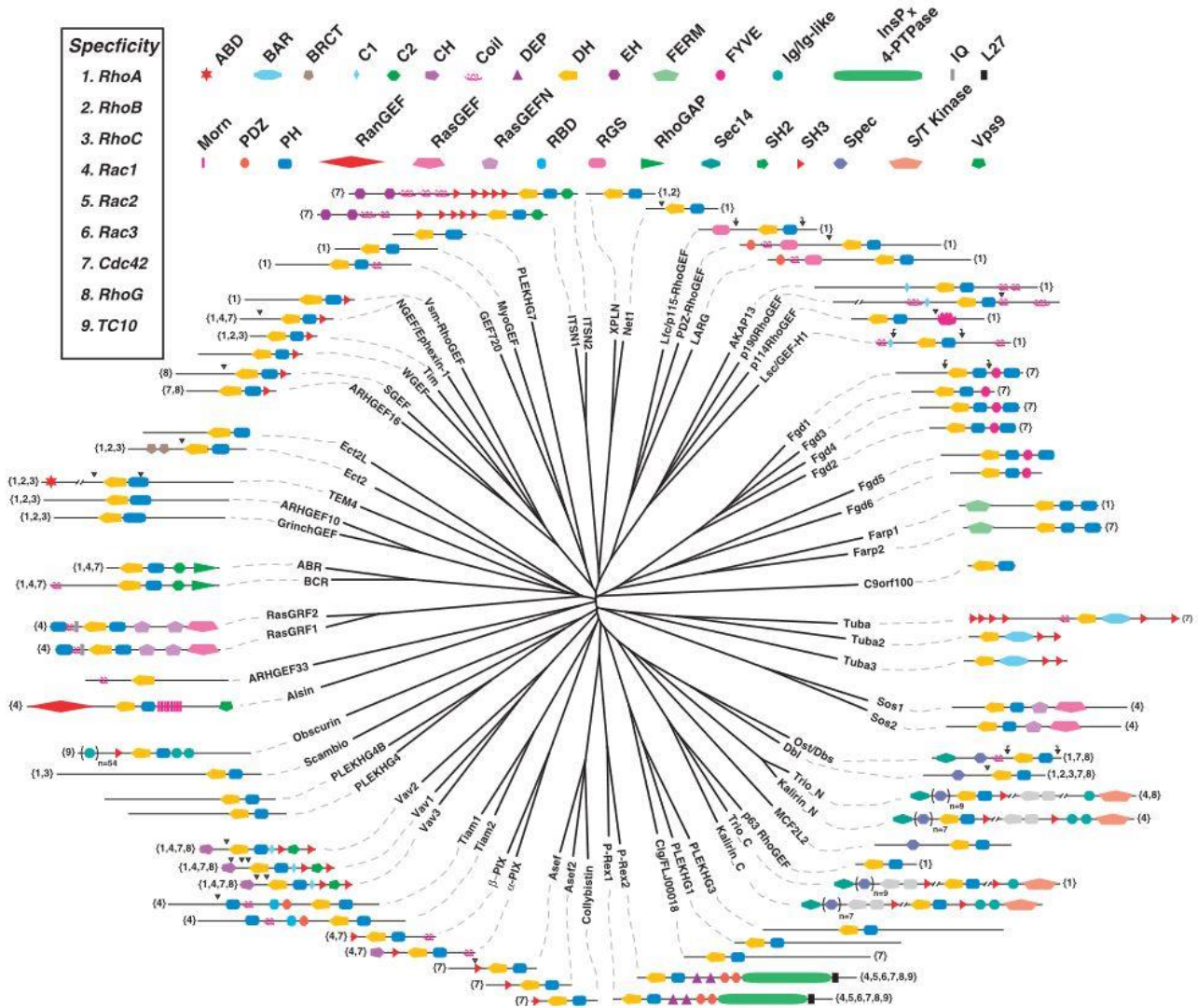


Figure 4 : Les GEFs à domaine DH (Cook, Rossman, et Der 2014)

Les différents domaines composants ces GEFs sont représentés avec notamment le domaine DH (jaune) et le domaine PH (rectangle bleu). La spécificité de ces GEFs pour les GTPases est également mentionnée.

Le mécanisme d'action des GEFs repose sur un changement de conformation des régions Switch I et II entraînant une modification de la poche nucléotidique et perturbant la fixation de l'ion Mg^{2+} (Vetter et Wittinghofer 2001; Rossman, Der, et Sondek 2005; Cherfils et Zeghouf 2013). Ces modifications structurales conduisent à la libération du GDP qui est remplacé par le GTP majoritaire dans le milieu intracellulaire. L'étude cristallographique de Rac1 liée aux domaines DH-PH de Tiam1 a permis de caractériser plus spécifiquement le mécanisme d'action de ces GEFs en identifiant les acides aminés clés et propres à cette réaction (Figure 5). Cette étude a mis en évidence que Tiam1 interagit avec les régions Switch I et II de Rac1. Des liaisons de type hydrogène sont établies entre un résidu d'acide glutamique de la

région CR1 du domaine DH de Tiam1 et les amides de la chaîne principale des acides aminés Thr35 et Val36 ainsi qu'avec l'hydroxyle de la chaîne latérale de la Tyr32 de la région Switch I de Rac1. Ces différentes interactions entre le domaine DH du GEF et la région Switch I de la GTPase entraînent une déstabilisation de la poche nucléotidique et un déplacement de la Thr35 qui participe à la coordination de l'ion Mg^{2+} . La région Switch II de Rac1 subit également des changements conformationnels qui sont dus aux interactions entre la région CR3 du domaine DH et l'Ala59 et la Tyr64 de Rac1. Ces modifications participent également à la déstabilisation du Mg^{2+} . En effet, le groupe méthyle présent dans la chaîne latérale de l'Ala59 est déplacé dans la poche nucléotidique et bloque le site de fixation du Mg^{2+} par encombrement stérique. L'ensemble de ces modifications conformationnelles des régions Switch I et II permettent une interaction entre l'acide aminé Glu62 et la Lys16 présente dans la boucle G1 de la GTPase. Cette interaction libère le β -phosphate du nucléotide qui était lié à la boucle G1. Ainsi, la perturbation de la liaison du Mg^{2+} et la déstabilisation de la boucle G1 sont des éléments clés permettant l'échange GDP/GTP (Worthylake, Rossman, et Sondek 2000; Hoffman et Cerione 2002; Toma-Fukai et Shimizu 2019).

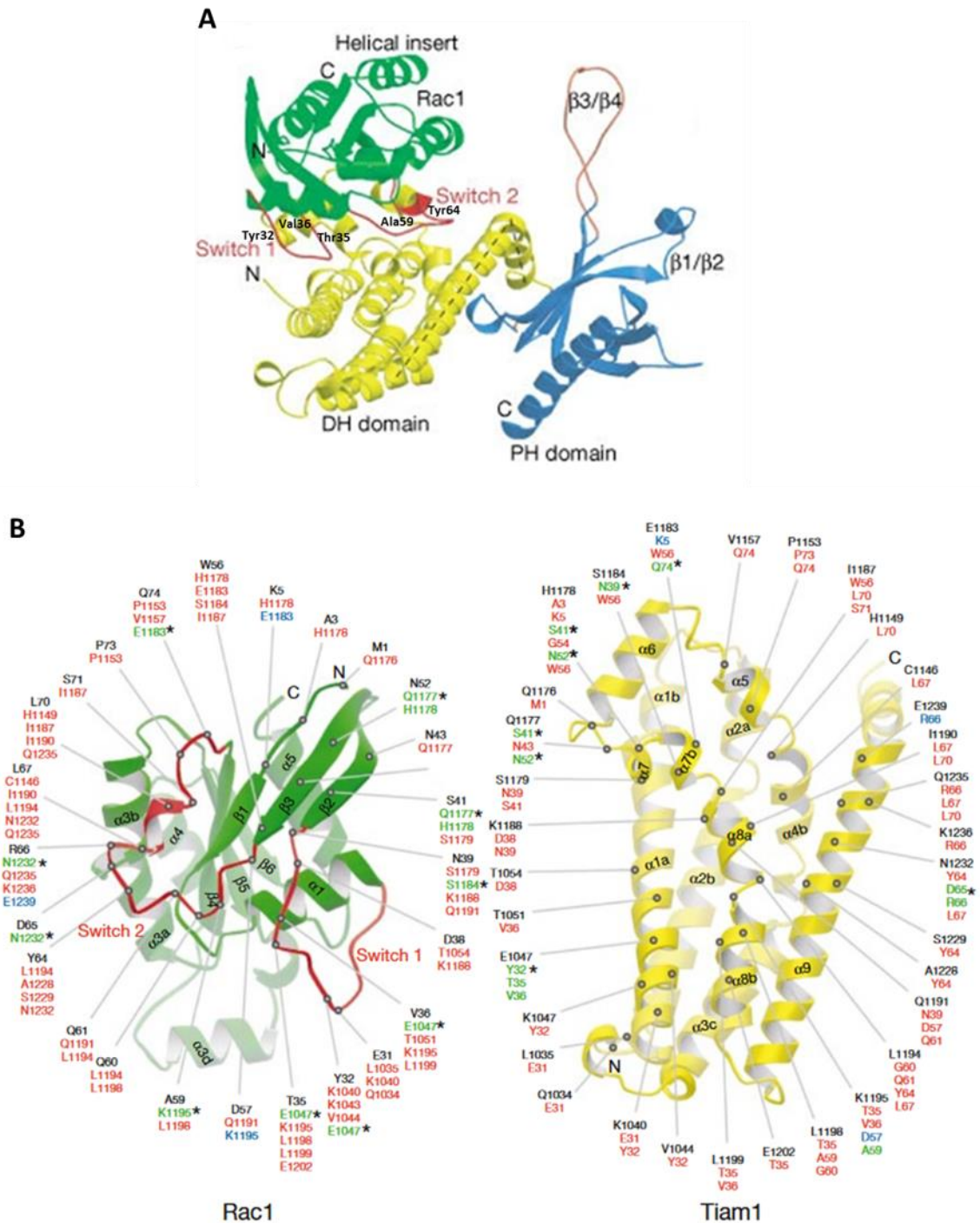


Figure 5 : Structure cristallographique du complexe Rac1/Tiam1 (d'après Worthylake, Rossman, et Sondek 2000)

(A) Structure cristallographique du complexe Rac1/Tiam1. La protéine Rac1 est représentée en vert avec ses domaines Switch I et II en rouge, les domaines DH et PH de Tiam1 sont respectivement en jaune et bleu. Les acides aminés de Rac1, Tyr32, Thr35, Val36, Ala59 et Tyr64, qui sont impliqués dans les interactions avec Tiam1 sont annotés. (B) Représentation des interactions entre Rac1 et Tiam1. Les liaisons hydrogènes sont annotées en vert, les interactions de Van der Waals en rouge, les liaisons ioniques en bleu et les étoiles représentent des liaisons non-ioniques faisant intervenir les atomes de la chaîne latérale de l'acide aminé.

L'activité des GEFs est régulée par différents mécanismes tels que la suppression de séquences inhibitrices intramoléculaire (López-Lago et al. 2000), des interactions protéine-protéine (Taya et al. 2001; Z. Chen et al. 2012) ou leur localisation intracellulaire (Fleming et al. 2004). De nombreux GEFs présentent des séquences de régulation qui bloquent leur propre activité par interaction intramoléculaire entre une séquence d'auto-inhibition et le domaine DH du GEF. Ce mécanisme de régulation a notamment été décrit pour Vav et Tiam1 qui possèdent à leur extrémité N-terminale une séquence d'auto-inhibition. Des études ont démontré que la phosphorylation des GEFs peut entraîner des modifications conformationnelles qui déplacent ces séquences d'auto-inhibition permettant alors aux GEFs d'exercer leur activité catalytique (López-Lago et al. 2000; Whalley et al. 2015; Azoitei et al. 2019). Pour le GEF Vav, il est nécessaire que la Tyr174 soit phosphorylée afin de démasquer son domaine DH contenant son site actif (Aghazadeh et al. 2000). L'activité des GEFs peut également dépendre de leur localisation intracellulaire. Par exemple, le GEF Tiam1 possède deux domaines PH, l'un en tandem avec le domaine DH qui participe à l'activité catalytique du GEF tandis que le second est responsable de son recrutement à la membrane (Crompton et al. 2000; Fleming et al. 2004).

La seconde famille de GEFs, les GEFs à domaine DHR, est constituée de 11 membres classés en quatre sous-groupes : DOCK-A, -B, -C et -D (Figure 6). Ces GEFs sont caractérisés par la présence de deux domaines conservés : la région d'homologie Dock-1 (DHR-1) qui permet la liaison du GEF aux lipides et la région DHR-2 qui est responsable de l'activité catalytique du GEF. Les GEFs des groupes DOCK-A et -B activent spécifiquement les GTPases de la sous-famille de Rac tandis que DOCK-D active spécifiquement Cdc42. Les GEFs de la sous-famille DOCK-C sont capables d'activer Rac et Cdc42 à l'exception de DOCK8 qui est spécifique de Cdc42 (Laurin et Côté 2014).

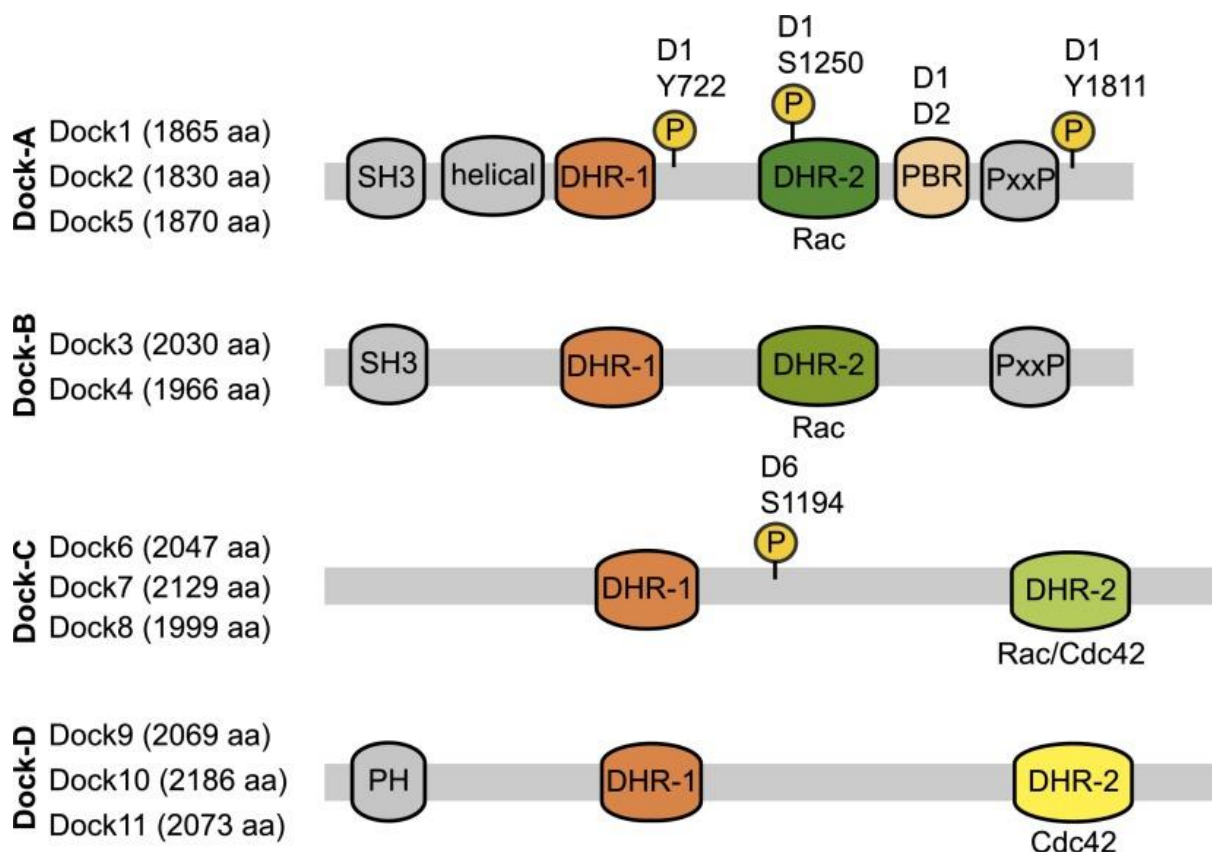


Figure 6 : Structure des GEFs de la famille DOCK (Laurin et Côté 2014)

Les GEFs de la famille DOCK sont subdivisées en 4 sous-familles qui possèdent toutes au minimum un domaine DHR-1 impliqué dans la liaison aux lipides et un domaine DHR-2 portant l'activité catalytique du GEF

Le mécanisme d'action de ces GEFs est moins bien connu que celui des GEFs à domaine DH. Ces GEFs sont décrits pour interagir avec les GTPases monomériques via leur domaine DHR2 et modifier uniquement la conformation de la région Switch I sans interagir avec la région Switch II. La fixation du GEF sur la GTPase entraîne un déplacement de la boucle G1 du domaine Switch I ce qui perturbe l'interaction entre la Phe28 et la base du GDP libérant le β -phosphate du nucléotide. Cette modification conformationnelle de Switch I permet l'insertion d'un résidu hydrophobe à proximité du site de fixation de l'ion Mg^{2+} ce qui a pour effet de déstabiliser la liaison entre cet ion et la GTPase monomérique (Thompson et al. 2021).

I.3.2- Les protéines activatrices de l'activité GTPasique (GAPs) :

Les protéines G monomériques de la famille Rho possèdent toutes une activité GTPasique intrinsèque mais celle-ci est lente et incompatible avec les différentes fonctions

régulées par les GTPases qui demandent une inactivation rapide des protéines. Les GAPs accélèrent la réaction d'hydrolyse du GTP en GDP.

La famille RhoGAP est constituée de plus de 70 membres dont chacun possède un domaine GAP, formant 9 hélices α , constitué de 190 acides aminés hautement conservés dont une arginine essentielle à l'activité catalytique (Mosaddeghzadeh et Ahmadian 2021). Ces protéines régulatrices possèdent également des régions DH, PH, SH2, SH3 et des régions riches en proline permettant de réguler leur activité et leur localisation subcellulaire (Figure 7). La région PH permet la liaison à la membrane plasmique et les régions SH2 et SH3 sont impliquées dans les interactions protéiques (Ligeti, Welti, et Scheffzek 2012).

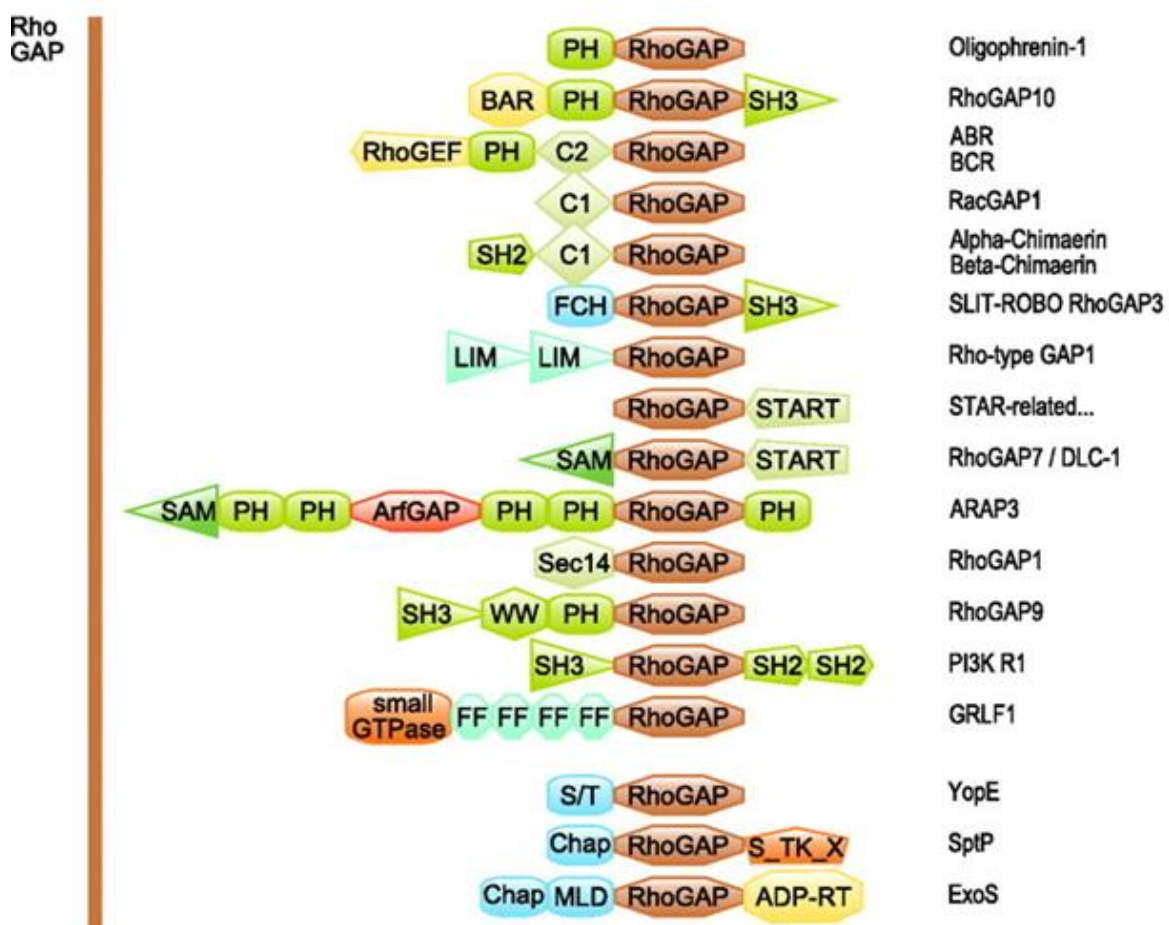


Figure 7 : Structure des protéines de la famille RhoGAP (Ligeti, Welti, et Scheffzek 2012)

Organisation structurale de différentes GAPs spécifiques des GTPases de la famille Rho avec un domaine GAP hautement conservé et d'autres régions telles que DH, PH, SH2, SH3.

Les GAPs interagissent avec les Rho GTPases au niveau de la boucle G1, les régions Switch I et Switch II. Une liaison est établie entre l'arginine catalytique du domaine GAP et le

carbonyle de la chaîne principale de la Gly12 de Rac1 permettant de stabiliser l'état de transition de l'hydrolyse du GTP. Cette interaction participe également à la stabilisation des charges négatives qui se forment lors de l'état de transition de l'hydrolyse du GTP au niveau du γ -phosphate et oriente la Gln61 de Rac1 afin qu'elle coordonne l'attaque nucléophile d'une molécule d'eau sur le γ -phosphate (Bos, Rehmann, et Wittinghofer 2007; Mosaddeghzadeh et Ahmadian 2021) (Figure 8).

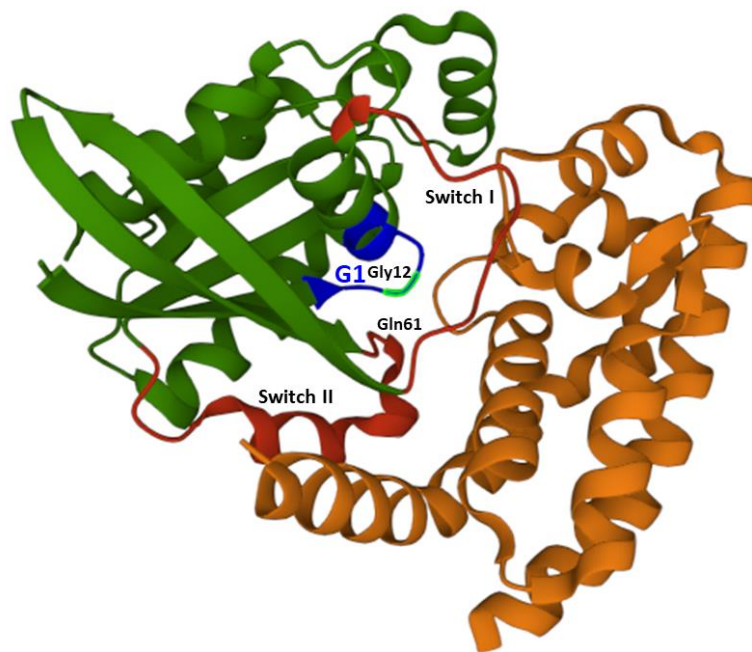


Figure 8 : Structure cristallographique du complexe Rac1/GAP (PDB : 1HE1)
La protéine Rac1 est représentée en vert avec ses domaines Switch I et Switch II en rouge et la boucle G1 en bleu, le domaine GAP de la toxine ExoS est en orange.

L'activité des GAPs est régulée de façon spatio-temporelle. Ainsi, certaines GAPs doivent être présentes au niveau de la membrane plasmique pour permettre l'inactivation des GTPases monomériques. Les RhoGAPs peuvent également être régulées par phosphorylation comme ARHGAP24, une GAP spécifique de Rac1, dont la phosphorylation de la Ser402 induit son activation cytoplasmique (Morishita, Tsutsumi, et Ohta 2015; Hodge et Ridley 2016).

I.3.3. Les protéines inhibitrices de la dissociation guanylique (GDIs) :

Les RhoGDIs empêchent la dissociation du nucléotide guanylique, le plus souvent le GDP, et maintiennent les GTPases sous forme inactive dans le cytoplasme. La famille des RhoGDIs se compose de trois membres : RhoGDI1, RhoGDI2, RhoGDI3. Le membre de la

famille majoritaire est RhoGDI1 qui a une expression ubiquitaire. RhoGDI2 est préférentiellement exprimée dans les cellules épithéliales et hématopoïétiques tandis que RhoGDI3 est exprimée dans le pancréas, les poumons et le cerveau (DerMardirossian et Bokoch 2005; Dovas et Couchman 2005; Garcia-Mata, Boulter, et Burridge 2011). Les RhoGDIs sont composées d'un domaine N-terminal avec un faisceau d'hélices α qui interagit avec les régions Switch de la GTPase et une extrémité C-terminale comprenant un sandwich β qui se lie au groupement prényle.

Le mécanisme d'interaction entre les GTPases monomériques et les GDIs se divise en deux étapes. Premièrement, le domaine N-terminal du GDI se lie aux domaines Switch I et II de la GTPase inhibant la dissociation du nucléotide. Les acides aminés de Rac1 essentiels à cette interaction ont été identifiés : la Thr35, la Tyr64, l'Arg66, l'His103 et l'His104 établissant des liaisons hydrogène avec la GDI (Garcia-Mata, Boulter, et Burridge 2011) (Figure 9). Deuxièmement, le groupement prényle de la GTPase monomérique est déplacé de la membrane plasmique vers la poche hydrophobe du GDI présente à son extrémité C-terminale ce qui empêche les interactions entre les lipides de la GTPase monomérique et la membrane plasmique (Dovas et Couchman 2005; Garcia-Mata, Boulter, et Burridge 2011). Suite à cette étape la GTPase monomérique est séquestrée dans le cytosol. Il a été observé que PAK (p-21 activated kinase) phosphoryle les Ser101 et Ser174 de RhoGDI permettant la dissociation du complexe protéique Rac1/RhoGDI et l'activation de la GTPase monomérique (Dovas et Couchman 2005).

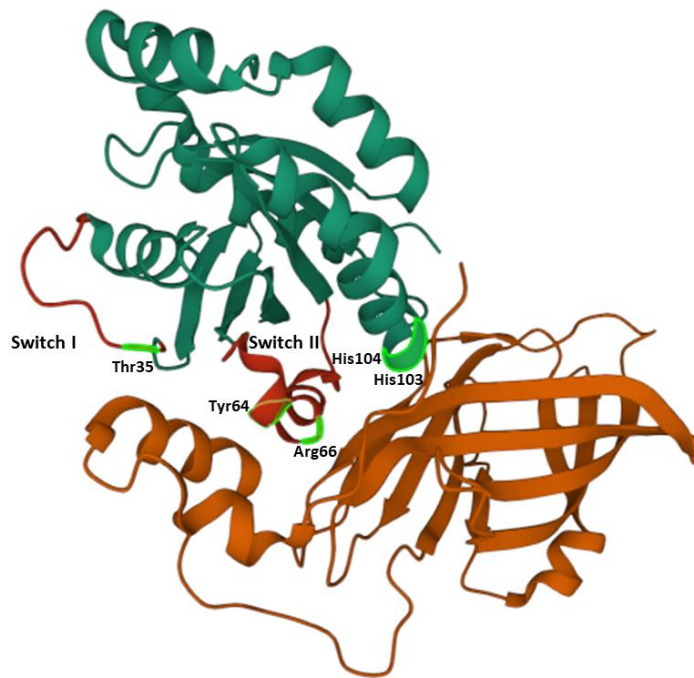


Figure 9 : Structure cristallographique du complexe Rac/GDI (PDB : 1DS6)

La protéine Rac est représentée en vert avec ses domaines Switch I et Switch II en rouge, les acides aminés impliqués dans les interactions avec la GDI sont mentionnés, la GDI est en orange.

II- Rôles physiologiques de la GTPase Rac1 :

En modulant l'organisation du cytosquelette d'actine, la protéine Rac1 régule des fonctions cellulaires essentielles telles que la migration, l'adhésion et la contraction cellulaire. Rac1 est également impliquée dans la transduction de signaux de croissance, la régulation de la transcription, le cycle cellulaire et le stress oxydant.

II.1- Organisation du cytosquelette d'actine et migration cellulaire :

Le cytosquelette d'actine est un système filamentaire dynamique qui s'étend dans le cytoplasme et régit la morphologie cellulaire. Il est composé de monomères globulaires d'actine qui s'assemblent pour former des microfilaments d'actine polarisés avec une extrémité à croissance rapide et une extrémité à croissance lente. Les filaments d'actine forment un réseau de filaments droits ou branchés associés aux protéines liant l'actine. La capacité d'assemblage/désassemblage de ce réseau d'actine confère aux cellules une certaine plasticité qui leur permet de s'adapter à leur environnement et notamment de migrer (Cooper 2000).

La protéine Rac1 régule l'organisation du cytosquelette d'actine notamment via la polymérisation directe de l'actine. Rac1, activée par le GEF Tiam1, interagit avec son effecteur IRSp53 favorisant la liaison de Rac1 aux protéines WAVE qui peuvent à leur tour activer le complexe Arp2/3. Cette cascade de signalisation participe à la formation de nouveaux polymères d'actine qui se ramifient aux filaments déjà existants et qui sont essentiels à la formation de lamellipodes (Miki et al. 2000; Millard, Sharp, et Machesky 2004; Ridley 2006). Les lamellipodes présents au niveau du front de migration des cellules sont des projections membranaires qui permettent à la cellule de se déformer et guident la migration cellulaire. Rac1 contrôle également la polymérisation de l'actine de façon indirecte via son effecteur PAK. Ce dernier phosphoryle et active les LIM-kinases (LIMKs) qui phosphorylent et inactivent la cofiline responsable de la dépolymérisation de l'actine (Ridley 2006; Mierke et al. 2020). De ce fait, Rac1 participe à la stabilisation des filaments d'actine (Figure 10).

La régulation de l'organisation du cytosquelette d'actine est un élément clé de la migration cellulaire. Par conséquent Rac1, tout comme les GTPases RhoA et Cdc42, est impliquée dans cette fonction cellulaire. Le mécanisme de migration cellulaire est régulé de façon spatio-temporelle. Premièrement, des protrusions membranaires de deux types se développent à l'avant de la cellule permettant d'orienter la migration. La formation de filopodes, de longs filaments d'actine droits, est sous le contrôle de l'activité de Cdc42 (L. Ma, Rohatgi, et Kirschner 1998, 42; Lawson et Ridley 2018) tandis que la formation de lamellipodes est régulée par Rac1. De nouveaux points d'adhésion doivent être établis entre la cellule et les substrats extracellulaires pour soutenir la formation de ces protrusions membranaires. Rac1, via son GEF β -Pix participe à la formation du complexe GIT/ β -Pix/PAK impliqué dans la mise en place de ces nouveaux points d'adhésion (Frank et Hansen 2008; Lawson et Ridley 2018) (Figure 10). Deuxièmement, le corps et l'arrière de la cellule doivent se contracter pour suivre l'extension vers l'avant de la cellule. Cette étape fait intervenir la GTPase RhoA qui participe à la formation de fibres de stress et module la force de contraction de l'actine-myosine régulant la contraction du corps et de l'arrière de la cellule (Etienne-Manneville et Hall 2002; Hall 2012).

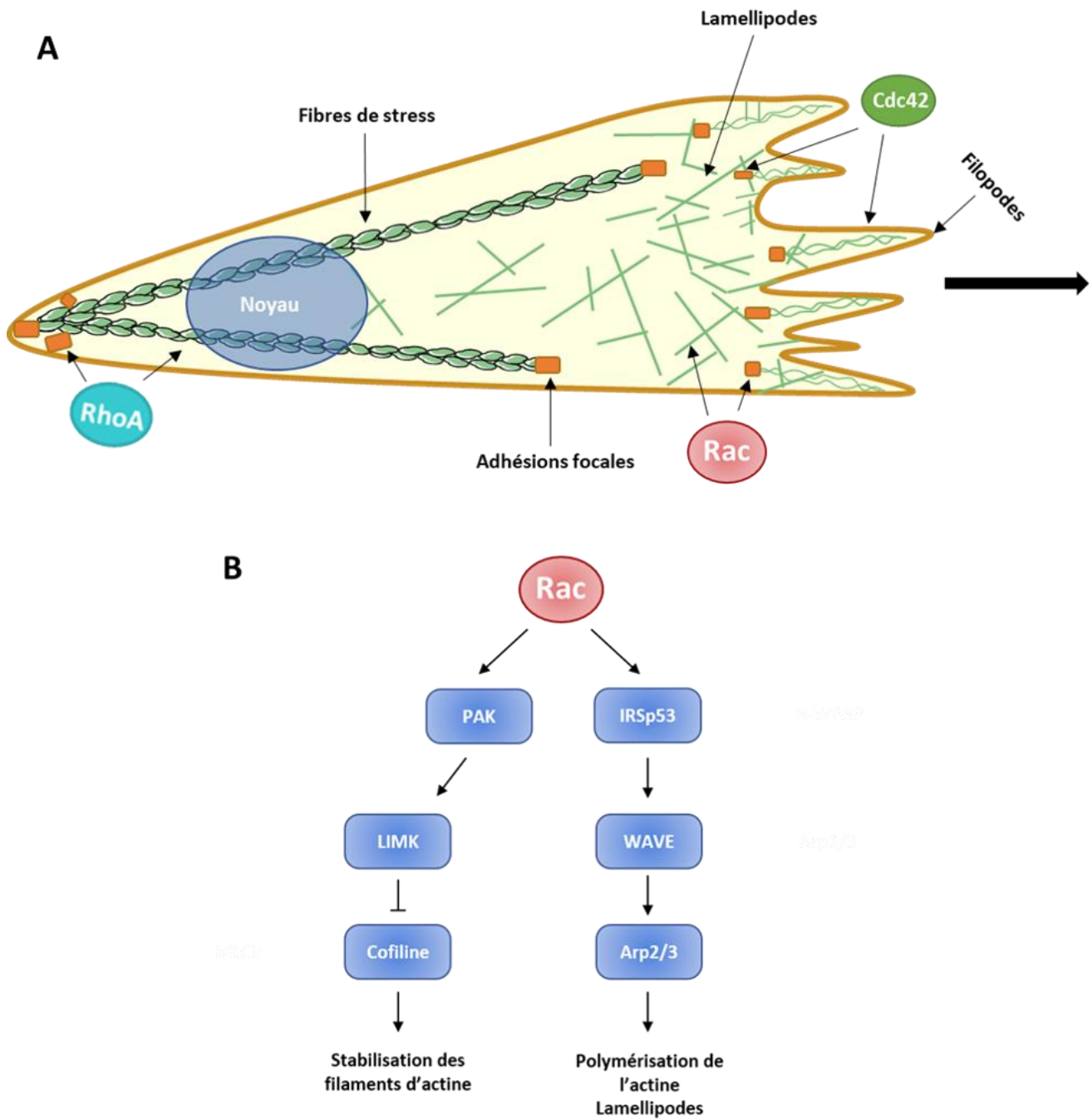


Figure 10 : Régulation de la migration cellulaire mésenchymateuse par les GTPases de la famille Rho

(A) Représentation schématique d'une cellule en cours de migration. Cdc42 régule la formation de filopodes et des complexes focaux d'adhésion, Rac1 contrôle la formation des lamellipodes et l'assemblage des complexes focaux d'adhésion, RhoA participe au développement des fibres de stress et régule la contraction du corps cellulaire. (B) Voies de signalisations moléculaires régulant l'organisation du cytosquelette d'actine et la migration cellulaire dépendante de Rac1.

II.2- Régulation du cycle cellulaire et de la prolifération :

Au cours du cycle cellulaire, la cycline D1 permet l'activation de kinases dépendantes de la cycline (cdk) cdk4 et cdk6 qui phosphorylent et inactivent la protéine rétinoblastome permettant la libération du facteur de transcription E2F. Ce dernier régule l'expression de gènes impliqués dans la transition G1/S. Différentes études ont démontré que Rac1 est capable de moduler l'expression de la cycline D1 tant au niveau transcriptionnel que traductionnel (Ridley 2001; Jaffe et Hall 2005).

La transcription de la cycline D1 est induite par différents facteurs de transcription dont NFκB. Il a été constaté que la liaison de NFκB sur le promoteur de la cycline D1 est stabilisée par Rac1 (Joyce et al. 1999). La transcription de la cycline D1 peut également être régulée par ERK. Rac1 interagit avec son effecteur PAK qui phosphoryle et active ERK induisant la transcription de la cycline D1 via ETS et AP-1 (Klein et al. 2007). Rac1 est également impliquée dans la régulation de la traduction de la cycline D1. Il a été démontré dans les cellules endothéliales que les intégrines activent SOS, un GEF de Rac1, qui active cette dernière et favorise la biosynthèse de la cycline D1 (Mettouchi et al. 2001). D'autres études ont mis en évidence qu'une inhibition de la protéine Rac1 bloque les cellules en phase G1 (L. Liu et al. 2014).

II.3- Régulation des NADPH oxydases :

Les NADPH (nicotinamide adénine dinucléotide phosphatase) oxydases (NOX) sont des complexes enzymatiques transmembranaires qui catalysent l'oxydation du NADPH menant à la formation de NADP⁺, H⁺ et de l'ion superoxyde O₂⁻. Le proton H⁺ et l'anion superoxyde O₂⁻ réagissent ensemble sous l'action de la superoxyde dismutase pour former du peroxyde d'hydrogène (H₂O₂). L'ion superoxyde et le peroxyde d'hydrogène font partie de la famille des espèces réactives de l'oxygène qui peuvent oxyder l'ADN (acide désoxyribonucléique), les protéines et les lipides. La famille des NOXs chez l'homme, est composée de sept isoenzymes : cinq NOXs (NOX1, NOX2, NOX3, NOX4 et NOX5) et deux DUOXs (DUOX1 et DUOX2) (Bedard et Krause 2007).

D'un point de vue structurelle, le complexe enzymatique NOX est composé de différentes sous-unités qui diffèrent selon les isoenzymes. Les NOX1, 2, 3 et 4 sont associées à la sous-unité membranaire p22phox ainsi qu'à des sous-unités régulatrices essentielles à la formation d'un complexe NOX actif au niveau membranaire (Bedard et Krause 2007; Panday et al. 2015) (Figure 11). Différentes études mettent en évidence le rôle essentiel de Rac1 dans la formation de ces complexes enzymatiques. Le recrutement des sous-unités régulatrices de NOX1 et NOX2 est possible grâce à une interaction directe entre ces sous-unités et les régions Switch I et Switch II de Rac1 (Kao et al. 2008). De ce fait, la protéine Rac1 régule l'activité de ces NOXs, la production de ROS (espèces réactives de l'oxygène) associée et participe au stress oxydant.

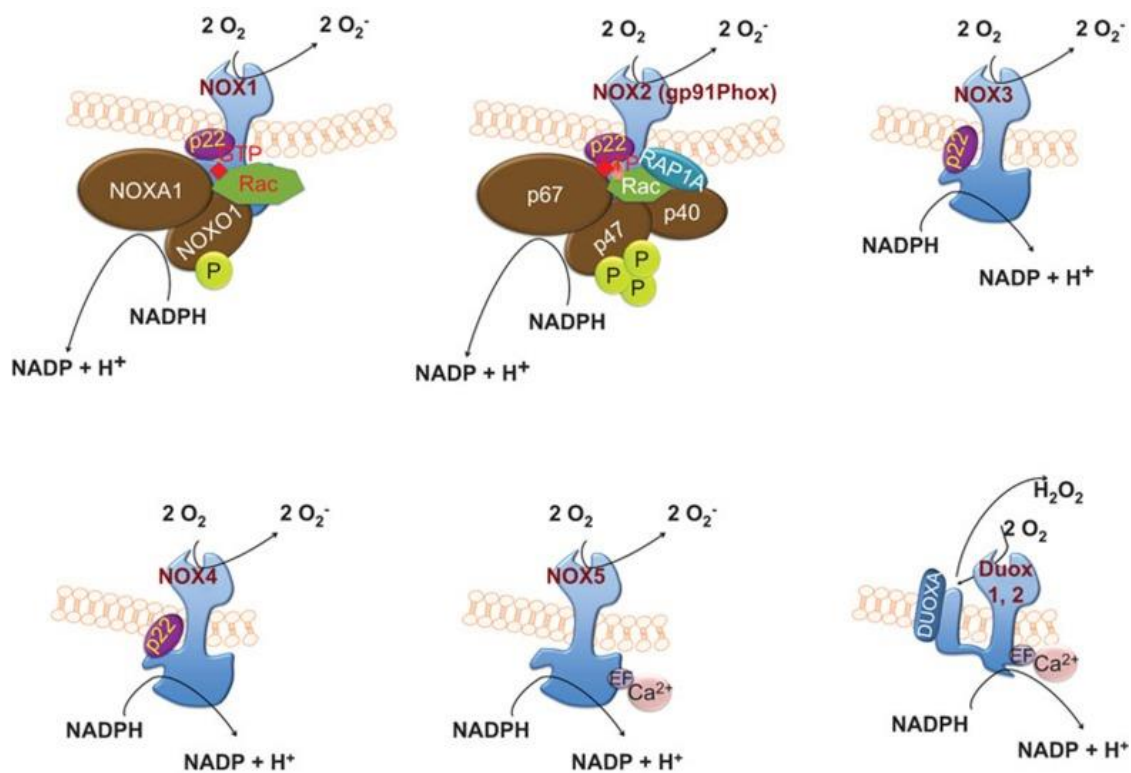


Figure 11 : Schéma d'assemblage et d'activation des NOXs (Panday et al. 2015)

L'activation de NOX1 et NOX2 dépend de la phosphorylation de NOXO1 et p47phox respectivement et nécessite la translocation des complexes régulateurs à la membrane, NOXA1 et Rac1 pour NOX1 et p67phox, p40phox et Rac1 pour NOX2. L'assemblage et l'activation des autres NOXs ne dépend pas de Rac1.

II.4- Régulation de la contraction des cellules musculaires lisses :

Le muscle lisse tapisse les parois de l'ensemble des organes creux du système respiratoire (trachée, bronches, bronchioles, alvéoles), du système gastro-intestinal (œsophage,

estomac et intestin), du système urino-génital (vessie, utérus) ainsi que la média des vaisseaux. La fonction principale des CMLs est la contraction permettant notamment de contrôler le diamètre des vaisseaux pour les CMLs vasculaires (CMLv) ou des bronches pour les CMLs bronchiques (CMLb).

La contraction des CMLs repose sur l'activité de la myosine qui est active lorsque sa chaîne légère (MLC₂₀) est phosphorylée. Deux enzymes, la phosphatase de la chaîne légère de la myosine (MLCP) et la kinase de la chaîne légère de la myosine (MLCK) régulent l'état de phosphorylation de la MLC₂₀ (Figure 12).

L'activation de la MCLK est nécessaire à la phosphorylation de la MLC₂₀ et est dépendante de la concentration intracellulaire en Ca²⁺. Une entrée de Ca²⁺ extracellulaire et/ou la libération des stocks calciques au niveau du réticulum sarcoplasmique via les récepteurs à l'IP₃ et les récepteurs à la ryanodine (RyR) induisent une augmentation de la concentration intracellulaire en Ca²⁺ (Hill-Eubanks et al. 2011; Amberg et Navedo 2013). Cette élévation de Ca²⁺ dans le cytosol permet la formation de complexes calcium-calmoduline et l'activation de la MLCK. Il a récemment été démontré dans les CMLb, que la protéine Rac1, en se fixant au domaine PH de la sous-unité β₂ de la phospholipase C, favorise la production d'IP₃, la libération de Ca²⁺ et finalement la contraction des CMLb (André-Grégoire et al. 2018).

La contraction des CMLs est également régulée indépendamment du Ca²⁺ par la voie de sensibilisation au Ca²⁺ de l'appareil contractile. Cette voie de signalisation implique la MLCP qui déphosphoryle la MLC₂₀ et favorise la relaxation. Les agonistes contractants activent généralement des récepteurs à sept segments transmembranaires qui activent la voie du Ca²⁺ mais également la GTPase monomérique RhoA. RhoA actif interagit avec son effecteur principal, Rho-kinase (ROCK), qui phosphoryle et inhibe l'activité de la MLCP (Feng et al. 1999). ROCK phosphoryle également la protéine CPI-17 qui inactive alors la MLCP (Koyama et al. 2000; Pagiatakis et al. 2012; Swärd et al. 2003). L'inhibition de la MLC permet de maintenir des taux élevés de MLC₂₀ phosphorylée et donc de maintenir une contraction maximale avec une faible concentration Ca²⁺ intracellulaire.

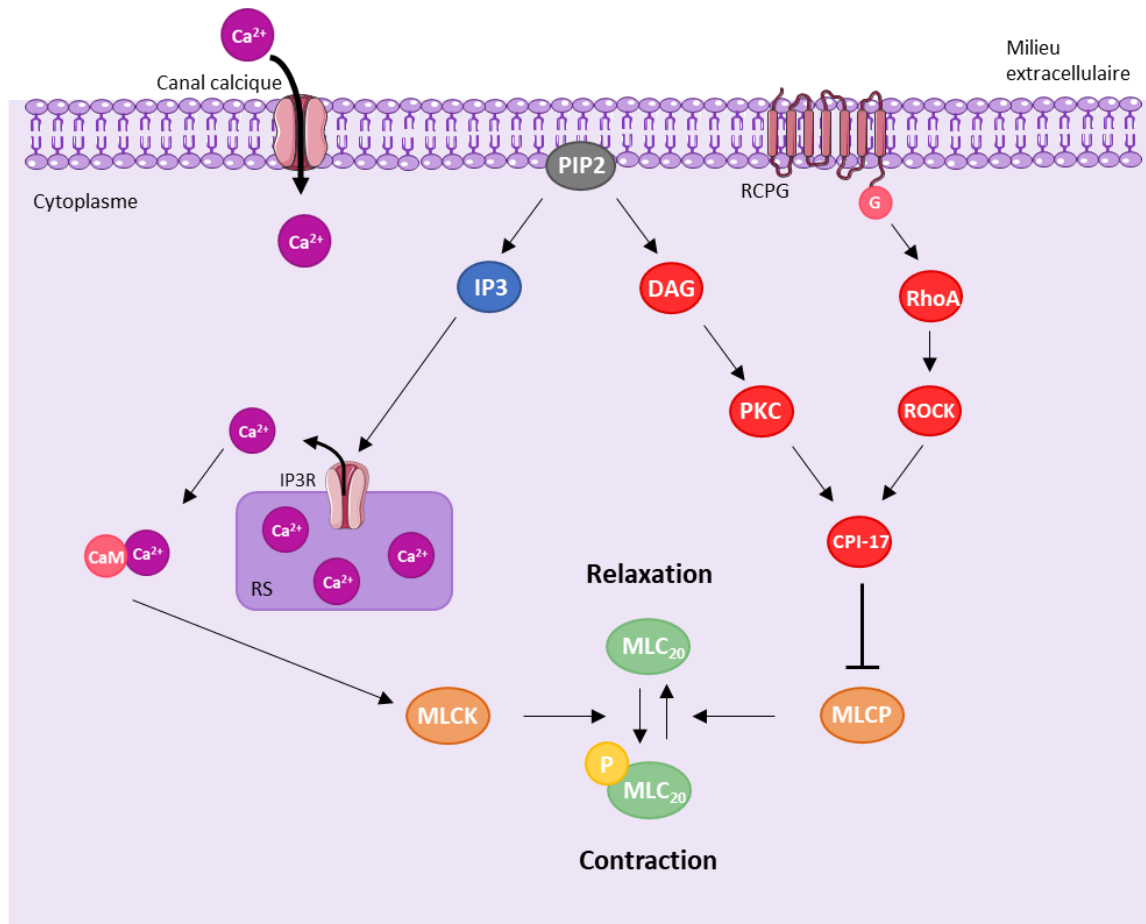


Figure 12 : Régulation de la contraction des CMLv

RCPG : récepteur couplé aux protéines G ; ROCK : Rho kinase ; PIP2 : phosphatidylinositol-4,5-bisphosphate ; IP3 : inositol 1,4,5-trisphosphate ; CaM : calmoduline ; MLCK : kinase de la chaîne légère de la myosine ; DAG : diacylglycérol ; PKC : protéine kinase C ; MLCP : phosphatase de la chaîne légère de la myosine ; MLC_{20} : chaîne légère de la myosine

III- Rôles physiopathologiques de Rac1 :

Comme décrit dans la partie précédente, Rac1 régule des fonctions cellulaires essentielles et une modification de son expression et/ou de son activité peut avoir de nombreuses répercussions physiopathologiques. Rac1 est décrit pour être impliqué dans des pathologies cardiovasculaires (Sawada, Li, et Liao 2010; Loirand, Sauzeau, et Pacaud 2013), inflammatoires (Winge et al. 2016), infectieuses (Eitel et al. 2012; Ravi et al. 2021) et dans différents cancers (Rathinam, Berrier, et Alahari 2011; Haga et Ridley 2016; Kazanietz et Caloca 2017). Au cours de ma thèse je me suis principalement intéressée aux rôles de Rac1 dans des pathologies associées aux CMLs et dans le cancer.

III.1- Rac1 dans la physiopathologie des CMLs :

III.1.1- La contractilité des CMLs :

Tous mécanismes menant à une augmentation de la contraction des CMLv participent à la hausse de la pression artérielle systémique et donc au développement de pathologies cardiovasculaires. Cette augmentation de la contraction des CMLv peut avoir deux origines : une élévation de la production de vasoconstricteurs et/ou une baisse de la synthèse de vasodilatateurs. La relaxation des CMLv est essentiellement régulée par les cellules endothéliales via la synthèse de monoxyde d'azote (NO). Dans un modèle murin haplo-insuffisant pour Rac1 dans les cellules endothéliales, il a été observé une diminution de l'expression et de l'activité de la NO synthase endothéliale (eNOS). La production de NO est réduite ainsi que la vasorelaxation des CMLv (Sawada et al. 2008). De même, la délétion spécifique de Rac1 dans les CMLs conduit également à un défaut de relaxation en réponse aux donneurs de NO et aux agents vasorelaxants (André et al. 2014; Fabbiano et al. 2014). Ce défaut de vasorelaxation induit une hypertension artérielle dans ces modèles murins. Ce défaut de relaxation artérielle en réponse au NO est également observé dans un modèle murin ayant une délétion du gène de Vav2, un GEF de Rac1 (Sauzeau et al. 2010). Ces études démontrent le rôle clé de la voie de signalisation Vav2/ Rac1 dans la relaxation des CMLv et dans le contrôle de la pression artérielle.

L'asthme et la bronchopneumopathie chronique obstructive sont des pathologies respiratoires majeures qui se caractérisent par une hyperréactivité bronchique (HRB). Chez les asthmatiques, il a été observé *ex vivo* que les CMLb ont une capacité contractile augmentée caractérisée par une contraction plus rapide et plus forte (X. Ma et al. 2002; Matsumoto et al. 2007). Dans notre laboratoire, nous avons observé dans un modèle de souris asthmatiques que la délétion de l'expression de Rac1 dans les CMLs ou son inhibition pharmacologique prévient le développement de l'HRB (André-Grégoire et al. 2018). Ces résultats démontrent le rôle de Rac1 dans la dérégulation des CMLb associée à l'asthme.

L'ensemble de ces études révèle le rôle essentiel de Rac1 dans la régulation de la contraction des CMLs. Toutefois, en fonction du type de CMLs étudié, son rôle est différent.

III.1.2- Le remodelage des CMLs :

Les CMLs sont décrites pour participer au remodelage tissulaire associé à de nombreuses pathologies telles que l'hypertension, l'athérosclérose, la resténose ou l'asthme

sévère. Dans ces différents contextes, il est observé une hypertrophie, une prolifération et une migration des CMLs.

Dans les pathologies vasculaires, plusieurs études ont démontré l'implication de Rac1 dans le remodelage tissulaire via la production de ROS. Comme décrit précédemment (II.3- Régulation des NADPH oxydases) Rac1 régule l'activité des NOXs et est donc impliquée dans la production des ROS. Au niveau des CMLv, les isoformes de NOX retrouvées principalement sont NOX1, NOX2 et NOX4 (Bedard et Krause 2007). L'activation de ces NOXs dépendante de Rac1 entraîne notamment l'activation des voies de signalisation dépendantes de p38 et ERK décrites pour promouvoir la prolifération et la migration des CMLv. L'expression du dominant négatif Rac1^{N17} dans les CMLv, tout comme un traitement avec des agents antioxydants, empêche l'activation de ces voies de signalisation et inhibe la migration des CMLv (C. Li et al. 2000; Gorin et al. 2004; Gerthoffer 2007). Il a également été mis en évidence que l'angioplastie active Rac1 qui participe à la prolifération des CMLv via la stimulation de l'ubiquitine-ligase Skp2 impliquée dans la progression du cycle cellulaire (Bond et al. 2008). Ces différents éléments mettent en lumière le rôle physiopathologique de Rac1 dans la production de ROS et l'activation de voies de signalisations menant à la prolifération et à la migration des CMLv.

III.2- Rac1 en oncologie :

En oncologie, plusieurs mutations de la GTPase monomérique Rac1 ont été identifiées dont Rac1^{P29S}, Rac1^{N92I}, Rac1^{C157Y} et Rac1^{P179L} (Kawazu et al. 2013; Davis et al. 2013). La mutation Rac1^{P29S} est la mieux décrite à ce jour et a été observée dans 9% des mélanomes induits par exposition aux rayons UV (Davis et al. 2013). Le résidu en position 29 de la protéine Rac1, fait partie de la région Switch I et cette mutation favorise l'interaction entre Rac1 et ses effecteurs. Une surexpression de la protéine a été observée dans différents types de cancers dont le cancer colorectal, pancréatique, mammaire et différentes leucémies (Lou et al. 2018) (Figure 13). Il a également été constaté que la suractivation de la protéine Rac1 pouvait être associée à une augmentation de son expression ou à une hyperactivation des GEFs responsables de son activation. De plus, une isoforme de Rac1, Rac1b, est décrite pour être surexprimée dans le cancer du sein, du côlon et du poumon (Jordan et al. 1999; Schnelzer et al. 2000; Stallings-Mann et al. 2012). Cette protéine Rac1b a un cycle d'échange du nucléotide plus rapide que la protéine Rac1 et présente les propriétés biochimiques caractéristiques des formes constitutivement actives des GTPases monomériques (Matos et al. 2000; Melzer et al. 2019).

L'activité de la protéine Rac1 est associée à la prolifération, la migration et la formation de métastases ainsi qu'à la chimiorésistance des cellules tumorales ainsi. L'expression du dominant négatif Rac1^{N17}, l'extinction de l'expression de Rac1 et son inhibition pharmacologique ont permis de redonner une chimiosensibilité à des cellules tumorales résistantes à différentes chimiothérapie dans le cas notamment du cancer du sein (Q. Li et al. 2020), du poumon (Q.-Y. Chen et al. 2011) et du carcinome épidermoïde de l'œsophage (Zeng et al. 2019).

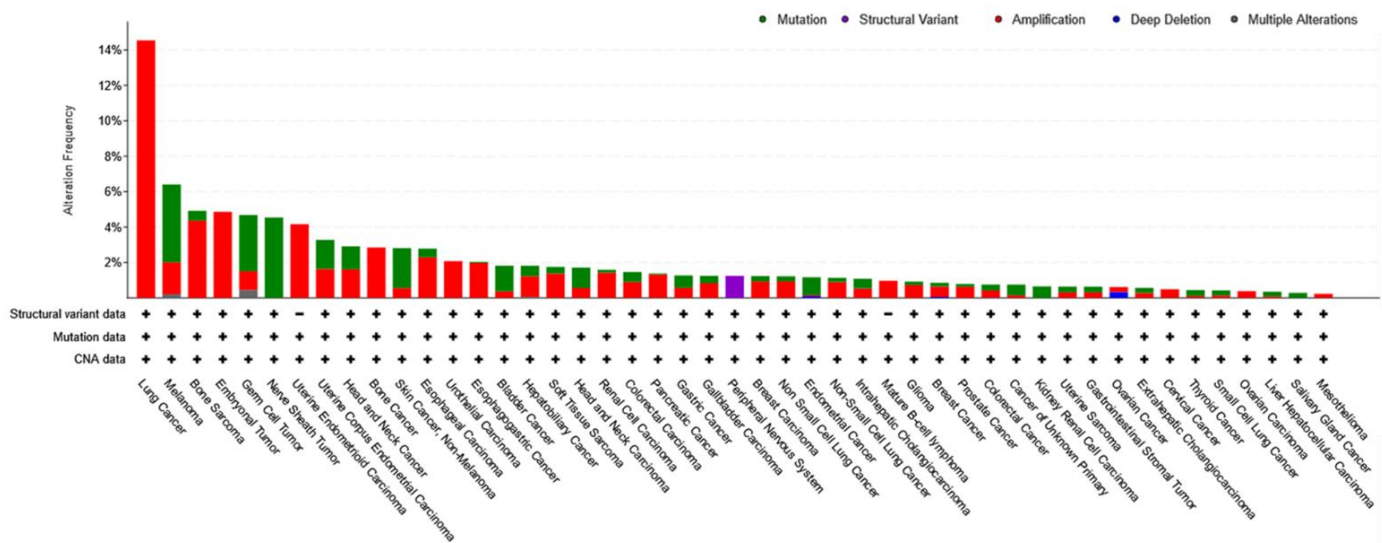


Figure 13 : Fréquence des modifications de séquence ou d'expression de Rac1 observées dans différents types de cancer (d'après cBioPortal)

Fréquence des modifications de Rac1 observées en différents types de cancer avec en vert les mutations, en violet les variants structuraux, en rouge l'augmentation de son expression, en bleu les délétions et en gris la présence de plusieurs types de modifications.

III.2.1- La prolifération des cellules tumorales :

Les cellules tumorales se caractérisent par une prolifération anormale en absence de signaux de croissance ce qui favorise leur survie. Rac1, de par son rôle dans l'activation des voies de signalisation pro-prolifératives, a été étudiée dans ce contexte.

La hausse de l'activation de Rac1 observée dans les cellules tumorales entraîne une suractivation de ses effecteurs dont PAK1 qui est décrit pour promouvoir la prolifération cellulaire. PAK1 participe à l'activation des cascades de signalisation de ERK, AKT et WNT impliquées dans la régulation du cycle cellulaire et donc la prolifération (Radu et al. 2014). Plus précisément, PAK1 phosphoryle Raf-1 et MEK1 qui activent à leur tour ERK. Cette voie de

signalisation favorise l'expression de la cycline D1 et la progression du cycle cellulaire en phase G1/S (L. Chen et al. 2019). Concernant l'implication de PAK1 dans la voie WNT- β -caténine, il a été démontré que PAK1 s'associe et phosphoryle la β -caténine au niveau de la Ser663 et de la Ser675. La β -caténine est alors stabilisée et est transloquée dans le noyau où elle régule la transcription de la cycline D1 et de la protéine myc, tous deux décrits pour favoriser la prolifération cellulaire (Arias-Romero et al. 2013) (Figure 14).

PAK1 est également décrit pour réguler l'apoptose. Il a été observé que la phosphorylation de Raf-1 par PAK1 entraîne sa translocation dans le noyau permettant sa liaison à BAD afin de le phosphoryler. BAD une fois phosphorylé ne peut plus interagir avec Bcl-2 ce qui inhibe cette voie de signalisation pro-apoptotique et favorise donc la survie des cellules tumorales (Schürmann et al. 2000). PAK1 est aussi capable d'activer la voie de NF κ B ce qui a pour effet de favoriser la résistance des cellules tumorales à l'apoptose comme cela a été observé dans des cellules épithéliales mammaires (Friedland et al. 2007). De plus, la protéine Rac1 régule l'activation des NOXs et la formation des ROS qui participent à l'activation de la voie dépendante de NF κ B favorisant la survie cellulaire (Figure 14).

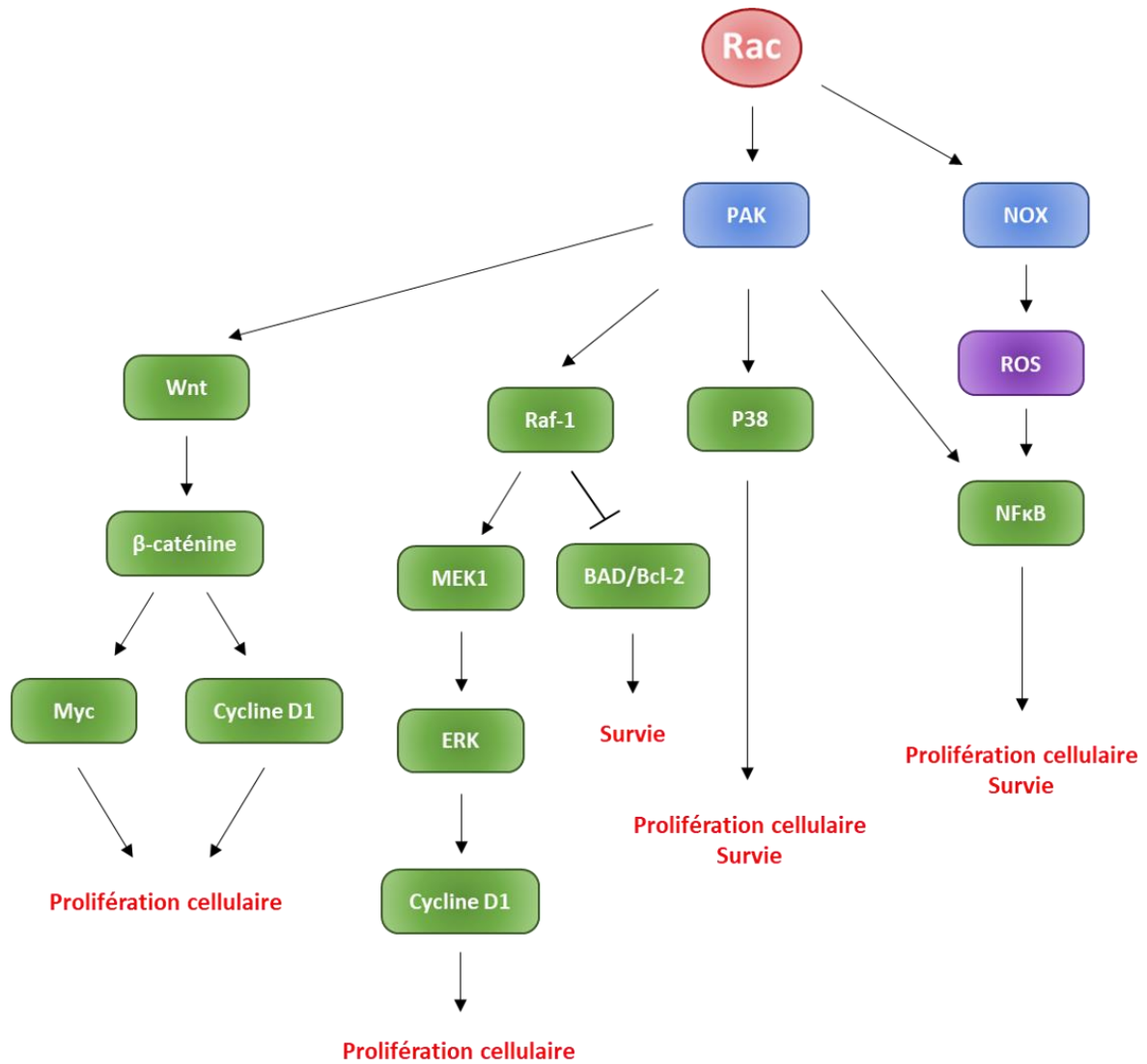


Figure 14 : Voies de signalisations moléculaires impliquant Rac1 dans la prolifération et la survie des cellules tumorales

L'activation de Rac1 entraîne différentes cascades de signalisations impliquées dans la prolifération et la survie qui participent à la tumorigénèse.

III.2.2- La formation de métastases :

La formation des métastases se définit par l'infiltration des cellules cancéreuses dans le système lymphatique et/ou sanguin qui s'extravasent ensuite pour nicher dans le ou les tissus cibles distants. Ainsi, la migration cellulaire joue un rôle clé dans la progression tumorale et la formation de métastases. Comme décrit précédemment (II.1 Organisation du cytosquelette d'actine et migration cellulaire), la voie de signalisation Rac/PAK/LIMK est impliquée dans la motilité cellulaire via la polymérisation de l'actine et la formation de lamellipodes. Une

augmentation de la motilité et de l'invasivité des lignées cellulaires, notamment du cancer du sein, est corrélée à une hausse de l'activité de PAK1 (Vadlamudi et al. 2000).

La migration des cellules nécessite la perte des adhésions cellule-cellule. Dans le cas du carcinome, les cellules épithéliales perdent ces adhésions et subissent une transition épithélio-mésenchymateuse (EMT). La délétion spécifique de l'E-cadhérine dans les cellules épithéliales murines entraîne une augmentation de la capacité d'invasion des cellules tumorales dans un modèle de carcinome (Derksen et al. 2006). Ainsi, la perte de l'E-cadhérine semble être impliquée dans l'invasion et la formation de métastases (Birchmeier et Behrens 1994). La diminution de l'expression de l'E-cadhérine est également observée lors de la surexpression de la forme constitutivement active de Rac1, Rac1^{V12}, dans les cellules de carcinomes (Hage et al. 2009). Par ailleurs, IQGAP1, un effecteur de Rac1, s'associe à différentes protéines formant les jonctions d'adhérence. IQGAP1 stabilise l'interaction entre l'E-cadhérine et la β -caténine au niveau du complexe jonctionnel lorsque Rac1 n'est pas active. Par conséquent, l'activation de Rac1 déstabilise le complexe de jonction en modifiant la distribution de l'E-cadhérine et de la β -caténine (Hage et al. 2009). L'ensemble de ces éléments démontrent le rôle central de l'activité de Rac1 dans l'invasion tumorale et la formation de métastases.

IV- Stratégies thérapeutiques régulant l'activité de la GTPase Rac1 :

L'ensemble de ces données bibliographique met en évidence que la protéine Rac1 est une cible thérapeutique potentielle dans de nombreux contextes pathologiques. C'est pourquoi depuis plusieurs décennies, différentes stratégies ont été développées pour de moduler son activité (Figure 15) : limiter la présence de Rac1 au niveau membranaire, cibler les interactions de Rac1 avec ses activateurs (GEFs) ou ses effecteurs (Tableau I).

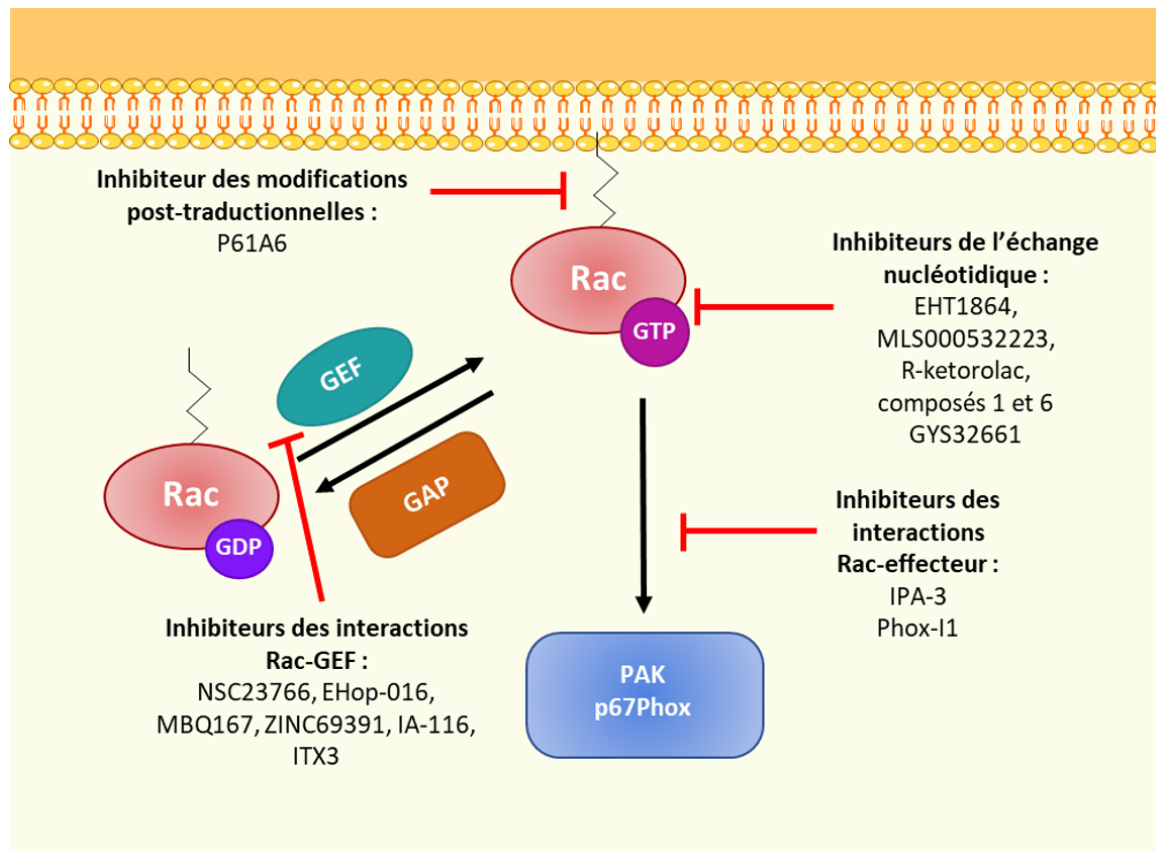


Figure 15 : Les différentes stratégies thérapeutiques ciblant Rac1

Il est possible de moduler l'activité de la protéine Rac1 en utilisant des inhibiteurs de ses modifications post-traductionnelles, des inhibiteurs des interactions Rac-GEF, des inhibiteurs ciblant l'incorporation du nucléotide ou des inhibiteurs limitant les interactions entre Rac1 et ses effecteurs

V.1- Utilisation de toxines inhibant Rac1 :

Il est également possible d'inhiber l'activité de la protéine Rac1 via l'utilisation de toxines bactériennes. Des bactéries pathogènes peuvent produire des toxines capables de modifier les Rho GTPases, dont Rac1, en bloquant leurs interactions avec leurs effecteurs. C'est le cas des toxines de la famille large clostridial cytotoxins (LCC) qui est composée des toxines A et B de *Clostridium difficile*, la toxine létale (LT) et la toxine hémorragique (HT) de *Clostridium sordelli* et la toxine alpha de *Clostridium novyi*. Toutes ces toxines sont constituées d'une seule chaîne polypeptidique abritant un domaine catalytique à leur extrémité N-terminale et un domaine de liaison cellulaire à leur extrémité C-terminale et entraînent une monoglycosylation des GTPases (Aktories et al. 2011). Les LCC peuvent avoir une spécificité de substrat et de cosubstrat différente. Ainsi, les toxines A et B, la toxine hémorragique de *C. sordellii* et la toxine de *C. novyi* modifient toutes les Rho GTPases tandis que la toxine létale

et la toxine B modifient Rac et Cdc42 (Z. Liu et al. 2021). Cette mono-glycosylation des GTPases induit un encombrement stérique qui va prévenir l'interaction entre la GTPase et ses effecteurs. De plus, la glycosylation des GTPases empêche l'échange nucléotidique médié par les GEFs et les rend également insensibles aux GAPs (Lerm, Schmidt, et Aktories 2000).

D'autres toxines peuvent également réguler l'activité des Rho GTPases en agissant comme des GAPs. Il s'agit des toxines dites injectées telles que SptP (protéine tyrosine phosphatase de *Salmonella typhimurium*), ExoS (exoenzyme S de *Pseudomonas aeruginosa*) et YopE (protéine externe E de *Yersinia pseudotuberculosis*) (Lerm, Schmidt, et Aktories 2000). La toxine SptP possède plusieurs domaines dont l'un à son extrémité C-terminale qui lui confère une activité tyrosine phosphatase. Il a été mis en évidence que cette toxine se fixe préférentiellement sur Rac1 et Cdc42 lorsque ces GTPases sont sous forme liées au GTP et stimule leur activité GTPasique intrinsèque comme le fait les RhoGAPs (Fu et Galán 1999). La toxine ExoS possède une activité d'ADP-ribosyltransférase de par son domaine C-terminal et agit également comme une RhoGAP pour Rac1, Cdc42 et RhoA grâce à son domaine N-terminal (Goehring et al. 1999). La toxine YopE présente également un domaine ayant une activité GAP à son extrémité N-terminale avec une forte homologie de séquence avec les domaines GAP de SptP et ExoS (Von Pawel-Rammingen et al. 2000). Ainsi, il a été mis en évidence que cette toxine catalyse l'activité GTPasique intrinsèque des GTPases, Rac1, Cdc42 et RhoA et favorise donc la présence de ces GTPases sous forme inactive.

V.2- Inhibiteurs des modifications post-traductionnelles de Rac1 :

La protéine Rac1 pour être active doit subir différentes modifications post-traductionnelles au niveau de son extrémité C-terminale. Rac1 fait l'objet de l'ajout d'un groupement géranylgeranyl, issu du géranylgeranyl-pyrophosphate, sur la Cys189 grâce à l'action de l'enzyme géranylgeranyltransférase de type 1 (GGTase-I). Cette modification post-traductionnelle permet à la protéine de s'ancrer à la membrane plasmique et d'interagir avec ses effecteurs. Au cours de ces dernières années, plusieurs molécules inhibant la GGTase-I ont été identifiées telles que le P61A6. Cette molécule inhibe la prolifération cellulaire dans différentes lignées de cellules cancéreuses humaines (Watanabe et al. 2008). De plus, il a été mis en évidence dans un modèle murin de cancer du pancréas, qu'un traitement au P61A6 diminue la croissance tumorale associé à une baisse de l'activité de la GTPase RhoA (Lu et al. 2009). Malgré ces résultats prometteurs, cette stratégie thérapeutique manque de spécificité puisque de nombreuses GTPases monomériques subissent cette modification post-

traductionnelle et l'utilisation clinique d'un inhibiteur de GGTase-I pourrait mener à de nombreux effets secondaires.

V.3- Inhibiteurs de la formation du complexe Rac1-GEF :

Pour inhiber Rac1, une autre stratégie est de bloquer son activation médiée par les GEFs. Cette stratégie paraît pertinente puisque certains GEFs sont exprimés spécifiquement dans certains tissus ou peuvent être activés en réponse à des stimuli particuliers. Par conséquent, le développement d'inhibiteurs de GEFs ou des interactions GEF/Rac1 permettraient d'être plus spécifique que les inhibiteurs de GGTase-I.

La première molécule développée et caractérisée comme étant un inhibiteur de l'interaction entre Rac1 et ses GEFs est le NSC23766. Cette molécule a été identifiée par criblage virtuel basé sur la structure de Rac1 en 2004 (Gao et al. 2004). L'étude de la structure cristallographique du complexe Rac1-Tiam1 a permis d'identifier le Trp56 comme étant un acide aminé indispensable à l'interaction spécifique entre Rac1 et Tiam1. Structuellement, cet acide aminé se trouve dans une poche formée par les résidus Lys5, Val7, Thr58, et Ser71 de Rac1 et les résidus His1178, Ser1184, Glu1183, et Ile1197 de Tiam1 (Worthylake, Rossman, et Sondek 2000; Gao et al. 2004). A partir de ces informations structurales, un screening de bibliothèques chimiques a été réalisé pour identifier les molécules se liant à Trp56 de Rac1. Après docking (Figure 16), la capacité des molécules à inhiber l'interaction Rac1/GEF a été évaluée. Le NSC23766 était la seule molécule capable d'inhiber significativement l'interaction entre le GEF Trio et Rac1 avec une $IC_{50} \sim 50 \mu M$. Cette molécule ne modifie pas la formation du complexe Cdc42/Intersectine, démontrant la spécificité du NSC23766 pour la GTPase Rac1 (Gao et al. 2004). Cette stratégie de design rationnelle de molécules a donc mené à l'identification du premier inhibiteur de GEF spécifique de Rac1. Les premiers tests fonctionnels ont démontré que le NSC23766 inhibe la croissance cellulaire des 3T3 stimulée par les GEFs de Rac1, Trio ou Tiam1, sans avoir d'effet sur la croissance stimulée par des GEFs de RhoA ou Cdc42 (Gao et al. 2004). D'autres études ont mis en évidence que l'utilisation du NSC23766 inhibe la prolifération, la migration et l'invasion des cellules tumorales (Thomas et al. 2007; Yoshida et al. 2010; Ji et al. 2015). Cependant le NSC23766 présente des effets sur d'autres cibles que la protéine Rac1. Il a été constaté que le NSC23766, à des concentrations

élevées ($\sim 100 \mu\text{M}$), entraîne une modification des glycoprotéines à la surface des plaquettes prévenant l'activation plaquettaire indépendamment de l'activité de Rac1 (Dütting et al. 2015).

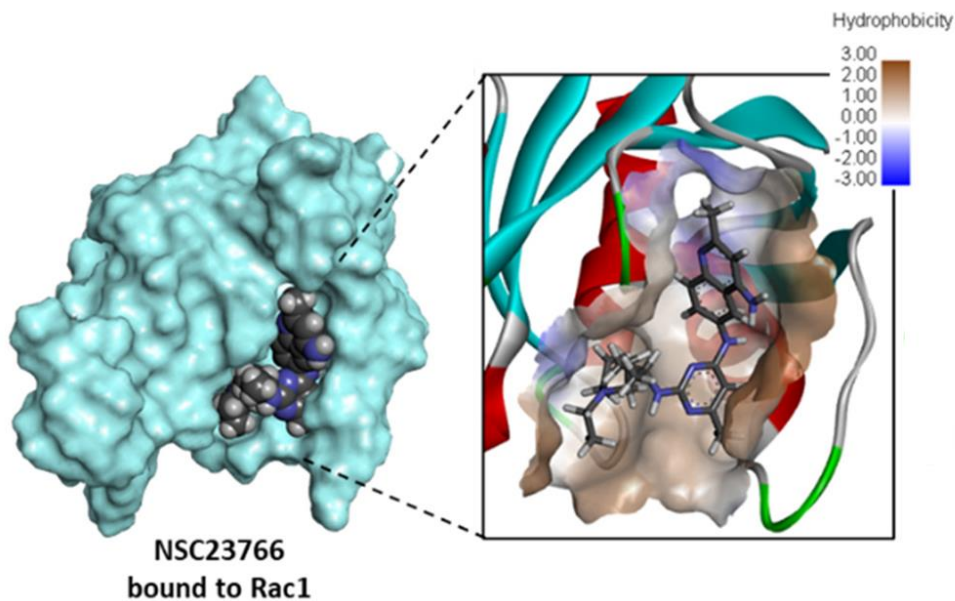


Figure 16 : Modèle de docking du NSC23766 sur la GTPase Rac1 (Sauzeau, Beignet, et Bailly 2022)

Modèle de docking de la molécule NSC23766 sur la protéine Rac1. La surface de la protéine est représentée en cyan, les interactions entre le NSC23766 et Rac1 sont modélisées et colorées en fonction de leurs types hydrophiles ou hydrophobes.

Etant la première molécule identifiée, la structure du NSC23766 a servi de base pour le développement d'autres molécules. C'est le cas notamment pour EHop-016 qui a été synthétisé et caractérisé en 2012 (Montalvo-Ortiz et al. 2012). Le docking de la molécule EHop-016 sur la structure de Rac1 a permis d'identifier les acides aminés Pro34, Thr35, Val36, Phe37, Asp38, Asn39, Trp56, Asp57, Thr58, Ala59, Tyr64, Leu67, Arg68, Leu70, et Ser71 comme étant essentiels pour l'interaction entre Rac1 et cette nouvelle molécule. EHop-016 empêche l'interaction GEF Vav2/Rac1. L'effet inhibiteur sur l'activité de Rac1 a été évalué sur une lignée cellulaire de mélanome avec une $IC_{50} \sim 1.1 \mu\text{M}$. In vitro, EHop-016 diminue la formation de lamellipodes et la migration cellulaire (Montalvo-Ortiz et al. 2012). L'effet d'EHop-016 a été également évalué *in vivo* dans un modèle murin immunodéficient de cancer du sein. Le traitement avec EHop-016 limite la croissance tumorale, l'angiogenèse ainsi que la formation de métastases (Castillo-Pichardo et al. 2014). Bien que la structure de EHop-016 semblerait plus favorable que celle du NSC23766, un autre dérivé de cette molécule a été développé récemment : le MBQ-167. Le docking de cette nouvelle molécule montre qu'elle se fixe dans

la poche de liaison avec Rac1 et interagit notamment par une liaison hydrogène avec le résidu Asn39 de Rac1 (Humphries-Bickley et al. 2017). La GTPase Cdc42 possède également cet acide aminé ce qui explique pourquoi le MBQ-167 inhibe aussi cette GTPase. Le MBQ-167 a une IC_{50} pour Rac1 de 103nM et de 78nM pour Cdc42 dans des cellules métastatiques de cancer de sein. Cette molécule permet d'inhiber la migration cellulaire et de réduire la viabilité des cellules du cancer du sein en réduisant l'activité de PAK et STAT3. Il a ainsi été mis en évidence que le MBQ-167 induit une perte de polarité des cellules métastatique du cancer de sein avec une diminution de la formation de lamellipodes médiée par Rac1 et de filopodes contrôlés par Cdc42. Cet effet est uniquement observé sur les cellules métastatiques du cancer du sein sans affecter les cellules non cancéreuses. L'utilisation de cette molécule dans un modèle murin immunodéficient de cancer du sein réduit la progression des tumeurs mammaires (Humphries-Bickley et al. 2017; Maldonado et al. 2019; Cruz-Collazo et al. 2021).

Un screening de la librairie chimique ZINC a été réalisé afin d'identifier de nouvelles molécules capables de cibler l'interaction entre Rac1 et ses GEFs. Ce criblage a mené à l'identification de la molécule ZINC69391 qui interfère dans l'interaction entre Rac1 et Tiam1. Différentes études *in vitro* ont mis en évidence la capacité de cette molécule à limiter la progression du cycle cellulaire et la migration de cellules issues de lignées de cancer du sein, de glioblastome et de leucémies (Cardama, Comin, et al. 2014; Cardama, Gonzalez, et al. 2014; Cabrera et al. 2017). L'utilisation *in vivo* de ZINC69391 réduit la formation de métastases pulmonaires dans un modèle murin syngénique de cancer du sein (Cardama, Comin, et al. 2014). Un analogue de cette molécule, 1A-116, a également été développé et caractérisé. La molécule 1A-116 prévient spécifiquement l'interaction entre Rac1 et P-Rex1 et a un effet inhibiteur plus important que la molécule ZINC69391 ($IC_{50} \sim 21\mu M$ pour 1A-116 et $IC_{50} \sim 48\mu M$ pour ZINC69391) (Cardama, Comin, et al. 2014). L'utilisation de cette molécule réduit également la prolifération, la migration cellulaire et l'invasion tumorale (Cardama, Comin, et al. 2014; Cardama, Gonzalez, et al. 2014; Cabrera et al. 2017).

V.4- Inhibiteurs de l'échange nucléotidique :

L'échange du GDP par le GTP est une étape indispensable à l'activation de la GTPase Rac1. Une stratégie d'inhibition de Rac1 possible consiste donc à inhiber cet échange nucléotidique en développant des molécules se liant spécifiquement à la GTPase Rac1. L'étude de la structure cristallographique de Rac1 liée au GDP et au GTP a permis d'identifier les acides

aminés clés impliqués dans la liaison au nucléotide et a mené au développement de molécules interagissant spécifiquement avec ces acides aminés.

L'EHT 1864 est décrit pour empêcher la fixation du nucléotide spécifiquement sur les isoformes de la protéine Rac, ce qui en fait un inhibiteur de l'échange nucléotidique. L'étude du mécanisme d'action de cet inhibiteur a mis évidence que l'EHT1864 entraîne une libération du nucléotide de la poche de Rac1 et diminue l'affinité de la GTPase pour le nucléotide présent empêchant donc son activation quel que soit le GEF impliqué dans ce processus (Shutes et al. 2007; Onesto et al. 2008). Ce mécanisme d'inhibition bloquant la liaison du GTP à Rac1 suggère que l'EHT1864 devrait inhiber l'interaction entre Rac1 et l'ensemble de ces effecteurs. De plus, la fixation de l'EHT4864 sur Rac1 a lieu au niveau des régions Switch I et Switch II qui sont impliquées dans la liaison de Rac1 à ses effecteurs. L'utilisation de l'EHT1864 induit une diminution de la formation de lamellipodes et de la migration associée dans des cellules 3T3 (Shutes et al. 2007; Onesto et al. 2008; Castoria et al. 2011). D'autres études menées sur des lignées de cellules de cancer du sein ont mis en évidence que l'EHT1864 inhibe l'adhésion, la prolifération cellulaire, induit l'apoptose et réduit la croissance tumorale dans un modèle murin de xénotransfert de cancer du sein (Molnár et al. 2015; Hampsch et al. 2017). Une étude a également montré que l'utilisation de l'EHT1864 pouvait avoir des effets secondaires au niveau plaquettaire et indépendamment de l'activité de la protéine Rac1. En effet, l'utilisation de l'EHT1864 à des concentrations de l'ordre de la centaine de micromolaire entraîne une apoptose des plaquettes et diminue l'expression des intégrines impliquées dans l'activation plaquettaires (Dütting et al. 2015).

D'autres molécules capables d'inhiber l'échange nucléotidique ont été développées suite à la découverte de l'EHT1864, c'est notamment le cas de MLS000532223, R-ketorolac et des composés 1 et 6. La molécule MLS000532223 a été découverte suite au screening de la librairie chimique MLSCN et empêche la fixation du GTP sur la GTPase Rac1 mais également Cdc42 et RhoA de manière dose-dépendante. L'utilisation de cette molécule sur une lignée de mastocytes a permis d'inhiber la formation de fibres stress médiée par RhoA, de lamellipodes médiée par Rac1 et de filopodes médiée par Cdc42 ainsi que la migration cellulaire associée (Surviladze et al. 2010). Le R-ketorolac est le R-énantiomère d'un anti-inflammatoire non stéroïdien déjà utilisé en thérapeutique. Cette molécule a été identifiée comme pouvant interagir avec les GTPases de la famille Rho dans une étude utilisant le screening de molécules ayant déjà reçu une autorisation de mise sur le marché et pouvant donc être repositionnée ou obtenir une extension d'application. Le docking de cette molécule au niveau de la poche de fixation du nucléotide sur Rac1 et Cdc42 suggère qu'elle interagit en neutralisant l'ion Mg^{2+} impliqué dans

l'échange nucléotidique (Oprea et al. 2015). Une étude sur des lignées cellulaires de cancer de l'ovaire a mis en évidence que le R-ketorolac inhibe la migration cellulaire, l'adhésion et l'invasion (Guo et al. 2015). L'utilisation de cette molécule *in vivo*, dans un modèle transgénique murin de cancer du sein spontané, a réduit la croissance tumorale (Peretti et al. 2018). Les composés 1 et 6 ont quant à eux été identifiés par screening virtuel et docking de molécules capables de se lier à la poche nucléotidique de la protéine Rac1. Le docking de ces deux molécules suggèrent qu'elles se fixent sur Rac1 au niveau de la poche nucléotidique. Ces deux molécules bloquent uniquement l'interaction entre le nucléotide et la GTPase Rac1 et n'ont pas d'effet sur RhoA ou encore Cdc42. L'inhibition de l'échange nucléotidique induit par ces molécules diminue l'interaction entre Rac1 et son effecteur PAK1 de manière dose-dépendante. De plus, il a été constaté que l'utilisation des composés 1 et 6 inhibe la prolifération, la migration cellulaire et diminue la survie de lignées cellulaires issues de cancer du pancréas (Arnst et al. 2017).

Récemment, un nouvel inhibiteur de Rac1 dérivé de la structure de l'EHT1864 a été développé par Revere Pharmaceuticals, le GYS32661. L'hétérocycle central 4-pyrone de l'EHT1864 a été remplacé par un imidazole ce qui a amélioré la capacité de la molécule à se lier à Rac1 et a donc amélioré son pouvoir inhibiteur ($IC_{50} \sim 1.18 \mu M$) (Goka et al. 2019). Cette molécule inhibe l'activité de Rac1 et de Rac1b et diminue la migration et prolifération de différentes lignées de cellules cancéreuses issues du cancer du côlon, du rein et de la prostate (Goka et al. 2019; Goka et al. 2020; Goka, Mesa Lopez, et Lippman 2021). Le GYS32661 réduit la migration des cellules endothéliales ainsi que le nombre de nouveaux vaisseaux sanguins formés dans un modèle murin de xénogreffe de cancer du rein démontrant que le GYS32661 a un effet anti-angiogénique (Goka et al. 2020). L'utilisation du GYS32661 *in vivo* dans différents modèles de xénogreffe de cancers du côlon et du rein a permis de limiter la croissance tumorale (Goka et al. 2019; Gola et al. 2020).

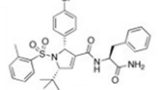
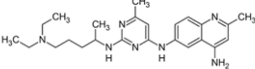
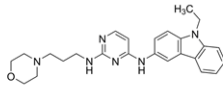
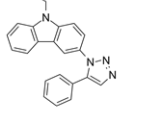
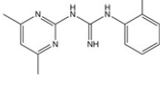
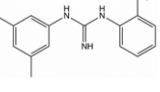
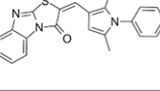
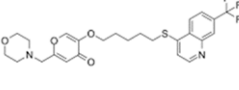
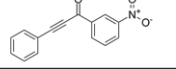
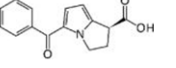
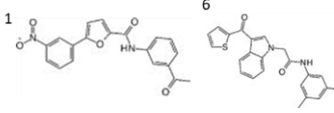
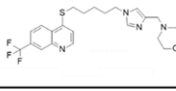
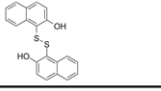
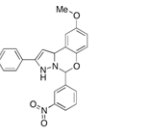
V.5- Inhibiteurs des interactions entre Rac1 et ses effecteurs :

La protéine Rac1 possède des effecteurs spécifiques qui vont déclencher des cascades de signalisation particulières et donc orienter l'effet cellulaire dépendant de l'activation de Rac1. Ainsi une stratégie thérapeutique possible vise à inhiber l'interaction entre Rac1 et ses effecteurs ou inhiber directement ses effecteurs en ciblant les voies de signalisation d'intérêt.

Dans cette optique, des inhibiteurs notamment de PAK ont été développés. La protéine PAK1 sous forme inactive forme un dimère entraînant l'auto-inhibition de la protéine. La

liaison de Rac1 sur PAK1 déstabilise sa configuration de dimère et permet l'autophosphorylation de la Thr423 de PAK1 qui est essentielle à la stabilisation de la forme monomérique et active de PAK1. Un des rôles de la protéine PAK1 active est de catalyser l'hydrolyse de l'ATP (adénosine triphosphate), c'est pourquoi des tests évaluant l'hydrolyse de l'ATP ont été utilisés pour identifier des molécules capables d'inhiber l'activation de PAK1. Cette stratégie de criblage a permis d'identifier la molécule IPA-3 comme potentiel inhibiteur de PAK1. Afin d'identifier la cible protéique de cette molécule des tests d'activité de kinase ont été réalisés et ont mis en évidence que IPA-3 inhibe l'autophosphorylation de la Thr423 de PAK1 impliquée dans l'activation de cette dernière. Ainsi la molécule IPA-3 est capable d'inhiber l'activation de la protéine PAK1 mais n'a pas d'effet lorsque celle-ci est déjà activée (Viaud et Peterson 2009). L'utilisation de l'IPA-3 a notamment pour effet d'empêcher la formation de lamellipodes, la prolifération cellulaire et limite la croissance tumorale dans un modèle murin de xénogreffe de cancer du foie (Takahashi et Suzuki 2009; Wong et al. 2013). Cet inhibiteur bloque donc l'activation de PAK1 et des voies de signalisations dépendantes de son activité. Un autre effecteur important de Rac1 est la NOX. Comme décrit précédemment (II.3 Régulation des NADPH oxydases), Rac1 interagit avec la sous-unité p67phox afin de permettre l'activation des NOXs et favoriser la production des ROS. L'étude de la structure du complexe Rac1-p67phox a mené à l'identification des résidus impliqués dans cette interaction, à savoir l'Arg38 et 102 de p67phox et la Thr25, Ans26 et Ala27 de la région Switch I de Rac1. Un screening virtuel de bibliothèques chimiques a été réalisé afin d'identifier les molécules capables de se lier spécifiquement à ces résidus de p67phox. Ce criblage a permis l'identification de la molécule Phox-II qui se lie à p67phox en interagissant avec l'Arg38 de la protéine empêchant donc la protéine Rac1 de se lier également à ce résidu. La molécule Phox-II est capable d'inhiber la production de ROS *in vitro* avec une $IC_{50} \sim 3 \mu M$ sans avoir d'effet sur les autres fonctions régulées par Rac1 notamment l'organisation du cytosquelette d'actine.

Tableau I : Les différents inhibiteurs de Rac1

Catégories d'inhibiteurs	Nom de la molécule	Cible	IC ₅₀	Structure	Effets	Commentaires
Inhibiteur de la géranylgéranylation	P61A6	GGTase-1	2.2 µM		Inhibe la prolifération cellulaire Limite la croissance tumorale	Non spécifique de Rac1 ou des GTPases
Inhibiteurs des interactions Rac-GEF	NSC23766	Rac-Tiam1 Rac-Trio	50 µM		Inhibe la prolifération, la migration et l'invasion tumorale	Spécifique de Rac1 Agrégation plaquettaire IC ₅₀ élevée pour utilisation thérapeutique
	EHop-016	Rac-Vav2	1 µM		Inhibe la formation de lamellipodes, la migration cellulaire Inhibe l'angiogenèse Limite la croissance tumorale et la formation de métastases	Spécifique Rac1
	MBQ167	Rac Cdc42	103 nM pour Rac1 78 nM pour Cdc42		Perte de polarité des cellules métastatiques Limite la progression tumorale	Effet sur Rac1 et Cdc42
	ZINC69391	Rac1-Tiam1	48 µM		Inhibe la prolifération et la migration cellulaire Limite la formation de métastases	Spécifique de Rac1
	IA-116	Rac-P-Rex1	21 µM		Inhibe la prolifération, la migration cellulaire et l'invasion	Spécifique de Rac1
	ITX3	Rac-Trio	76 µM			Spécifique de l'interaction TrioN-Rac1 IC ₅₀ élevée pour utilisation thérapeutique
Inhibiteurs de l'échange nucléotidique	EHT1864	Rac1	25 µM		Inhibe la migration, l'adhésion, la prolifération cellulaire Induit l'apoptose Limite la croissance tumorale	Spécifique de Rac1 et ses isoformes Agrégation plaquettaire
	MLS000532223	Rac1, RhoA, Cdc42	10 µM		Inhibe la formation de lamellipodes, filopodes et fibres de stress	Non spécifique de Rac1
	R-ketorolac	Rac1, Cdc42	0.5 µM pour Rac1 1 µM pour Cdc42		Inhibe l'adhésion, la migration cellulaire et l'invasion Limite la croissance tumorale	Effet sur Rac1 et Cdc42 Approuvé en mélange racémique par la FDA
	Composés 1 et 6	Rac1	95 ± 21 nM pour le composé 1 88 ± 48 nM pour le composé 6		Inhibent la prolifération et la migration cellulaire Diminuent la survie cellulaire dans des lignées cancéreuses	Spécifique de Rac1
	GYS32661	Rac1 et Rac1b	1.18 µM		Inhibe la prolifération, et la migration cellulaire Limite la croissance tumorale Effet anti-angiogénique	Spécifique de Rac1 et du variant Rac1b
Inhibiteurs des interactions Rac-effecteur	IPA-3	Pak1	2,5 µM		Inhibe l'autophosphorylation de la Thr423 de Pak1	Spécifique de Pak1
	Phox-11	p67phox	3 µM		Inhibe l'activation de NOX2 et la production de ROS	Spécifique de la sous-unité p67phox de NOX2

OBJECTIFS DE THESE

La GTPase Rac1 régule des fonctions cellulaires essentielles et participe de ce fait à de nombreux processus physiopathologiques. Notre équipe a démontré que Rac1 est activée dans les CMLb de patients asthmatiques. L'asthme sévère se caractérise par une hyperréactivité bronchique et un profond remodelage des voies respiratoires associé à une hypertrophie et une hyperplasie du muscle lisse. Le premier objectif de mon travail de thèse a été d'identifier le rôle de la suractivation de Rac1 dans les CMLb au cours de l'asthme allergique sévère et de valider l'intérêt thérapeutique de cibler Rac1 dans l'asthme.

L'ensemble des données bibliographiques présentées précédemment (IV- Stratégies thérapeutiques régulant l'activité de la GTPase Rac1) montrent que de nombreux inhibiteurs de cette protéine ont été développés et utilisés en recherche afin d'élucider le rôle de Rac1 dans différents mécanismes cellulaires et contextes pathologiques. Cependant, aujourd'hui aucun de ces inhibiteurs n'est utilisé en clinique. Mon second objectif a donc consisté à identifier et à caractériser un nouvel inhibiteur spécifique de la GTPase Rac ayant des paramètres physico-chimiques ainsi que des effets biologiques permettant son développement et son utilisation en clinique.

RESULTATS

Première partie : Rôle de Rac1 dans les cellules musculaires lisses bronchiques et le remodelage des voies aériennes associés à l'asthme allergique sévère

L'asthme est une pathologie chronique des voies aériennes qui touchent plus de 250 millions de personnes à travers le monde et son incidence ne fait qu'augmenter (D'Amato et al. 2016). En France, 6 à 7% de la population adulte souffre de cette pathologie et est responsable chaque année de près de 1000 décès en France. Cette pathologie respiratoire hétérogène se caractérise par des symptômes respiratoires variés qui consistent en une respiration sifflante, de la toux, une oppression thoracique associés à une limitation variable des débits expiratoires et à une inflammation bronchique chronique (Papi et al. 2018). Les traitements actuels reposent sur l'utilisation de corticostéroïdes inhalés associés à des bronchodilatateurs à action courte ou de longue durée afin de contrôler les symptômes de la maladie (Reddel et al. 2015). Pour les patients qui souffrent d'asthme dit sévère, 5 à 10% des patients asthmatiques, les traitements actuels ne sont pas efficaces pour contrôler les symptômes. La société thoracique américaine et la société thoracique européenne ont défini l'asthme sévère comme étant un asthme nécessitant un traitement reposant sur l'utilisation de fortes doses de corticoïdes inhalés en association avec un autre traitement, ou une corticothérapie orale, dans le but de maintenir le contrôle de la pathologie ou qui reste non contrôlé malgré ce traitement conséquent (Chung et al. 2014). Les patients souffrants d'asthme sévère ont une fonction respiratoire dégradée de façon plus importante, des exacerbations plus fréquentes et plus graves en comparaison aux autres patients asthmatiques.

D'un point de vue physiopathologique l'asthme se définit par trois composantes importantes : l'inflammation, l'hyperréactivité bronchique et le remodelage des voies aériennes.

La composante inflammatoire, grandement étudiée, définit les phénotypes et endotypes d'asthme et est responsable de la grande hétérogénéité de la maladie. On trouve ainsi deux grandes familles d'asthme : l'asthme éosinophilique et non éosinophilique. Le phénotype d'asthme éosinophilique se caractérise par une forte présence de lymphocytes de type Th2 qui

vont sécréter trois cytokines principales, IL-4, IL-5 et IL-13. L'IL-4 participe à la polarisation des lymphocytes T auxiliaires et la hausse de l'expression des IgE. L'IL-5 participe à l'activation et au recrutement des éosinophiles tandis que l'IL-13 participe à l'HRB et au remodelage des voies aériennes (Carr, Zeki, et Kraft 2018; Mubarak, Shakoor, et Masood 2019). L'asthme non éosinophilique est moins bien connu et caractérisé que l'asthme éosinophilique.

L'HRB est définie comme une contraction exagérée des bronches via les CMLb en réponse à différents stimuli et peut être médiée par l'inflammation.

Le remodelage des voies aériennes est caractérisé par des modifications structurelles de la paroi bronchique dont une altération de l'épithélium bronchique, une augmentation de l'épaisseur de la membrane basale et une hyperplasie et hypertrophie des CMLs. L'altération de l'épithélium bronchique peut être dû à un défaut de prolifération des cellules épithéliales et une augmentation de l'apoptose. L'épaississement de la membrane peut s'expliquer, en partie, par l'augmentation des dépôts de collagène de type I et III ainsi que de fibronectine. L'hyperplasie du muscle lisse bronchique est induite par une augmentation de la prolifération de ces dernières en réponse soit à l'inflammation soit à des facteurs mitogènes (Sumi et Hamid 2007; Shifren et al. 2012; Fehrenbach, Wagner, et Wegmann 2017). L'unique solution thérapeutique permettant de lutter contre l'hyperplasie du muscle lisse est la thermoplastie bronchique qui vise à réduire la masse des CMLb. Les essais cliniques ont montré une amélioration de la qualité de vie des patients ayant subis cette intervention avec une diminution du nombre d'exacerbations et des visites d'urgences pendant 5 ans après la thermoplastie bronchique (Laxmanan et Hogarth 2015). Ces résultats démontrent l'intérêt thérapeutique de cibler les CMLs bronchiques dans l'asthme. Il est nécessaire d'élucider les mécanismes moléculaires impliqués dans l'hyperplasie du muscle lisse bronchique pour identifier de nouvelles cibles pharmacologiques. Comme décrit précédemment la GTPase Rac1 régule la migration, la prolifération et l'adhésion des cellules notamment les CMLs ainsi que leur contraction. Nous avons donc émis l'hypothèse que Rac1 pourrait également être impliquée dans l'hyperplasie des CMLs et donc dans le remodelage des voies aériennes associées à l'asthme sévère. Ainsi l'objectif de cette partie de ma thèse a été d'étudier le rôle de Rac1 dans les CMLb au cours de l'asthme sévère.

Mes résultats mettent en évidence que l'activation de la protéine Rac1 induit la prolifération des CMLb via la voie de signalisation de STAT3. Dans notre modèle murin d'asthme allergique sévère, la délétion de Rac1 dans les CML prévient le développement de l'hyperplasie du muscle lisse bronchique caractéristique du remodelage des voies aériennes associé à cette pathologie. De plus, l'administration d'un inhibiteur de Rac1, le NSC23766, par nébulisation a prévenu l'hyperplasie du muscle lisse bronchique et également l'inflammation de type éosinophilique. Ces résultats mettent donc en évidence l'intérêt thérapeutique de cibler la protéine Rac1 dans cette pathologie.

Ce travail a fait l'objet de la publication d'un article original (Article 1: Essential role of smooth muscle Rac1 in severe asthma associated-airway remodeling). Pour cette étude j'ai réalisé les études histologiques, de biologie cellulaire, de signalisation cellulaire, de biochimie ainsi que la caractérisation de nos modèle murins. Mon travail a également fait l'objet d'une revue (Article 2: Bronchial smooth muscle cell in asthma: where does it fit?). Une étude similaire portant sur le rôle de Rac1 dans les CMLv au cours de l'hypertension artérielle pulmonaire a été menée au laboratoire au cours de ma thèse (Annexe 1: Smooth muscle Rac1 contributes to pulmonary hypertension).

Article 1: Essential role of smooth muscle Rac1 in severe asthma associated-airway remodeling

Article publié dans le journal Thorax



Original research

Essential role of smooth muscle Rac1 in severe asthma-associated airway remodelling

Florian Dilasser,¹ Lindsay Rose,¹ Dorian Hassoun,¹ Martin Klein,¹ Morgane Rousselle,¹ Carole Brosseau,² Christophe Guignabert,³ Camille Taillé,⁴ Marie Christine Dombret,⁵ Leonarda Di Candia,⁴ Nicolas Heddebaut,⁶ Gregory Bouchaud,¹ Marina Pretolani,⁶ Antoine Magnan,⁷ Gervaise Loirand,¹ Vincent Sauzeau¹

¹Inserm UMR 1087, Nantes, France

²Centre de recherche en transplantation, Inserm 1064, Nantes, France

³Inserm U999, Le Plessis Robinson, France

⁴Service de Pneumologie et Centre de Référence des Maladies Pulmonaires Rares, Hôpital Bichat - Claude-Bernard, Paris, France

⁵APHP, Paris, France

⁶Inserm 1152, Paris, France

⁷Institut du Thorax UMR1087 CNRS 6291, Inserm, Université de Nantes, CHU de Nantes, DHU2020, Nantes, France

Correspondence to

Dr Vincent Sauzeau, Inserm UMR 1087, Nantes, France; vincent.sauzeau@inserm.fr

FD and LR contributed equally.

Received 28 September 2020

Revised 20 November 2020

Accepted 2 December 2020

Published Online First

4 February 2021



© Author(s) (or their employer(s)) 2021. Re-use permitted under CC BY-NC. No commercial re-use. See rights and permissions. Published by BMJ.

To cite: Dilasser F, Rose L, Hassoun D, et al. *Thorax* 2021;**76**:326–334.

ABSTRACT

Background Severe asthma is a chronic lung disease characterised by inflammation, airway hyperresponsiveness (AHR) and airway remodelling. The molecular mechanisms underlying uncontrolled airway smooth muscle cell (aSMC) proliferation involved in pulmonary remodelling are still largely unknown. Small G proteins of the Rho family (RhoA, Rac1 and Cdc42) are key regulators of smooth muscle functions and we recently demonstrated that Rac1 is activated in aSMC from allergic mice. The objective of this study was to assess the role of Rac1 in severe asthma-associated airway remodelling.

Methods and results Immunofluorescence analysis in human bronchial biopsies revealed an increased Rac1 activity in aSMC from patients with severe asthma compared with control subjects. Inhibition of Rac1 by EHT1864 showed that Rac1 signalling controlled human aSMC proliferation induced by mitogenic stimuli through the signal transducer and activator of transcription 3 (STAT3) signalling pathway. In vivo, specific deletion of Rac1 in SMC or pharmacological inhibition of Rac1 by nebulisation of NSC23766 prevented AHR and aSMC hyperplasia in a mouse model of severe asthma. Moreover, the Rac1 inhibitor prevented goblet cell hyperplasia and epithelial cell hypertrophy whereas treatment with corticosteroids had less effect. Nebulisation of NSC23766 also decreased eosinophil accumulation in the bronchoalveolar lavage of asthmatic mice.

Conclusion This study demonstrates that Rac1 is overactive in the airways of patients with severe asthma and is essential for aSMC proliferation. It also provides evidence that Rac1 is causally involved in AHR and airway remodelling. Rac1 may represent as an interesting target for treating both AHR and airway remodelling of patients with severe asthma.

INTRODUCTION

Asthma is a heterogeneous and complex disease that affects more than 300 million people worldwide.^{1,2} The disease expression includes wheezy dyspnoea, expiration blocking, cough and thoracic oppression in a context of chronic bronchial inflammation.³ Current treatments are based on anti-inflammatory therapies (inhaled and oral corticosteroids) and inhaled bronchodilators. Severe asthma is defined as asthma that is not improved by standard treatment and that requires a combination of high doses of inhaled corticosteroids with an add-on therapy to

key message

What is the key question?

► The objective of this study was to assess the role of Rac1 in severe asthma-associated airway remodelling.

What is the bottom line?

► The current study unveils an overactivation of smooth muscle Rac1 in bronchi from severe asthmatics, and highlights a leading role of Rac1 in airway remodeling.

Why read on?

► Rac1 appears as a new attractive therapeutic target in severe asthma.

be controlled, or that remains uncontrolled or even worsens despite these treatments.⁴ Severe asthma leads to a poor quality of life and important health-care expenses due to direct (care visits and treatments) and indirect (day off work) costs.^{5,6} Thus, improving the therapeutic management of these patients represents a major public health challenge.

In addition to chronic inflammation, severe asthma is characterised by airway hyperresponsiveness (AHR) and structural changes of the airway wall. This airway remodelling includes goblet cell hyperplasia, thickening of the basal membrane, angiogenesis and airway smooth muscle cells (aSMCs) hypertrophy and hyperplasia.^{7–9} The extent of this remodelling correlates with the severity of asthma and the degree of airflow obstruction.¹⁰ Currently, the only available treatment targeting airway remodelling is bronchial thermoplasty, a bronchoscopy procedure that consists in reducing the aSMC mass through the local delivery of controlled radiofrequency energy. Although bronchial thermoplasty has been shown to be effective in controlling asthma in severe asthmatics,^{11–13} its long-term effects are not known and the selection of patients who could benefit from this invasive procedure remains challenging. Nevertheless, the use of this procedure demonstrated the therapeutic value of targeting aSMCs in severe asthma and the need of developing new pharmacologic strategies for limiting aSMC proliferation and airway remodelling in severely affected patients.

It has been widely demonstrated in vitro that the small G protein Rac1 activity controls aSMC



proliferation.^{14 15} We thus hypothesised that Rac1 may be implicated in the proliferation of aSMC and consequently in the deleterious airway remodelling associated with severe asthma. By using human bronchial biopsies, human aSMC cultures and a mice model of severe allergic asthma sensitised to house dust mite (HDM) that closely mimics human pathology, we demonstrated that activation of Rac1 is causally involved in aSMCs proliferation and airway remodelling associated with severe asthma. We also show that in vivo pharmacological inhibition of Rac1 prevents asthma-associated airway remodelling thus confirming Rac1 as an alternative potential target for the treatment of severe asthma.

METHODS

Human bronchial biopsies

Bronchial biopsies were obtained by bronchial endoscopy from severe asthmatics as previously described.¹⁶ All enrolled patients gave written approval. Control samples were obtained from donor lung transplants under NaRacAS (expression and activity of Rac1 in bronchial smooth muscle cells from from asthmatic patients) protocol (NCT03325088). Clinical protocols were previously approved by relevant ethic committees.

Analysis of Rac1 activity

Human pulmonary biopsies paraffin-embedded sections were deparaffinised and permeabilised (phosphate buffered saline (PBS)+0.1% Triton-X100) before incubation with anti-Rac-GTP antibody (26903, NewEast Biosciences, King of Prussia, Pennsylvania) (1/1000) overnight at room temperature (RT). After three washes in PBS, sections were incubated for 1 hour at RT with the secondary Alexa568-labelled anti-rabbit antibody (1/1000). Anti-SM22 α antibody (Abcam) (1/500 O/N at RT) with Alexa488-labelled anti-mouse antibody (1/1000 1 hour at RT) were used to localise smooth muscle. To quantify Rac-GTP levels within the smooth muscle, Rac-GTP fluorescence intensities were measured inside a mask delimited by SM22a-positive cells and normalised to the control condition.

aSMCs proliferation

Primary aSMCs were isolated from human bronchial biopsies. Additional detail on the method is provided in an online data supplement. Human aSMCs were seeded into 24-well plates (10 000 aSMCs/well) and allowed to adhere during 6 hour before serum starvation during 24 hours. When indicated, human aSMCs were treated with the Rac inhibitor, EHT1864 (10^{-5} M; Tocris Bioscience), P21-activated kinases (Pak) inhibitor IPA3 (10^{-5} M; Tocris Bioscience), Akt inhibitor VIII (10^{-5} M; Calbiochem), MEK inhibitor PD98059 (10^{-5} M; ThermoFisher), JAK inhibitor ruxolitinib (10^{-5} M; InvivoGen) added 30 min before stimulation with bFGF (25 ng/mL; Miltenyi Biotech), PDGF-bb (25 ng/mL; Miltenyi Biotech), interleukins (IL)-13 (10 ng/mL; Miltenyi Biotech), IL-33 (10 ng/mL; Miltenyi Biotech), IL-17 (20 ng/mL; Miltenyi Biotech), IL-9 (10 ng/mL; Miltenyi Biotech) or TSLP (10 ng/mL; Miltenyi Biotech) for 48 hours. Cells were stained with EdU for 12 hours at 10^{-5} M according to the manufacturer's indications (EdU Staining Proliferation Kit iFluor 488, ID: ab219801, Abcam). Proliferation was quantified by the ratio of EdU-positive cells over the total number of cells. Proliferative signalling pathways were analysed by immunoblotting detailed in an online data supplement.

Allergic asthma models

C57Bl/6 Rac1^{lox/lox} and SMMHC-Rac1^{lox/lox} mice were obtained as previously described.¹⁷ Rac1 deletion in smooth muscle cells (SMCs) was induced in 8-week-old SMMHC-Rac1^{lox/lox} males

by intraperitoneal injection of tamoxifen (1 mg/day in sunflower oil) for five consecutive days during 2 weeks. Tamoxifen-treated Rac1^{lox/lox} mice were used as control. Allergic asthma was induced in mice using a total HDM extract (*Dermatophagoides farinae*, from Stallergenes Greer, Antony, France), as described previously.¹⁸ Additional details on the method for experimental models and the analyses of bronchoalveolar lavage fluid and airways reactivity are provided in an online data supplement.

Histology

To assess smooth muscle hypertrophy/hyperplasia, lung sections were stained by immunohistochemistry with SM22a antibody (Abcam). Hyperplasia was expressed as the ratio of SM22a-positive area to the total bronchial area and normalised to the control condition. Additional detail on the method for making pulmonary sections is provided in an online data supplement.

Statistics

Mann-Whitney test was performed for two-group comparisons. For multiple comparisons, the non-parametric Kruskal-Wallis test was used followed by Dunns' post-test to specifically compare indicated groups. The two-way ANOVA test was used for multiple comparisons of bronchial contractility studies. Data analysis was performed using the GraphPad Prism software. The threshold for statistical significance was set at $p < 0.05$.

RESULTS

Rac1 activity is increased in aSMC from patients with severe asthma

To validate the potential role of Rac1 in airway remodelling associated with severe asthma, we determined the level of Rac1 activity in bronchial biopsies from healthy subjects and from patients with severe asthma (table 1). Asthmatic donors of bronchial biopsies were mainly 50-year-old female patients with adult asthma onset. They suffered from hypereosinophilic exacerbation-prone asthma for a mean duration of 24.7 years, with pulmonary function tests moderately altered but predominantly characterised by fixed airflow obstruction. These patients were uncontrolled (mean values of asthma control test=8.5) and they showed poor quality of life (mean values of Asthma Quality-of-Life Questionnaire=2.3) (table 1), despite an optimal treatment with high doses of inhaled corticosteroids associated with another controller, sometimes in combination with oral corticosteroids. Immunofluorescence measurements of Rac1 activity, using an antibody that specifically recognises the active GTP-bound form of Rac1, revealed a greater intensity in bronchial biopsies from asthmatic patients than from controls (figure 1A,B). Labelling of aSMC by anti-SM22a antibody showed that the aSMC area was larger in bronchial biopsies of severe asthmatics than in control subjects (figure 1A,B). Furthermore, the high level of Rac1-GTP detected in biopsies of patients with severe asthma is mainly localised in SM22a-positive area indicating that it results from an increase in Rac1 activity in aSMC (figure 1A,B). The activation of Rac1 observed within the aSMC is thus consistent with our hypothesis of a potential role of Rac1 signalling in airway remodelling and in aSMC hyperplasia in severe asthmatics.

aSMCs proliferation depends on Rac1 activity

Several growth factors, cytokines and chemokines have been proposed to participate in airway remodelling in severe asthma by promoting aSMC proliferation.¹⁹⁻²⁴ We therefore assessed the role of Rac1 in primary human aSMC proliferation in response to different mitogenic stimuli. Among the mitogen factors used, only bFGF and PDGFbb induced a significant proliferation of control

Table 1 Clinical and paraclinical data of asthmatic and control donors.

	Asthma control p value (n=11) (n=4)
Age (years)	50.4±12.4 50.8±11.4 NS
Gender (F/H)	7/4 3/1 NS
BMI (kg.m ⁻²)	29.2±9.4 24.0±5 0.34
Atopy (Y/N)	8/3 0/4 0.025
Total IgE (IU/mL)	333±274
Asthma duration (years)	24.7±20.3
Eosinophils (mm ⁻³)	294±177
Pulmonary function test	
FEV1 (% predicted)	59±16
FEV1/FVC	0.58±0.12
Reversibility (Y/N)	2/
Treatment	
Daily OCS (Y/N)	6/5
OCS posology (mg/day)	23±20
ICS (µg/day)	2091±831
LABA (Y/N)	10/1
Daily nebulisation (Y/N)	7/4
Exacerbation annual rate	9.3±7.1
Hospitalisation annual rate	2.2±4
Control and quality of life score	
ACT Score	8.5±3
<20 (Y/N)	11/0
AQLQ Score	2.3±0.7

ACT, asthma control test; AQLQ, Asthma Quality-of-Life Questionnaire; BMI, body mass index; FEV1, Forced Expiratory Volume in one second; FVC, forced vital capacity; ICS, inhaled corticosteroids; IgE, immunoglobulin E; LABA, long acting beta2 agonists; OCS, oral corticosteroids. SEM). Fisher statistical test was used to compare Control and Asthmatic patients.

human aSMC (online supplemental figure E1). Interestingly, both in basal condition and on exposure to bFGF, the proliferation rate of aSMC from severe asthma patients was significantly higher than that of aSMC from control subjects (figure 2A,B). These differences are abolished by the Rac inhibitor, EHT1864, that prevented both spontaneous and bFGF- and PDGFbb-induced proliferation of aSMC from control and severe asthmatics (figure 2A,C). These results suggest that Rac1 activity is involved in the mitogenic effect of bFGF and PDGFbb on human aSMC and participates to the high proliferation rate of aSMC of asthmatic patients. To validate this hypothesis, we assessed the activation of the Rac1 signalling pathway, by measuring the phosphorylation of Pak, one of the main downstream targets of Rac1, by western blot (figure 3A). Stimulation of control aSMC with bFGF and PDGFbb indeed increased Pak phosphorylation and this response was prevented by EHT1864, thereby confirming the activation of Rac1 (figure 3A).

Rac1/Pak1/STAT3 signaling pathway is involved in growth factor-induced aSMCs proliferation

Transduction pathways activated by mitogens involved in asthmatic airway remodelling have been shown to converge to a relatively limited number of intracellular signalling modules, mainly P44/42 mitogen-activated protein kinases (MAPK), phosphoinositide 3-kinase (PI3K)/Akt and JAK/STAT.^{24–28} Indeed, we confirm

that bFGF and PDGFbb rapidly increased the phosphorylation levels of P44/42, Akt, and signal transducer and activator of transcription 3 (STAT3) in control human aSMCs (figure 3A and online supplemental figure E2). Inhibition of these signalling pathways by PD98059, Akt VIII inhibitor and ruxolitinib, respectively, reduced the proliferation of control human aSMCs at baseline and after bFGF and PDGFbb stimulation, attesting the role of these signalling pathways in this process (figure 3B). Phosphorylation of STAT3 induced by bFGF and PDGFbb was prevented by the Rac1 inhibitor EHT1864 (figure 3A), which had no effect on P44/42 activation in response to the two mitogenic factors (online supplemental figure E2). EHT1864 also downregulated Akt phosphorylation in bFGF-treated human aSMC, but not in aSMC stimulated by PDGFbb (online supplemental figure E2). These results demonstrated the essential role of Rac1 in the activation of the STAT3 pathway by mitogenic stimuli in human aSMC.

SM Rac1 deletion prevents airway remodeling in a mouse model of severe asthma

To establish the role of Rac1 in airway remodelling in vivo, we developed a murine model of severe allergic asthma induced by a percutaneous sensitisation and repeated intranasal challenges with HDM. This model allows the observation of major changes of the airway wall including aSMCs hyperplasia (figure 4A,B), AHR of bronchial rings to methacholine (figure 4C), and mixed inflammation with eosinophil and neutrophil accumulation in bronchoalveolar lavage (BAL) fluid (figure 4D). Nebulisation of the reference corticosteroid, beclomethasone at 150 µg/kg²⁹ had no significant effect on airway inflammation in this severe asthma model, whereas it prevented BAL eosinophilia and neutrophilia in an acute allergic asthma model (online supplemental figure E3). These results show that this severe allergic asthma model closely mimics the main features of severe asthma in humans, including the corticosteroid resistance.

We next submitted tamoxifen-inducible SM-Rac1-KO mice¹⁴ to the severe allergic asthma protocol. ASM area and AHR were significantly reduced in SM-Rac1-KO mice compared with SM-Rac1^{lox/lox} (figure 4B,C), whereas the histological grade, inflammatory cells accumulation in BAL and mucus production (figure 4A,D) remained unchanged. These results suggest a causal role of Rac1 in SMC hyperplasia and the resulting airway remodelling associated with severe allergic asthma.

Inhalation of a Rac1 inhibitor prevents aSMC hyperplasia, AHR, and pulmonary inflammation in a murine allergic severe asthma model

As a proof of concept to demonstrate the therapeutic value of pharmacological inhibition of Rac1 to limit airway remodelling associated with severe asthma, the Rac1 inhibitor NSC23766 was administered by repeated nebulisations before each HDM challenge. NSC23766 abrogated SMC hyperplasia and AHR of bronchial rings in response to methacholine (figure 5A-C), but also peri-bronchial/vascular infiltrates of inflammatory cells (figure 5A,B). This effect of NSC23766 on inflammatory cell infiltration was confirmed by the significant decrease of the number of macrophages and eosinophils in BAL fluid of NSC23766-treated mice, as compared with vehicle-treated mice (figure 5D). The efficiency of NSC23766 on airway remodelling and pulmonary inflammation was shown to be higher than that of current reference treatments such as repeated high doses of beclomethasone inhalations (1500 µg/kg), or the long-lasting β2-agonist, formoterol (figure 5A,B,D). Despite a significant reduction of inflammatory cell infiltrate, beclomethasone failed to

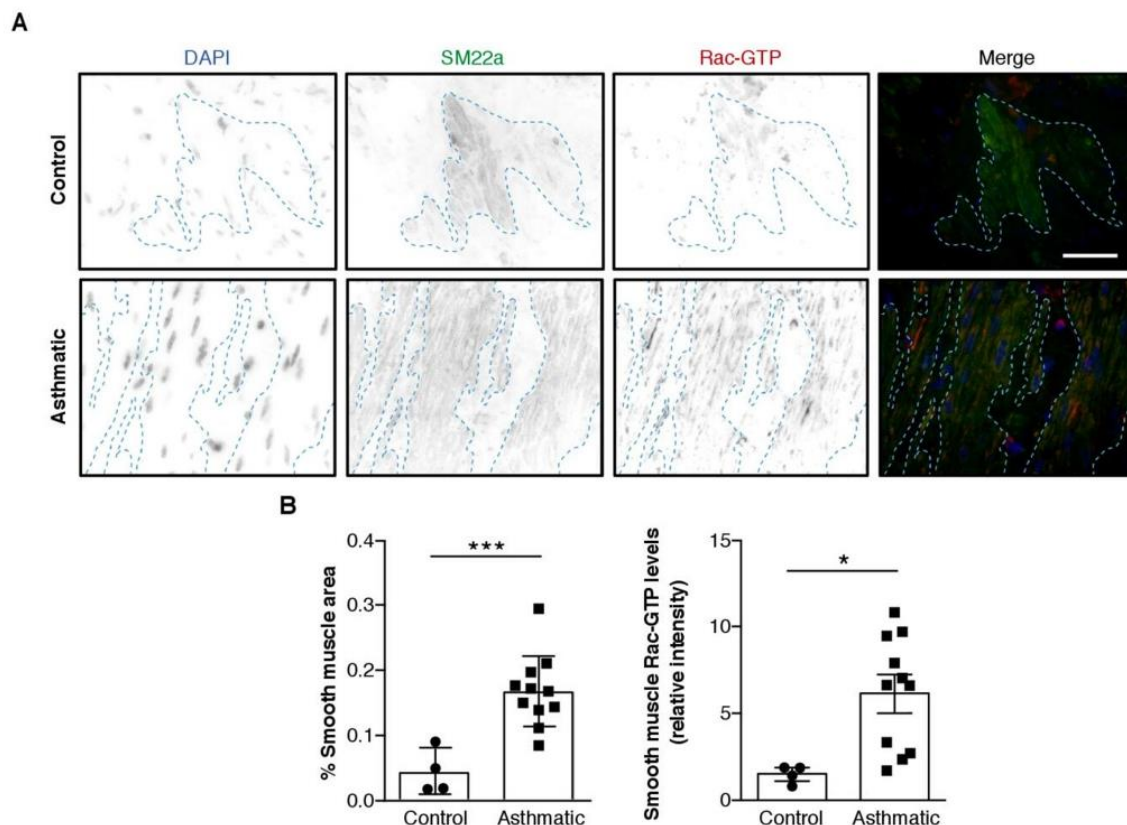


Figure 1 Rac activity is increased in airway smooth muscle contained in bronchial biopsies from asthmatics. (A) Representative images of Rac-GTP immunofluorescence (red) in biopsies sections from control (n=4) and patients with severe asthma (n=11). Nuclei were detected by 4',6-diamidino-2-phenylindole staining (blue) and smooth muscle by SM22a immunofluorescence (green). Scale bar, 100 μ m. (B) Quantification of smooth muscle area, mean fluorescence intensity of the Rac1-GTP signal within the biopsy and within the smooth muscle layer. Data are presented as mean \pm SEM. Mann-Whitney statistical test was used to compare control and asthmatic groups. * P <0.05, *** p <0.001.

prevent aSMC hyperplasia, and formoterol had no effect on lung inflammation and remodelling.

DISCUSSION

Our current study revealed a leading role of Rac1 in airway remodelling and in aSMC hyperplasia associated with severe asthma, by promoting STAT3-dependent aSMC proliferation. This involvement of Rac1 in the pathological remodelling in the human disease is consistent with its overactivation observed in bronchi from severe asthmatics.

The increase of aSMC mass is one of the main features of airway remodelling associated with asthma and is considered as a marker of disease severity.^{12,19} It relies on a high proliferation rate of aSMC in patients with severe asthma compared with mild and moderate asthma, or control subjects.³⁰ A number of mediators can operate in concert to stimulate aSMC proliferation, including growth factors (PDGFbb and bFGF), cytokines and chemokines, which are produced by inflammatory and airway structural cells, and by products of mast cells infiltrating the aSMC bundles, such as histamine, tryptase, and leukotrienes.^{22,23} Although initially described as the main intracellular signalling pathway mediating cytokine responses, the JAK/STAT signalling pathway has been shown to be activated by many different ligands and receptors, including growth factor/tyrosine kinase receptors and G protein coupled receptors.³¹ Consistent with our results, Rac1 has been shown to be required for growth

factor receptor-mediated and G protein coupled-receptor-mediated activation of the JAK/STAT pathway, thus defining Rac1 as a hub in signalling networks that control human aSMC proliferation.^{24,32,33} This role of Rac1 is in agreement with the strong activity of Rac1 systematically observed in the remodelled airway wall of patients with severe asthma compared with control subjects, even though the number of samples analysed was limited. Recently, P-Rex1, a Rac1 exchange factor, has been shown to be aberrantly upregulated in lung tissue from patients with asthma and to potentiate growth factor-induced human aSMC proliferation.³⁴ Therefore, it can be hypothesised that the activation of aSMC Rac1 observed in severe asthma patients could be related, at least in part, to this aberrant upregulation of P-Rex1 expression, and would be responsible for the increased aSMC proliferation in asthma.

The increase in aSMC mass in asthma patients was associated with airflow obstruction.^{9,10} Indeed, aSMC are not only responsible for AHR through their contractile activity, but also contribute to the inflammatory process by modifying the extracellular matrix and producing mediators that act on inflammatory cells. Pharmacological targeting of aSMC thus appears as an attractive strategy for novel asthma therapies. Current therapeutic strategies remain based on the chronic use of high dose inhaled or oral corticosteroids, resulting in various and harmful long-term side effects.^{35,36} New therapeutic strategies such as monoclonal antibodies anti-IgE (omalizumab), anti-IL-5 (mepolizumab, reslizumab), anti-IL-5 receptor

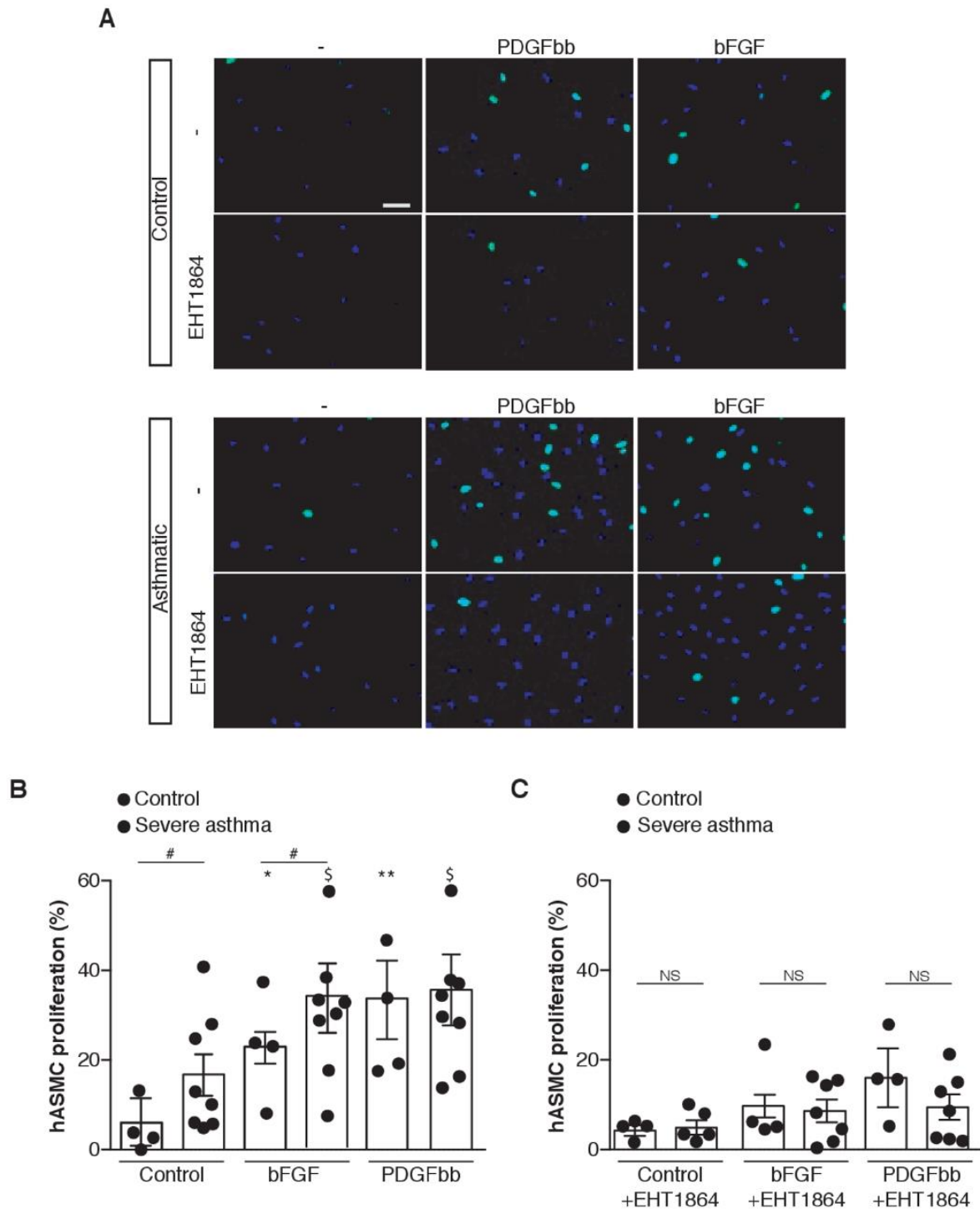
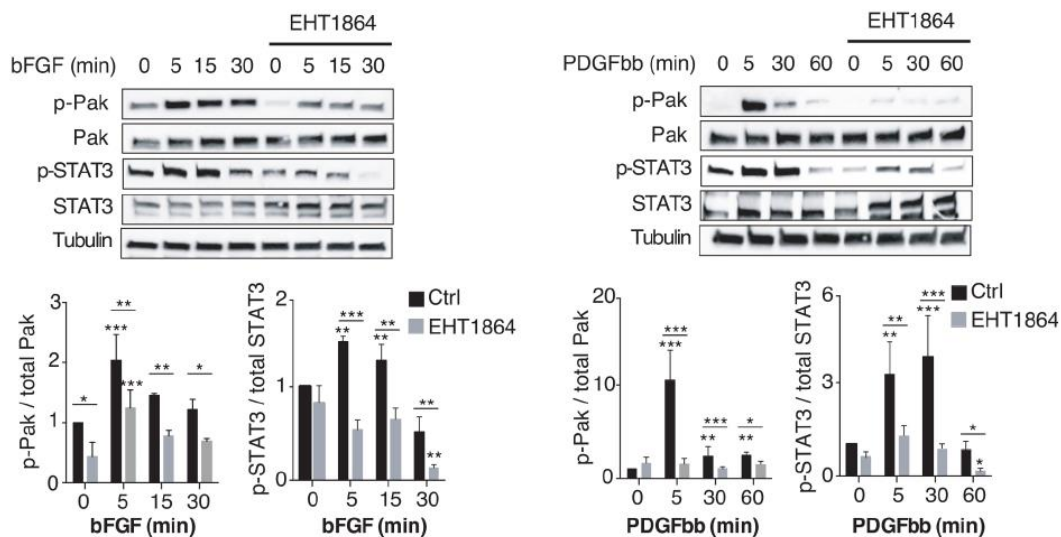


Figure 2 Rac1 inhibition reduces bFGF-induced and PDGFbb-induced aSMCs proliferation. (A) Representative images of airway smooth muscle cell (aSMC) proliferation from control and severe asthmatics induced by bFGF and PDGFbb, in the absence and in the presence of the Rac1 inhibitor, EHT1864. Nuclei are detected by 4',6-diamidino-2-phenylindole staining (blue) and aSMC proliferation by EdU staining (green). Scale bar, 25 μ m. (B,C) Quantification of aSMC proliferation by EdU staining in the absence (B) and in the presence (C) of EHT1864. The results are expressed as the percentage of cell proliferation (EdU-positive cells) (mean \pm SEM of n=3 independent experiments). Kruskal-Wallis test followed by Dunns' post-test were used. *P<0.05, **p<0.01 versus untreated cells from control subjects; $^{\#}$ P<0.05 versus untreated cells from patients with severe asthma; $^{\$}$ p<0.05 versus cells from control subjects.

A



B

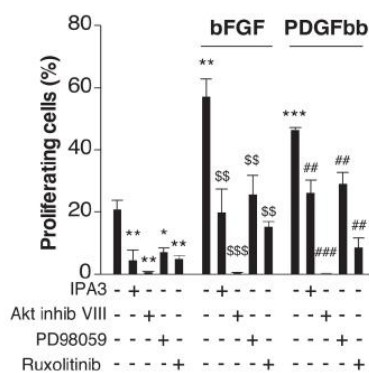
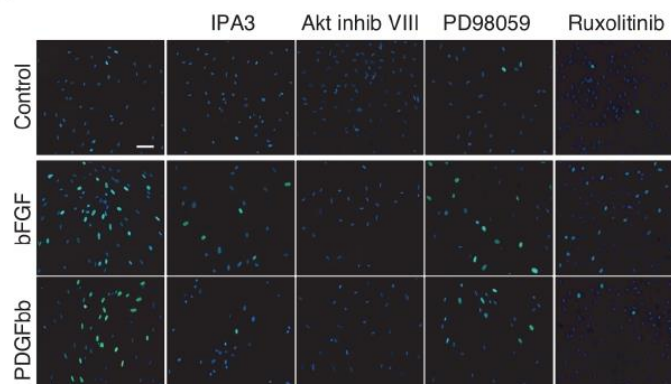


Figure 3 Role of Rac1/P21-activated kinases (Pak1) in bFGF-induced activation of Akt-dependent signalling pathway. (A) Immunoblot analysis and corresponding quantification of Pak and STAT3 expression and phosphorylation in control airway smooth muscle cell (aSMCs) stimulated with bFGF or PDGFbb at different time points, in the absence, or in the presence of EHT1864 ($n=4-5$ independent experiments). (B) Control aSMC proliferation induced by bFGF and PDGFbb, in the absence and in the presence of inhibitors of PAK (IPA3), Akt (Akt Inhib VIII), P44/42 (PD98059) or JaAK2 (ruxolitinib). Nuclei are detected by 4',6-diamidino-2-phenylindole staining (blue) and haSMC proliferation by EdU staining (green). Scale bar, 25 μ m. Quantification of aSMC proliferation by EdU staining. The results are expressed as the percentage of EdU-positive cells. ($n=3-4$ independent experiments). Data are presented as mean \pm SEM. Kruskal-Wallis test followed by Dunns' post-test were used. * $P<0.05$, ** $p<0.01$, *** $p<0.001$ versus untreated cells; \$\$\$ $p<0.001$, \$\$\$ $p<0.001$ versus bFGF treated cells; ## $p<0.01$, ### $p<0.001$ versus PDGFbb treated cells.

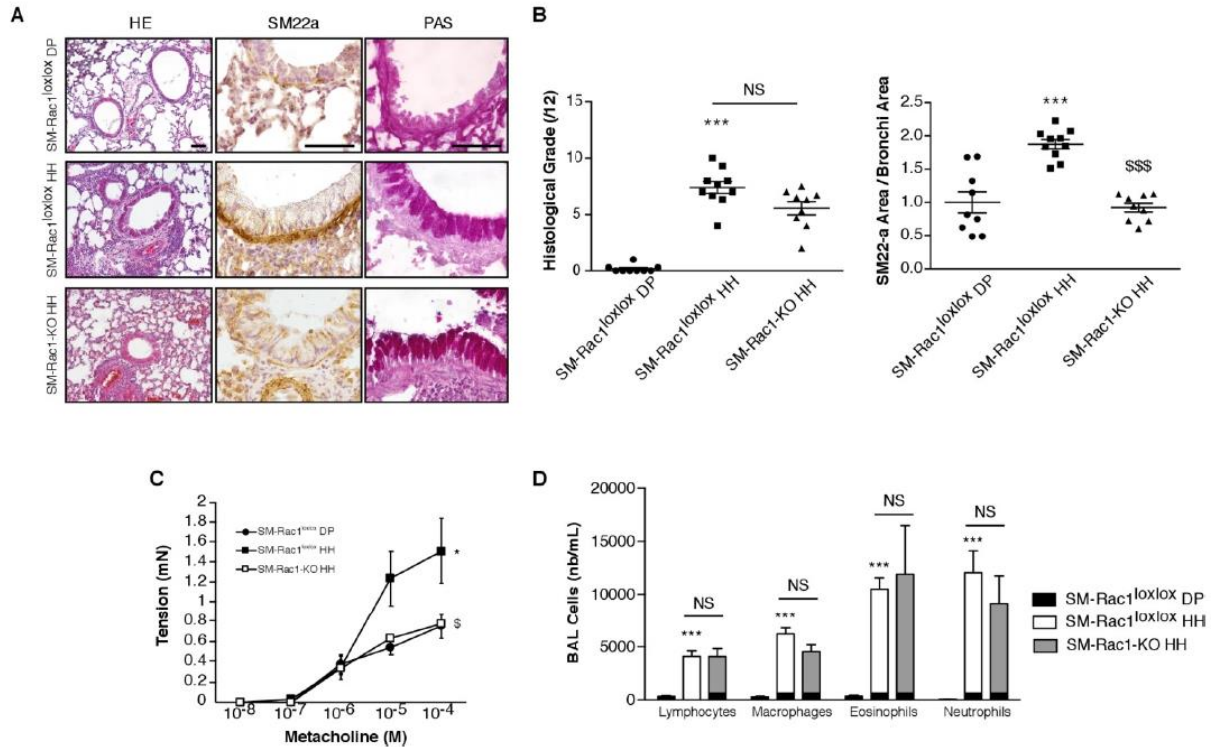


Figure 4 SM-Rac1 deletion prevents smooth muscle hyperplasia associated in an experimental model of severe allergic asthma. (A) Hematoxylin/Eosin (HE staining, SM22a immunohistochemistry and Periodic acid–Schiff (PAS) staining of lung sections from naïve (DP) or house dust mite-sensitised (HH) mice of the indicated genotypes. Images are representative of 9–10 mice in each experimental condition. Scale bars, 100 μ m. (B) Histological grade and smooth muscle hyperplasia quantification on lung sections from DP and HH mice of the indicated genotypes (n=9–10 mice). (C) Contractile responses to increasing concentration of methacholine of bronchial rings from DP and HH mice of the indicated genotypes (n=3–4). (D) Infiltrating cells in bronchoalveolar lavage fluid from DP and HH mice of the indicated genotypes (n=8–14). Data are expressed as mean \pm SEM. Kruskal-Wallis test followed by Dunns' post-test were used for (B) and (D). Two-way analysis of variance test was used for (C). NS, not significant. * $P < 0.05$, *** $p < 0.001$ versus SM-Rac1^{lox/lox} DP mice; ^S $p < 0.05$, ^{SSS} $p < 0.001$ versus SM-Rac1^{lox/lox} HH mice.

(benralizumab) and anti-IL-4/IL-13 receptor (dupilumab) significantly improve exacerbations rate and asthma control, and lower oral corticosteroid use in patients with severe asthma.^{37–41} However, these strategies focus on specific inflammatory endotypes,^{39–42–44} and the potential impacts of these new strategies on airway remodelling are still missing. In this context, our demonstration that Rac1 is a node in signalling pathways that plays a major role in the contraction and proliferation of aSMC makes this protein a pharmacological target of choice for severe asthma. The efficiency of SMC Rac1 deletion and repeated inhalations of the Rac1 inhibitor NSC23766 to prevent AHR and aSMC hyperplasia validate this hypothesis in a severe allergic asthma model in mice that recapitulate the human disease. Moreover, in addition to these expected effects, Rac1 inhibition also reduced eosinophilic inflammation, thus demonstrating that the anti-inflammatory action of Rac1 inhibitor already described in an acute murine model of allergic asthma,⁴⁴ is also effective in severe chronic asthma. To our knowledge, this is the first demonstration of a drug able to combine all the desired effects for the treatment of severe asthma, that is, limiting aSMC contraction and proliferation and reducing inflammation. Since Rac1 is known to have ubiquitous expression and multiple functions,⁴⁵ an open and important question that remains to be addressed is the possible side effects of Rac1 inhibitor. However, in asthma, the opportunity of administrating the treatment locally might be an effective way to limit potential adverse effects. Indeed, repeated administration of

NSC23766 by nebulisation failed to alter blood pressure, whereas SMC Rac1 deletion has been shown to elicit this effect.⁴⁶

In conclusion, we suggest that Rac1 may represent a relevant target to develop new drugs of clinical interest for the treatment of severe asthma. Our data support the concept that inhibition of Rac1-dependent signalling pathway may simultaneously limit aSMC hyperplasia, AHR and inflammation, thereby providing a novel approach to reverse airway remodelling and restore airway function in patients with severe asthma. The development of Rac1 inhibitors may thus offer a new therapeutic option for patients who are refractory to current treatments.

Acknowledgements The authors thank Marie-Aude Cheminant (institut du thorax) for expert technical assistance. We also value the support provided by the animal facility units of the University of Nantes. We thank Therassay, Micropicell and Cytocell core facilities (SFR François Bonamy, University of Nantes) for the functional and cellular explorations, Philippe LACOSTE (MD, PhD) and Meggy BERNARD (Nantes university hospital) for the collection of human bronchial samples from lung transplants. The authors also thank the support of the cluster LUNG innovation (LUNG O2; Programme d'Investissements d'Avenir ANR-16-IDEX-0007).

Contributors Conception and design: MP, AM, GL and VS. Experimentation: FD, LR, DH, MK, MR, CB, CT, MCD, LDC., NH, GB and VS. Analysis and interpretation: FD, MP, GL and VS. Drafting the manuscript: FD, GL and VS. Authors FD and LR contributed equally to this work.

Funding This work was supported by grants from the Institut de Recherche en Santé Respiratoire des Pays de la Loire (G-Rar and NARACAS projects), the

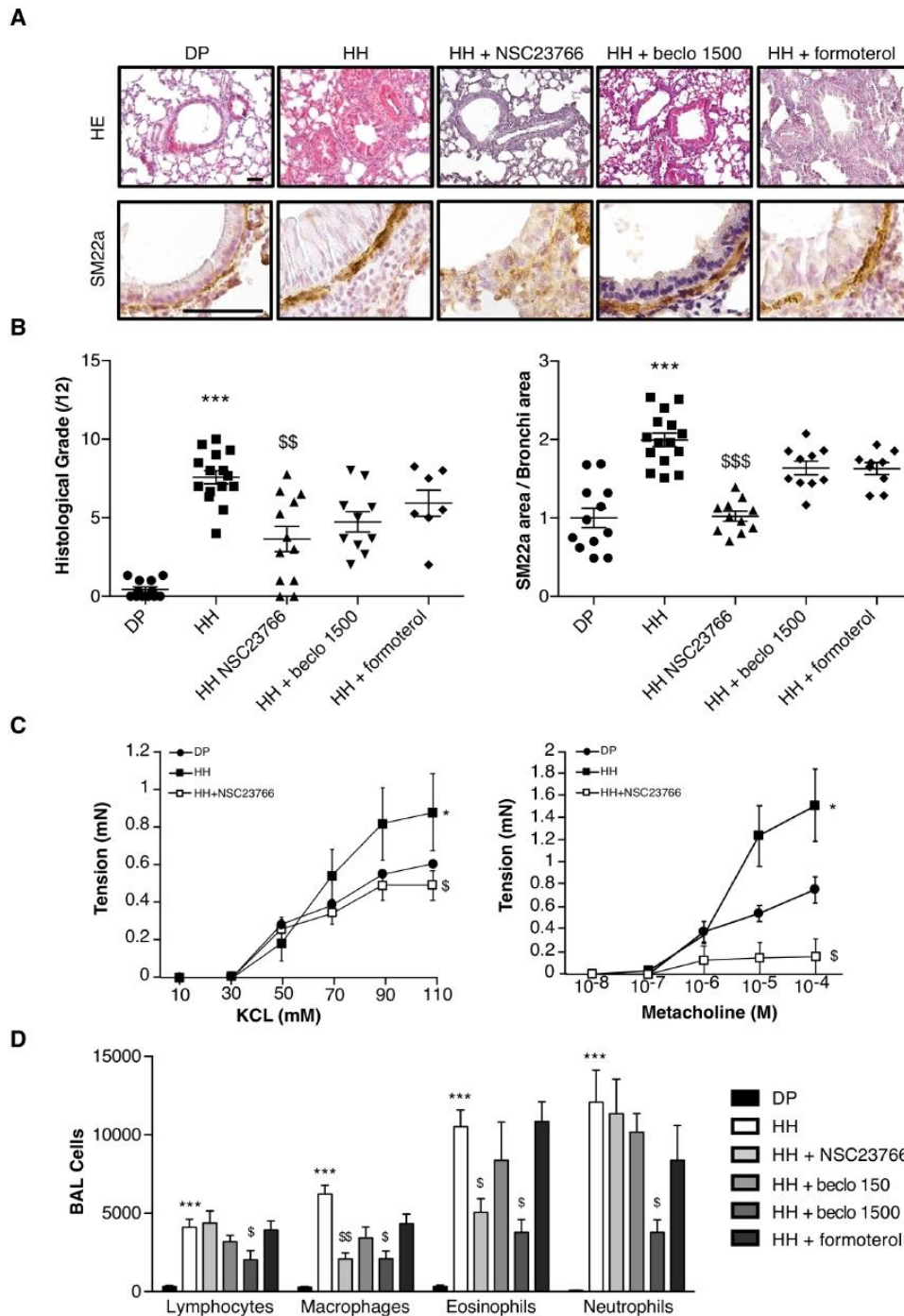


Figure 5 NSC23766 inhalations reduce pulmonary remodelling and smooth muscle hyperplasia associated with severe allergic asthma. (A) Hematoxylin/Eosin (HE) staining and SM22a immunohistochemistry of lung sections from naïve (DP) or house dust mite-sensitised (HH) mice treated with NaCl, NSC23766, beclomethasone (1500 µg/kg) or formoterol. Images are representative of 9–15 mice in each experimental condition. Scale bars, 100 µm. (B) Histological grade and smooth muscle hyperplasia measured on lung sections from DP and HH mice treated with NaCl, NSC23766, beclomethasone or formoterol (n=9–15 mice). (C) Contractile responses to increasing concentrations of KCl and methacholine of bronchi rings from DP and HH mice treated with NaCl or NSC23766 (n=4–5). (D) Infiltrating cells in bronchoalveolar lavage fluid from DP and HH mice treated with NaCl, NSC23766, beclomethasone (150 or 1500 µg/kg), or formoterol (n=9–14 mice). Data are represented as mean±SEM. Kruskal-Wallis test followed by Dunns' post-test were used for (B) and (D). Two-way analysis of variance test was used for (c). *P<0.05, ***p<0.001 versus DP NaCl; [§]p<0.05, ^{§§}p<0.01 and ^{§§§}p<0.001 versus HH NaCl.

Société d'Accélération du Transfert de Technologie (project number STRAS-2117) and the Institut National de la Santé et de la Recherche Médicale (INSERM). LR was supported by a grant from MRES. FD and DH were supported by a grant from Fondation Recherche Médicale.

Competing interests None declared.

Patient consent for publication Not required.

Ethics approval All experimental procedures and animal care were performed in accordance with the Regional Ethical Committee for Animal Experiments of the Pays de la Loire and conform to the ARRIVE guidelines.

Provenance and peer review Not commissioned; externally peer reviewed.

Data availability statement All data relevant to the study are included in the article or uploaded as supplementary information. Vincent SAUZEAU, PhDvincent.sauzeau@inserm.fr.

Open access This is an open access article distributed in accordance with the Creative Commons Attribution Non Commercial (CC BY-NC 4.0) license, which permits others to distribute, remix, adapt, build upon this work non-commercially, and license their derivative works on different terms, provided the original work is properly cited, appropriate credit is given, any changes made indicated, and the use is non-commercial. See: <http://creativecommons.org/licenses/by-nc/4.0/>.

REFERENCES

- Variations in the prevalence of respiratory symptoms, self-reported asthma attacks, and use of asthma medication in the European community respiratory health survey (ECRHS). *Eur Respir J* 1996;9:687–95.
- Worldwide variation in prevalence of symptoms of asthma, allergic rhinconjunctivitis, and atopic eczema: Isaac. The International study of asthma and allergies in childhood (Isaac) Steering Committee. *Lancet Lond. Engl* 1998;351:1225–32.
- Reddel HK, Bateman ED, Becker A, et al. A summary of the new GINA strategy: a roadmap to asthma control. *Eur Respir J* 2015;46:622–39.
- Chung KF, Wenzel SE, Brozek JL, et al. International ERS/ATS guidelines on definition, evaluation and treatment of severe asthma. *Eur Respir J* 2014;43:343–73.
- Lane S, Molina J, Plusa T. An international observational prospective study to determine the cost of asthma exacerbations (COAX). *Respir Med* 2006;100:434–50.
- Moore WC, Bleeker ER, Curran-Everett D, et al. Characterization of the severe asthma phenotype by the National heart, lung, and blood Institute's severe asthma research program. *J Allergy Clin Immunol* 2007;119:405–13.
- Bento AM, Hershenson MB. Airway remodeling: potential contributions of subepithelial fibrosis and airway smooth muscle hypertrophy/hyperplasia to airway narrowing in asthma. *Allergy Asthma Proc* 1998;19:353–8.
- Jeffery PK. Remodeling in asthma and chronic obstructive lung disease. *Am J Respir Crit Care Med* 2001;164:528–38.
- Prakash YS. Emerging concepts in smooth muscle contributions to airway structure and function: implications for health and disease. *Am J Physiol Lung Cell Mol Physiol* 2016;311:L1113–40.
- James AL, Bai TR, Mauad T, et al. Airway smooth muscle thickness in asthma is related to severity but not duration of asthma. *Eur Respir J* 2009;34:1040–5.
- Castro M, Rubin A, Laviolette M, et al. Persistence of effectiveness of bronchial thermoplasty in patients with severe asthma. *Ann Allergy Asthma Immunol* 2011;107:65–70.
- Castro M, Rubin AS, Laviolette M, et al. Effectiveness and safety of bronchial thermoplasty in the treatment of severe asthma: a multicenter, randomized, double-blind, sham-controlled clinical trial. *Am J Respir Crit Care Med* 2010;181:116–24.
- Thomson NC, Rubin AS, Niven RM, et al. Long-Term (5 year) safety of bronchial thermoplasty: asthma intervention research (air) trial. *BMC Pulm Med* 2011;11:8.
- Liu Y, Li W, Ye C, et al. Gambogic acid induces G0/G1 cell cycle arrest and cell migration inhibition via suppressing PDGF receptor β tyrosine phosphorylation and Rac1 activity in rat aortic smooth muscle cells. *J Atheroscler Thromb* 2010;17:901–13.
- Page K, Li J, Hodge JA, et al. Characterization of a Rac₁ Signaling Pathway to Cyclin D₁ Expression in Airway Smooth Muscle Cells. *J Biol Chem* 1999;274:22065–71.
- Aubier M, Thabut G, Hamidi F, et al. Airway smooth muscle enlargement is associated with protease-activated receptor 2/ligand overexpression in patients with difficult-to-control severe asthma. *J Allergy Clin Immunol* 2016;138:729–39.
- André-Grégoire G, Dilasser F, Chesné J, et al. Targeting of Rac1 prevents bronchoconstriction and airway hyperresponsiveness. *J Allergy Clin Immunol* 2018;142:824–33.
- Chesné J, Braza F, Chadeuf G, et al. Prime role of IL-17A in neutrophilia and airway smooth muscle contraction in a house dust mite-induced allergic asthma model. *J Allergy Clin Immunol* 2015;135:1643–5.
- Hashimoto M, Tanaka H, Abe S. Quantitative analysis of bronchial wall vascularity in the medium and small airways of patients with asthma and COPD. *Chest* 2005;127:965–72.
- Hoshino M, Takahashi M, Aoike N. Expression of vascular endothelial growth factor, basic fibroblast growth factor, and angiogenin immunoreactivity in asthmatic airways and its relationship to angiogenesis. *J Allergy Clin Immunol* 2001;107:295–301.
- Redington AE, Roche WR, Madden J, et al. Basic fibroblast growth factor in asthma: measurement in bronchoalveolar lavage fluid basally and following allergen challenge. *J Allergy Clin Immunol* 2001;107:384–7.
- Vignola AM, Chanez P, Chiappara G, et al. Transforming growth factor-beta expression in mucosal biopsies in asthma and chronic bronchitis. *Am J Respir Crit Care Med* 1997;156:591–9.
- Bossé Y, Rola-Pleszczynski M. Fgf2 in asthmatic airway-smooth-muscle-cell hyperplasia. *Trends Mol Med* 2008;14:3–11.
- Simeone-Penney MC, Severgnini M, Rozo L, et al. Pdgf-Induced human airway smooth muscle cell proliferation requires STAT3 and the small GTPase Rac1. *Am J Physiol Lung Cell Mol Physiol* 2008;294:L698–704.
- Zhou L, Hershenson MB. Mitogenic signaling pathways in airway smooth muscle. *Respir Physiol Neurobiol* 2003;137:295–308.
- Yap HM, Israf DA, Harith HH, et al. Crosstalk between signaling pathways involved in the regulation of airway smooth muscle cell hyperplasia. *Front Pharmacol* 2019;10:1148.
- Jee S-H, Chu C-Y, Chiu H-C, et al. Interleukin-6 induced basic fibroblast growth factor-dependent angiogenesis in basal cell carcinoma cell line via JAK/STAT3 and PI3-kinase/Akt pathways. *J Invest Dermatol* 2004;123:1169–75.
- Shi H, Lin B, Huang Y, et al. Basic fibroblast growth factor promotes melanocyte migration via activating PI3K/Akt-Rac1-FAK-JNK and ERK signaling pathways. *IUBMB Life* 2016;68:735–47.
- Hrvacic B, Bosnjak B, Tudja M, et al. Applicability of an ultrasonic nebulization system for the airways delivery of beclomethasone dipropionate in a murine model of asthma. *Pharm Res* 2006;23:1765–75.
- Johnson PR, Roth M, Tamm M, et al. Airway smooth muscle cell proliferation is increased in asthma. *Am J Respir Crit Care Med* 2001;164:474–7.
- Bousoik E, Montazeri Aliabadi H. "Do We Know Jack" About JAK? A Closer Look at JAK/STAT Signaling Pathway. *Front Oncol* 2018;8:287.
- Pelletier S, Duhamel F, Coulombe P, et al. Rho family GTPases are required for activation of JAK/STAT signaling by G protein-coupled receptors. *Mol Cell Biol* 2003;23:1316–33.
- Movassagh H, Shan L, Halayko AJ, et al. Neuronal chemorepellent semaphorin 3E inhibits human airway smooth muscle cell proliferation and migration. *J Allergy Clin Immunol* 2014;133:560–7.
- Huang Y, Xie Y, Jiang H, et al. Upregulated P-Rex1 exacerbates human airway smooth muscle hyperplasia in asthma. *J Allergy Clin Immunol* 2019;143:778–81.
- Buchman AL. Side effects of corticosteroid therapy. *J Clin Gastroenterol* 2001;33:289–94.
- Volmer T, Effenberger T, Trautner C, et al. Consequences of long-term oral corticosteroid therapy and its side-effects in severe asthma in adults: a focused review of the impact data in the literature. *Eur Respir J* 2018;52. doi:10.1183/13993003.00703-2018. [Epub ahead of print: 25 10 2018].
- Normansell R, Walker S, Milan SJ, et al. Omalizumab for asthma in adults and children. *Cochrane Database Syst Rev* 2014;CD003559.
- Pavord ID, Korn S, Howarth P, et al. Mepolizumab for severe eosinophilic asthma (DREAM): a multicentre, double-blind, placebo-controlled trial. *Lancet* 2012;380:651–9.
- Bleeker ER, FitzGerald JM, Chanez P, et al. Efficacy and safety of benralizumab for patients with severe asthma uncontrolled with high-dosage inhaled corticosteroids and long-acting β_2 -agonists (SIROCCO): a randomised, multicentre, placebo-controlled phase 3 trial. *The Lancet* 2016;388:2115–27.
- Castro M, Zangrilli J, Wechsler ME, et al. Reslizumab for inadequately controlled asthma with elevated blood eosinophil counts: results from two multicentre, parallel, double-blind, randomised, placebo-controlled, phase 3 trials. *Lancet Respir Med* 2015;3:355–66.
- FitzGerald JM, Bleeker ER, Nair P, et al. Benralizumab, an anti-interleukin-5 receptor α monoclonal antibody, as add-on treatment for patients with severe, uncontrolled, eosinophilic asthma (CALIMA): a randomised, double-blind, placebo-controlled phase 3 trial. *The Lancet* 2016;388:2128–41.
- FitzGerald JM, Bleeker ER, Menzies-Gow A, et al. Predictors of enhanced response with benralizumab for patients with severe asthma: pooled analysis of the SIROCCO and CALIMA studies. *Lancet Respir Med* 2018;6:51–64.
- Haldar P, Brightling CE, Singapuri A, et al. Outcomes after cessation of mepolizumab therapy in severe eosinophilic asthma: a 12-month follow-up analysis. *J Allergy Clin Immunol* 2014;133:921–3.
- Hanania NA, Wenzel S, Rosén K, et al. Exploring the effects of omalizumab in allergic asthma: an analysis of biomarkers in the extra study. *Am J Respir Crit Care Med* 2013;187:804–11.
- Jaffe AB, Hall A. Rho GTPases: biochemistry and biology. *Annu Rev Cell Dev Biol* 2005;21:247–69.
- André G, Sandoval JE, Retailleau K, et al. Smooth muscle specific Rac1 deficiency induces hypertension by preventing p116RIP3-dependent RhoA inhibition. *J Am Heart Assoc* 2014;3:e000852.

Online data supplement

1
2
3
4
5
6
7
8
9
10
11
12
13
14
15
16
17
18
19
20
21
22
23
24
25

Supplemental Methods

Cell culture. Primary aSMCs were isolated from human bronchial biopsies. Tissues were cleaned manually and the muscular layer was further digested for 1 hour with collagenase II (1 mg/mL, Worthington Biochemical, Lakewood, NJ) at 37°C under agitation. Cells grew up in Dulbecco modified Eagle medium (Gibco; Invitrogen ThermoFisher Scientific, Waltham, Mass) containing 10% FBS, 100 units/mL penicillin, and 100 mg/mL streptomycin at 37°C and 5% CO₂. The culture medium was changed every 72 hours. All experiments were performed between passages 1 and 6.

Allergic asthma models. For acute allergic asthma model, mice were sensitized on days D0, D7, D14, and D21 by skin application of 500 µg Der f in 20 µL of dimethyl sulfoxide (Sigma) onto the ears. Control mice were sensitized with dimethyl sulfoxide. Intranasal challenges were performed with 250 µg of Der f in 40 µL of sterile PBS on D27 and D34. For severe allergic asthma model, mice were submitted to the same protocol but were intranasally challenged on days D26, D27, D28 and D33, D34, D35. When indicated, allergic asthma mice were treated by repeated inhalations of NSC23766 (40 µg/kg in 400 µL PBS), formoterol (125 µg/kg in 400 µL PBS) or beclomethasone (150 or 1500 µg/kg in 400 µL PBS) before each challenge. All mice were sacrificed 24 hours after last intranasal challenge for analysis.

Bronchoalveolar lavage (BAL) fluid analysis. Mice were tracheotomized and 1 mL of sterile PBS was administrated intratracheally through a catheter. Cells and supernatants from recovered fluid were separated by centrifugation. Total cell number was counted on Kova slides by optical microscopy. Identification of immune cell subpopulations was performed by

26 flow cytometry analysis²⁰. Acquisition was performed on LSR II (BD Bioscience) and analyzed
27 with FlowJo software.

28 **Airways reactivity ex vivo.** Murine primary bronchi were cleaned, cut in rings, and mounted
29 on a multichannel isometric myograph in Krebs-Henseleit physiological solution (118.4 mM
30 NaCl, 4.7 mM KCl, 2 mM CaCl₂, 1.2 mM MgSO₄, 1.2 mM KH₂PO₄, 25 mM NaHCO₃, and 11 mM
31 glucose) at 37°C and gassed with a mixture of 95%O₂/5%CO₂. A pretension of 0.5 mN was
32 applied. We constructed dose-response curves to methacholine (Sigma-Aldrich, Paris, France).
33 The wire myograph was connected to a digital data recorder (MacLab/4e, AD Instruments,
34 Paris, France) and recordings were analyzed using LabChart v7 software (AD Instruments).

35 **Histology.** Paraformaldehyde (4% in PBS, 1 mL) was administered intratracheally in the lungs
36 through a flexible catheter, trachea was ligatured, and lungs were excised. Lungs were fixed
37 in 4% paraformaldehyde for 48 h and embedded into paraffin. Sections measuring 6 mm in
38 size were stained with periodic acid-Schiff or hematoxylin/eosin for morphological studies.
39 Histological grade (over 12 points) was determined to assess inflammation (0-8) and
40 pulmonary remodeling (0-4) as previously described²⁰.

41 **Immunoblotting.** Primary aSMCs were incubated on ice with lysis buffer supplemented with
42 protease and phosphatase inhibitor cocktails (Sigma Aldrich, Saint Quentin Fallavier, France)
43 and sodium orthovanadate. Lysates were subjected to SDS-PAGE, transferred to nitrocellulose
44 membranes, and incubated with specific antibodies: p-Akt (9271), Akt (9272), p-P44/42
45 (9101), P44/42 (4695), p-Pak (2605), Pak1 (2602), p-STAT3 (9131) and STAT3 (4904) antibodies
46 were from Cell Signaling Technology (Leiden, The Netherlands). Equal loading was checked by
47 reprobing of the membrane with an anti-tubulin antibody (Beckman Coulter; Villepinte,
48 France). Immune complexes were detected with appropriate secondary antibodies and

49 enhanced chemiluminescence reagent (Clarity ECL BioRad, Marnes la Coquette, France).
50 Protein band intensities were quantified using ImageJ Software (NIH software, Bethesda, Md).
51

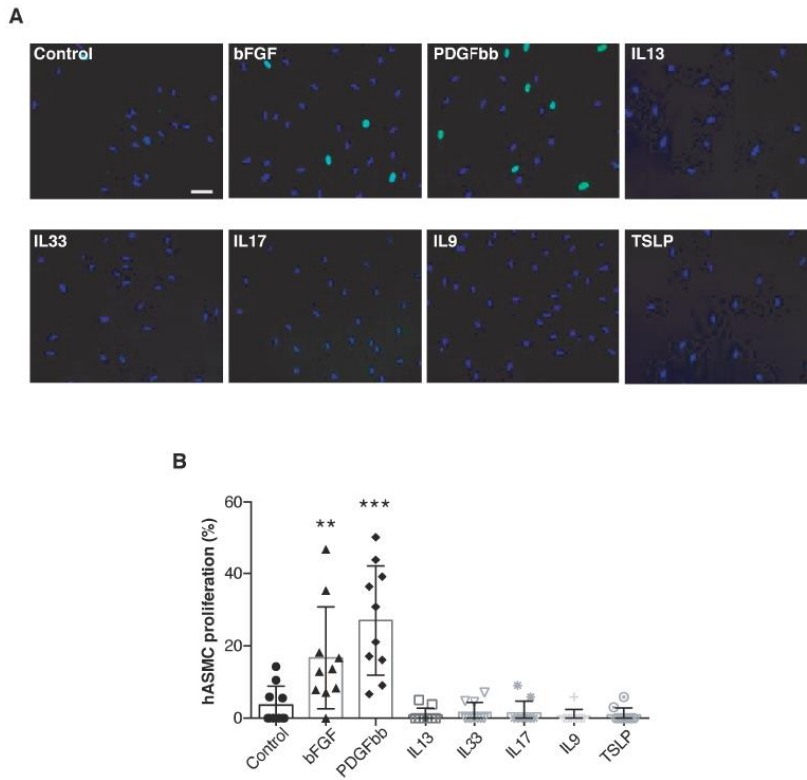
52 Supplemental legends

53
54 **Figure E1. aSMC proliferation is induced by bFGF and PDGFbb. (A)** Representative images of
55 aSMC proliferation by indicated factors. Nuclei are detected by DAPI staining (blue) and aSMC
56 proliferation by EdU staining (green). Scale bar, 25 μ m. **(B)** Proliferation of haSMC induced by
57 bFGF, PDGFbb, IL-13, IL-33, IL-17, IL-9 and TSLP. Detection and quantification of haSMC
58 proliferation by EdU staining. Results are expressed as the percentage of EdU positive cells
59 (n=10). Data are presented as mean \pm SEM. Kruskal-Wallis test followed by Dunns' posttest
60 were used. ** P <0.01, *** P <0.001 vs control cells.

61
62 **Figure E2. Activation of Akt and P44/42 in response to bFGF and PDGFbb. (A)** Immunoblot
63 analysis of Akt and P44/42 expression and phosphorylation in haSMCs stimulated with bFGF
64 or PDGFbb at different time points. When indicated, EHT1864 was preincubated 30 min before
65 stimulation. **(B)** Quantification of phosphorylation and expression of Akt and P44/42 (n=4-5).
66 Data are expressed as mean \pm SEM. Kruskal-Wallis test followed by Dunns' posttest were used.
67 * P <0.05, ** P <0.01, *** P <0.001.

68
69 **Figure E3. Effect of beclomethasone on pulmonary inflammatory cells infiltrate in an acute**
70 **allergic asthma murine model.** Infiltrating cells in BAL fluid from DP and HH mice from the
71 acute allergic asthma protocol treated with beclomethasone (150 or 1500 μ g/kg) or NaCl (n =
72 10 mice). Data are expressed as mean \pm SEM. Kruskal-Wallis test followed by Dunns' posttest
73 were used. *** P <0.001 vs DP NaCl; § P <0.05 vs HH NaCl.

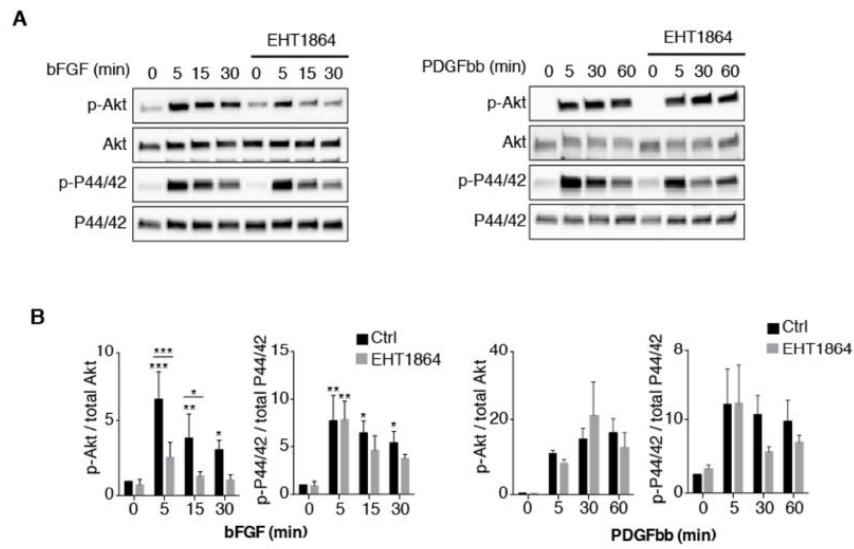
Figure E1



74

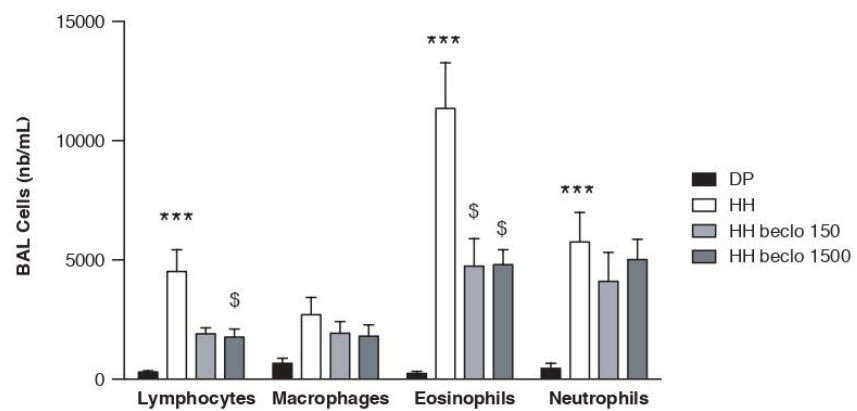
75

Figure E2



77

Figure E3



Article 2: Bronchial smooth muscle cell in asthma: where does it fit?

Article publié dans BMJ Open Respiratory Research

Bronchial smooth muscle cell in asthma: where does it fit?

Dorian Hassoun,¹ Lindsay Rose,² François-Xavier Blanc ,¹ Antoine Magnan,^{3,4} Gervaise Loirand,² Vincent Sauzeau²

To cite: Hassoun D, Rose L, Blanc F-X, et al. Bronchial smooth muscle cell in asthma: where does it fit?. *BMJ Open Resp Res* 2022;**9**:e001351. doi:10.1136/bmjresp-2022-001351

DH and LR contributed equally.

Received 27 June 2022
Accepted 4 September 2022



© Author(s) (or their employer(s)) 2022. Re-use permitted under CC BY-NC. No commercial re-use. See rights and permissions. Published by BMJ.

¹Nantes Université, CHU Nantes, CNRS, INSERM, l'institut du thorax, F-44000 Nantes, France

²Nantes Université, CNRS, INSERM, l'institut du thorax, F-44000 Nantes, Pays de la Loire, France

³INRAe, UMR 0892, Hôpital Foch, Suresnes, France

⁴Université Versailles-Saint-Quentin-en-Yvelines Paris-Saclay, Versailles, France

Correspondence to

Dr Vincent Sauzeau;
vincent.sauzeau@inserm.fr

ABSTRACT

Asthma is a frequent respiratory condition whose pathophysiology relies on altered interactions between bronchial epithelium, smooth muscle cells (SMC) and immune responses. Those leads to classical hallmarks of asthma: airway hyper-responsiveness, bronchial remodelling and chronic inflammation. Airway smooth muscle biology and pathophysiological implication in asthma are now better understood. Precise deciphering of intracellular signalling pathways regulating smooth muscle contraction highlighted the critical roles played by small GTPases of Rho superfamily. Beyond contractile considerations, active involvement of airway smooth muscle in bronchial remodelling mechanisms is now established. Not only cytokines and growth factors, such as fibroblasts growth factor or transforming growth factor- β , but also extracellular matrix composition have been demonstrated as potent phenotype modifiers for airway SMC. Although basic science knowledge has grown significantly, little of it has translated into improvement in asthma clinical practice. Evaluation of airway smooth muscle function is still limited to its contractile activity. Moreover, it relies on tools, such as spirometry, that give only an overall assessment and not a specific one. Interesting technics such as forced oscillometry or specific imagery (CT and MRI) give new perspectives to evaluate other aspects of airway muscle such as bronchial remodelling. Finally, except for the refinement of conventional bronchodilators, no new drug therapy directly targeting airway smooth muscle proved its efficacy. Bronchial thermoplasty is an innovative and efficient therapeutic strategy but is only restricted to a small proportion of severe asthmatic patients. New diagnostic and therapeutic strategies specifically oriented toward airway smooth muscle are needed to improve global asthma care.

INTRODUCTION

Airway smooth muscle cells (aSMC) derive mainly during embryogenesis from mesenchymal precursors, in parallel with epithelial buds, and are associated with the correct development of the airways tree.¹ Present all along the respiratory tree from the trachea to the bronchioles, it is conserved in vertebrae through evolution.² aSMCs are thought to maintain basal tone in bronchi and homogeneous lung ventilation through modulation of local airflow resistance.³ Though, its real

physiological role after development remains controversial in part due to the difficulties to design experimental procedure to test specific hypothesis (impact on mucus expulsion and cough, ventilation to perfusion matching etc).⁴ However, while the physiological role of aSMC is controversial, their involvement in airways diseases, especially in asthma, is now better understood.

Asthma is a respiratory condition defined by the association of variable respiratory symptoms, such as acute dyspnoea, chest tightness, wheezing and chronic cough, associated with impaired airflow and chronic bronchial inflammation.⁵ It is a frequent disease affecting around 250 million patients worldwide with an increased incidence for the last decade.⁶ Asthma treatment is mainly based on inhaled corticosteroids associated with long-acting and short-acting bronchodilators. The main objective of those treatments is to achieve a complete control of the disease.⁷

Asthma pathophysiological hallmark can principally be divided into three inter-related components: airway inflammation, airway hyper-responsiveness and airway remodelling (figure 1).

Inflammatory pathways involved in asthma course have been extensively studied. Two main pathophysiological pathways are now commonly accepted: eosinophilic (or type-2-driven asthma) and non-eosinophilic.⁸ Considering type-2-driven asthma, key inflammatory cytokines can be highlighted: interleukine (IL)-4 implicated in T-helper 2 polarisation and IgE switching, IL-5 associated with eosinophils production and trafficking and IL-13 that plays a central role in airway remodelling. Some biotherapies targeting those cytokines pathways had proven their efficiency in selected severe asthmatics and are now available in clinical practice.⁹ On the contrary, non-eosinophilic asthma, including paucigranulocytic and neutrophilic asthma, remains poorly understood.

Airway remodelling is defined by an association of structural modifications of bronchial

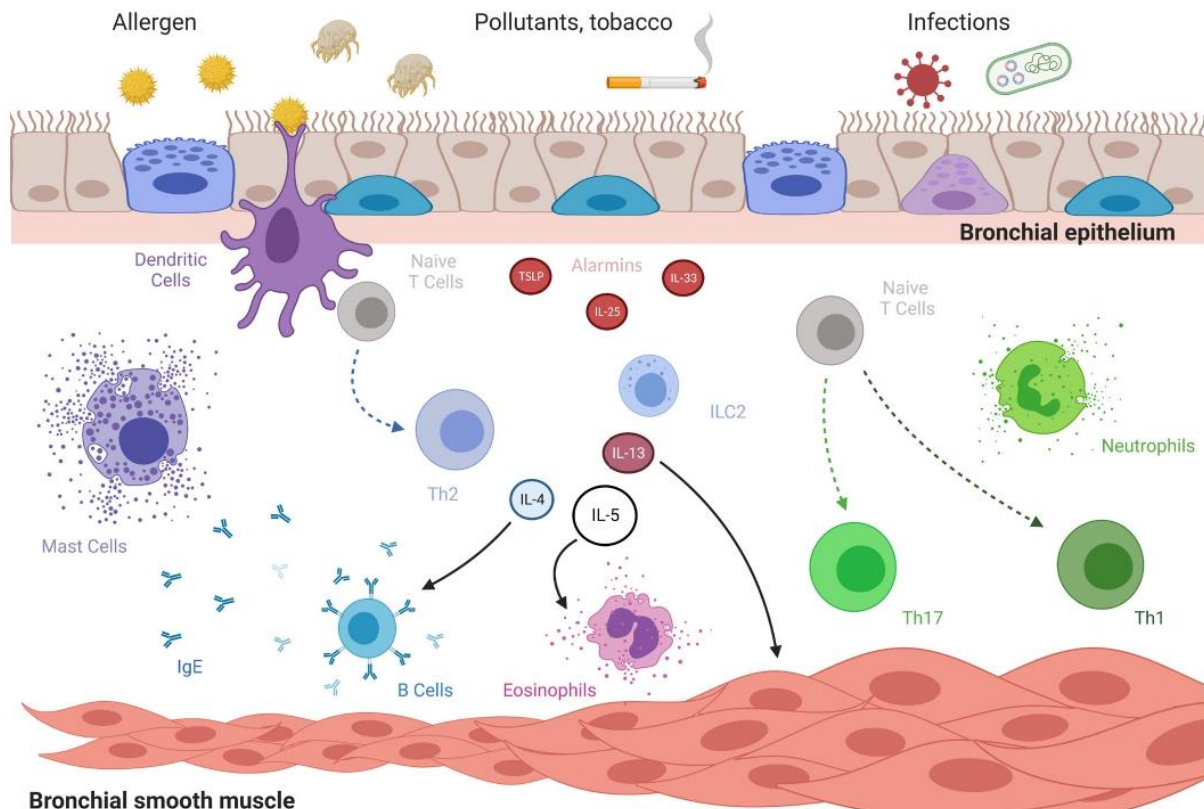


Figure 1 Pathophysiology of asthma. Under stimulation by noxious and/or harmless environment, bronchial epithelium secretes alarmins. Such molecules stimulate innate and adaptive immunity giving rise to infiltration of bronchi by eosinophils or neutrophils or both. Conversely, under sustained inflammation, bronchial remodelling developed with increased basal membrane thickness and hypertrophy and hyperplasy of bronchial smooth muscle. Along with specific bronchial smooth muscle cells acquired hypercontractility, all those mechanisms participate to airway hyper-responsiveness. IgE, immunoglobulin E; IL, interleukine; Th, T-helper cell, TSLP, thymic stromal lymphopoietin. Created with BioRender.com.

wall including aSMC alterations, epithelial dysfunction, reticular membrane thickening and oedema.^{10 11} Such lesions can be irreversible and lead to the progressive loss of respiratory function through time.¹² Airway remodelling unlinked with airway smooth muscle biology is presented elsewhere.¹³

Airways hyper-responsiveness (AHR) is defined by an exaggerated response of airways to harmless or harmful stimuli. This altered response of bronchi to environment depends on bronchial smooth muscle's activity, principal actor of bronchoconstriction. Noteworthy, inflammation, by acting on bronchial smooth muscle, is also closely linked to this phenomenon.

Although recent biotherapies critically improved asthma outcomes in severe asthmatic patients, some inflammatory endotypes, noteworthy non-eosinophilic asthma, remain orphan of efficient treatment.¹⁴⁻¹⁷ New strategies are evaluated in preclinical setup on non-inflammatory components, notably in aSMC. In this review, we will discuss the biological dysfunctions of the bronchial smooth muscle during asthma, the different techniques of evaluation of these dysfunctions in the

clinic as well as the existing or developing therapeutic strategies to manage them.

Biology of aSMC and role in asthma pathophysiology

aSMC contraction dysfunction in asthma

aSMC is essential in the development and sustainment of AHR. Ex vivo studies demonstrated that aSMC harvested from asthmatic subjects displayed increased maximum capacity and shortening velocity compared with controls.¹⁸ Moreover, aSMCs isolated from asthmatic patients presented a stronger contraction in response to histamine compared with controls.¹⁹ Contractile capacity of bronchial SMC principally depends on the phosphorylation of the 20 kDa myosin light chain (MLC₂₀), which leads to the activation of the contractile apparatus (figure 2). The phosphorylation level of MLC₂₀ is regulated by two enzymes: the myosin light chain kinase (MLCK) and the myosin light chain phosphatase (MLCP). Two distinct signalling pathways regulate the activity of these enzymes: the Ca²⁺ and the Ca²⁺ sensitisation pathway.

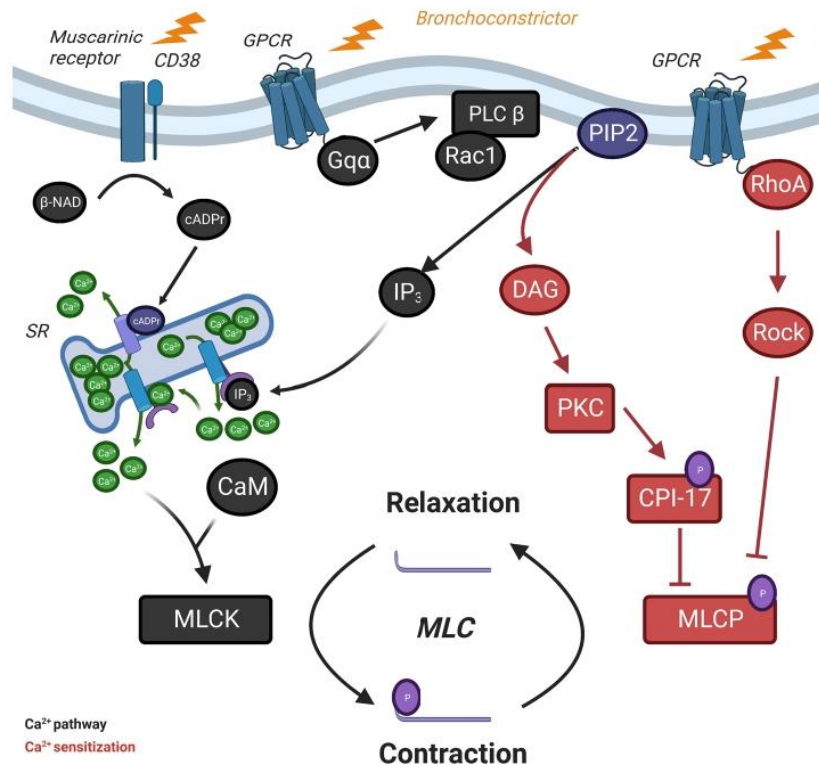


Figure 2 Intracellular regulation of airway smooth muscle cells contraction. Smooth muscle cells contraction and relaxation cycle depends on phosphorylation and dephosphorylation of MLC, respectively. Increase of intracellular Ca²⁺ concentration in response to bronchoconstrictor stimuli leads to the CaM-dependent activation of MLCK, which phosphorylates MLC: it is the Ca²⁺ pathway. In parallel, activation of RhoA–Rock pathways and CPI-17 deactivates MLCP, which prevents MLC from dephosphorylation: it is the Ca²⁺ sensitisation. β-NAD, beta-nicotinamide adenine dinucleotide; cADPr, cyclic adenosine diphosphate ribose; CaM; calmodulin; CD, cluster of differentiation; DAG, diacylglycerol; GPCR, G protein-coupled receptors; IP₃, inositol triphosphate; MLC, myosin light chain; MLCK, myosin light chain kinase; MLCP, myosin light chain phosphatase; PKC, protein kinase C; PLC, phospholipase C; PIP₂, phosphatidylinositol-4,5-bisphosphate; Rac1, Rac family small GTPase 1; ROCK, Rho kinase; RhoA, Rho family small GTPase A; SR, sarcoplasmic reticulum.

Considering the Ca²⁺ pathway, the phosphorylation of MLC₂₀ by MLCK leads to cross bridges with actin that conducts the aSMC contraction cycle. Interestingly, overexpression of MLCK in aSMC has been observed during asthma associated with its overcontractility.^{18–20} MLCK activity is principally controlled by the rise in cytosolic Ca²⁺ concentration coming from extracellular calcium influx through ion channels and sarcoplasmic reticulum (SR) calcium stores.²¹ SR stores release is principally triggered by the inositol 1,4,5-trisphosphate (IP₃) produced by activated phospholipase C (PLC) after the binding of contractile agonists to G protein-coupled receptors or to M₃ muscarinic receptors.²²

Recently, this signalling pathway has been complemented by studies demonstrating the involvement of the monomeric GTPase Rac1 in aSMC contraction. Rac1 protein is activated in murine and human aSMC by bronchoconstrictors such as methacholine leading to its association with the pleckstrin homology domain of PLC β₂ to potentiate the production of IP₃ required for aSMC contraction.²³ The relevance of this signalling pathway in

aSMC was highlighted by demonstrating that Rac1 was overactivated in aSMC from asthmatic patients as well as in aSMC from mice developing allergic asthma. In this experimental model, deletion of the Rac1 gene specifically in SMCs or pharmacological inhibition of Rac1 activity prevents AHR. These results identify the Rac1 protein as a new therapeutic target in respiratory pathologies associated with AHR.²³

Independently of IP₃ production, cyclic adenosine diphosphate ribose (cADPr) could activate the ryanodine receptors channel (RyR) on the SR leading to the liberation of Ca²⁺ from the internal SR stores.^{24–25} Such metabolite is produced from beta-nicotinamide adenine dinucleotide next to the stimulation of the muscarinic receptor M₃. Moreover, Ca²⁺ liberation is increased by Ca²⁺-induced Ca²⁺ release through RyRs, resulting in Ca²⁺ wave propagation and the simultaneous aSMC twitching.²⁶ In asthma, overexpression of CD38 induced by proinflammatory cytokines such as IL-1β, IL-13 and tumor necrosis factor-α leads to increased RyR activation by cADPr.^{24–27}



Calcium uptake and sustainment of ATP synthesis by mitochondria are essential to smooth muscle contraction.²⁸ Calcium uptake is mediated by the mitochondrial Ca^{2+} uniporter while its release mainly depends on $\text{Na}^{2+}/\text{Ca}^{2+}$ or $\text{H}^{+}/\text{Ca}^{2+}$ exchanger.²⁹ In aSMC from asthmatic patients, mitochondrial dysfunction can be observed. Downregulation of the expression of sarcoendoplasmic Ca^{2+} ATPases 2 is associated with the dysregulation of Ca^{2+} homeostasis in asthma.³⁰

The Ca^{2+} sensitisation pathway leads to a maximal contraction independently of the intracellular Ca^{2+} concentration by the regulation of the MLC_{20} phosphorylation state by MLCP. On the one hand, activation of protein kinase C by diacylglycerol leads to the phosphorylation of protein kinase C-potentiated phosphatase inhibitor protein of 17 kDa (CPI-17), which binds to the catalytic subunit of MLCP, inhibiting its phosphatase activity.³¹ On the other hand, activated RhoA interacts with its downstream effector Rho kinase (ROCK), which inactivates MLCP by phosphorylating its myosin-binding subunit.³² Moreover, ROCK can also regulate the activity of MLCP by the phosphorylation of CPI-17.^{31,33} Interestingly, expression and activity of CPI-17 are increased in aSMC from rats model of allergic asthma.³⁴ In parallel, several studies have shown an increase of RhoA expression in aSMC in animal models.³⁵ Inhibition of RhoA activity prevents and reverses AHR induced in allergic asthma models of guinea pigs.³⁶ Conversely, inflammatory cytokines can significantly influence Ca^{2+} sensitisation pathway. IL17A, a cytokine secreted by Th17 cells, is able to induce an upregulation of RhoA protein in human aSMC.³⁷ Conversely, it can also increase aSMC contraction by the activation of RhoA–ROCK2 through NF- κ B pathway.³⁸ Targeting IL-17 pathway with neutralising antibody decreased the expression of NF- κ B, ROCK-I and ROCK-II in lung parenchyma in a mouse model of asthma compared with controls.³⁹ Interestingly, it has been recently proven in mouse that combination of anti-IL17 antibodies along with ROCK inhibitor (Y-27632) significantly improved respiratory resistance, bronchial remodelling and inflammation.⁴⁰ Similar findings were observed with IL-13, which induces an increase in RhoA expression by aSMC.⁴¹ Those results suggest a potential role of Ca^{2+} sensitisation pathway dysfunction associated with asthma AHR.

Aside inflammatory cytokines, small molecules can also interact with the contractile apparatus such as nitric oxide (NO). In physiological conditions, NO is a potent bronchodilator through the production of cGMP by activated cytosolic guanylate cyclase leading to decreased intracellular Ca^{2+} .⁴² Bronchial NO mainly derived from epithelial cells on the one hand and inhibitory non-adrenergic non-cholinergic nerve terminals.^{43,44} Inhibition of NO synthesis by L-NG-Nitro arginine methyl ester in vitro and in vivo in guinea pigs enhances the airway hyper-responsiveness in response to histamine.⁴⁵ Though, its precise role in the context of asthma remains controversial.⁴⁶ Indeed, inflammatory environment, especially type

2 driven, is a potent activator of inducible NO synthase of type 2 in epithelial cells.^{47,48} Exhaled NO measured in asthmatic patients is correlated with AHR.^{49,50} Association of NO with worsened AHR, despite its physiological bronchodilator effect, can be partly explained by collateral damages linked with peroxynitrite production and side effects on vessels with increased permeability and bronchial oedema.

Autonomous innervation of aSMCs is another modulator of AHR. TRPA1 channels are located at sensory nerves, predominantly on C fibres and is also expressed in non-neuronal cells including airway inflammatory cells, SMC, epithelial cells and fibroblasts.⁵¹ Activation of TRPA1 by environmental irritants such as cigarette smoke or air pollution leads to the activation of bronchopulmonary C fibres in an experimental model and is implicated in cough.⁵² Inhibition or knockout of TRPA1 channels leads to an inhibition of neuropeptide release and airway hyperreactivity in an ovalbumin-challenged mice model of asthma.⁵³ Whether such pathway is implicated in human asthma pathophysiology remains to be demonstrated.

aSMC beyond contraction: bronchial remodeling

Airway remodelling presentation may differ between groups of moderate-to-severe asthmatic patients in terms of aSMC mass and basement membrane thickening.⁵⁴ Interestingly, airway remodelling can appear early in asthma, even in children.^{55,56} Significant bronchial remodelling in childhood, characterised by reticular basement thickening and increased aSMC mass, is associated with severe disease.⁵⁷ Moreover, airway remodelling is also associated with persistent obstruction in severe asthmatic children.⁵⁸ Those elements are in favour of an early role played by airway remodelling in asthma natural course.

Physiologically, aSMC presents low proliferation capacities and a contractile phenotype characterised by the expression of sm- α -actin, smooth muscle γ -actin, smooth muscle myosin heavy chain, calponin, h-caldesmon, SM22, smoothelin and metavinculin.⁵⁹ Though, in inflammatory environment, aSMC have the ability to switch their phenotype with an increase of their proliferation and migration capacity leading to hyperplasia.⁶⁰ Mitochondria biogenesis is also affected. In proliferative aSMC from asthmatic patients, increased mitochondrial mass and activity can be observed associated with altered calcium homeostasis.⁶¹

Phenotype switch can be induced in vitro by several growth factors and cytokines presented in table 1. Analysis of induced sputum in asthmatics showed that many of these molecules are indeed oversecreted.⁶² Bronchial inflammation associated with remodelling can be driven by the environment through the ability of bronchial epithelium to secrete alarmins, namely thymic stromal lymphopoietin (TSLP), IL-25 and IL-33, in response to harm.¹¹ It has been demonstrated that human aSMC expressed receptor to TSLP and IL-25 and that their

Table 1 Mitogenic factors of aSMC

Factors	Cellular source	Effects	Ref
Growth factors			
PDGF	Platelets, monocytes/macrophages, ASMC, epithelium	Pro-proliferative	123–126
FGF	Extracellular matrix, monocytes/macrophages, ASMC	Pro-proliferative	126–129
EGF	Epithelium, platelets	Pro-proliferative	130
Cytokines			
TGF- β	ASMC, T-lymphocytes, epithelium	Pro-proliferative	128 131–133
TNF- α	ASMC, epithelium, T cells, monocytes/macrophages	Pro-proliferative, antiproliferative	126 134–136
IL-1 β	T cells, monocytes/macrophages, ASMC, epithelium	Pro-proliferative	137 138
IL-6	T cells, monocytes/macrophages, ASMC, epithelium	Pro-proliferative	135 138
IFN- γ	T cells, NK cells	Antiproliferative	139
IL-4	T-cell, mast cells	Antiproliferative	140 141
Inflammatory mediators			
Histamine	Mast cells, basophils	Pro-proliferative	142 143
Thromboxane A2	Mast cells, monocytes/macrophages	Pro-proliferative	144 145
Sphingosine 1-phosphate	Plasma, platelets	Pro-proliferative	146
Enzymes and diverse			
Tryptase	Mast cells	Pro-proliferative	143 147
Thrombin	Plasma	Pro-proliferative	148
Elastase	Neutrophils	Pro-proliferative	149
Reactive oxygen species	Monocytes–macrophages, neutrophils, eosinophils, mast cells	Pro-proliferative	150

aSMC, airway smooth muscle cells; EGF, epidermal growth factor; FGF, fibroblast growth factor; IFN, interferon; IL, interleukine; PDGF, platelet-derived growth factor; TGF- β , transforming growth factor- β ; TNF- α , tumor necrosis factor- α .

stimulation lead to proinflammatory and synthetic phenotypes.^{63 64} Conversely, it has been shown by air–liquid interface coculture that injured epithelial cells stimulate aSMC proliferation through the production of proinflammatory molecules (IL-6, IL-8, monocyte chemoattractant protein-1) and matrix metalloproteinase-9.⁶⁵ Mechanical stimulation of epithelial cells is another path leading to phenotype switch of aSMC. A significant proliferation of aSMC could be induced in vitro by compression of epithelial cells.⁶⁶ Combination of inflammatory cytokines, such as type 2 cytokines, leads to complex modification of aSMC phenotype. For example, whereas IL-13 alone have an antiproliferative effect on cultured aSMC, it also increases the expression of CysLT1 receptor enhancing leukotriene induced proliferation.^{67 68} Interestingly, stimulated aSMC are also able to synthesise proinflammatory factors such as the platelet-derived growth factor (PDGF), fibroblasts growth factor, IL-1 β , transforming growth factor- β , IL-5, IL-6, IL-8, IL-17, which further amplifies phenotype switch.³

Composition of the extracellular matrix (ECM) itself also influences the phenotype and functions of aSMC.⁶⁹ Laminin reduces the aSMC proliferation and increases the expression of contractile proteins such as sm- α -actin and smooth muscle myosin heavy chain.⁷⁰ On the contrary, fibronectin promotes the aSMC proliferation

but decreases the expression of contractile proteins.⁷⁰ During asthma, the synthesis of laminin is reduced while the fibronectin synthesis is increased promoting the switch of aSMC to a proliferative phenotype.⁷¹ In response, aSMC participate to the deposition of the ECM through increased MMP-9 and MMP-12 expressions as it has been shown in bronchial biopsies from severe asthmatic patients.⁷²

At a cell signalling level, aSMC proliferation is principally under the control of extracellular signal-regulated kinase (ERK) and PI3K pathways by increased expression of cyclin D1. ERK protein, a member of the MAPK family, is a central regulator of cell cycle entry and G1 progression essential to aSMC proliferation.⁷³ In parallel, Akt1, an effector of PI3K, inhibits the constitutively active glycogen synthase kinase 3 and an activator mTOR and p70 S6 kinase which are important for transcriptional activation and protein translation leading to aSMC proliferation and hypertrophy.⁷⁴ PI3K can also activate Rac1 and Cdc42 in order to promote the cell proliferation thanks to cyclin D1.⁷⁵ In addition, Rac1 forms part of the Nicotinamide Adenine Dinucleotide Phosphate (NADPH) oxidase complex and also participates in the reactive oxygen species production which is involved in the aSMC mitogenesis.⁷⁶ We recently demonstrated that Rac1 was essential to the increased proliferation capacities of aSMC



from asthmatic patients in comparison to controls in basal condition and after mitogenic stimulation.⁷⁷ We identified the signal transducer and activator of transcription 3 as the main effectors involved in such Rac1-dependent mechanism. Interestingly, inhibition of Rac1 activity in a mouse model of asthma prevented aSMC hyperplasia. aSMC hyperplasia also results from the migration of aSMC or progenitors in response to mitogen factors such as the PDGF, the vascular endothelial growth factor, the transforming growth factor β (TGF- β) or IL-1 β . The P38 MAPK, PI3K and ERK pathways are involved in migration as their inhibition leads to decreased aSMC migration due to reduced phosphorylation of heat shock protein 27 implicated in the F-actin polymerization necessary for cell motility.⁷⁸ Moreover, the migration of aSMC in response to PDGF is significantly impacted by the inhibition of PI3K, ERK or ROCK pathway.^{79,80}

Aside its proliferative capacity, activated aSMC also demonstrate improved capacity to interact with immune cells through increased expression of their surface molecules such as VCAM-1, ICAM-1, CD44 and LFA-1.⁸¹ Noteworthy, aSMC display closed interaction with mast cells and are able to synthesize powerful mastocyte chemotactic agents such as the stem cell factor but also TGF- β 1 and tumour suppressor in lung cancer-1.⁸² In parallel, aSMC express both CD44 and CD51 which are involved in the mast cell adhesion.⁸³ Interaction of mast cells with aSMC promotes the degranulation and cytokines production by mast cells ultimately leading to aSMC contraction and proliferation.⁸⁴ aSMC can also interact with other immune cell types such as T cells via CD44, which induces DNA synthesis of aSMC and promotes its proliferation.⁸⁵

As presented, aSMC has important impacts on asthma pathophysiology not solely due to their contractile activity but also to their ability to interact with other cell types leading to complex remodelling activity. Such a broad involvement makes the clinical evaluation of its action at a patent level complex, as it is discussed in the next section.

Bronchial smooth muscle in asthma clinical practice

In routine practice, evaluation of aSMC's function cannot be fulfilled directly. Indeed, conventional pulmonary function tests, such as spirometry and plethysmography only give access to an overall sight of their implication in airway obstruction. New tools currently developed to further assess new facets of its function are described below.

Airway obstruction in asthma

Airway obstruction is necessary to asthma diagnosis along with relevant and consistent respiratory symptoms. Pulmonary function tests in asthma, particularly forced spirometry, are standardised and aim to prove such obstruction.⁸⁶ Evolution of obstruction through time is critical considering asthma care. Data from birth cohorts showed that children with low forced expiratory volume

in one second (FEV1)/forced vital capacity (FVC) ratio had a steeper slope of evolution of FEV1/FVC ratio through time until adulthood that increases the risk of developing asthma.⁸⁷ In parallel, patients self-reporting asthma experienced a faster decline of FEV1 through time than healthy volunteers in a 15-year prospective study performed in Denmark.⁸⁸

Bronchodilators response tests are available to assess the role of bronchial smooth muscle contraction in obstruction for an individual patient.⁸⁶ However, negative bronchodilator test does not imply that aSMC are not relevant in asthma symptoms. Indeed, a fixed obstruction (FEV1/FVC ratio under lower limit of normal values and/or FEV1 under 80% of predicted value after bronchodilators) can appear in about 20% of never ever-smoking adult asthmatic patients after 10 years of follow-up.⁸⁹ Such persistent airway obstruction had been linked with increased airway smooth muscle area in a population of severe asthmatics under standardised high dose anti-inflammatory treatment.⁹⁰ Though, airway remodelling is not only dependent on aSMC. It has been shown recently by cluster analysis of pathological examination of bronchial biopsies from asthmatic patients and healthy individuals that bronchial remodelling could be classified into several groups depending on the component involved (bronchial smooth muscle, basal membrane).⁵⁴

Considering small airways impairment in asthma, available explorations are currently imperfect. A study highlighted that mid-expiratory and instantaneous flows (FEF25-75 and FEF75) did not significantly add informations to FEV1 and FEV1 to FVC ratio.⁹¹ Use of impulse oscillometry and nitrogen breath washout technics identified around 1/3 of asthmatic patients displaying markers of small airways dysfunction.⁹² Though, data clearly linking pathology with oscillometric data are still lacking. Conversely, specific imagery approaches are currently assessed. Non-invasive evaluation of obstruction by hyperpolarized ³HE MRI showed that ventilation defects due to obstruction often persisted in time and location under stable or provoked (methacholine) conditions in a small series of patients.⁹³ Interestingly, markers of ventilation heterogeneity linked to small airways involvement inversely correlated with variation of asthma control score under inhaled corticosteroid treatment of asthmatic patients.⁹⁴ Nevertheless, MRI lacks availability needed for clinical practice.

Airway hyper-responsiveness in asthma

AHR is an important argument in favour of asthma diagnosis that can be sought by direct and indirect provocation bronchial tests.^{95,96} Methacholine and histamine tests are the principal direct provocation tests available. They aim at triggering direct bronchial smooth muscle contraction through inhalation of determined cumulative doses of stimulant. However, this test explores only selected pathways of bronchial smooth muscle contraction to the exclusion of the others described in the previous sections. In addition, its overall sensitivity is around 60%–90% and

Table 2 Effect of approved biotherapies on pulmonary function tests in allergic and eosinophilic severe asthma (phase III trials)

Phenotype Endotype	Molecule Type	Target	Main inclusion criteria	Effect on respiratory function	Ref
Allergic	Omalizumab Humanised monoclonal antibody	IgE	Severe asthma with high dose ICS Positive SPT to aeroallergen Serum total IgE 30–700 IU/mL	Improved morning PEF +2.8% predicted FEV1 in comparison with placebo	15 106
Eosinophilic	Mepolizumab Humanised monoclonal antibody	IL-5	Severe asthma with high dosage ICS. Peripheral blood eosinophils count $\geq 150/\text{mm}^3$ at screening or $\geq 300/\text{mm}^3$ during the previous year. + Maintenance treatment with systemic corticosteroids (5–35 mg of prednisone or equivalent) ⁴	Slight improvement of pre-BD and post-BD FEV1 (+98 mL, +138 mL, respectively) in comparison with placebo Statistically non-significant improvement of pre-BD and post-BD FEV1 in the corticosteroid weaning trial	14 151
Eosinophilic	Reslizumab Humanised monoclonal antibody	IL-5	Inadequately controlled asthma despite at least medium dosage ICS. Peripheral blood eosinophils count $\geq 400/\text{mm}^3$	Statistically significant improvement of pre-BD FEV1 in comparison with placebo (+0.11 L LS mean)	152
Eosinophilic	Benralizumab Humanised monoclonal antibody	IL-5 receptor	Severe asthma with high dosage ICS. Baseline peripheral blood eosinophils count $\geq 300/\text{mm}^3$	Statistically significant improvement of pre-BD FEV1 in comparison with placebo in SIROCCO and CALIMA studies (+159 mL and +116 mL, respectively, LS mean)	16 153 154
Type-2 inflammation	Dupilumab Fully human monoclonal antibody	IL-4 receptor α	Uncontrolled asthma despite medium to high dosage ICS and up to two controller	Statistically significant improvement of pre-BD FEV1 in comparison with placebo at 12 wks (+130 mL LS mean) and 24 wks (+ 220 mL LS mean).	17 108
Eosinophilic and non-eosinophilic	Tezepelumab Fully human monoclonal antibody	TSLP	Uncontrolled asthma despite medium to high dosage ICS	Statistically significant improvement of pre-BD FEV1 in comparison with placebo at 52 wks (+130 mL LS mean)	110

BD, bronchodilators; FEV1, forced expiratory volume in one second; ICS, inhaled corticosteroid; IgE, immunoglobuline E; IL-5, interleukine 5; LS, least squares; PEF, peak expiratory flow; SPT, skin prick test; TSLP, thymic stromal lymphopoietin; wks, weeks.

specificity around 90%.⁹⁷ Its use in clinical practice is then principally reserved to intermediate probability of asthma at diagnosis and is not recommended for follow-up.

Indirect tests mainly include exercise-induced and eucapnic hyperventilation tests. The objective of such tests is to provoke a deshydration of respiratory airways that stimulates the secretion of various cytokines and inflammatory mediators by bronchial epithelium and sub-mucosa triggering hypersensitive aSMC contraction.⁹⁶ Exercise-induced bronchoconstriction is associated with asthma with a good specificity but low sensitivity. In an overall population, exercise-induced bronchoconstriction under standardised exercise correlated with airflow limitation (FEV1) but also with age and sex.⁹⁸ Noteworthy, some patients displaying significant positive indirect AHR tests would not react to direct stimulation of airway smooth muscle contraction.⁹⁹

Unmet needs in aSMC functional evaluation in asthma

Diagnostic tools determining the exact role played by bronchial smooth muscle in asthma at an individual level

need to be developed. Indeed, spirometry isn't sufficient to precisely incriminate the responsible agent (inflammation, bronchial smooth muscle, infection triggers, combination of those). Tests specifically exploring bronchial contractility and its determinants could potentially be of interest in order to guide therapy, particularly concerning the use of long-acting bronchodilators. Conversely, it would be interesting to evaluate the proliferative activity of bronchial smooth muscle in order to early detect and prevent bronchial remodelling. Finally, the improvement of physiopathological knowledge could lead to the development of new targeted therapeutic strategies alongside their specific biomarkers.

aSMC as a target in asthma

Conventional therapies: inhaled and oral treatments

Conventional therapies in asthma principally target 2 pathophysiological mechanisms: inflammation and bronchoconstriction. Inhaled bronchodilators (beta-2 agonist and anticholinergic) directly target aSMC by decreasing



its contractility in order to improve airflow and limit chronic and acute symptoms. Though, pharmacological researches mainly focused on the improvement of the length and/or delay of action. Interestingly, a proof-of-concept clinical trial showed in a small cohort of severe asthmatics (31 patients) that gallopamil, a calcium ion channel inhibitor, could reduce the aSMC bronchial area and thickness after 1 year of treatment in comparison with baseline associated with reduced exacerbation after the end of treatment.¹⁰⁰ However, further clinical trials were withdrawn by the pharmaceutical companies.

Even if inhaled corticosteroids target principally inflammatory effectors, it also affects aSMC contractility and proliferation. Glucocorticoids reduce the expression of α -smooth actin and the short isoform of MLCK by aSMC in response to TGF- β which dampens its contractility.¹⁰¹

It also decreases the expression and phosphorylation of CPI-17 by aSMC in a rat model leading to lower MLC phosphorylation and improved AHR.¹⁰² Furthermore, ciclesonide effectively reduced key bronchial remodeling features, such as goblet cell hyperplasia or immune reactive aSMC, in a rat model of asthma.¹⁰³ Considering bronchial remodeling, high doses of inhaled steroids also improved the submucosal hypervascularity but also the basement membrane thickness in small clinical studies.^{104,105}

Biotherapies and aSMC

No biotherapy directly targeting aSMC is currently under clinical development to our knowledge. However, available biotherapies that target inflammation can have implication in aSMC (table 2).

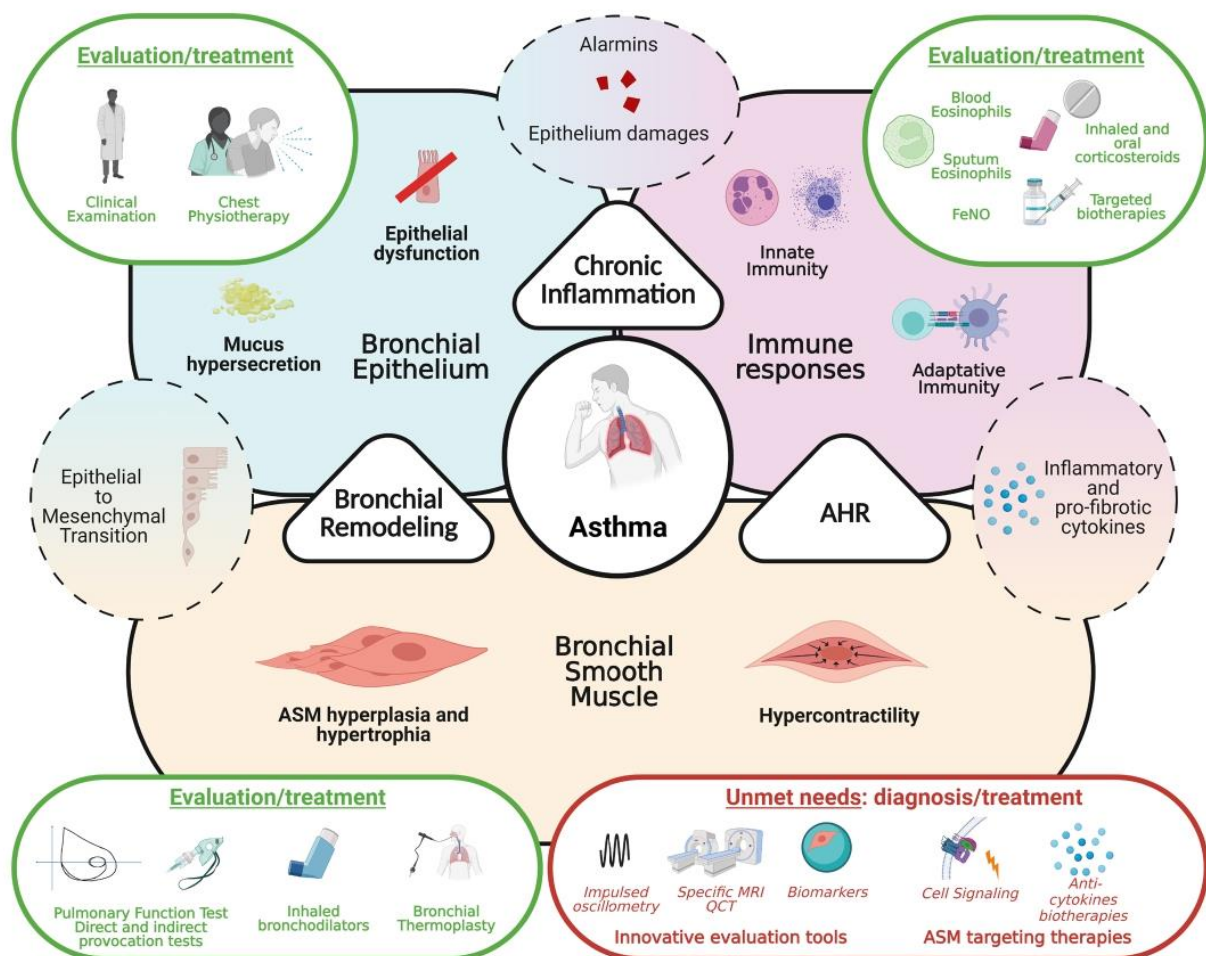


Figure 3 Bronchial smooth muscle cells in asthma from pathophysiological consideration to evaluation and treatments. Asthma development relies on three main pathophysiological processes, bronchial remodeling, chronic inflammation and airway hyper-responsiveness, consequences of alteration of bronchial epithelium and ASM and development of inadequate immune responses. Whereas anti-inflammatory therapeutic strategies got significantly improved in the last years, little progress has been made considering ASM. Innovative precise evaluation tools of ASM function along with specific targeting strategies need to be developed. AHR, airway hyper-responsiveness; ASM, airway smooth muscle; FeNO, exhaled fraction of azote monoxide.

Omalizumab is a humanised monoclonal antibody targeting immunoglobulin (Ig) E to treat severe allergic asthmatic patients. Phase III study demonstrated that omalizumab significantly improves asthma exacerbation rate compared with placebo.^{15 106} It also showed that omalizumab could slightly improve morning peak expiratory flow and FEV1. Monoclonal antibodies targeting IL-5 pathway namely mepolizumab, reslizumab and benralizumab are now approved to be used to treat severe eosinophilic asthma.¹⁰⁷ Considering improvement of prebronchodilator and postbronchodilator FEV1, biotherapies targeting IL-5 reached statistical significance overall, though clinical significance remains questionable (about +100 mL vs placebo). Conversely, dupilumab, a fully human monoclonal antibody targeting IL-4 receptor α also demonstrated a significant reduction of exacerbation rate and efficient oral corticosteroid tapering in patients suffering of uncontrolled moderate to severe asthma.^{17 108} Interestingly, a significant improvement of FEV1 under treatment with dupilumab was observed at 24 weeks of treatment with mean difference above 200 mL.¹⁰⁸ In a real-life asthma cohort, dupilumab also improved FEV1 by 10% (predicted values) after 1 year of treatment.¹⁰⁹ Recently, a treatment with tezepelumab, a human monoclonal antibody targeting the TSLP, lead to a 130 mL increase of pre bronchodilator FEV1 in comparison with the control group.¹¹⁰ Such improvements, to be confirmed in the long term, tends to underline the importance of the interactions between inflammation and bronchial smooth muscle and the interest in simultaneously targeting multiple actors.

Few trials specifically studied the effect of biotherapies on pulmonary functions. Benralizumab failed to significantly improve prebronchodilator FEV1 and hyperinflation in SOLANA trial.¹¹¹ To note, this trial aimed at assessing benralizumab efficiency at short-term (84 days) and potentially lack interesting effects on obstruction through prolonged treatment. Small-sized clinical studies have shown that mepolizumab could possibly improve small airway function evaluated by multiple-breath nitrogen washout test and forced oscillometry after a few months of treatments.¹¹²

Bronchial thermoplasty

In order to specifically target bronchial wall including aSMC, an interventional endoscopic technic was developed: bronchial thermoplasty. Its objective is to lower the airway wall thickness by direct thermic energy application. In AIR-2 clinical trial, bronchial thermoplasty significantly improved quality of life with a trend in favour of better asthma control through lower exacerbation rate in comparison with the sham group.¹¹³ Good long-term tolerance has been shown after 5 years of follow-up.¹¹⁴ Considering bronchial remodelling, in a small prospective case series (n=11), bronchial thermoplasty slightly decreased the airway wall thickness and air-trapping 2 years after the procedure, even if no significant improvement of airway lumen could be observed.¹¹⁵ However,

no significant effect had been observed on small airways evaluated by oscillometry 6 months after the procedure, despite significantly improved clinical markers.¹¹⁶ Interestingly, a proof-of-concept pilot study found that bronchial thermoplasty could nevertheless improve dynamic hyperinflation in selected patients.¹¹⁷ Though, such results need to be confirmed in larger and control clinical studies.

Data about bronchial thermoplasty effects on airways physiology and asthma pathophysiology are now available. aSMC area (α -SMA staining) significantly decreased in short term (6 weeks) after bronchial thermoplasty consistent with lower smooth muscle mass.¹¹⁸ The TASMA randomised clinical study confirmed such data by including a parallel delayed bronchial thermoplasty group of severe asthmatic patients as controls.¹¹⁹ Nevertheless, modification of aSMC mass did not correlate with improvement of asthma control and related quality of life scores (Asthma Control Questionnaire, Asthma Quality of Life Questionnaire). In parallel, it was recently reported that bronchial thermoplasty induced a decrease of mucus production assessed by MUC5AC epithelial expression at 12 months post procedure.¹²⁰ Bronchial thermoplasty can also modify cell cross-talk between the different components of airway wall. It has been reported that it blocked the production and secretion of heat-shock protein-60 by the epithelium that triggered in part remodelling in asthma by fibroblasts.¹²¹

Unmet needs in targeted treatment of aSMC in asthma

Few innovative strategies targeting specifically aSMC are available. Although bronchial thermoplasty has shown interesting results, this technique remains complex and reserved to a limited number of patients. Besides, in an era of precision medicine, tools that predict response to a treatment strategy in an individual setting are essential. Few studies are available concerning such biomarkers to predict efficacy of bronchial thermoplasty. Fixed or reversible obstruction status was not significantly associated with clinical response to bronchial thermoplasty.¹²² Small molecules that directly target key signalling pathways implicated in aSMC contraction and proliferation could be an interesting therapeutic opportunity. For example, inhibition of Rho and Rac activation could potentially reduce airway hyper-responsiveness and remodelling. Nevertheless, those have long been considered as undruggable due to their ubiquitous expression and critical biological roles that could lead to serious side effects. The identification of tissue and condition specific regulators of Rho superfamily activation, such as guanine exchange factors, could be a promising way to overcome such limit.

CONCLUSION

Asthma represents a broad-spectrum disease involving at different levels epithelial dysfunction, sustained bronchial inflammation and bronchial smooth muscle



dysfunction. Knowledge about bronchial smooth muscle role in asthma pathophysiology had been considerably improved (figure 3). Mechanisms of bronchial contraction are better understood and new intracellular pathways had been discovered. However, aSMC should not be only considered as simple contraction actors. Indeed, implication of aSMC airway remodelling and their secretion capacities are far more important than previously expected.

In routine practice, aSMC functions are mainly assessed through pulmonary function tests and provocation tests. Innovative tools such as forced oscillometry and dedicated imaging are used in clinical research but did not reach clinical practice yet. In parallel, improvement of basic sciences comprehension of airway smooth muscle biology doesn't lead to real targeted strategies for now. On the one hand, bronchodilators developed for the last decades mainly targeted the same pathways (adrenergic and muscarinic receptors) and on the other hand, bronchial thermoplasty still lacks predictors of success even though promising results have been described. Development of tools to better assess aSMC activity in clinical practice along with new targeted treatment are mandatory to identify patients for whom SMC dysfunction is preponderant and need to be specifically treated.

Contributors DH, LR and VS drafted the manuscript. DH and LR drew the figures. F-XB, AM, GL and VS critically revised the manuscript. All authors gave their final approval for publication.

Funding This work was supported by a grant from the French Regional Council of Pays de la Loire, IRSR-PL project StaRac. DH is supported by a scholarship from Foundation pour la Recherche Médicale, poste pour internes et assistants program, FDM201906008829.

Competing interests None declared.

Patient consent for publication Not applicable.

Ethics approval Not applicable.

Provenance and peer review Not commissioned; externally peer reviewed.

Open access This is an open access article distributed in accordance with the Creative Commons Attribution Non Commercial (CC BY-NC 4.0) license, which permits others to distribute, remix, adapt, build upon this work non-commercially, and license their derivative works on different terms, provided the original work is properly cited, appropriate credit is given, any changes made indicated, and the use is non-commercial. See: <http://creativecommons.org/licenses/by-nc/4.0/>.

ORCID iD

François-Xavier Blanc <http://orcid.org/0000-0001-7644-2188>

REFERENCES

- 1 Badri KR, Zhou Y, Schuger L. Embryological origin of airway smooth muscle. *Proc Am Thorac Soc* 2008;5:4–10.
- 2 Cieri RL. Pulmonary smooth muscle in vertebrates: a comparative review of structure and function. *Integr Comp Biol* 2019;59:10–28.
- 3 Berger P, Marthan R, Tunon de Lara J-M. [The pathophysiological role of smooth muscle cells in bronchial inflammation]. *Rev Mal Respir* 2002;19:778–94.
- 4 Mitzner W. Airway smooth muscle: the appendix of the lung. *Am J Respir Crit Care Med* 2004;169:787–90.
- 5 Reddel HK, Bateman ED, Becker A, et al. A summary of the new GINA strategy: a roadmap to asthma control. *Eur Respir J* 2015;46:622–39.
- 6 D'Amato G, Vitale C, Molino A, et al. Asthma-related deaths. *Multidiscip Respir Med* 2016;11:37.
- 7 Chung KF, Wenzel SE, Brozek JL, et al. International ERS/ATS guidelines on definition, evaluation and treatment of severe asthma. *Eur Respir J* 2014;43:343–73.
- 8 Carr TF, Zeki AA, Kraft M. Eosinophilic and Noneosinophilic asthma. *Am J Respir Crit Care Med* 2018;197:22–37.
- 9 Agache I, Beltran J, Akdis C, et al. Efficacy and safety of treatment with biologicals (benralizumab, dupilumab, mepolizumab, omalizumab and reslizumab) for severe eosinophilic asthma. A systematic review for the EAACI Guidelines - recommendations on the use of biologicals in severe asthma. *Allergy* 2020;75:1023–42.
- 10 Pascual RM, Peters SP. Airway remodeling contributes to the progressive loss of lung function in asthma: an overview. *J Allergy Clin Immunol* 2005;116:quiz 487:477–86.
- 11 Lambrecht BN, Hammad H. The airway epithelium in asthma. *Nat Med* 2012;18:684–92.
- 12 Bumbacea D, Campbell D, Nguyen L, et al. Parameters associated with persistent airflow obstruction in chronic severe asthma. *Eur Respir J* 2004;24:122–8.
- 13 Hough KP, Curtiss ML, Blain TJ, et al. Airway remodeling in asthma. *Front Med* 2020;7:191.
- 14 Ortega HG, Liu MC, Pavord ID, et al. Mepolizumab treatment in patients with severe eosinophilic asthma. *N Engl J Med* 2014;371:1198–207.
- 15 Holgate ST, Chuchalin AG, Hebert J. Omalizumab 011 International study G. efficacy and safety of a recombinant anti-immunoglobulin E antibody (omalizumab) in severe allergic asthma. *Clin Exp Allergy* 2004;34:632–8.
- 16 FitzGerald JM, Bleecker ER, Nair P, et al. Benralizumab, an anti-interleukin-5 receptor α monoclonal antibody, as add-on treatment for patients with severe, uncontrolled, eosinophilic asthma (CALIMA): a randomised, double-blind, placebo-controlled phase 3 trial. *Lancet* 2016;388:2128–41.
- 17 Castro M, Corren J, Pavord ID, et al. Dupilumab efficacy and safety in moderate-to-severe uncontrolled asthma. *N Engl J Med* 2018;378:2486–96.
- 18 Ma X, Cheng Z, Kong H, et al. Changes in biophysical and biochemical properties of single bronchial smooth muscle cells from asthmatic subjects. *Am J Physiol Lung Cell Mol Physiol* 2002;283:L1181–9.
- 19 Matsumoto H, Moir LM, Oliver BGG, et al. Comparison of gel contraction mediated by airway smooth muscle cells from patients with and without asthma. *Thorax* 2007;62:848–54.
- 20 Benayoun L, Druilhe A, Dombret M-C, et al. Airway structural alterations selectively associated with severe asthma. *Am J Respir Crit Care Med* 2003;167:1360–8.
- 21 Murray RK, Fleischmann BK, Kotlikoff MI. Receptor-activated Ca influx in human airway smooth muscle: use of Ca imaging and perforated patch-clamp techniques. *Am J Physiol* 1993;264:C485–90.
- 22 Sanderson MJ, Delmotte P, Bai Y, et al. Regulation of airway smooth muscle cell contractility by Ca²⁺ signaling and sensitivity. *Proc Am Thorac Soc* 2008;5:23–31.
- 23 André-Grégoire G, Dilasser F, Chesné J, et al. Targeting of Rac1 prevents bronchoconstriction and airway hyperresponsiveness. *J Allergy Clin Immunol* 2018;142:e823:824–33.
- 24 Deshpande DA, Walseth TF, Panettieri RA, et al. CD38/Cyclic ADP-ribose-mediated Ca²⁺ signaling contributes to airway smooth muscle hyper-responsiveness. *Faseb J* 2003;17:452–4.
- 25 Deshpande DA, White TA, Guedes AGP, et al. Altered airway responsiveness in CD38-deficient mice. *Am J Respir Cell Mol Biol* 2005;32:149–56.
- 26 Perez JF, Sanderson MJ. The frequency of calcium oscillations induced by 5-HT, ACh, and KCl determine the contraction of smooth muscle cells of intrapulmonary bronchioles. *J Gen Physiol* 2005;125:535–53.
- 27 Deshpande DA, Dogan S, Walseth TF, et al. Modulation of calcium signaling by interleukin-13 in human airway smooth muscle: role of CD38/cyclic adenosine diphosphate ribose pathway. *Am J Respir Cell Mol Biol* 2004;31:36–42.
- 28 Tarasov AI, Griffiths EJ, Rutter GA. Regulation of ATP production by mitochondrial Ca²⁺. *Cell Calcium* 2012;52:28–35.
- 29 Delmotte P, Sieck GC. Interaction between endoplasmic/sarcoplasmic reticulum stress (ER/SR stress), mitochondrial signaling and Ca²⁺ regulation in airway smooth muscle (ASM). *Can J Physiol Pharmacol* 2015;93:97–110.
- 30 Mahn K, Hirst SJ, Ying S, et al. Diminished sarco/endoplasmic reticulum Ca²⁺ ATPase (SERCA) expression contributes to airway remodelling in bronchial asthma. *Proc Natl Acad Sci U S A* 2009;106:10775–80.
- 31 Sakai H, Hirano T, Takeyama H, et al. Acetylcholine-Induced phosphorylation of CPI-17 in rat bronchial smooth muscle: the roles of Rho-kinase and protein kinase C. *Can J Physiol Pharmacol* 2005;83:375–81.

- 32 Feng J, Ito M, Ichikawa K, *et al.* Inhibitory phosphorylation site for Rho-associated kinase on smooth muscle myosin phosphatase. *J Biol Chem* 1999;274:37385–90.
- 33 Koyama M, Ito M, Feng J, *et al.* Phosphorylation of CPI-17, an inhibitory phosphoprotein of smooth muscle myosin phosphatase, by Rho-kinase. *FEBS Lett* 2000;475:197–200.
- 34 Sakai H, Chiba Y, Hirano T, *et al.* Possible involvement of CPI-17 in augmented bronchial smooth muscle contraction in antigen-induced airway hyper-responsive rats. *Mol Pharmacol* 2005;68:145–51.
- 35 Chiba Y, Ueno A, Shinozaki K, *et al.* Involvement of RhoA-mediated Ca²⁺ sensitization in antigen-induced bronchial smooth muscle hyperresponsiveness in mice. *Respir Res* 2005;6:4.
- 36 Schaafsma D, Bos IST, Zuidhof AB, *et al.* The inhaled Rho kinase inhibitor Y-27632 protects against allergen-induced acute bronchoconstriction, airway hyperresponsiveness, and inflammation. *Am J Physiol Lung Cell Mol Physiol* 2008;295:L214–9.
- 37 Chiba Y, Tanoue G, Suto R, *et al.* Interleukin-17A directly acts on bronchial smooth muscle cells and augments the contractility. *Pharmacol Rep* 2017;69:377–85.
- 38 Kudo M, Melton AC, Chen C, *et al.* IL-17A produced by $\alpha\beta$ T cells drives airway hyper-responsiveness in mice and enhances mouse and human airway smooth muscle contraction. *Nat Med* 2012;18:547–54.
- 39 Camargo LdoN, Righetti RF, Aristóteles LRdeCRB, *et al.* Effects of Anti-IL-17 on inflammation, remodeling, and oxidative stress in an experimental model of asthma exacerbated by LPS. *Front Immunol* 2017;8:1835.
- 40 Dos Santos TM, Righetti RF, Camargo LdoN, *et al.* Effect of Anti-IL17 antibody treatment alone and in combination with Rho-kinase inhibitor in a murine model of asthma. *Front Physiol* 2018;9:1183.
- 41 Chiba Y, Nakazawa S, Todoroki M, *et al.* Interleukin-13 augments bronchial smooth muscle contractility with an up-regulation of RhoA protein. *Am J Respir Cell Mol Biol* 2009;40:159–67.
- 42 Carvajal JA, Germain AM, Huidobro-Toro JP, *et al.* Molecular mechanism of cGMP-mediated smooth muscle relaxation. *J Cell Physiol* 2000;184:409–20.
- 43 Ward JK, Barnes PJ, Springall DR, *et al.* Distribution of human i-NANC bronchodilator and nitric oxide-immunoreactive nerves. *Am J Respir Cell Mol Biol* 1995;13:175–84.
- 44 Asano K, Chee CB, Gaston B, *et al.* Constitutive and inducible nitric oxide synthase gene expression, regulation, and activity in human lung epithelial cells. *Proc Natl Acad Sci U S A* 1994;91:10089–93.
- 45 Nijkamp FP, van der Linde HJ, Folkerts G. Nitric oxide synthesis inhibitors induce airway hyperresponsiveness in the guinea pig in vivo and in vitro. Role of the epithelium. *Am Rev Respir Dis* 1993;148:727–34.
- 46 Prado CM, Martins MA, Tibério IFLC. Nitric oxide in asthma physiopathology. *ISRN Allergy* 2011;2011:832560.
- 47 Hamid Q, Springall DR, Riveros-Moreno V, *et al.* Induction of nitric oxide synthase in asthma. *Lancet* 1993;342:1510–3.
- 48 Dweik RA, Sorkness RL, Wenzel S, *et al.* Use of exhaled nitric oxide measurement to identify a reactive, at-risk phenotype among patients with asthma. *Am J Respir Crit Care Med* 2010;181:1033–41.
- 49 Jatakanon A, Lim S, Kharitonov SA, *et al.* Correlation between exhaled nitric oxide, sputum eosinophils, and methacholine responsiveness in patients with mild asthma. *Thorax* 1998;53:91–5.
- 50 Dupont LJ, Rochette F, Demedts MG, *et al.* Exhaled nitric oxide correlates with airway hyperresponsiveness in steroid-naive patients with mild asthma. *Am J Respir Crit Care Med* 1998;157:894–8.
- 51 Grace MS, Baxter M, Dubuis E, *et al.* Transient receptor potential (TRP) channels in the airway: role in airway disease. *Br J Pharmacol* 2014;171:2593–607.
- 52 Birrell MA, Belvisi MG, Grace M, *et al.* TRPA1 agonists evoke coughing in guinea pig and human volunteers. *Am J Respir Crit Care Med* 2009;180:1042–7.
- 53 Caceres AI, Brackmann M, Elia MD, *et al.* A sensory neuronal ion channel essential for airway inflammation and hyperactivity in asthma. *Proc Natl Acad Sci U S A* 2009;106:9099–104.
- 54 Siddiqui S, Shikotra A, Richardson M, *et al.* Airway pathological heterogeneity in asthma: visualization of disease microclusters using topological data analysis. *J Allergy Clin Immunol* 2018;142:1457–68.
- 55 Saglani S, Payne DN, Zhu J, *et al.* Early detection of airway wall remodeling and eosinophilic inflammation in preschool wheezers. *Am J Respir Crit Care Med* 2007;176:858–64.
- 56 Regamey N, Ochs M, Hilliard TN, *et al.* Increased airway smooth muscle mass in children with asthma, cystic fibrosis, and non-cystic fibrosis bronchiectasis. *Am J Respir Crit Care Med* 2008;177:837–43.
- 57 Bossley CJ, Fleming L, Gupta A, *et al.* Pediatric severe asthma is characterized by eosinophilia and remodeling without T(H)2 cytokines. *J Allergy Clin Immunol* 2012;129:e913:974–82.
- 58 Tillie-Leblond I, de Blic J, Jaubert F, *et al.* Airway remodeling is correlated with obstruction in children with severe asthma. *Allergy* 2008;63:533–41.
- 59 Halayko AJ, Salari H, Ma X, *et al.* Markers of airway smooth muscle cell phenotype. *Am J Physiol* 1996;270:L1040–51.
- 60 Berair R, Saunders R, Brightling CE. Origins of increased airway smooth muscle mass in asthma. *BMC Med* 2013;11:145.
- 61 Trian T, Benard G, Begueret H, *et al.* Bronchial smooth muscle remodeling involves calcium-dependent enhanced mitochondrial biogenesis in asthma. *J Exp Med* 2007;204:3173–81.
- 62 Zou H, Fang Q-H, Ma Y-M, *et al.* Analysis of growth factors in serum and induced sputum from patients with asthma. *Exp Ther Med* 2014;8:573–8.
- 63 Shan L, Redhu NS, Saleh A, *et al.* Thymic stromal lymphopoietin receptor-mediated IL-6 and CC/CXC chemokines expression in human airway smooth muscle cells: role of MAPKs (ERK1/2, p38, and JNK) and STAT3 pathways. *J Immunol* 2010;184:7134–43.
- 64 Lajoie-Kadoch S, Joubert P, Létuvé S, *et al.* Tnf-Alpha and IFN-gamma inversely modulate expression of the IL-17E receptor in airway smooth muscle cells. *Am J Physiol Lung Cell Mol Physiol* 2006;290:L1238–46.
- 65 Malavia NK, Raub CB, Mahon SB, *et al.* Airway epithelium stimulates smooth muscle proliferation. *Am J Respir Cell Mol Biol* 2009;41:297–304.
- 66 Lan B, Mitchel JA, O'Sullivan MJ, *et al.* Airway epithelial compression promotes airway smooth muscle proliferation and contraction. *Am J Physiol Lung Cell Mol Physiol* 2018;315:L645–52.
- 67 Risse P-A, Jo T, Suarez F, *et al.* Interleukin-13 inhibits proliferation and enhances contractility of human airway smooth muscle cells without change in contractile phenotype. *Am J Physiol Lung Cell Mol Physiol* 2011;300:L958–66.
- 68 Espinosa K, Bossé Y, Stankova J, *et al.* CysLT1 receptor upregulation by TGF-beta and IL-13 is associated with bronchial smooth muscle cell proliferation in response to LTD4. *J Allergy Clin Immunol* 2003;111:1032–40.
- 69 Keglłowicz LF, Borger P. The three A's in asthma - airway smooth muscle, airway remodeling & angiogenesis. *Open Respir Med J* 2015;9:70–80.
- 70 Hirst SJ, Twort CH, Lee TH. Differential effects of extracellular matrix proteins on human airway smooth muscle cell proliferation and phenotype. *Am J Respir Cell Mol Biol* 2000;23:335–44.
- 71 Tran T, McNeill KD, Gerthoffer WT, *et al.* Endogenous laminin is required for human airway smooth muscle cell maturation. *Respir Res* 2006;7:117.
- 72 Araujo BB, Dolhnikoff M, Silva LFF, *et al.* Extracellular matrix components and regulators in the airway smooth muscle in asthma. *Eur Respir J* 2008;32:61–9.
- 73 Orsini MJ, Krymskaya VP, Eszterhas AJ, *et al.* Mapk superfamily activation in human airway smooth muscle: mitogenesis requires prolonged p42/p44 activation. *Am J Physiol* 1999;277:L479–88.
- 74 Krymskaya VP, Penn RB, Orsini MJ, *et al.* Phosphatidylinositol 3-kinase mediates mitogen-induced human airway smooth muscle cell proliferation. *Am J Physiol* 1999;277:L65–78.
- 75 Schaafsma D, Roscioni SS, Meurs H, *et al.* Monomeric G-proteins as signal transducers in airway physiology and pathophysiology. *Cell Signal* 2008;20:1705–14.
- 76 Page K, Li J, Hodge JA, *et al.* Characterization of a Rac1 signaling pathway to cyclin D(1) expression in airway smooth muscle cells. *J Biol Chem* 1999;274:22065–71.
- 77 Dilasser F, Rose L, Hassoun D, *et al.* Essential role of smooth muscle Rac1 in severe asthma-associated airway remodelling. *Thorax* 2021;76:326–334.
- 78 Hedges JC, Dechert MA, Yamboliev IA, *et al.* A role for p38(MAPK)/HSP27 pathway in smooth muscle cell migration. *J Biol Chem* 1999;274:24211–9.
- 79 Carlin SM, Roth M, Black JL. Urokinase potentiates PDGF-induced chemotaxis of human airway smooth muscle cells. *Am J Physiol Lung Cell Mol Physiol* 2003;284:L1020–6.
- 80 Parameswaran K, Cox G, Radford K, *et al.* Cysteinyl leukotrienes promote human airway smooth muscle migration. *Am J Respir Crit Care Med* 2002;166:738–42.
- 81 Tliba O, Panettieri RA. Noncontractile functions of airway smooth muscle cells in asthma. *Annu Rev Physiol* 2009;71:509–35.
- 82 Yang W, Kaur D, Okayama Y, *et al.* Human lung mast cells adhere to human airway smooth muscle, in part, via tumor suppressor in lung cancer-1. *J Immunol* 2006;176:1238–43.



- 83 Girodet P-O, Ozier A, Trian T, *et al.* Mast cell adhesion to bronchial smooth muscle in asthma specifically depends on CD51 and CD44 variant 6. *Allergy* 2010;65:1004–12.
- 84 Hamawy MM, Mergenhagen SE, Siraganian RP. Adhesion molecules as regulators of mast-cell and basophil function. *Immunol Today* 1994;15:62–6.
- 85 Lazaar AL, Albelda SM, Pilewski JM, *et al.* T lymphocytes adhere to airway smooth muscle cells via integrins and CD44 and induce smooth muscle cell DNA synthesis. *J Exp Med* 1994;180:807–16.
- 86 Graham BL, Steenbruggen I, Miller MR, *et al.* Standardization of spirometry 2019 update. an official American thoracic Society and European respiratory Society technical statement. *Am J Respir Crit Care Med* 2019;200:e70–88.
- 87 Karmaus W, Mukherjee N, Janjanam VD, *et al.* Distinctive lung function trajectories from age 10 to 26 years in men and women and associated early life risk factors - a birth cohort study. *Respir Res* 2019;20:98.
- 88 Lange P, Parnar J, Vestbo J, *et al.* A 15-year follow-up study of ventilatory function in adults with asthma. *N Engl J Med* 1998;339:1194–200.
- 89 Ulrik CS, Backer V. Nonreversible airflow obstruction in life-long nonsmokers with moderate to severe asthma. *Eur Respir J* 1999;14:892–6.
- 90 Ferreira DS, Carvalho-Pinto RM, Gregório MG, *et al.* Airway pathology in severe asthma is related to airflow obstruction but not symptom control. *Allergy* 2018;73:635–43.
- 91 Quanjer PH, Weiner DJ, Pretto JJ, *et al.* Measurement of FEF25–75% and FEF75% does not contribute to clinical decision making. *Eur Respir J* 2014;43:1051–8.
- 92 Kjellberg S, Houtz BK, Zetterström O, *et al.* Clinical characteristics of adult asthma associated with small airway dysfunction. *Respir Med* 2016;117:92–102.
- 93 de Lange EE, Altes TA, Patrie JT, *et al.* The variability of regional airflow obstruction within the lungs of patients with asthma: assessment with hyperpolarized helium-3 magnetic resonance imaging. *J Allergy Clin Immunol* 2007;119:1072–8.
- 94 Farah CS, King GG, Brown NJ, *et al.* The role of the small airways in the clinical expression of asthma in adults. *J Allergy Clin Immunol* 2012;129:e381:381–7.
- 95 Coates AL, Wanger J, Cockcroft DW, *et al.* ERS technical standard on bronchial challenge testing: general considerations and performance of methacholine challenge tests. *Eur Respir J* 2017;49. doi:10.1183/13993003.01526-2016. [Epub ahead of print: 01 05 2017].
- 96 Hallstrand TS, Leuppi JD, Joos G, *et al.* ERS technical standard on bronchial challenge testing: pathophysiology and methodology of indirect airway challenge testing. *Eur Respir J* 2018;52. doi:10.1183/13993003.01033-2018. [Epub ahead of print: 15 11 2018].
- 97 Sumino K, Sugar EA, Irvin CG, *et al.* Methacholine challenge test: diagnostic characteristics in asthmatic patients receiving controller medications. *J Allergy Clin Immunol* 2012;130:e66:69–75.
- 98 Satia I, Priel E, Al-Khazraji BK, *et al.* Exercise-induced bronchoconstriction and bronchodilation: investigating the effects of age, sex, airflow limitation and FEV₁. *Eur Respir J* 2021;58:2004026.
- 99 Anderson SD, Charlton B, Weiler JM, *et al.* Comparison of mannitol and methacholine to predict exercise-induced bronchoconstriction and a clinical diagnosis of asthma. *Respir Res* 2009;10:4.
- 100 Girodet P-O, Dournes G, Thumerel M, *et al.* Calcium channel blocker reduces airway remodeling in severe asthma. A proof-of-concept study. *Am J Respir Crit Care Med* 2015;191:876–83.
- 101 Goldsmith AM, Hershenson MB, Wolbert MP, *et al.* Regulation of airway smooth muscle alpha-actin expression by glucocorticoids. *Am J Physiol Lung Cell Mol Physiol* 2007;292:L99–106.
- 102 Goto K, Chiba Y, Sakai H, *et al.* Glucocorticoids inhibited airway hyperresponsiveness through downregulation of CPI-17 in bronchial smooth muscle. *Eur J Pharmacol* 2008;591:231–6.
- 103 Leung SY, Eynott P, Nath P, *et al.* Effects of ciclesonide and fluticasone propionate on allergen-induced airway inflammation and remodeling features. *J Allergy Clin Immunol* 2005;115:989–96.
- 104 Chetta A, Zanini A, Foresi A, *et al.* Vascular component of airway remodeling in asthma is reduced by high dose of fluticasone. *Am J Respir Crit Care Med* 2003;167:751–7.
- 105 Ward C, Pais M, Bish R, *et al.* Airway inflammation, basement membrane thickening and bronchial hyperresponsiveness in asthma. *Thorax* 2002;57:309–16.
- 106 Humbert M, Beasley R, Ayres J, *et al.* Benefits of omalizumab as add-on therapy in patients with severe persistent asthma who are inadequately controlled despite best available therapy (GINA 2002 step 4 treatment): INNOVATE. *Allergy* 2005;60:309–16.
- 107 Holguin F, Cardet JC, Chung KF, *et al.* Management of severe asthma: a European respiratory Society/American thoracic Society guideline. *Eur Respir J* 2020;55. doi:10.1183/13993003.00588-2019. [Epub ahead of print: 02 01 2020].
- 108 Rabe KF, Nair P, Brusselle G, *et al.* Efficacy and safety of Dupilumab in glucocorticoid-dependent severe asthma. *N Engl J Med* 2018;378:2475–85.
- 109 Dupin C, Belhadi D, Guillemainault L, *et al.* Effectiveness and safety of dupilumab for the treatment of severe asthma in a real-life French multi-centre adult cohort. *Clin Exp Allergy* 2020;50:789–98.
- 110 Menzies-Gow A, Corren J, Bourdin A, *et al.* Tezepelumab in adults and adolescents with severe, uncontrolled asthma. *N Engl J Med* 2021;384:1800–9.
- 111 Panettieri RA, Welte T, Shenoy KV, *et al.* Onset of effect, changes in airflow obstruction and lung volume, and health-related quality of life improvements with Benralizumab for patients with severe eosinophilic asthma: phase IIIb randomized, controlled trial (SOLANA). *J Asthma Allergy* 2020;13:115–26.
- 112 Farah CS, Badal T, Reed N, *et al.* Mepolizumab improves small airway function in severe eosinophilic asthma. *Respir Med* 2019;148:49–53.
- 113 Castro M, Rubin AS, Laviolette M, *et al.* Effectiveness and safety of bronchial thermoplasty in the treatment of severe asthma: a multicenter, randomized, double-blind, sham-controlled clinical trial. *Am J Respir Crit Care Med* 2010;181:116–24.
- 114 Thomson NC, Rubin AS, Niven RM, *et al.* Long-term (5 year) safety of bronchial thermoplasty: asthma intervention research (air) trial. *BMC Pulm Med* 2011;11:8.
- 115 Konietzke P, Weinheimer O, Wielpütz MO, *et al.* Quantitative CT detects changes in airway dimensions and air-trapping after bronchial thermoplasty for severe asthma. *Eur J Radiol* 2018;107:33–8.
- 116 Langton D, Ing A, Sha J, *et al.* Measuring the effects of bronchial thermoplasty using oscillometry. *Respirology* 2019;24:431–6.
- 117 Guibert N, Guillemainault L, Lepage B. Bronchial thermoplasty in patients with dynamic hyperinflation: results from the proof-of-concept heat trial. *Eur Respir J* 2020.
- 118 Ichikawa T, Panariti A, Audusseau S, *et al.* Effect of bronchial thermoplasty on structural changes and inflammatory mediators in the airways of subjects with severe asthma. *Respir Med* 2019;150:165–72.
- 119 Goorsenberg AWM, d'Hooghe JNS, Srikanthan K. Bronchial thermoplasty induced airway smooth muscle reduction and clinical response in severe asthma: the TASMA randomized trial. *Am J Respir Crit Care Med* 2020.
- 120 Haj Salem I, Gras D, Joubert P, *et al.* Persistent reduction of mucin production after bronchial thermoplasty in severe asthma. *Am J Respir Crit Care Med* 2019;199:536–8.
- 121 Sun Q, Fang L, Roth M, *et al.* Bronchial thermoplasty decreases airway remodelling by blocking epithelium-derived heat shock protein-60 secretion and protein arginine methyltransferase-1 in fibroblasts. *Eur Respir J* 2019;54:1900300.
- 122 Langton D, Ing A, Fielding D, *et al.* Bronchodilator responsiveness as a predictor of success for bronchial thermoplasty. *Respirology* 2019;24:63–7.
- 123 Hirst SJ, Barnes PJ, Twort CH. Quantifying proliferation of cultured human and rabbit airway smooth muscle cells in response to serum and platelet-derived growth factor. *Am J Respir Cell Mol Biol* 1992;7:574–81.
- 124 Hirst SJ, Barnes PJ, Twort CH. PDGF isoform-induced proliferation and receptor expression in human cultured airway smooth muscle cells. *Am J Physiol* 1996;270:L415–28.
- 125 Simeone-Penney MC, Severgnini M, Rozo L, *et al.* PDGF-Induced human airway smooth muscle cell proliferation requires STAT3 and the small GTPase Rac1. *Am J Physiol Lung Cell Mol Physiol* 2008;294:L698–704.
- 126 Stamatiou R, Paraskeva E, Gourgoulisian K, *et al.* Cytokines and growth factors promote airway smooth muscle cell proliferation. *ISRN Inflamm* 2012;2012:731472.
- 127 Ediger TL, Toews ML. Synergistic stimulation of airway smooth muscle cell mitogenesis. *J Pharmacol Exp Ther* 2000;294:1076–82.
- 128 Bossé Y, Thompson C, Stankova J, *et al.* Fibroblast growth factor 2 and transforming growth factor beta1 synergism in human bronchial smooth muscle cell proliferation. *Am J Respir Cell Mol Biol* 2006;34:746–53.
- 129 Zou H, Nie X-hong, Zhang Y, *et al.* Effect of basic fibroblast growth factor on the proliferation, migration and phenotypic modulation of airway smooth muscle cells. *Chin Med J* 2008;121:424–9.
- 130 Krymskaya VP, Hoffman R, Eszterhas A, *et al.* EGF activates ErbB-2 and stimulates phosphatidylinositol 3-kinase in human airway smooth muscle cells. *Am J Physiol* 1999;276:L246–55.

- 131 Chen G, Khalil N. Tgf-Beta1 increases proliferation of airway smooth muscle cells by phosphorylation of MAP kinases. *Respir Res* 2006;7:2.
- 132 Cohen MD, Ciocca V, Panettieri RA. TGF-Beta 1 modulates human airway smooth-muscle cell proliferation induced by mitogens. *Am J Respir Cell Mol Biol* 1997;16:85–90.
- 133 Xie S, Sukkar MB, Issa R, et al. Mechanisms of induction of airway smooth muscle hyperplasia by transforming growth factor-beta. *Am J Physiol Lung Cell Mol Physiol* 2007;293:L245–53.
- 134 Stewart AG, Tomlinson PR, Fernandes DJ, et al. Tumor necrosis factor alpha modulates mitogenic responses of human cultured airway smooth muscle. *Am J Respir Cell Mol Biol* 1995;12:110–9.
- 135 Knobloch J, Yanik SD, Körber S, et al. TNFalpha-Induced airway smooth muscle cell proliferation depends on endothelin receptor signaling, GM-CSF and IL-6. *Biochem Pharmacol* 2016;116:188–99.
- 136 Li X, Zou F, Lu Y, et al. Notch1 contributes to TNF- α -induced proliferation and migration of airway smooth muscle cells through regulation of the Hes1/PTEN axis. *Int Immunopharmacol* 2020;88:106911.
- 137 De S, Zelazny ET, Souhrada JF, et al. Interleukin-1 beta stimulates the proliferation of cultured airway smooth muscle cells via platelet-derived growth factor. *Am J Respir Cell Mol Biol* 1993;9:645–51.
- 138 De S, Zelazny ET, Souhrada JF, et al. Il-1 beta and IL-6 induce hyperplasia and hypertrophy of cultured guinea pig airway smooth muscle cells. *J Appl Physiol* 1995;78:1555–63.
- 139 Amrani Y, Tliba O, Choubey D, et al. IFN-Gamma inhibits human airway smooth muscle cell proliferation by modulating the E2F-1/Rb pathway. *Am J Physiol Lung Cell Mol Physiol* 2003;284:L1063–71.
- 140 Hawker KM, Johnson PR, Hughes JM, et al. Interleukin-4 inhibits mitogen-induced proliferation of human airway smooth muscle cells in culture. *Am J Physiol* 1998;275:L469–77.
- 141 Shim JY, Park SW, Kim DS, et al. The effect of interleukin-4 and amphiregulin on the proliferation of human airway smooth muscle cells and cytokine release. *J Korean Med Sci* 2008;23:857–63.
- 142 Panettieri RA, Yadavish PA, Kelly AM, et al. Histamine stimulates proliferation of airway smooth muscle and induces c-fos expression. *Am J Physiol* 1990;259:L365–71.
- 143 Chhabra J, Li Y-Z, Alkhoury H, et al. Histamine and tryptase modulate asthmatic airway smooth muscle GM-CSF and RANTES release. *Eur Respir J* 2007;29:861–70.
- 144 Noveral JP, Grunstein MM. Role and mechanism of thromboxane-induced proliferation of cultured airway smooth muscle cells. *Am J Physiol* 1992;263:L555–61.
- 145 Capra V, Habib A, Accomazzo MR, et al. Thromboxane prostanoid receptor in human airway smooth muscle cells: a relevant role in proliferation. *Eur J Pharmacol* 2003;474:149–59.
- 146 Ammit AJ, Hastie AT, Edsall LC, et al. Sphingosine 1-phosphate modulates human airway smooth muscle cell functions that promote inflammation and airway remodeling in asthma. *FASEB J* 2001;15:1212–4.
- 147 Berger P, Perng DW, Thabrew H, et al. Tryptase and agonists of PAR-2 induce the proliferation of human airway smooth muscle cells. *J Appl Physiol* 2001;91:1372–9.
- 148 Panettieri RA, Hall IP, Maki CS, et al. Alpha-thrombin increases cytosolic calcium and induces human airway smooth muscle cell proliferation. *Am J Respir Cell Mol Biol* 1995;13:205–16.
- 149 Huang C-D, Chen H-H, Wang C-H, et al. Human neutrophil-derived elastase induces airway smooth muscle cell proliferation. *Life Sci* 2004;74:2479–92.
- 150 Brar SS, Kennedy TP, Sturrock AB, et al. NADPH oxidase promotes NF-kappaB activation and proliferation in human airway smooth muscle. *Am J Physiol Lung Cell Mol Physiol* 2002;282:L782–95.
- 151 Bel EH, Wenzel SE, Thompson PJ, et al. Oral glucocorticoid-sparing effect of mepolizumab in eosinophilic asthma. *N Engl J Med* 2014;371:1189–97.
- 152 Castro M, Zangrilli J, Wechsler ME, et al. Reslizumab for inadequately controlled asthma with elevated blood eosinophil counts: results from two multicentre, parallel, double-blind, randomised, placebo-controlled, phase 3 trials. *Lancet Respir Med* 2015;3:355–66.
- 153 Bleecker ER, FitzGerald JM, Chanez P, et al. Efficacy and safety of benralizumab for patients with severe asthma uncontrolled with high-dosage inhaled corticosteroids and long-acting β_2 -agonists (SIROCCO): a randomised, multicentre, placebo-controlled phase 3 trial. *Lancet* 2016;388:2115–27.
- 154 Nair P, Wenzel S, Rabe KF, et al. Oral glucocorticoid-sparing effect of Benralizumab in severe asthma. *N Engl J Med* 2017;376:2448–58.

Deuxième partie : Identification et caractérisation d'un nouvel inhibiteur pharmacologique de Rac1

Rac1 joue un rôle important dans le développement et la progression du cancer. Le cancer est aujourd'hui, dans de nombreux pays, la première cause de mortalité précoce avant 70 ans (Figure 17). En 2020, on estime à 19,3 millions le nombre de nouveaux cas de cancer dans le monde et 10 millions de décès sont imputables au cancer à travers le monde. Le cancer du sein de la femme est le cancer pour lequel le nombre de nouveau cas (hommes et femmes confondus) est le plus important en 2020 et représente plus de 2,26 millions de nouveaux cas suivi par le cancer du poumon avec 2,2 millions de nouveaux cas. Le cancer du poumon est la première cause de décès par cancer (hommes et femmes confondus) en 2020 avec 1,7 millions de décès tandis que le cancer du sein chez la femme est le 5^e avec plus de 684 mille décès (Sung et al. 2021).

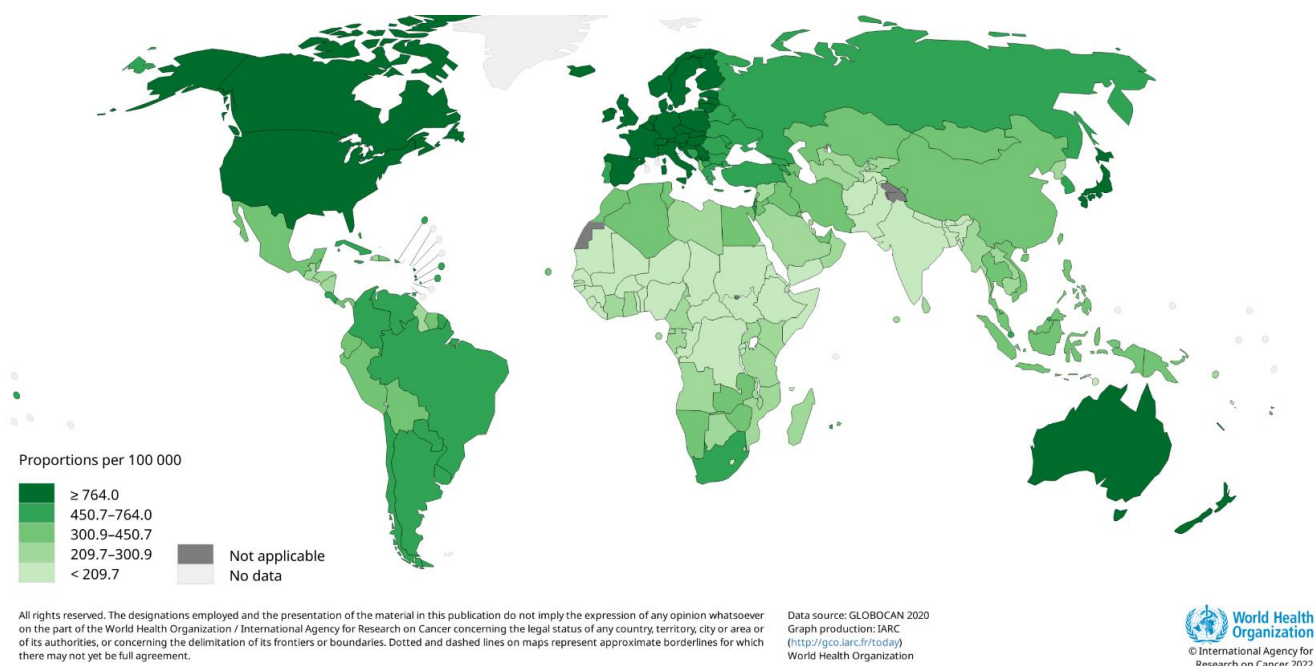


Figure 17 : Prévalence du cancer à travers le monde en 2020 (GLOBOCAN 2020)

La prévalence de tous types de cancer, âges et sexes confondus est représentée en proportion pour 100 000 habitants en 2020.

Comme décrit précédemment (III.2- Rac1 en oncologie), Rac1 participe à la prolifération et la survie des cellules tumorales ainsi qu'à leur migration et la formation de métastases. Ces éléments font donc de Rac1 une cible thérapeutique d'intérêt également en oncologie.

Différentes stratégies thérapeutiques et inhibiteurs de Rac1 ont déjà été développés (IV-Stratégies thérapeutiques régulant l'activité de la GTPase Rac1) et plus ou moins caractérisés. Ces différents inhibiteurs sont plus ou moins spécifiques de Rac1 ou de ses effecteurs, ont pour certains des effets sur d'autres cibles non négligeables ou encore des IC₅₀ trop élevés pour une utilisation envisageable en clinique. Ces molécules sont aujourd'hui utilisées comme des outils pour caractériser l'effet de l'inhibition de Rac1 sur différentes fonctions cellulaires et dans divers contextes physiopathologiques. De plus, l'étude des différentes stratégies de criblage utilisées pour le développement de ces diverses molécules ainsi que leurs structures chimiques sont utiles au développement de nouveaux inhibiteurs spécifiques de Rac1.

Pendant ma thèse j'ai identifié et caractériser un nouvel inhibiteur pharmacologique spécifique de Rac1. Pour cela une approche de criblage virtuel associé à des tests *in vitro* ont été utilisés et ont permis notamment de valider sa spécificité et d'identifier son mécanisme d'action. Cet inhibiteur agit comme un compétiteur réversible du GTP en se liant à Rac1 au niveau de la poche nucléotidique et empêche ainsi son activation. L'utilisation de cet inhibiteur dans un modèle murin de cancer du sein triple négatif a permis de réduire la croissance tumorale, d'améliorer la survie et a empêché la formation de métastases.

Pour cette étude j'ai réalisé les étapes de biologie cellulaire, signalisation cellulaire, biochimie, l'étude pharmacocinétique de l'A4.1 ainsi que la caractérisation de ses effets dans nos modèles murins de cancer du sein triple négatif.

Article 3: A Rac GTPase-Specific Small Molecule Inhibitor targets metastasis
in triple negative breast cancer

Article en cours de rédaction

A Rac GTPase-Specific Small Molecule Inhibitor targets metastasis in triple negative breast cancer.

Florian DILASSER, PhD.^{a*} Lindsay ROSE, MSc.^{a*} Agnès QUEMENER, MSc.^{e,f} Yann FERANDEZ, PhD.^c Dorian HASSOUN, MD.^a Camille TROUILLET, PhD.^d Morgane ROUSSELLE, BSc.^a Gwennan ANDRE, PhD.^a Mike MAILLASSON, MSc.^{e,f,g} Mickael CROYAL, PhD.^a Mathieu RIVIERE, MSc.^d Didier DUBREUIL, PhD.^d Sylvain COLLET, PhD.^d Frédérique SOUAZE, PhD.^e Mario CAMPONE, MD.^e Anne PATSOURIS, MD.^e Philippe JUIN, PhD.^e Jacques LEBRETON, PhD.^d Arnaud TESSIER, PhD.^d Jacqueline CHERFILS, PhD.^c Gervaise LOIRAND, PhD.^a Vincent SAUZEAU, PhD.^{a,*}

^a Université de Nantes, CHU Nantes, CNRS, INSERM, l'institut du thorax, Nantes, France

^c Laboratory of biology and applied pharmacology, CNRS, ENS Paris-Saclay, Paris, France

^d Chimie Et Interdisciplinarité : Synthèse, Analyse, Modélisation, CNRS, UNIV Nantes, Nantes, France

^e Nantes Université, Inserm, CNRS, CRCI2NA, Nantes - France

^f LabEx IGO, Immunotherapy, Graft, Oncology, Nantes, France

^g Université de Nantes, Inserm, CNRS, CHU Nantes, SFR Santé, FED 4203, Inserm UMS 016, CNRS UMS 3556, IMPACT Platform, Nantes, France

* These authors have contributed equally to this work and are listed in alphabetical order.

Short title:

Total word Count:

Disclosures:

The authors have reported that they have no relationships with industry relevant to the contents of this paper to disclose.

Funding:

This work was supported by grants from the Institut de Recherche en Santé Respiratoire des Pays de la Loire (STARac project), the TTO Ouest Valorisation (Oracle and Oracle2 projects) and the Institut National de la Santé et de la Recherche Médicale (INSERM). LR was supported by a grant from MRES. DH was supported by a grant from Fondation de la Recherche Médicale.

*** Reprint requests and correspondence:**

Vincent SAUZEAU, PhD

l'institut du thorax

Inserm UMR 1087, CNRS UMR 6291

IRS-UN, 8 quai Moncoussu

44007 Nantes cedex 1, France

E-mail: vincent.sauzeau@univ-nantes.fr

Acknowledgements:

The authors value the support provided by the animal facility units of the University of Nantes. We thank Therassay, Micropicell and Cytocell core facilities (SFR François Bonamy, University of Nantes) for the functional and cellular explorations.

Abstract

The Rho GTPase Rac regulates essential cell functions including actin cytoskeleton organization implicated in cell migration and invasion. Rac1 activity is involved in many steps of cancerogenesis such as initiation, progression, invasion and metastasis. Rac hyperactivation and overexpression are associated with aggressive cancers. For these reasons there is an extensive interest in the development of new Rac GTPase inhibitors. In this study we achieved a pharmacophore and by docking-based virtual screening we identified a new Rac inhibitor, A4.1. A4.1 is a specific and efficient inhibitor of Rac1 which is able to inhibit Rac1 activity *in vitro* and *in vivo*. *In vitro* A4.1 inhibited the colony formation and invasion in triple negative breast cancer (TNBC) cell line. *In vivo* A4.1 reduced the tumor growth after primary tumor resection in immunodeficient and immunocompetent murine models of TNBC. The treatment with A4.1 also reduced metastasis frequency and improve mice survival in these two models of TNBC. Therefore, A4.1, is a promising Rac1 inhibitor for the treatment of metastatic cancers with high Rac activity.

Introduction

Rac1, the Ras-related small GTPase member of the Rho family, is a binary molecular switch cycling between an inactive GDP-bound “OFF” state and an active GTP-bound “ON” state to regulate essential cellular functions including actin cytoskeleton organization, NADPH oxidase activity, and modulation of gene expression (Loirand et al., 2013; Ridley, 2015). When this activation/inactivation cycling is compromised, Rac1 activity is implicated in various steps of oncogenesis including initiation, progression, invasion, and metastasis (Jansen et al., 2018; Kazanietz and Caloca, 2017). Overexpression of Rac1 has been reported in colorectal (Kawasaki et al., 2003), pancreatic (Crnogorac-Jurcevic et al., 2001), breast (Tian et al., 2018; Andr es Lopez-Cortes. Scientific reports, 2020), and testicular cancers (McIver et al., 2013) and in various leukemia (Durand-Onayli et al., 2018; Hasan et al., 2018; Wang et al., 2009). Recently, it was observed that the mRNA expression levels of Rac1 is gradually increased in breast cancer tissues of stages I, II, III and IV ; indicating that the high expression level of Rac1 is associated with high pathological stage and more aggressive tumor subtypes (Tian et al., 2018). Moreover, aberrant activation of upstream regulators of Rac1, such as the Rac exchange factors TIAM1, PREX1, ECT2 and Vav family members, have been implicated in various cancers (Kazanietz and Caloca, 2017; Lin and Zheng, 2015). In addition, the discovery of a hotspot mutation in *RAC1* (c.85C>T) in up to 9% of sun-exposed melanomas identified Rac1 as a new actor of melanoma genesis (Reid, T.S, Terry, K.L J Mol Biol 2004; Goa, Y., Dickerson, J.B PNAS 2004). There is also emerging evidence that Rac may be mutationally activated [Rac1(N92I), Rac1(C157Y), Rac2(P29L), and Rac2(P29Q)] in other forms of cancer such as head and neck tumors as well as a breast tumor (Kawazu et al., 2013). This oncogenic role of Rac1 was confirmed by targeting depletion of its expression that reduced the rate of proliferation and invasion in cancer cells (Shutes, A. et al. JBC 2007; Duttings JTH

2015), pointing that Rac1 blocking may have therapeutic value in repressing tumor progression and metastasis.

To date, there is no clinically available drugs targeting Rac1. Over the two last decades, it has been challenging to directly target Ras superfamily proteins with therapeutic molecules. These proteins are deemed to be undruggable: they are too smooth, too floppy and have few pockets where a molecule might bind tightly (Ledford, 2015). However, several strategies have been considered to inhibit Rac1 activity (Lin and Zheng, 2015). Some bacterial toxins (exoenzyme C3 transferase, toxin A and B) could modify Rho GTPases activity and they have been widely used to decipher physiological functions of Rho GTPases. However, these toxins are non-specific and cannot be used clinically. HMG-CoA reductase and geranylgeranyltransferase inhibitors are also used to inhibit the translocation of Rac1 to the membrane and thus prevent its activation. As observed with toxins, these inhibitors are not specific and have not demonstrated significant therapeutic efficiency. To activate Rac1, Guanine Exchange Factors (GEF) promote the GDP/GTP nucleotide exchange. The NSC23766 compound is the first Rac1 specific inhibitor to be described impairing Rac/GEFs interaction. Another strategy was to identify molecules blocking the interaction between Rac1 and its effectors to inhibit Rac1-dependent cellular functions. That was the strategy used to develop the EHT1864 compound. However, further studies have demonstrated that EHT1864 is a non-competitive inhibitor that promotes nucleotide dissociation and locks Rac1 in an inactive state. In addition, it has been described that NSC23766 and EHT1864 present some critical off-targets like inhibition of Rac1-independent platelet activation (Sebti *SM Oncogene* 2000, Sousa *SF Cur Med Chem* 2008), thus highlighting the obvious need to discover new specific Rac1 inhibitors.

In this study, we carried out a pharmacophore and docking-based virtual screening and we identify the compound A4.1 as the first potent and efficient Rac1 inhibitor able to inhibit

Rac activity *in vivo*. Herein, we designed experiments to demonstrate the pharmacological/therapeutical potential of this new potent Rac inhibitor in human metastatic cancer such as triple negative breast cancer (TNBC).

Results

Pharmacophore modeling, virtual screening and docking

We first used a pharmacophore model generated on the basis of the crystal structure of RAC1 in complex with NSC23766 (Zheng, Y., Nassar, N., and Skowronek, K. R. (2010) United States Patent 17,826,982) and virtual screening to search for new small molecules that bind to RAC1 and potentially inhibit its activity (**Fig. 1**). From the docking of candidates retrieved from the virtual screening, the top scoring 100 chemicals have been purchased for testing their ability to inhibit RAC-dependent cell processes and EGF-induced RAC activation. The ranking of the molecules according to their efficacy compared to the known RAC inhibitors, EHT1864 and NSC23766, has placed the molecule A4 at the top of the list (**Supp. Table 1**). Further examination of A4 structure and docking to characterize its binding mode and interactions with RAC1 revealed possible interaction with the nucleotide binding pocket of RAC1. Indeed, prediction of A4 binding modes by docking studies, showed that interaction of A4 with RAC1 involves mainly hydrophobic interactions when it was docked to the NSC23766 binding site of RAC1 (the one used for the virtual screening), while it consists of more hydrogen bonds, when the nucleotide binding site was explored, resulting in a docking score more in favor of the last site (**Figure 1b**). Chemical modifications of A4 affected the docking score in the nucleotide binding pocket (**Table 1**). To confirm these virtual data, A4 and its analogs have been synthesized and their ability to inhibit Rac1-dependent processes has been experimentally assessed by quantifying their inhibitory action on membrane ruffle formation. Of note, we observed a very good correlation between the docking score and the potency of the analogues to inhibit the Rac1-dependent process for 5 out of tested 6 molecules (**Table 1**). The substitution of sulfur atom by oxygen (A4.14) slightly affect the docking score and the inhibition of ruffle formation while the modification in the carbon chain length (A4.16) in the western part of the molecule decreased the docking score and the inhibition of ruffle formation. More drastically,

the removal of the aromatic ring (A420) or the replacement of the sulfonamide functional group by an amide functional group (A4.15) molecule leads to the loss of RAC inhibition, suggesting the essential role of these functional groups in the inhibitory activity. The A4.1 analog bearing a change in the methoxy group position on the benzene ring showed a better docking score than A4 and a higher potency to inhibit membrane ruffle formation as shown by the decrease of the IC_{50} from 3.10^{-8} M for A4 to $0.67.10^{-9}$ M for A4.1 (**Table 1 and Fig. 1b**). The inhibitory action of A4.1 on RAC1-dependent cell function and its superiority to NSC23766 was further confirmed on cell migration (**Supp. Fig. 2a**) and cell adhesion (**Supp. Fig. 2b**). A4.1 thus emerged as the best small molecule candidate and was considered as the lead molecule of this chemical series. A4.15 was identified as a negative control molecule and results from our structure activity relationship allows to propose a chemical skeleton model of small molecule RAC inhibitor (**Supp. Figure 3**).

Compound A4.1 is a potent and selective inhibitor of RAC proteins

To further characterized A4.1 properties, we next directly assessed its effects on RAC1 activity both in cell and *in vitro*. In 3T3 fibroblasts, measured of the amount of active GTP-bound RAC1 by pull-down assay shows that A4.1 (10^{-5} M) totally prevented EGF-induced RAC1 activation, while NSC23766 and A4.15 had no significant effect (**Figure 1d**). *In vitro*, A4.1 efficiently inhibits the guanine nucleotide exchange catalyzed by the DH-PH of the RAC GEF Trio on RAC1 (**Figure 2a**). A4.1 also significantly reduced the activation of RAC2 by Trio but has no effect on Trio-induced RhoG activation (**Figure 2a**). These observations are consistent with a direct effect of A4.1 on RAC proteins. We similarly used fluorescence kinetics to test potential effect of A4.1 on guanine nucleotide exchange on RHOA and CDC42 (**Figure 2b**). A4.1 has no effect on Arhgef1-induced RHOA activation and Tiam-induced CDC42 activation. Thus, A4.1, seems to display a remarkable specificity for RAC proteins.

To confirm the specificity of A4.1 for RAC proteins and to validate whether A4.1 directly binds to RAC, we used surface plasmon resonance to measure its interaction with the RHO family proteins RAC1, RHOA and CDC42 (**Figure 2c**). Surface plasmon resonance sensograms clearly show that A4.1 binds to RAC1 but not to RHOA and CDC42, confirming a direct, selective and reversible interaction of A4.1 with RAC proteins.

A4.1 is a competitive nucleotide binding inhibitor of RAC1

The observed direct interaction of A4.1 with RAC1 and the inhibition of its activity, together with its docking in the nucleotide binding pocket leads us to hypothesize that A4.1 could exert its inhibitory effect by competing with the guanine nucleotide binding to RAC. To assess this hypothesis, we carried out nucleotide exchange assay to test the inhibition of RAC activation by A4.1 under conditions where A4.1 concentration was held fixed (5 μM) while increasing the concentration of GTP (**Figure 3a**). The inhibitory effect of A4.1 was decreased by increasing the mant-GTP concentration from 1 μM to 2,5 μM and abolished at 5 μM (**Figure 3a**). These results are thus consistent with A4.1 behaves as a reversible competitive inhibitor of guanine nucleotide binding on RAC1.

We next wanted to experimentally validate the binding of A4.1 to the nucleotide binding pocket of RAC1. Unfortunately, our attempts to obtain the crystal structure of RAC1 in complex with A4.1 were unsuccessful. Therefore, we performed photolabeling coupled with liquid chromatography-high resolution mass spectrometry (*LC-HRMS*) for identifying sites of A4.1-RAC1 interaction. A phenylazide derivative of A4.1 ([N3]-A4.1), forming a reactive nitrene intermediate by activation by ultraviolet irradiation has been synthesized and used to allow to light-induced covalent binding of the molecule to RAC1. *LC-HRMS* chromatograms show that irradiation of RAC1 did not alter its protein profile, while in the presence of [N3]-A4.1, slight modifications of both chromatographic profile and mass spectrum, associated with an increased

noise level suggest that RAC1 was modified. Deconvoluted mass spectra clearly identified the two typically states of RAC1 corresponding to the protein with (25.0 kDa) and without (24.5 kDa) bound nucleotide (**Figure 3b**). In the presence of [N3]-A4.1, the peak of the smallest RAC1 isoform is reduced, and a third states with a molecular weight of 25.1 kDa corresponding to the theoretical labeling of nucleotide-free RAC1 with a single molecule [N3]-A4.1 appears (**Figure 3b**). Samples of RAC1 alone and compound treated RAC1 were then reduced, alkylated, and trypsin-digested prior to additional LC-HRMS and LC-MS/MS analyses. Trypsin digestion led to the formation of 14 detectable peptides corresponding to a 88% sequence coverage of RAC1. The spectrum of peptides from the [N3]-A4.1 treated RAC1 sample, shows that it contains an additional peptide corresponding to CVVVG DGAVGK (position 6-16) with a mass shift of 485.1 Da and a retention time of 8.5 min (**Figure 3c**). MS/MS fragmentation of both labeled and unlabeled CVVVG DGAVGK peptide revealed that the lysine16 residue (K) is the reactive amino-acid linking the inhibitor. Lys16 belongs to the phosphate-binding loop (P-loop) of RAC1 (position 12-17) corresponding to a conserved GxGxxxxGK[ST] sequence motif found in mononucleotide-binding *proteins* (Ihara et al. 1998). This conserved lysine residue forms hydrogen bonds (H-bonds) with β - and γ -phosphate groups, while the next Ser/Thr residue coordinates the Mg^{2+} ion, which, in its turn, coordinates β - and γ -phosphates from the other side of the phosphate chain. The interaction between Lys16 and A4.1 thus confirms that the inhibitor compound binds to the guanine nucleotide binding pocket of RAC1 (**Figure 3d**).

Despite the conservation of this Lys residue in other Rho proteins (**Supp. Fig. 4**) A4.1 displays a remarkable specificity of A4.1. Examination of the sequences of neighboring regions that contain 7 amino acids involved in the nucleotide binding confirmed the very high homology of the N-terminal region of RAC1 and RAC2 with CDC42, RHOG and RHOA on which A4.1 did not bind and had no effect. Nevertheless, a common difference between RAC proteins and

A4.1-insensitive Rho proteins lies on Gly30, which is only found in RAC proteins. Glycine is a unique amino acid as it only contains a hydrogen as its side chain, which makes glycine the most flexible amino acid (Yan and Sun, 1997). Its conformation has greater freedom providing flexibility for adjacent residues. Gly30 can thus confers to RAC proteins a unique flexibility of the nucleotide binding region that does not exist in the other Rho proteins. To address this hypothesis, we substituted Gly30 of RAC1 by a serine residue (G30S-RAC1), to mimic the sequence of CDC42. Kinetics of guanine nucleotide exchange on G30S-RAC1 are similar in the absence and in the presence of A4.1(Figure 3e). Thus, the point mutation of Gly30 on RAC1 made it resistant to A4.1, suggesting that flexibility of the nucleotide binding region provided by Gly30 allows unique accessibility and selectivity of A4.1 to RAC proteins.

To further characterize the inhibitory action of A4.1 on RAC proteins we tested its potency on the fact-cycling P29S-RAC1 and the constitutively active RAC1B oncomutants. The activity of these mutants analyzed by pull-down assay was strongly reduced by A4.1 indicating that in addition to being effective on wild-type RAC1 activity, A4.1 is also able to limit oncogenic RAC overactivation (**Figure 3f**).

A4.1 inhibits RAC activity, colony formation and invasion in TNBC cell line

We next sought to characterize *in vitro* the biological effect of A4.1 in cancer cells by using the TNBC MDA-MB-468 Luc cell line (**Figure 4**). A4.1 (10 μ M) decreased by more than 50% the active RAC1-GTP levels in MDA-MB-468 Luc cells, while at same concentration, EHT1864 and NSC23766 have respectively no or little effects on RAC1 activity (**Figure 4a**). Clonogenic assay revealed that incubation of MDA-MB-468 Luc cells with increasing concentrations of A4.1 significantly inhibited colony formation in a dose-dependent manner (**Figure 4b**). A similar inhibitory effect of A4.1 was also obtained on colony formation in other breast cancer cell lines and in other types of cancer cell lines regardless of their oncogenic

mutations (**Figure 4c** and **Supp. Table 2**). This suggests that intracellular downstream transducers of these oncogenic mutations are, at least in part, RAC dependent-processes. Indeed, hyperactivation of Akt, known to play a central role in the oncogenicity of a variety of mutations including, *KRAS*, *PTEN* and *PI3K* is reduced by A4.1, while p44/42 activation is unchanged (**Supp. Fig. 5**). We next assessed the potential effect of A4.1 on MDA-MB-468 invasion in 3D collagen (**Figure 4d**). A4.1 strongly reduced the migration area of the MDA-MB-468 spheroids (**Figure 4d**). In the presence of A4.1, the size of the spheroids was not affected but appeared to be darker compared to untreated spheroids. These results suggest that A4.1 would not have an effect on the cell density of spheroids, thus on cell survival, but only on cell migration. In addition to the migratory capacity of cancer cells, tumor progression, invasion and metastasis is critically dependent on cancer-associated fibroblasts (CAFs) (Asif PJ et al, 2021). Interestingly, this anti-invasion property of A4.1 seen on cancer cells was also observed in human breast CAF spheroids (**Figure 4d**). This results therefore suggest that A4.1 may have anti-metastatic properties.

Compound A4.1 has suitable properties for *in vivo* testing

In order to assess the anti-tumor properties of A4.1 *in vivo*, we first would like to make sure of the safety and the absence of major off-target effects of A4.1. In vitro binding assays on a panel of targets (membrane receptors, ion channel, kinases, ...) revealed only very limited off-target binding (**Supp. Table 3**). Conventional approaches that have been used to detect potential genotoxic effects of A4.1 (bacterial toxicity, Ames fluctuations, and micronucleus test) have excluded such effects in the concentration range 10^{-7} - 10^{-4} M (**Supp. Table 4-6**). *In vivo* safety has been addressed by following various biological parameters in mice chronically receiving daily intraperitoneal A4.1 injection (1, 10 and 25 mg/Kg) for 1 month. None of the parameters measured, nor the weight of the mice was affected by the chronic A4.1 treatment

(Supp. Fig. 6). No deaths were recorded and visual inspection showed no signs of suffering or abnormal behavior of A4.1-treated mice. We then analyzed pharmacokinetics and tissue distribution of A4.1 following intraperitoneal injection of A4.1 (25 mg/Kg). A4.1 rapidly reached its peak plasma concentration, which then declined over 2-3 h (**Supp Table 7 and Supp. Figure 7**). A4.1 was detected in the liver, heart and lungs. The highest concentration of A4.1 was found in the kidney, indicating renal uptake and subsequent clearance in drug disposition. A4.1 was found at extremely low concentration in brain, which indicated that it could not cross the blood-brain barrier (**Supp. Figure 7**). Taken together, all these data suggest that A4.1 is suitable for *in vivo* testing in a mouse TNBC model.

Compound A4.1 prevents metastasis frequency in a mouse model of TNBC

The anti-metastatic potential of A4.1 was assessed in a TNBC xenograft model by orthotopic injection of MDA-MB-468 Luc cells into the mammary fat pad of 4-week-old NMRI nude mice randomized in 2 groups. The tumor gradually growth over time. At the 50th day post-grafting, when a volume of ~1000 mm³ was reached, the tumor was resected, which corresponded to tumor mass of approximately 0.6 g (**Supp. Figure 8a**). Treatment of the mice with A4.1 (25 mg/kg/jour by IP) or vehicle was then started for 4 weeks. Monitoring of the weight of the mice throughout the experiment, especially during the 4 weeks of treatment, shows that there were no differences between the 2 groups (**Supp. Figure 8b**). Longitudinal post-resection *in vivo* bioluminescence imaging (BLI) clearly showed a decrease in the primary tumor regrowth in the A4.1 group compared to control mice (**Figure 5a and Supp. Figure 8c**). *Ex vivo* BLI in relevant organs harvested at 4 weeks-post-resection did not detect metastasis in the liver and pancreas in both groups of mice. In contrast, it revealed the presence secondary tumors in leg bones, lungs, kidneys, ovaries and uterus with a significant higher frequency in control than in A4.1-treated mice (**Figure 5b**). Moreover, *ex vivo* luminescence intensity of

femur and ovaries and uterus is significantly lower in the A4.1-treated than in the control mice (**Figure 5c**).

These results demonstrate that A4.1 limits tumor regrowth and metastases in a TNBC xenograft model in immunocompromised mice, which lacks the immune system component known to participate to the multi-step processes of tumor growth and dissemination. To circumvent this limitation and confirm the effect of A4.1 in a model closer to human breast cancer, we next used a similar protocol in a syngeneic model using implantation of murine 4T1 tumor cells into the mammary fat pad of immunocompetent BALB/c mice the *4T1* murine *TNBC* cell line allografted. A4.1 treatment after primary tumor resection significantly decreased the frequency of primary tumor re-growth which was observed in 80% of control mice at 4 weeks post-resection but in only 40% of A4.1-treated mice (**Figure 5d**), and also significantly reduced metastasis frequency (**Figure 5e**). These beneficial effect of chronic A4.1 treatment in immunocompetent mice is not accompanied by changes in white cell blood counts, suggesting that A4.1 did not exhibit an immunosuppressive effect (**Supp. Table 8**). Finally, treatment with A4.1 remarkably increased the survival rate from 30% in controls to 80% in treated mice (**Figure 5f**).

RAC1 activity as poor prognostic factor of TNBC

The observed effect of A4.1 on tumor growth and invasion is in agreement with a key role of Rac1 in cancerogenesis and metastasis. Indeed, extraction and analysis of data related to *RAC1* mRNA expression in cancer tissue from the Cancer Genome Atlas (**Supp. Figure 9**). This analysis attests that high level of *RAC1* expression in many types of cancer is correlated with a high mortality rate of patient. However, the overexpression of *RAC1* is not necessarily associated with an increase in its activity. Thus, we analyzed the levels of active *RAC1* (*RAC*-GTP) in a panel of human breast cancer samples. A comparison of *RAC1* activity was carried

out in Luminal B-like (immunohistochemically defined by hormone receptor (HR) dissociated expression, HER2 negative status and mitotic grade > 1) and in triple negative (defined by lack of ER and PR expressions, HER2 negative) tumors (**Supp. Table 9**). With the follow-up over several years, each patient group was divided into total remission or recurrence (metastatic relapse) cancer to evaluate a possible association between RAC1 activity and breast cancer aggressiveness. Regardless of breast cancer subtype, we observed by immunofluorescence a high level of active RAC1 in tumors from breast cancer patients who developed metastases within five years after sampling, while levels of RAC1-GTP are low or undetectable in primary tumors of patients who went into remission (**Figure 6a**). This analysis suggests for the first time that detection of RAC1 activity levels in primary tumor could be predictive of metastasis relapses in breast cancer with a high specificity and sensitivity in TNBC (**Figure 6b**). These results reinforce the hypothesis that activation of RAC1 is involved in the initiation of metastases and the therapeutic necessity in developing this new potent RAC1 inhibitor A4.1.

Discussion

Since the discovery of hotspot mutations in RAC1 in various human cancers (i.e: melanoma and breast cancer) and that the level of RAC1 expression is associated with high pathological stage and more aggressive tumor subtypes, RAC1 attracts increasing interest as a potential marker to predict cancer prognosis and therapeutic target against tumor progression and metastasis. Despite intensive research, traditional strategies have failed to identify specific inhibitor of small GTPases and these proteins have been considered undruggable for decades.

The analysis of different crystallographic structures combined with an understanding of RAC1 protein dynamics has allowed us to set up a pharmacophore and docking-based virtual screening of compounds libraries and to succeed in the identification of new RAC1 inhibitors. The lead compound A4.1 is the first potent and selective RAC inhibitor able to inhibit RAC activity *in vivo*. This structure-based methodology for small GTPase inhibitors seems to be the most relevant strategy to discover specific inhibitors. Indeed, this same approach also lead to identify the first multivalent small-molecule Pan-Ras inhibitor termed 3144, displaying anti-tumor activity in mouse cancer models(Welsch et al., 2017).

Inhibiting RAC1 activity by targeting the nucleotide binding could raise some concerns about the biological specificity and innocuity of a such molecule. Indeed, RAC1 GTPase is involved in various essential and vital cell functions (Jaffe Ann Revell Dev Biol 2005). The total inhibition of its activity could lead to considerable off-targets, impeding with clinical development of a such drug. However, we didn't detect toxicity and off-target activity of A4.1 *in vitro* and in mice. These results could be explained by the observation that A4.1 affinity to RAC1 is lower than nucleotides, thus preventing RAC1 to be fully inhibited. This specification would allow A4.1 to limit the overactivation of RAC1 observed in this study in breast cancer patients who developed metastases, and in various cancer(André-Grégoire et al. 2017) or other pathological processes(Marei et Malliri 2017).

To demonstrate the pharmacological/therapeutic potential of this innovative RAC1 inhibitors in metastatic cancer, we showed in two different experimental models, that the chronic administration of A4.1 significantly reduces the frequency of metastases compared to control and with a therapeutic efficacy comparable to the molecules used in the clinic. This beneficial effect results in the increase of the survival curve, suggesting that this potent RAC inhibitor A4.1 can be a promising therapeutic agent to limit metastasis spreading in invasive cancers.

Acquired resistance to specific therapeutics remains a fundamental cause of relapses and failure. The treatment of resistance tumors has proved a major challenge to the field of cancer therapeutics. It was recently observed that constitutive mutants of RAC1(Li Q Nat Comm. 2020) or an overactivity of the main RAC effector p21-activated kinase (PAK) confer resistance to chemotherapy by mTOR pathway activation and inhibition of apoptosis. In addition, a high-throughput functional screen using RNAi to targeting genes commonly amplified in breast tumors with acquired resistance identified RAC1 as one of the most relevant protein involved in the mechanisms of resistance. They demonstrated that the inhibition of RAC1 expression restored sensitivity to chemotherapies (Wetterskog et al 2013 Oncogene). Herein, we have observed that A4.1 is able of inhibiting wild-type and oncomutant RAC1 activities such as RAC1b and RAC^{P29S}. Thus, this clinical development of A4.1 would, in addition to preventing metastases, restore tumors' sensitivity to chemotherapy agents.

Methods

In silico screening. The structure of RAC1 was first extracted from the crystal structure of RAC1-NSC23766 complex (Zheng, Y., Nassar, N., and Skowronek, K. R. (2010) United States Patent 17,826,982). Pharmacophore models were created from the binding site of NSC23766 with RAC1 using the Receptor-Ligand Pharmacophore Generation tools within Accelrys Discovery Studio 4.0 (DS4.0) software package. The pharmacophore models were built using HBA (hydrogen bond acceptor), HBD (hydrogen bond donor) and hydrophobic features. These features were created based on the observation of RAC1/NSC23766 interactions either directly from the ligand or in projection on RAC1 structure. The models consist of several combinations of four features, two main features (one HBA oriented towards the hydroxyl group of Ser71 and one HBD pointed to the O atom of Leu70), an accessory feature (one HBA oriented towards the amine group of Gln74) and several hydrophobic features facing residues Val36, Ala59, Tyr64, and leu67 of RAC1, completed by thirteen exclusion spheres centered on the main residues of the defined binding site (Val36, Asn39, Trp56, Asp57, Thr58, Ala59, Tyr64, Leu67, Arg68, Leu70, Ser71, Pro73 and Asn74).

The pharmacophore models were used as a search query against three dimensional multi-conformational molecular databases. The 2013 edition of the HitFinderTM collection (14,400 compounds) from Maybridge (www.maybridge.com), the DIVERSetTM-EXP (50,000 compounds) and the DIVERSetTM-CL (50,000 compounds) from Chembridge (www.chembridge.com) were used in the virtual screening. For the preparation of ligands, duplicate structures were removed and 3D coordinates were generated. A multi-conformational ligand database was then created using Catalyst within the Build 3D Database tool under DS4.0. The query was performed using the Search 3D Database tool with the FAST search method under DS4.0, retrieving as hits only compounds matching all features of the query.

The docking studies were performed using LigandFit option of receptor-ligand interactions protocol section available in DS4.0. Initially, RAC1 protein was prepared, by adding the hydrogen atoms and removing the water molecules, and then minimized using CHARMM force field. The protein molecule thus prepared was then defined as the total receptor. The ligand molecules retained by the pharmacophore models were docked into the binding site of the RAC1 and the interaction energies in the form of dock score (Venkatachalam et al, 2003) between each ligand and the protein were calculated. Docking was performed using CFF as the energy grid. Penalty of 200kcal/mol/atom was set up to reduce the dock score of poses that occurred outside of the binding site. The conformational search of the ligand poses was performed by the Monte Carlo trial method. Maximum internal energy was set at 10000kcal/mol. A short rigid body minimization was then performed (steepest descent and Broyden Fletcher Goldfarb Shanno (BFGS) minimizations). Ten poses were saved for each ligand after docking and 100 steps of BFGS rigid body minimization were then carried out. Scoring was performed with the scoring functions: LigScore1 and Ligscore2 (Krammer et al, 2005), using CFF force field. Best scored compounds were retained based on the calculation of a consensus score and binding free energies after *in situ* ligand minimization under DS4.0.

The potential binding mode of the hit A4 in the NSC23766 binding site as well as in the nucleotide binding pocket of RAC1 was predicted by additional docking experiments using the crystal structure of RAC1 extracted from NSC23766/RAC1 complex (Zheng, Y., Nassar, N., and Skowronek, K. R. (2010) United States Patent 17,826,982) and the RAC1 structure extracted from RAC1/Arfaptin complex (PDB code 1I4D, Tarricone C, et al. 2001) respectively. Both LigandFit and C-Docker programs were used, the latter being another docking program using CHARMM-based molecular dynamics docking algorithm and implemented under DS4.0 (Wu et al, J Comp Chem 2003). For both docking programs, best poses among the 50 saved were retained based on consensus score (LigandFit) or C-Docker

energy (C-Docker), and then compared based on the calculation of binding free energy after *in situ* ligand minimization.

Cell culture. NIH3T3 cells grew up in DMEM (Gibco; Invitrogen) containing 1 g/L glucose, 10% foetal bovine serum, 100 units/mL penicillin and 100 µg/mL streptomycin at 37°C and 5% CO₂. MDA-MB-468Luc, MDA-MB-231, MDA-MB-435s and A375 cells grew up in DMEM (Gibco; Invitrogen) containing 4,5 g/L glucose, 10% foetal bovine serum, 100 units/mL penicillin and 100 µg/mL streptomycin at 37°C and 5% CO₂. Other cancer cell lines grew up in RPMI 1640 (Gibco; Invitrogen) containing 10% foetal bovine serum, 100 units/mL penicillin and 100 µg/mL streptomycin at 37°C and 5% CO₂.

Cell imaging by immunofluorescence. After indicated treatments, cells were fixed with 4% paraformaldehyde and permeabilized in PBS 0.5% Triton X-100. To assess Rac1 activity, cells were then incubated with Rac-GTP antibody (26903, NewEast Biosciences, King of Prussia, Pa) (dilution 1/500) overnight at room temperature, followed by secondary Alexa568-labeled anti-mouse antibody (dilution 1/1000). Cancer cells were detected with firefly luciferase antibody (ab21176, Abcam) (dilution 1/500) overnight at room temperature, followed by secondary Alexa488-labeled anti-rabbit antibody (dilution 1/1000). To assess cytoskeleton organization, cells were incubated with Alexa Fluor 488 phalloidin (A12379, Invitrogen) to visualize F-actin. After staining, cells were mounted in Prolong gold antifade reagent with DAPI and images were captured by a fluorescence microscope.

Focus formation assays. 1000 cells/well from the indicated cancer cell lines were seeded in 6-wells plates and allowed to grow 2 days before treatments. When indicated, cells were then treated three times a week with indicated doses or 10⁻⁵M (when not indicated) of A4.1. When the untreated well reached 70% of confluence, cells were fixed with 4% paraformaldehyde and colored with 0,1% Coomassie Blue. The area occupied by the cells was then quantified with ImageJ software.

Immunoblotting. After indicated treatments, MDA-MB-468Luc cells were incubated on ice with lysis buffer supplemented with proteases and phosphatases inhibitor cocktails (Sigma Aldrich, Saint Quentin Fallavier, France) and sodium orthovanadate. Lysates were subjected to SDS-PAGE, transferred to nitrocellulose membranes, and incubated with specific antibodies. P-Akt (9271), Akt (9272), pP44/42 (9101) and P44/42 (4695) antibodies were from Cell Signaling Technology (Leiden, The Netherlands). Tubulin was from Beckman Coulter (Villepinte, France). Immune complexes were detected with appropriate secondary antibodies and enhanced chemiluminescence reagent (Clarity ECL BioRad, Marnes la Coquette, France). Protein band intensities were quantified using ImageJ Software (NIH software, Bethesda, Md).

Rac-GTP pull-down assays. Pull-down assay using GST-PBD fusion proteins were performed on NIH3T3 lysates to assess Rac1 activity as previously described (Guilluy et al. 2011). The precipitated active Rac was subjected to SDS-PAGE and detected by immunoblot with anti-Rac1 antibody (BD biosciences) (dilution 1/1000).

Surface plasmon resonance studies. SPR immobilization was performed at 25 °C. Rac1, RhoA and Cdc42 purified proteins (respectively RH01, RC01 and CD01, Cytoskeleton) were diluted to 5 µg/mL in Na⁺ acetate buffer (pH 5.0) and injected into sensor chip CM5 (GE Healthcare) in a Biacore T200 (GE Healthcare) that was activated with NHS/EDC buffer. Approximately 5,000 response units of the purified protein were captured on the biosensor chip. Biosensor chips were blocked by an injection of 1 mM ethanolamine (pH 8.5). SPR analysis was performed at 25°C in HBSEP running buffer (5% DMSO).

1D cell migration. NIH3T3 cells (1000/well) were seeded in a 96 well plate with 10mm fibronectin stripes (CytoPlates Motility, CYTOO) in medium with 1% SVF and allowed to spread for 4 hours before capturing time-lapse images for 24 hours (image/10 minutes) on a Widefield Leica DMI 6000B drove with Metamorph software. Cells speed was measured with ImageJ software.

Cell adhesion assay using impedance technology. NIH3T3 cells (10000/well) were seeded in a 96 well plate microtiter xCELLigence assay plate (E-Plate) (ACEA Biosciences Inc.) and placed on the Real-time xCELLigence Cell Analyzer (Roche Applied Science) platform at 37°C to measure the “cell index” every 5 min for a period of 6 hours. The cell index unit is defined as $(R_n - R_b)/15$. R_n is the cell electrode impedance of the well when it contains cells. R_b is the background impedance of the well with the media alone.

Proteins. Full-length Rac1 carrying a 6xHis tag in C-terminus was purified as previously described (Cherfils et al. 2011). Full-length Rac2, RhoG, RhoA and Cdc42 were purified as previously described (Cherfils et al. 2011; Jang et al. 2010). Full-length Rac1G30S was obtained by directed mutagenesis on the pET-3a-Rac1HisCter plasmid using Quick change II site directed mutagenesis kit (Agilent technologies) accordingly to the manufacturer instructions (Primer for: CAATGCATTTTCCTTCAGAATATATCCCTAC / Primer rev: GTAGGGATATATTCTGAAGGAAATGCATTG). Small GTPases were loaded with GDP prior to nucleotide exchange by incubation of 250 μ M GTPase with 1.5 μ M GDP and 10 μ M EDTA for 30 min at room temperature. Nucleotide exchange was stopped by the addition of 20 mM MgCl₂. Removal of excess nucleotides and buffer exchange was done by gel filtration. Trio^{DH1PH1} was purified as previously described (Ferrandez et al. 2017). Tiam^{DHPH} is a kind gift of Scott Hansen (University of California, Berkeley). Tiam^{DHPH} was expressed in Rosetta (DE3) pLysS Escherichia coli strains in LB medium by induction with 0.5 mM IPTG overnight at 20 °C. Bacterial pellet was resuspended in lysis buffer (20 mM Tris pH 8.0, 500 mM NaCl, 2 mM β -mercaptoethanol, 2 mM MgCl₂, 10% glycerol, 0.5% tween-20, anti-protease cocktail) and frozen in liquid nitrogen. After thawing, benzonase was added to 7.5 U/mL and cells were disrupted using a French press, cleared by centrifugation at 14 000 g for 30 minutes and the supernatant was filtered over a 0.22 μ m filter. Proteins were first purified by an affinity step using a 5 mL His-Trap column (GE Healthcare) with elution at 500 mM imidazole, followed

by gel filtration on a Superdex 200 column (GE Healthcare) equilibrated with 20 mM Tris pH 8.0, 150 mM NaCl, 2 mM β -mercaptoethanol, 1 mM $MgCl_2$, 5% glycerol. P115RhoGEF^{DHPH} (residues 388-799) was cloned into a pFastBac HTA vector (EcoRI-KpnI sites) for expression in insect cells. After sequencing, the plasmid pFastBac HTA was transposed into a bacmid by transformation into DH10Bac competent cells. After extraction and screening of the recombinant bacmids, Sf21 cells were transfected. After obtaining the viral stock, expression tests in 24-well plates were performed. P115RhoGEF^{DHPH} was expressed in insect cells and purified by affinity chromatography on a HisTrap column followed by gel filtration with a Superdex 75 XK16 / 61 column (Amersham), and then concentrated at 30mg/ml in 50mM Hepes pH 7.4, 100mM NaCl, 2mM β -mercaptoethanol. Specific exchange activity towards RhoA determined by fluorescence kinetics is $0.04\text{ s}^{-1}\text{M}^{-1}$.

Nucleotide exchange kinetics. Nucleotide exchange kinetics were measured by recording the increase in fluorescence following association of mant-GTP ($\lambda_{\text{Ex}} = 360\text{ nm}$, $\lambda_{\text{Em}} = 440\text{ nm}$). All reactions were performed at 30°C in a buffer containing Tris 20mM pH 8, NaCl 150mM and $MgCl_2$ 1mM. Purified GTPases were at $0.5\ \mu\text{M}$, indicated GEFs at $0.01\ \mu\text{M}$, GTP at $1\ \mu\text{M}$, A4.1 at $5\ \mu\text{M}$. K_{obs} were determined by a single exponential over the entire kinetics, which was preferred over analysis initial velocities which can be affected by the intrinsic fluorescence of chemical compounds as described here (Cherfils et al. 2011; Ferrandez et al. 2017). All experiments were done at least in triplicate.

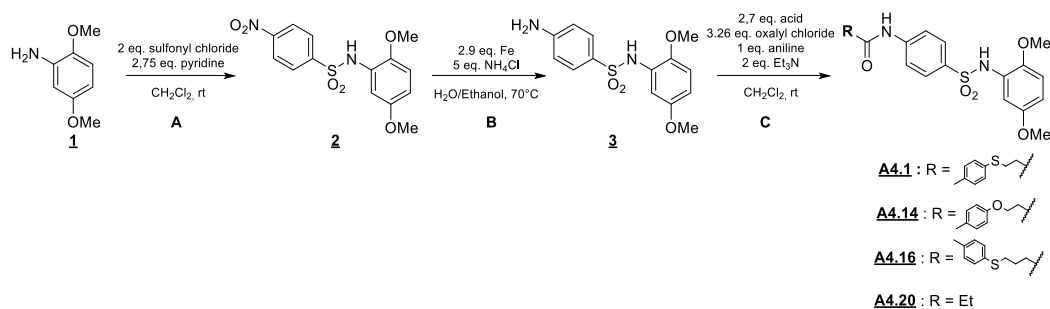
Histology. Paraformaldehyde (4% in PBS, 1 mL) was administered intratracheally in the lungs through a flexible catheter, trachea was ligatured, and lungs were excised. Lungs were fixed in 4% paraformaldehyde for 48 hours and embedded into paraffin. Sections measuring 6 mm in size were stained with hematoxylin/eosin for morphological studies. Histological grade (/12 points) was determined to assess inflammation (0-8) and pulmonary remodeling (0-4). To

assess smooth muscle hypertrophy/hyperplasia, sections were stained by immunochemistry with SM22 α antibody (Abcam).

Synthesis of chemical materials. *General considerations for the synthesis of Rac1 inhibitors:*

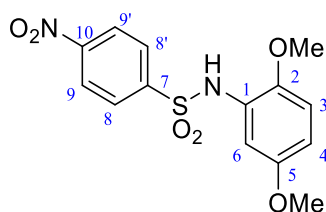
Solvents were purified and dried by standard methods prior to use; alternatively, the MB SPS-800-dry solvent system was used to dry dichloromethane. Commercially available reagents were purchased from Sigma Aldrich and were used without purification. Dry dichloromethane was obtained by refluxing solvent on calcium hydride for an hour and distilled under argon. Glassware used for reaction was either flame dried under vacuum or under argon stream for several minutes. Reactions were carried out under rigorous anhydrous conditions and argon stream/positive pressure of argon. ^1H and ^{13}C NMR spectra were recorded on a *Bruker Avance 300* spectrometer fitted with a 5 mm i.d. BBO probe carefully tuned to the recording frequency of 300.13 MHz (for ^1H) and 75.47 MHz (for ^{13}C), the temperature of the probe was set at room temperature (around 293-294 K), on a *Bruker Avance 400* spectrometer fitted with a 5 mm i.d. BBFO+ probe carefully tuned to the recording frequency of 400.13 MHz (for ^1H) and 100.61 MHz (for ^{13}C). The spectra are referenced to the solvent in which they were run (7.26 ppm for ^1H CDCl_3 and 77.16 ppm for ^{13}C CDCl_3 , 2.5 ppm for ^1H DMSO and 39.52 ppm for ^{13}C DMSO). Chemical shifts (δ) are given in ppm, and coupling constants (J) are given in Hz with the following splitting abbreviations: s = singlet, d = doublet, t = triplet, q = quartet, qt = quintet, sx = sextuplet, sp = septuplet, m = massif and br = broad. All assignments were confirmed with the aid of two-dimensional ^1H , ^1H (COSY), or ^1H , ^{13}C (HSQC, HMBC) experiments using standard pulse programs. All reactions were monitored by TLC on commercially available precoated plates (Kieselgel 60 F254), and the compounds were visualized with KMnO_4 solution [KMnO_4 (3 g), K_2CO_3 (20 g), NaOH (5% aq.; 5 mL), H_2O (300 mL)] and heating or by UV (254 nm) when possible. Flash column chromatography was carried out using high purity grade (Merck grade 9385) pore size 60 \AA , 230-400 mesh particle size silica gel (Sigma Aldrich). Solvents used for chromatography were prior distilled on a Buchi rotavapor R-220-SE. Low resolution mass spectrometry (MS) were recorded on a ThermoFinnigan DSQII quadripolar spectrometer (coupled with a TracUltra GC apparatus) for Chemical Ionization (CI), on a ThermoFinnigan LCQ Advantage spectrometer for ElectroSpray Ionisation (ESI). High resolution mass spectrometry (HRMS) were recorded on a ThermoFinnigan MAT95XL spectrometer (for CI) and on a ThermoFisher Scientific LTQ-Orbitrap spectrometer (for ESI).

Synthesis of inhibitors **A4.1**, **A4.14**, **A4.16**, **A4.20**



Synthesis of A4.1 :

2 : N-(2,5-dimethoxyphenyl)-4-nitrobenzenesulfonamide :

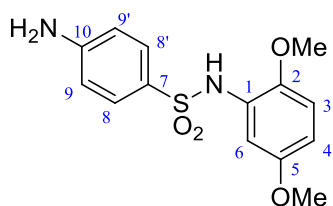


General procedure A :

To a suspension of commercial 4-nitrobenzenesulfonyl chloride (3g, 13.54 mmol) in CH_2Cl_2 (35 mL) were added dropwise commercial 2,5-dimethoxyaniline **1** (1.037g, 6.77 mmol) and pyridine (1.53 mL, 18.62 mmol) in CH_2Cl_2 (20 mL) at rt. After 3 hours of stirring at rt, the reaction mixture was quenched with water. The aqueous layer was extracted three times with CH_2Cl_2 . The combined organic layers were washed with a saturated aqueous NaHCO_3 solution and brine, dried over MgSO_4 , filtered and concentrated *in vacuo*. The crude was purified by column chromatography over silica gel (PE/AcOEt : 7/3) affording the expected compound **2** as a yellow solid (4.15g, 90%).

R_f : 0.42 (PE/ AcOEt : 7/3) **m.p.** : 160°C **¹H NMR** : (400 MHz, CDCl_3 , 25 °C) δ : 8.23 (m, 2H, H₉ et H_{9'}), 7.93 (m, 2H, H₈ et H_{8'}), 7.16 (d, ⁴J = 2.86 Hz, 1H, H₆), 7.10 (s, 1H, NH), 6.66 (d, ³J = 8.97 Hz, 1H, H₃), 6.60 (dd, ⁴J = 2.86 Hz, ³J = 8.97 Hz, 1H, H₄), 3.76 (s, 1H, OCH₃₍₅₎), 3.59 (s, 1H, OCH₃₍₂₎), **¹³C NMR** : (100 MHz, CDCl_3 , 25 °C) δ : 154.1 (C₅), 150.3 (C₁₀), 144.9 (C₇), 144.0 (C₂), 128.6 (C₈ et C_{8'}), 125.5 (C₁), 124.1 (C₉ et C_{9'}), 111.7 (C₃), 110.9 (C₄), 108.4 (C₆), 56.2 (OCH₃₍₂₎), 55.9 (OCH₃₍₅₎) **HRMS** : (ES-) m/z calculated for C₁₄H₁₃N₂O₆ [M-H]⁻, 337.0494; found 337.0505 **FT-IR** : $\nu(\text{NH}_{\text{sulfonamide}})$: 3309, $\nu(\text{CH}_{\text{ar}})$: 3107, $\nu(\text{CH}_{\text{Me}})$: 2945, 2839, $\nu_{\text{as}}(\text{NO}_2)$: 1533, $\nu_{\text{s}}(\text{NO}_2)$: 1346, $\nu_{\text{s}}(\text{SO})$: 1173, $\nu(\text{CN})$: 858.

3 : 4-amino-N-(2,5-dimethoxyphenyl)benzenesulfonamide :

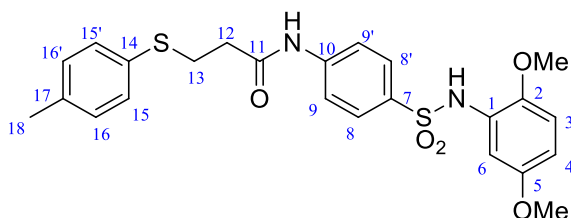


General procedure B :

To a solution of *N*-(2,5-dimethoxyphenyl)-4-nitrobenzenesulfonamide **2** (2 g, 6.48 mmol) in EtOH (100 mL) were successively added iron (1.06 g, 19 mmol) and an aqueous solution of NH₄Cl (1.72 g, 32.46 mmol in 20 mL of water). After stirring over 6 hours at 70 °C, the reaction mixture was filtered through a pad of celite on sintered funnel. After successive washings with acetone, CH₂Cl₂ and AcOEt, the biphasic mixture was separated. The aqueous layer was extracted twice with CH₂Cl₂. The combined organic layers were dried over MgSO₄ and the solvents were concentrated under vacuum. The crude was purified by chromatography over silica gel (PE/AcOEt : 1/1) affording the expected compound **3** as a light brown solid (1.37 g, 68%).

R_f : 0.22 (PE/ AcOEt : 1/1) **m.p.** : 115°C **¹H NMR** : (300 MHz, *d6*-DMSO, 25 °C) δ : 8.81 (s, 1H, NH), 7.38 (m, 2H, H₉-H_{9'}), 6.82 (d, 1H, H₃, ³J = 8.9 Hz), 6.78 (d; 1H, H₆, ⁴J = 2.9 Hz), 6.56 (dd, 1H, H₄, ³J = 8.8 Hz, ⁴J = 2.9 Hz), 6.52 (m, 2H, H₈-H_{8'}), 5.96 (s, 2H, NH₂), 3.63 (s, 3H, OCH₃₍₅₎), 3.56 (s, 3H, OCH₃₍₂₎) **¹³C NMR** : (75 MHz, *d6*-DMSO, 25 °C) δ : 152.8 (C₅ and C₁₀), 144.9 (C₂), 128.7 (C₈-C_{8'}), 127.3 (C₇), 124.8 (C₁), 112.5 (C₃), 112.3 (C₉-C_{9'}), 108.7 (C₄), 108.5 (C₆), 56.2 (OCH₃₍₅₎), 55.2 (OCH₃₍₂₎) **HRMS** : (ES+) *m/z* calculated for C₁₄H₁₆N₂O₄SNa [M-Na]⁺, 331.0728; found 331.0727 **FT-IR** : ν(NH_{amine}) : 3461, 3366 ; ν(NH_{sulfonamide}): 3218 ; ν(CH_{ar}) : 3110 ; ν(CH_{Me}) : 2939, 2839 ; ν_{as}(SO) : 1304 ; ν (CN) : 1257; ν_s(SO): 1144.

A4.1 : N-(4-(N-(2,5-dimethoxyphenyl)sulfamoyl)phenyl)-3-(p-tolylthio)propanamide



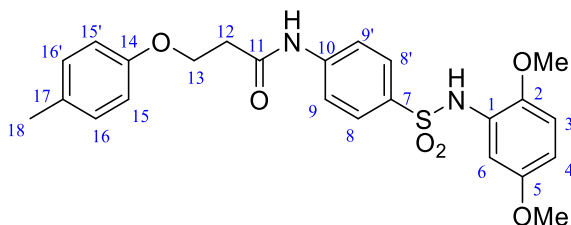
General procedure C :

In a 50 mL flask, commercial 3-(*p*-tolylthio)propanoic acid (0.38 g, 1.95 mmol) was dissolved in dry CH₂Cl₂ (10 mL) under argon atmosphere. Oxalyl chloride (0.17 mL, 1.95 mmol) and DMF (0.03 mL) were successively added to the reaction mixture at 0°C. After 15

minutes of stirring, bubbling stopped and an NMR analysis confirmed total conversion to the acyl chloride. Oxalyl chloride and CH_2Cl_2 were removed under reduced pressure. To a solution of the resulting 3-(*p*-tolylthio)propanoyl chloride in dry CH_2Cl_2 (10 mL) were added dropwise at 0°C 4-amino-*N*-(2,5-dimethoxyphenyl)benzenesulfonamide **3** (0.6 g, 1.95 mmol) and Et_3N (0.15 mL, 1.95 mmol) dissolved in dry CH_2Cl_2 (10 mL). After completion, the reaction mixture was quenched with an aqueous 5% NaHCO_3 solution. The aqueous layer was extracted three times with CH_2Cl_2 . The combined organic layers were washed successively with a molar solution of HCl and brine, dried over MgSO_4 , filtered and concentrated *in vacuo*. The crude was purified by chromatography over silica gel (PE/AcOEt/ CH_2Cl_2 : 5/3/2) then affording the expected compound **A4.1** as a white solid (0.745 g, 78%).

R_f : 0.15 (PE/ AcOEt/ CH_2Cl_2 : 5/3/2) **m.p.** : 129°C $^1\text{H NMR}$: (300 MHz, CDCl_3 , 25°C) δ ppm: 7.70 (m, 2H, $\text{H}_8\text{-H}_{8'}$), 7.60 (s, 1H, CONH), 7.53 (m, 2H, $\text{H}_9\text{-H}_{9'}$), 7.29 (m, 2H, $\text{H}_{15}\text{-H}_{15'}$), 7.13 (d, 1H, H_6 , $^4\text{J} = 2,8$ Hz), 7.10 (m, 2H, $\text{H}_{16}\text{-H}_{16'}$), 7.03 (s, 1H, SO_2NH), 6.65 (d, 1H, H_3 , $^3\text{J} = 8,8$ Hz), 6.53 (dd, 1H, H_4 , $^3\text{J} = 8,9$ Hz, $^4\text{J} = 2,9$ Hz), 3.74 (s, 3H, $\text{OCH}_{3(5)}$), 3.61 (s, 3H, $\text{OCH}_{3(2)}$), 3.21 (t, 2H, H_{12} , $^3\text{J} = 6,9$ Hz), 2.62 (t, 2H, H_{13} , $^3\text{J} = 6,9$ Hz), 2.30 (s, 3H, H_{18}) $^{13}\text{C NMR}$: (75 MHz, CDCl_3 , 25°C) δ ppm: 169.6 (C_{11}), 153.9 (C_2), 143.49 (C_{10}), 141.8 (C_5), 137.2 (C_{17}), 133.9 (C_7), 130.9 ($\text{C}_{15}\text{-C}_{15'}$), 130.7 (C_{14}), 130.0 ($\text{C}_{8\text{-}8'}$), 128.6 ($\text{C}_{16}\text{-C}_{16'}$), 126.5 (C_1), 119.1 ($\text{C}_9\text{-C}_9'$), 111.5 (C_3), 109.7 (C_4), 107.1 (C_6), 56.2 ($\text{OCH}_{3(5)}$), 55.8 ($\text{OCH}_{3(2)}$), 37.2 (C_{12}), 29.9 (C_{13}), 21.0 (C_{18}) **HRMS** : (ES+) m/z calculated for $\text{C}_{24}\text{H}_{27}\text{N}_2\text{O}_5\text{S}_2$ [M-H] $^+$, 487.1361 ; found 487.1362 **FT-IR** : $\nu(\text{NH}_{\text{amide}})$: 3310 ; $\nu(\text{NH}_{\text{sulfonamide}})$: 3242 ; $\nu(\text{CH}_{\text{ar}})$: 3125, 3066 ; $\nu(\text{CH}_{\text{OMe}})$: 2953, 2833 ; $\nu(\text{C=O})$: 1689 ; $\nu_{\text{as}}(\text{SO})$: 1330; $\nu_{\text{s}}(\text{SO})$: 1149.

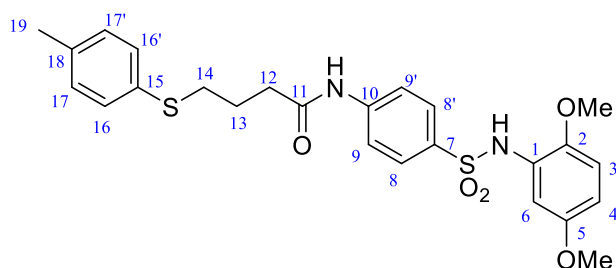
A4.14 : **N-(4-(N-(2,5-dimethoxyphenyl)sulfamoyl)phenyl)-3-(*p*-tolylthio)propanamide**



A4.14 was obtained following general procedure **C**, using commercial 3-(*p*-tolylthio)propanoic acid (0.36 g, 2 mmol), oxalyl chloride (0.17 mL, 2 mmol), 4-amino-*N*-(2,5-dimethoxyphenyl)benzenesulfonamide **3** (0.308 g, 1 mmol) and Et_3N (0.21 mL, 1.5 mmol). After purification (PE/AcOEt : 1/1), it afford the expected compound **A4.14** as a white solid (0.26 g, 55%). R_f : 0.46 ($\text{CH}_2\text{Cl}_2/\text{AcOEt}$: 9/1) **m.p.** : 145°C $^1\text{H NMR}$: (300 MHz, CDCl_3 , 25°C)

°C) δ ppm: 8.15 (s, 1H, CONH), 7.71 (m, 2H, H₈-H_{8'}), 7.55 (m, 2H, H₉-H_{9'}), 7.14 (d, 1H, H₆, $^4J = 2.9$ Hz), 7.10 (m, 2H, H₁₅-H_{15'}), 7.03 (s, 1H, SO₂NH), 6.83 (m, 2H, H₁₆-H_{16'}) 6.65 (d, 1H, H₃, $^3J = 8.9$ Hz), 6.52 (dd, 1H, H₄, $^3J = 8.9$ Hz, $^4J = 2.9$ Hz), 4.28 (t, 2H, H₁₃, $^3J = 5.7$ Hz), 3.74 (s, 3H, OCH₃₍₅₎), 3.61 (s, 3H, OCH₃₍₂₎), 2.82 (t, 2H, H₁₂, $^3J = 5.7$ Hz), 2.31 (s, 3H, H₁₈) ^{13}C NMR : (75 MHz, CDCl₃, 25 °C) δ ppm: 169.5 (C₁₁), 155.8 (C₁₄), 154.1 (C₂), 143.7 (C₁₀), 142.1 (C₅), 134.1 (C₇), 131.4 (C₁₇), 130.3 (C₁₆-C_{16'}), 128.7 (C₈-C_{8'}), 126.7 (C₁), 119.3 (C₉-C_{9'}), 114.7 (C₁₅-C_{15'}), 111.7 (C₃), 110.0 (C₄), 107.3 (C₆), 64.3 (C₁₃), 56.4 (OCH₃₍₅₎), 55.9 (OCH₃₍₂₎), 37.9 (C₁₂), 20.6 (C₁₈) HRMS : (ES⁺) m/z calculated for C₂₄H₂₆N₂O₆SNa [M-Na]⁺, 493.1409; found 493.1410 FT-IR : ν (NH) : 3242 ; ν (CH_{ar}) : 3065 ; ν (CH_{OMe}) : 2837 ; $\nu_{\text{as}}(\text{SO})$: 1321 ; ν (CN): 1283 ; $\nu_{\text{s}}(\text{SO})$: 1152.

A4.16 : N-(2,5-dimethoxyphenyl)-4-(3-(p-tolylthio)butanamido)benzamide

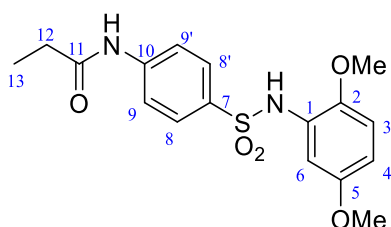


4-methyl-thiophenol (1.77 g, 14.3 mmol) was dissolved in DMF (18 mL). To the stirred solution at 0°C was added carefully in four times sodium hydride (0.57 g, 23.8 mmol, 60 %). The reaction mixture was kept stirring at 0°C for 30 min. γ -lactone was then added dropwise. After stirring at 0°C for 15 min, the reaction was warmed to rt, and finally to 90°C. After cooling down at rt, the reaction mixture was diluted with AcOEt and quenched with HCl (1M). The two layers were separated and the organic phase was washed with water and brine, dried over Na₂SO₄, filtered and concentrated off under vacuo. A purification of the crude (CH₂Cl₂/EtOAc : 9/1) was performed to obtain 4-(p-tolylthio)butanoic acid as a light yellow solid (0.9 g, 30%) ^1H NMR (300 MHz, CDCl₃) : 7.27 (m, 2H, H₆-H_{6'}), 7.10 (m, 2H, H₇-H_{7'}), 2.93 (t, 2H, $^3J = 7.2$ Hz, H₄), 2.51 (t, 2H, $^3J = 7.2$ Hz, H₂), 2.32(s, 3H, H₉), 1.92 (quint, 2H, $^3J = 7.2$ Hz, H₃) ^{13}C NMR (75 MHz, CDCl₃) : 178.8 (C₁), 136.5 (C₈), 131.9 (C₅), 130.4 (C₇-C_{7'}), 129.8 (C₆-C_{6'}), 33.6 (C₂), 32.5 (C₄), 24.0 (C₃), 21.0 (C₉).

A4.16 was obtained following general procedure **C**, using the corresponding 4-(p-tolylthio)butanoyl chloride obtained from 4-(p-tolylthio)butanoic acid (0.42 g, 2 mmol), oxalyl chloride (0.17 mL, 2 mmol), 4-amino-N-(2,5dimethoxyphenyl)benzenesulfonamide **3** (0.2 g, 0.65 mmol) and Et₃N (0.11 mL, 0.78 mmol). After purification by precipitation in iPrOH, the expected compound **A4.16** is isolated as a white solid (0.1 g, 20%). **R_f** : 0.12 (CH₂Cl₂) **m.p.** :

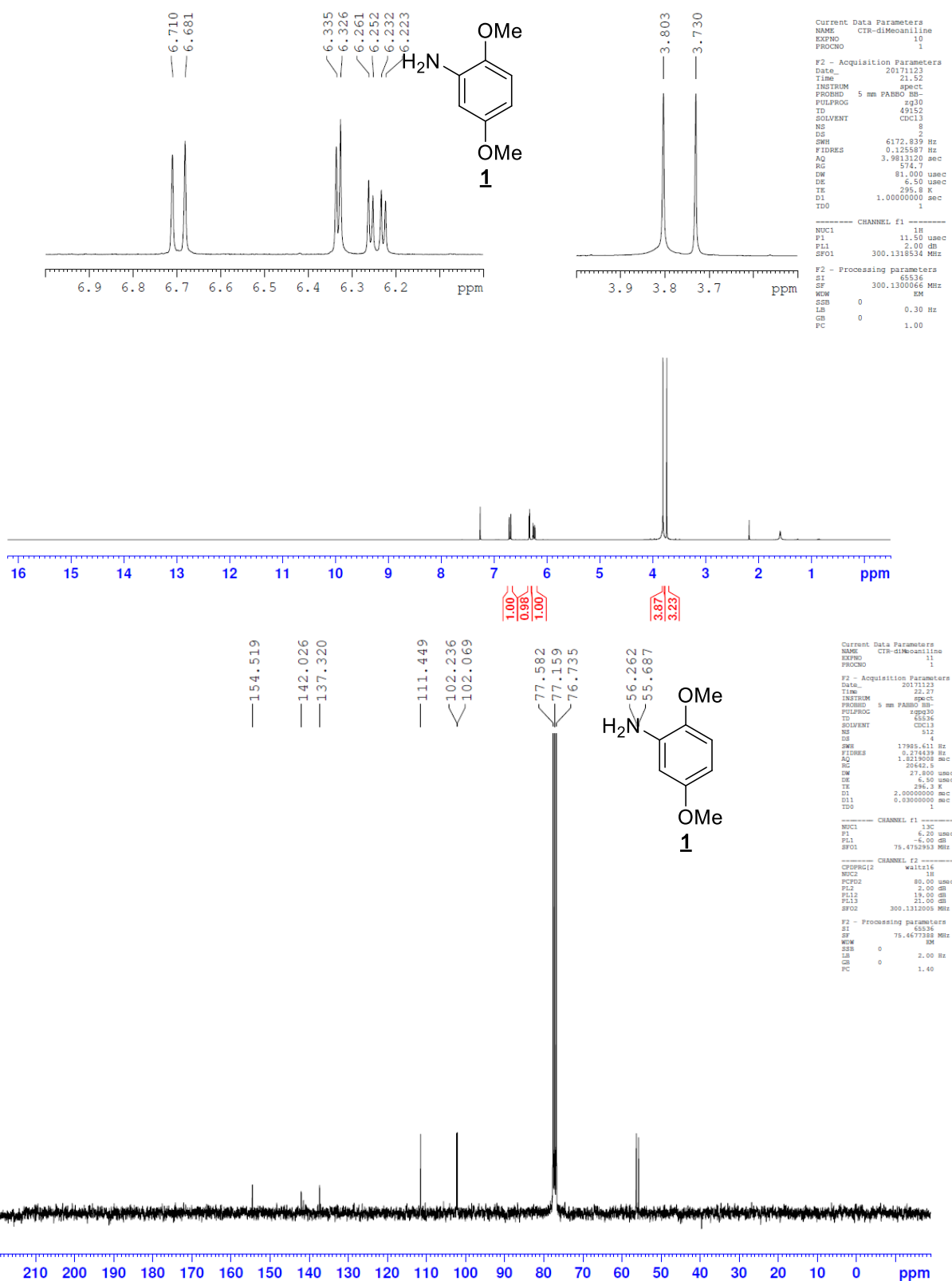
153°C $^1\text{H NMR}$ (300 MHz, CDCl_3) : 7.70 (m, 2H, H₈-H_{8'}), 7.52 (m, 2H, H₉-H_{9'}), 7.40 (s, 1H, CONH), 7.24 (m, 2H, H₁₆-H_{16'}), 7.13 (d, 1H, H₆, $^4J = 2.8$ Hz), 7.07 (m, 2H, H₁₇-H_{17'}), 7.04 (s, 1H, SO₂NH), 6.64 (d, 1H, H₃, $^3J = 8.9$ Hz), 6.53 (dd, 1H, H₄, $^4J = 2.8$ Hz, $^3J = 8.9$ Hz), 3.74 (s, 3H, OCH₃₍₅₎), 3.61 (s, 3H, OCH₃₍₂₎), 2.96 (t, 2H, H₁₄, $^3J = 6.8$ Hz), 2.51 (t, 2H, H₁₂, $^3J = 7.2$ Hz), 2.96 (s, 3H, H₁₉), 2.01 (q, 2H, H₇, $^3J = 7.0$ Hz) $^{13}\text{C NMR}$ (75 MHz, CDCl_3) : 170.9 (C₁₁), 154.0 (C₅), 143.7 (C₁₀), 142.1 (C₂), 136.7 (C₁₈), 133.9 (C₇), 131.9 (C₁₅), 130.5 (C₁₆-C_{16'}), 130.0 (C₁₇-C_{17'}), 128.7 (C₈-C_{8'}), 126.7 (C₁), 119.1 (C₉-C_{9'}), 111.6 (C₆), 109.9 (C₃), 107.2 (C₄), 56.4 (OCH₃₍₅₎), 55.9 (OCH₃₍₂₎), 35.8 (C₁₂), 33.8 (C₁₄), 24.5 (C₁₃), 21.1 (C₁₉) **HRMS** : (ES+) m/z calculated for C₂₆H₂₈N₂O₄SNa [M-Na]⁺, 523.1337; found 523.1340 **FT-IR** : $\nu(\text{NH})$: 3312 ; $\nu(\text{CH}_{\text{ar}})$: 2917 ; $\nu(\text{CH}_{\text{OMe}})$: 2832 ; $\nu_{\text{as}}(\text{SO})$: 1325 ; $\nu(\text{CN})$: 1304 ; $\nu_{\text{s}}(\text{SO})$: 1157.

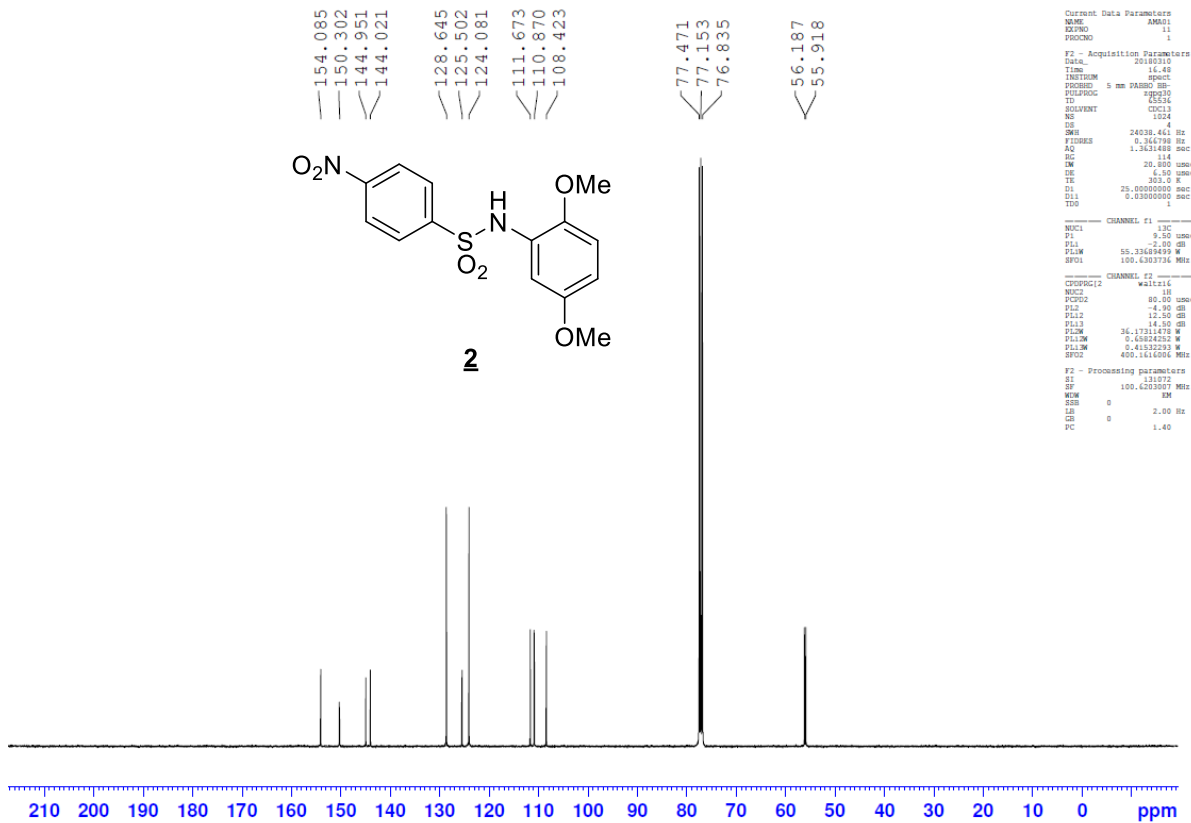
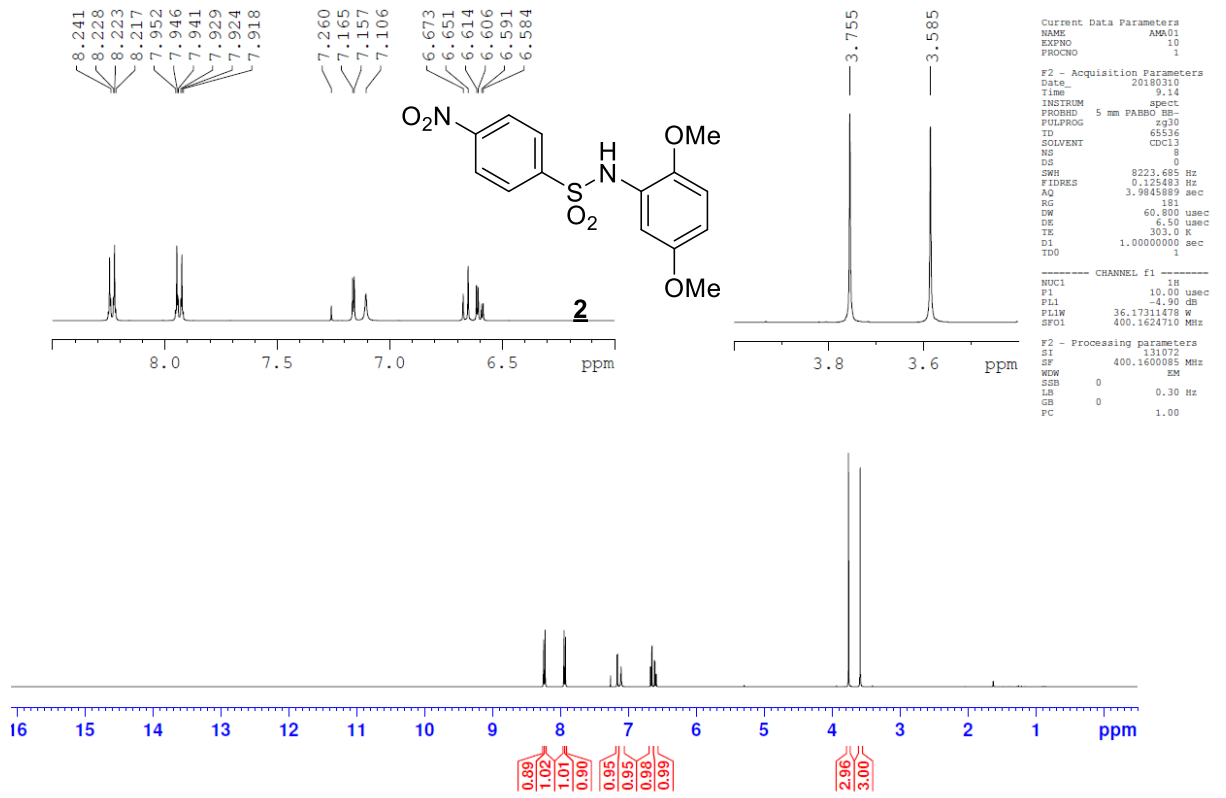
A4.20 : N-(2,5-dimethoxyphenyl)-4-(propanamido)benzamide

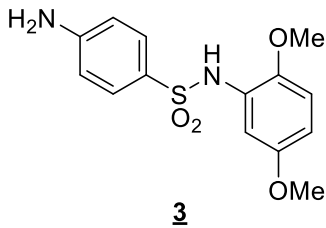
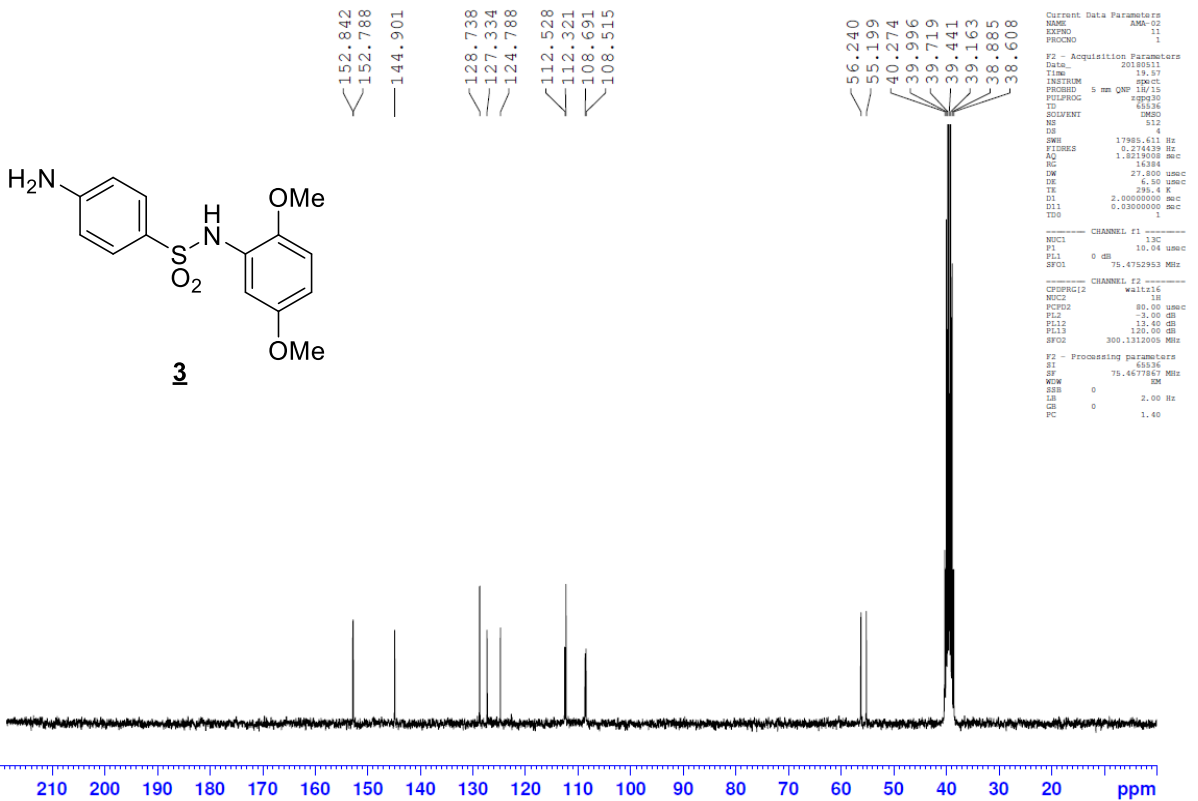
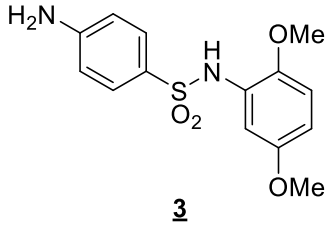
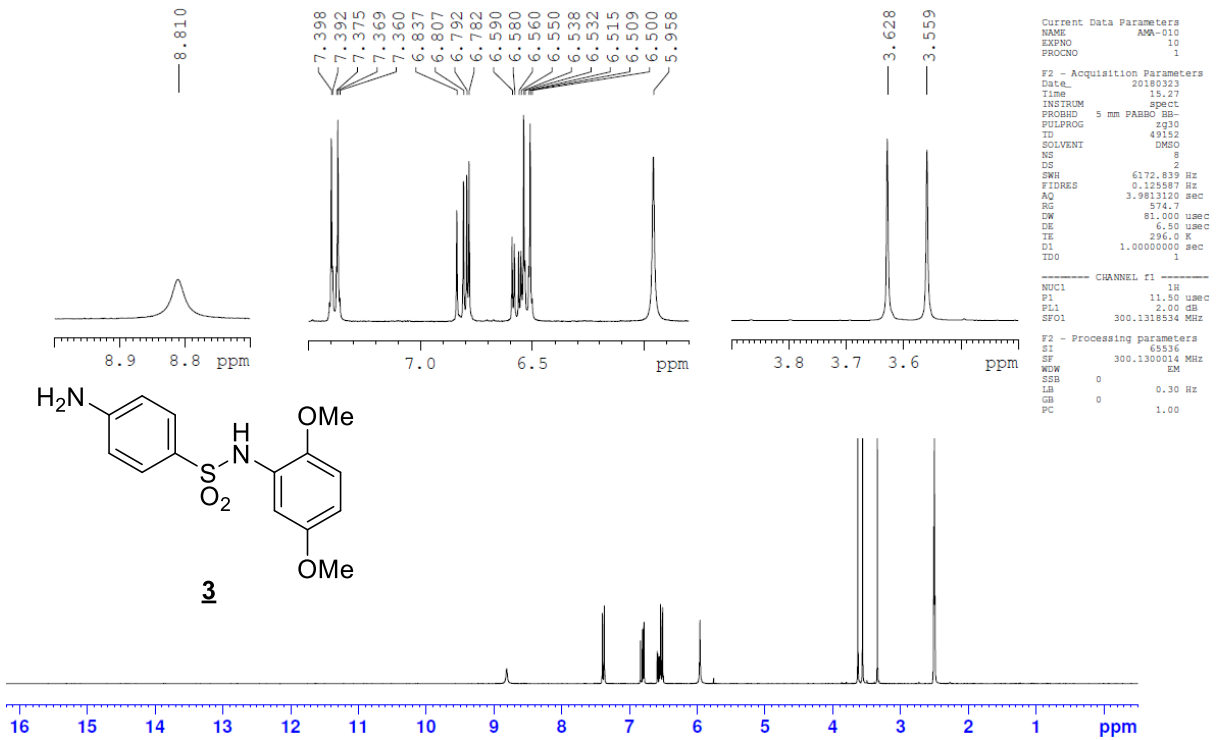


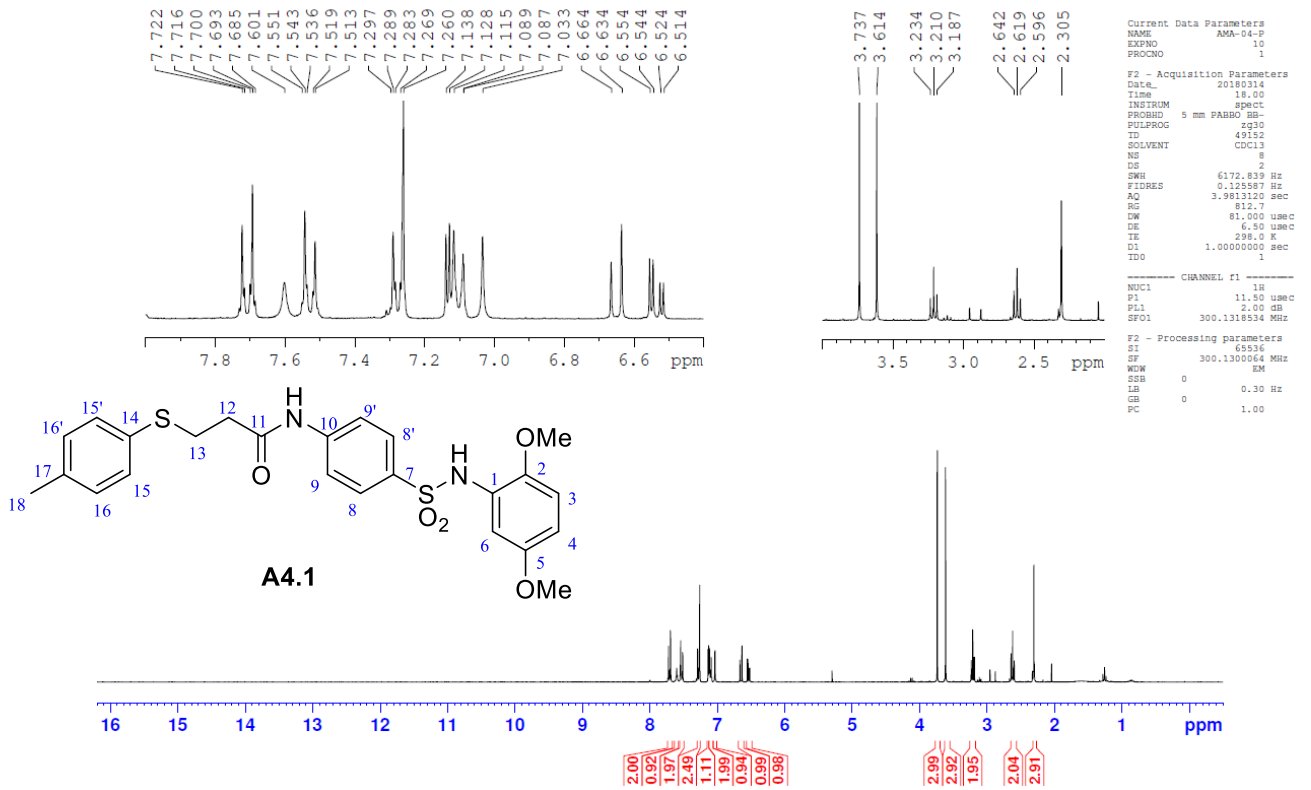
A4.20 was obtained following general procedure **C**, using the corresponding propanoyl chloride obtained from commercial propionic acid (0.36 g, 4.8 mmol), oxalyl chloride (0.41 mL, 4.8 mmol), 4-amino-N-(2,5dimethoxyphenyl)benzenesulfonamide **3** (0.5 g, 1.6 mmol) and Et₃N (0.67 mL, 4.8 mmol). After purification by precipitation in hexane, the expected compound **A4.16** is obtained as a white solid (0.15 g, 73%) **R_f**: 0.05 (CH_2Cl_2) m.p. : 170°C $^1\text{H NMR}$: (300 MHz, *d4*-MeOD, 25 °C) δ ppm: 7.65 (s, 4H, H₈-H_{8'} and H₉-H_{9'}), 7.03 (d, 1H, H₆, $^4J = 3.3$ Hz), 6.74 (d, 1H, H₃, $^3J = 8,9$ Hz), 6.62 (dd, 1H, H₄, $^3J = 8.9$ Hz, $^4J = 3.3$ Hz), 3.72 (s, 3H, OCH₃₍₅₎), 3.52 (s, 3H, OCH₃₍₂₎), 2.39 (q, 2H, H₁₂, $^3J = 7.5$ Hz), 1.18 (t, 3H, H₁₃, $^3J = 7.5$ Hz) $^{13}\text{C NMR}$: (75 MHz, *d4*-MeOD, 25 °C) δ ppm: 175.6 (C₁₁), 155.1 (C₅), 147.0 (C₁₀), 144.2 (C₂), 135.4 (C₇), 129.4 (C₈-C_{8'}), 127.8 (C₁), 120.0 (C₉-C_{9'}), 113.0 (C₃), 111.6 (C₄), 111.3 (C₆), 56.6 (OCH₃₍₅₎), 56.1(OCH₃₍₂₎), 31.1 (C₁₂), 9.9 (C₁₃) **HRMS** : (ES+) m/z calculated for C₁₇H₂₀N₂O₅SNa [M-Na]⁺, 387.0991; found 387.0977 **FT-IR** : $\nu(\text{NH})$: 3342, 3171 ; $\nu(\text{CH}_{\text{ar}})$: 2993 ; $\nu(\text{CH}_{\text{al}})$: 2925 ; $\nu(\text{CH}_{\text{OMe}})$: 2834 ; $\nu_{\text{as}}(\text{SO})$: 1329 ; $\nu(\text{CN})$: 1307 ; $\nu_{\text{s}}(\text{SO})$: 1152.

NMR spectra of the intermediates **1**, **2**, **3** and final compounds **A4.1**, **A4.14**, **A4.16**, **A4.20**

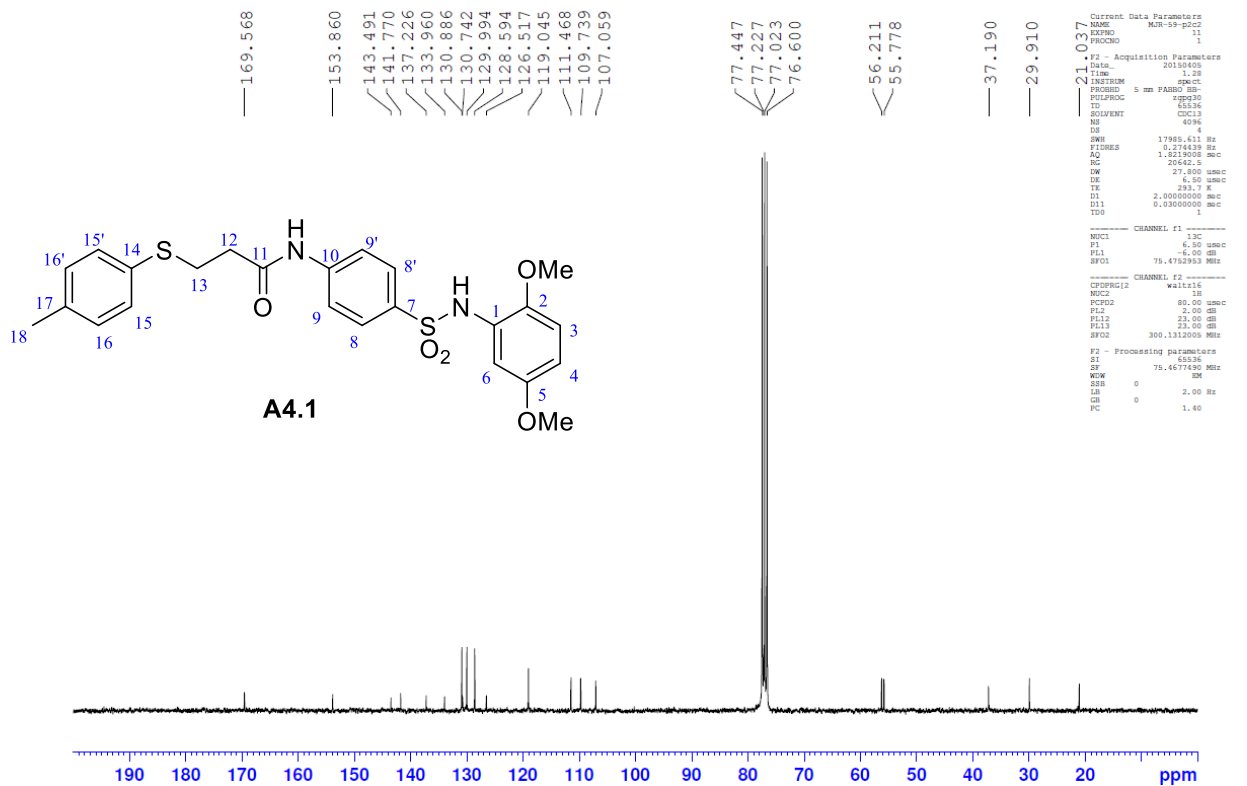


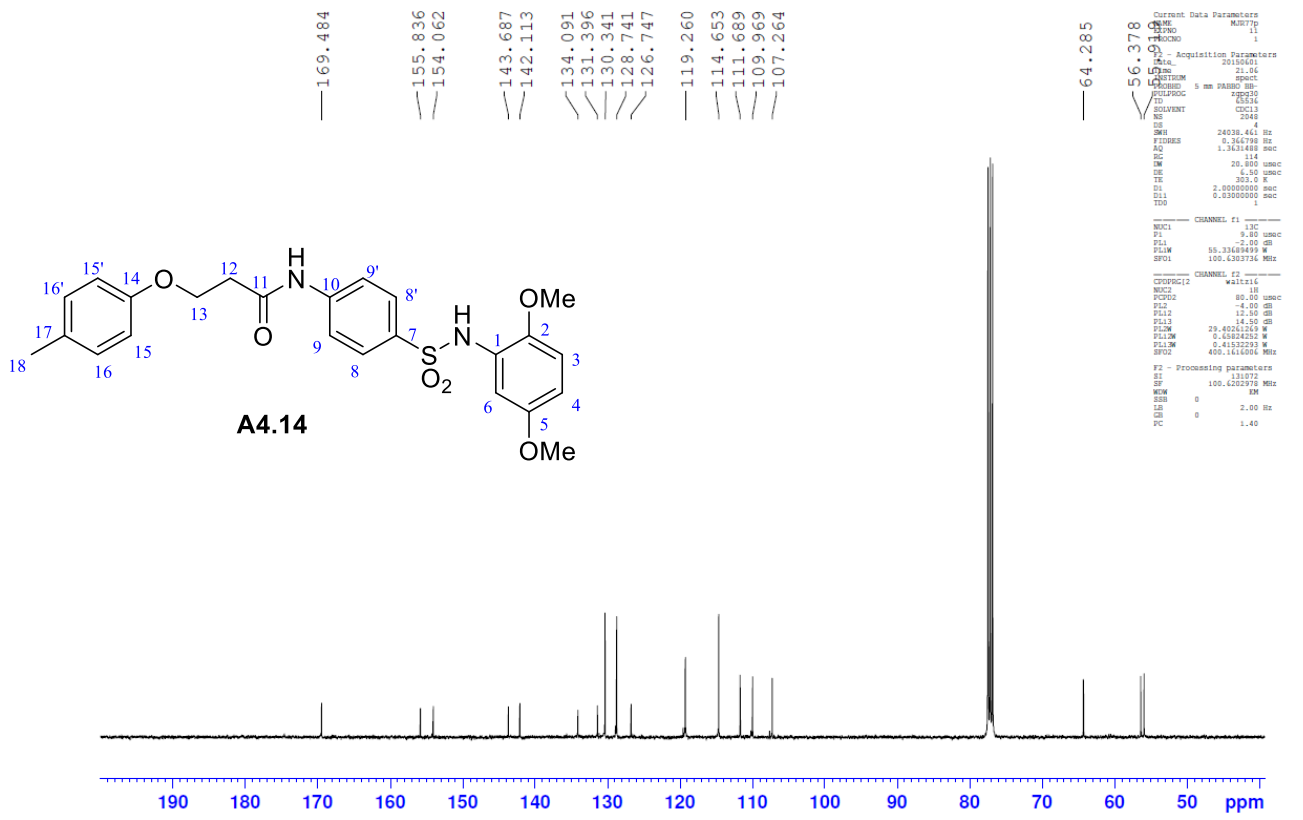
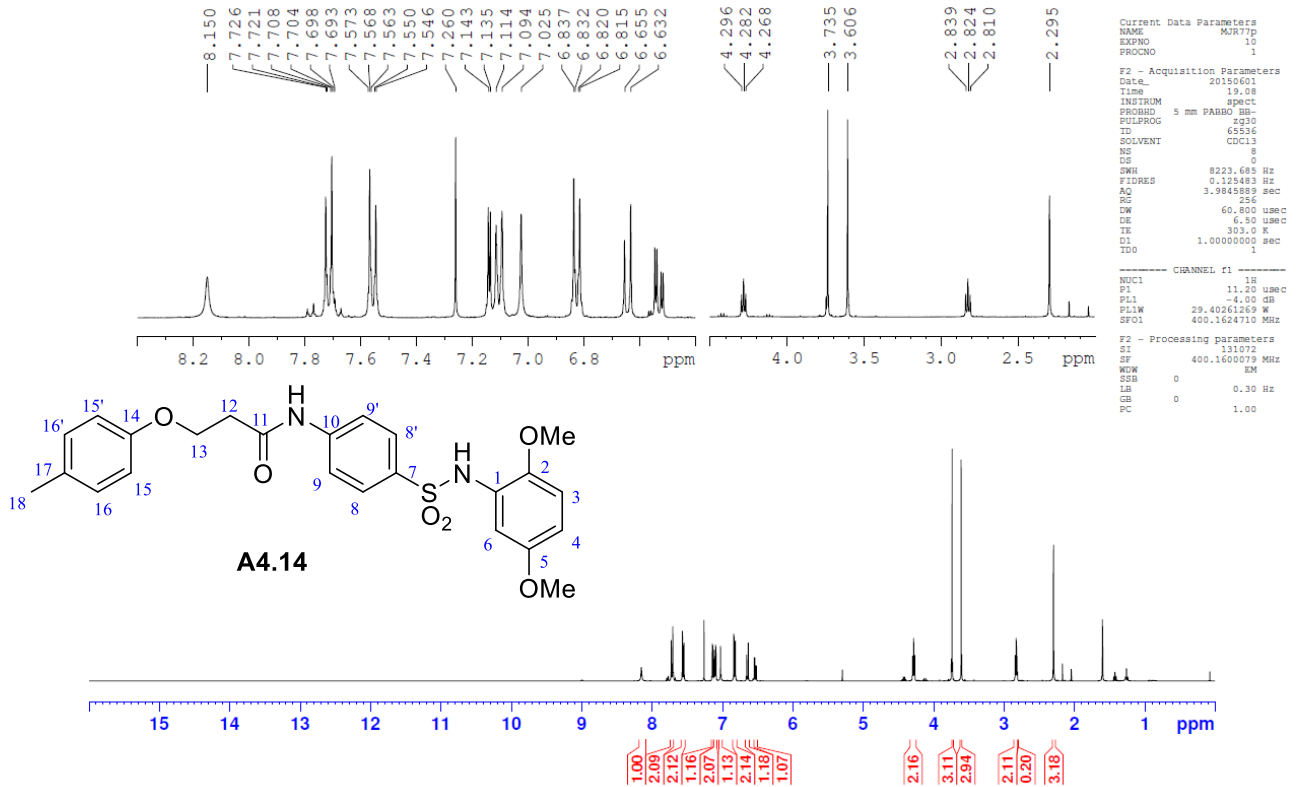


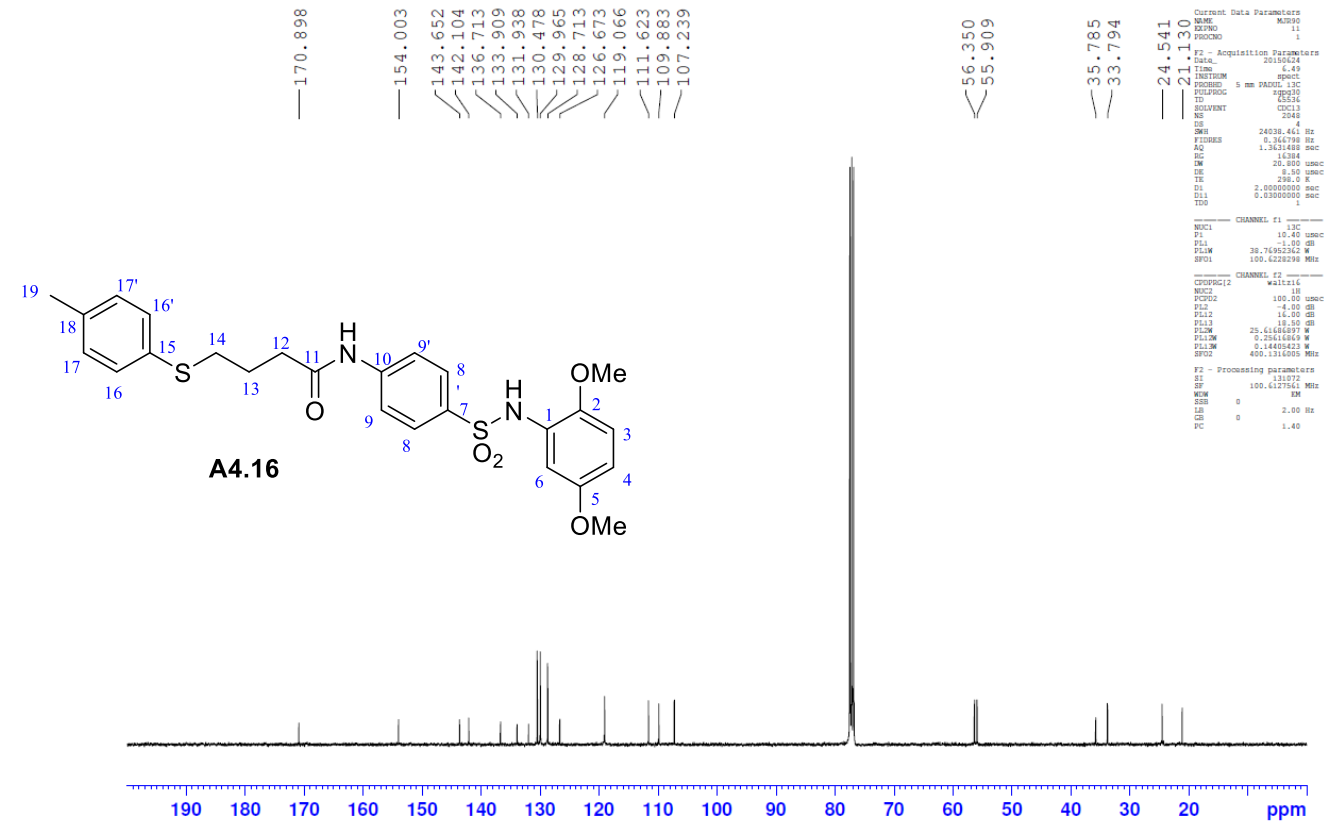
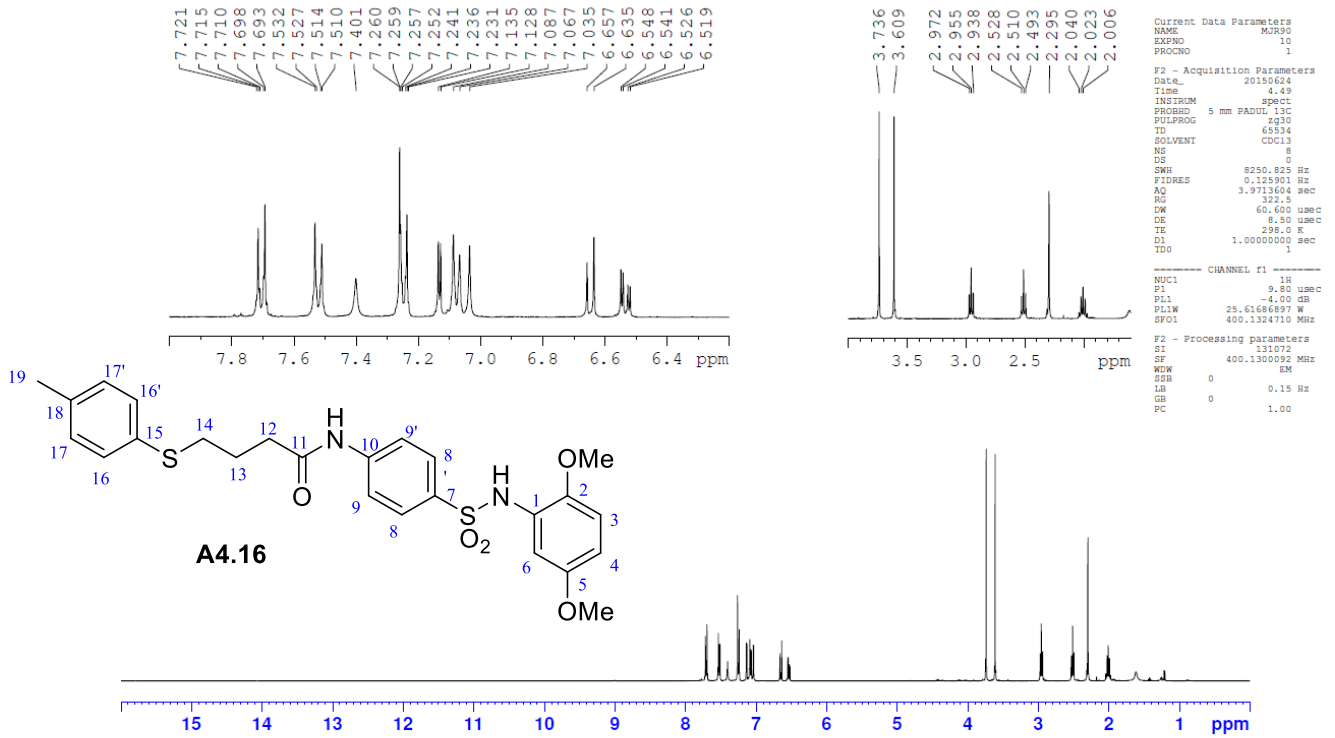


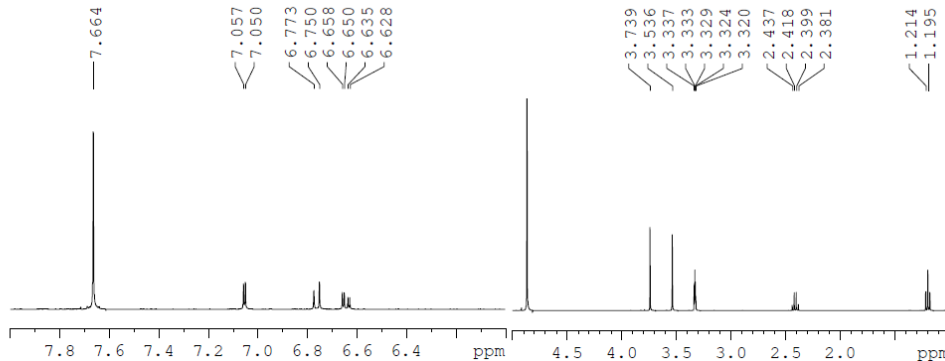


MJR-59-p2c2







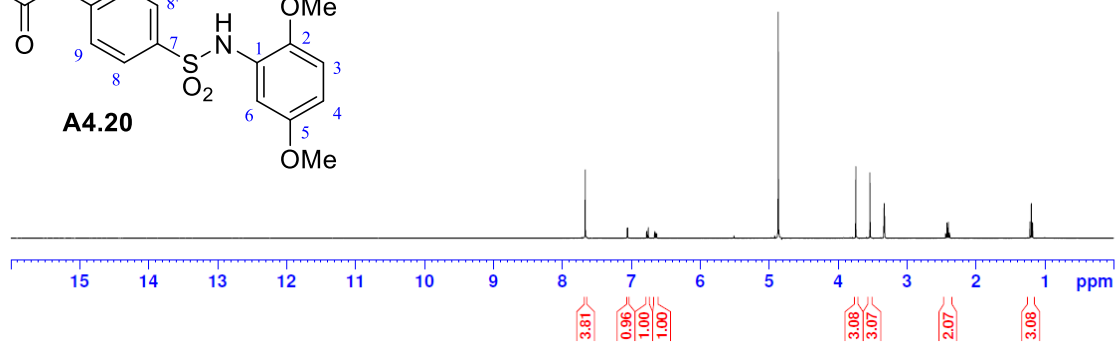
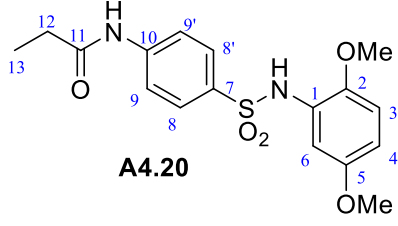


Current Data Parameters
 NAME MTR-101pp
 EXPNO 13
 PROCNO 1

F2 - Acquisition Parameters
 Date_ 20150721
 Time 21:40
 INSTRUM spect
 PROBHD 5 mm PADUL 13C
 PULPROG zgpg30
 TD 65536
 ID WEO
 SOLVENT MeOD
 NS 8
 DS 4
 SWH 8250.825 Hz
 FIDRES 0.125901 Hz
 AQ 1.3713604 sec
 RG 456.1
 DW 60.660 usec
 DE 8.50 usec
 TE 298.0 K
 IE 1.0000000 sec
 TD0 1

==== CHANNEL f1 =====
 NUC1 1H
 P1 9.80 usec
 PL1 -4.00 dB
 PL1W 25.61686897 W
 SFO1 400.1324710 MHz

F2 - Processing parameters
 SI 131072
 SF 400.1300000 MHz
 NDM EM
 SSB 0
 LB 0.30 Hz
 GB 0
 PC 1.00



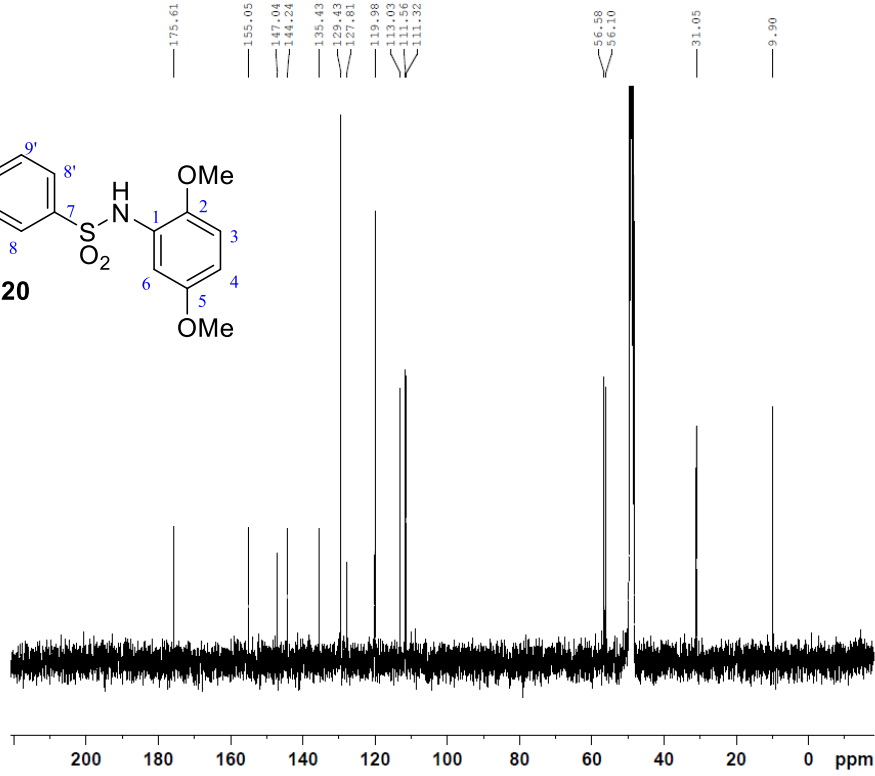
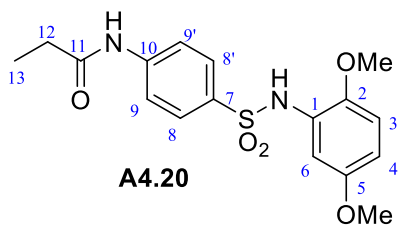
Current Data Parameters
 NAME MTR-101pp
 EXPNO 11
 PROCNO 1

F2 - Acquisition Parameters
 Date_ 20150721
 Time 23:39
 INSTRUM spect
 PROBHD 5 mm PADUL 13C
 PULPROG zgpg30
 TD 65536
 ID WEO
 SOLVENT MeOD
 NS 2048
 DS 4
 SWH 24038.461 Hz
 FIDRES 0.366798 Hz
 AQ 1.3631488 sec
 RG 9195.2
 DW 20.800 usec
 DE 8.50 usec
 TE 298.0 K
 IE 2.00000000 sec
 D11 0.03000000 sec
 TD0 1

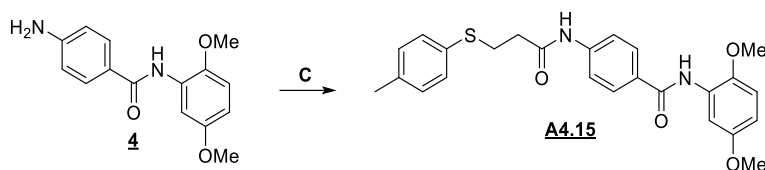
==== CHANNEL f1 =====
 NUC1 13C
 P1 10.40 usec
 PL1 -1.00 dB
 PL1W 38.76952362 W
 SFO1 100.6228298 MHz

==== CHANNEL f2 =====
 CPDPRG2 waltz16
 NUC2 1H
 PCPD2 100.00 usec
 PL2 -4.00 dB
 PL12 16.00 dB
 PL13 18.50 dB
 PL2W 25.61686897 W
 PL12W 0.25616869 W
 PL13W 0.14405423 W
 SFO2 400.1316005 MHz

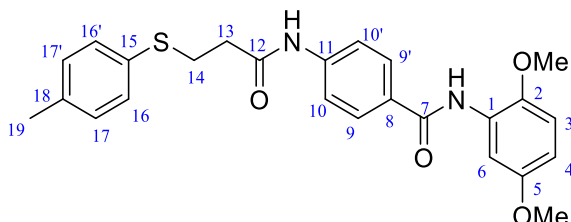
F2 - Processing parameters
 SI 131072
 SF 100.6126273 MHz
 NDM EM
 SSB 0
 LB 2.00 Hz
 GB 0
 PC 1.40



Synthesis of inhibitor A4.15

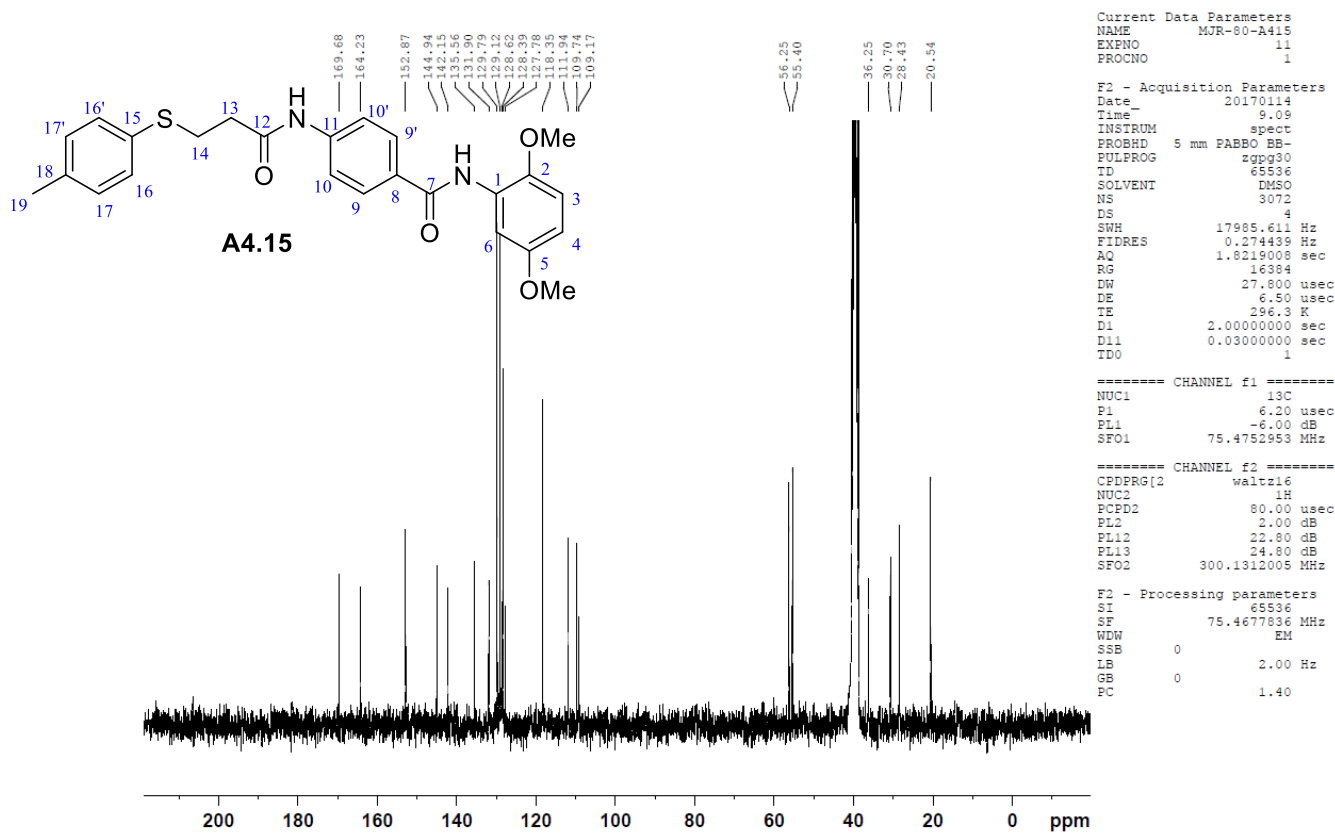
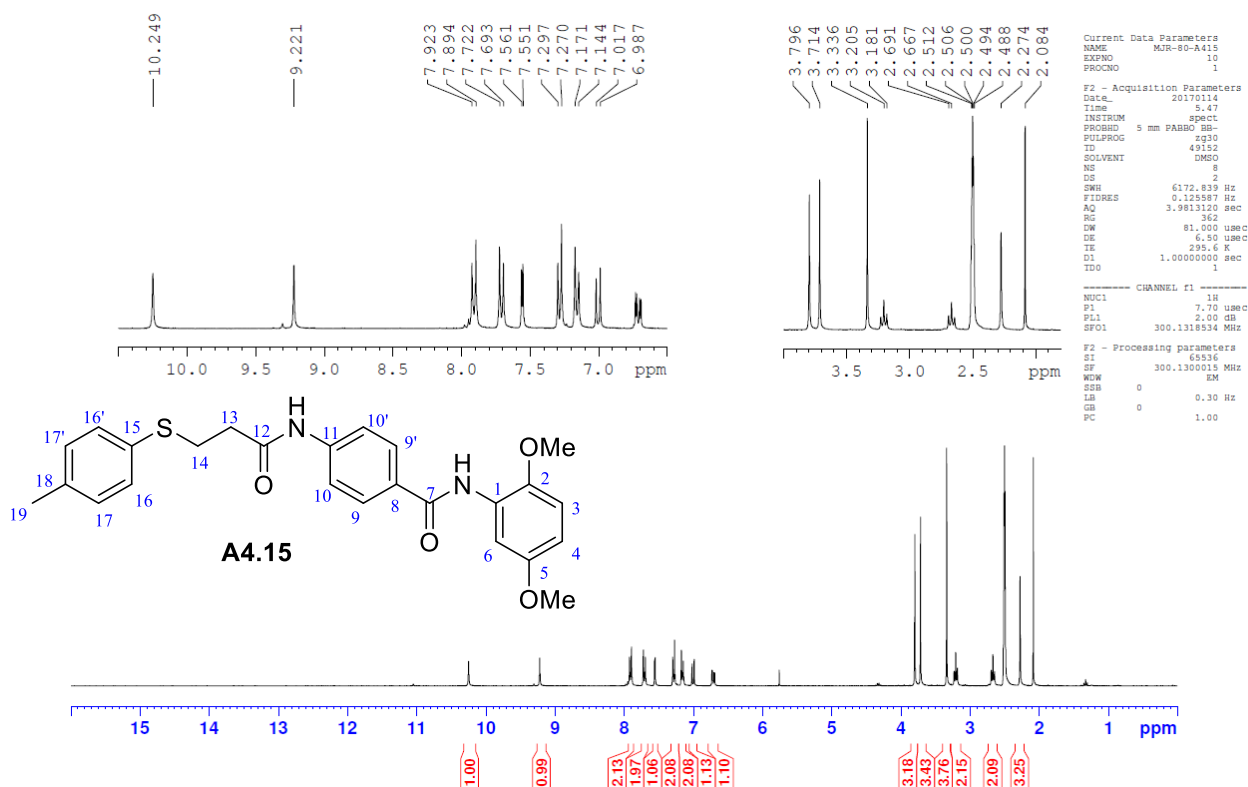


A4.15 : N-(2,5-dimethoxyphenyl)-4-(3-(p-tolythio)propanamido)benzamide

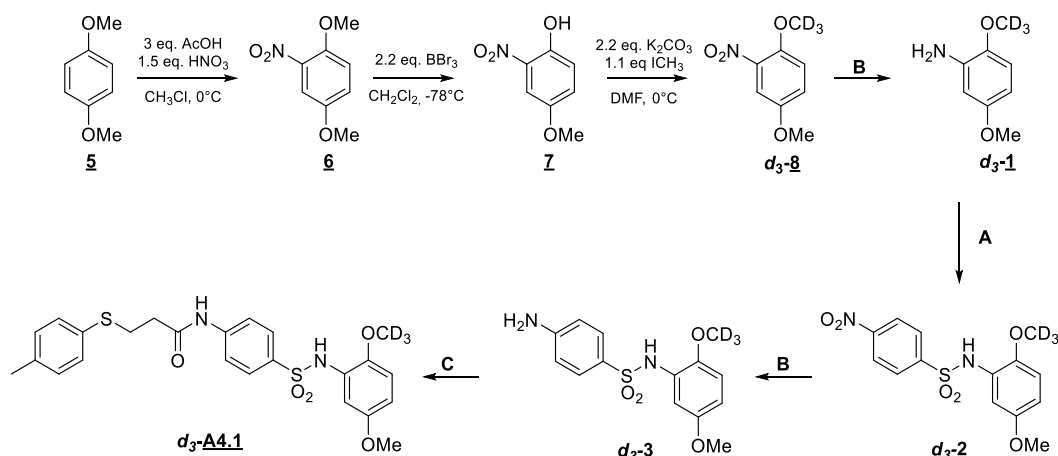


A4.15 was obtained following general procedure **C**, using commercial 3-(p-tolyloxy)propanoic acid (0.588 g, 3 mmol), oxalyl chloride (0.26 mL, 3 mmol), commercial 4-amino-N-(2,5-dimethoxyphenyl)benzamide **4** (0.5 g, 1.6 mmol) and Et₃N (0.17 mL, 1.2 mmol). After purification (CH₂Cl₂/EtOAc: 100/0 to 9/1), it afford the expected compound **A4.15** as a white solid (0.05 g, 10%) **R_f**: 0.35 (CH₂Cl₂/AcOEt: 9/1) **m.p.**: 153°C **¹H NMR**: (300 MHz, *d6*-DMSO, 25 °C) δ ppm: 10.25 (s, 1H, C₍₁₂₎ONH), 9.22 (s, 1H, C₍₇₎ONH), 7.91 (m, 2H, H₁₀-H_{10'}), 7.71 (m, 2H, H₉-H_{9'}), 7.56 (d, 1H, H₆, ⁴J = 3.1 Hz), 7.29 (m, 2H, H₁₆-H_{16'}), 7.16 (m, 2H, H₁₇-H_{17'}), 7.01 (d, 1H, H₃, ³J = 9.0 Hz), 6.72 (dd, 1H, H₄, ⁴J = 3.1 Hz, ³J = 9.0 Hz), 3.80 (s, 3H, OCH₃₍₅₎), 3.71 (s, 3H, OCH₃₍₂₎), 3.21 (t, 2H, H₁₄, ³J = 7.2 Hz), 2.67 (t, 2H, H₁₃, ³J = 7.2 Hz), 2.27 (s, 3H, H₁₉) **¹³C NMR**: (75 MHz, *d6*-DMSO, 25 °C) δ ppm: 169.7 (C₁₂), 164.2 (C₇), 152.9 (C₅), 144.9 (C₁₁), 142.2 (C₂), 135.6 (C₁₈), 131.9 (C₁₅), 129.8 (C₁₇-C_{17'}), 129.1 (C₁₆-C_{16'}), 128.6 (C₈), 128.4 (C₁₀-C_{10'}), 127.8 (C₁), 118.4 (C₉-C_{9'}), 111.9 (C₄), 109.7 (C₆), 109.2 (C₃), 56.3 (OCH₃₍₅₎), 55.4 (OCH₃₍₂₎), 36.3 (C₁₃), 28.5 (C₁₄), 20.5 (C₁₉) **HRMS**: (ES⁺) *m/z* calculated for C₂₅H₂₆N₂O₄SNa [M-Na]⁺, 473.1511; found 473.1510 **FT-IR**: ν(NH): 3316; ν(CH_{ar}): 3005; ν(CH_{OMe}): 2838; ν_{as}(SO): 1366; ν(CN): 1302; ν_s(SO): 1163.

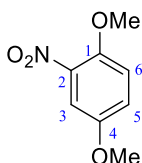
NMR spectra of the compounds A4.15



Synthesis of inhibitor d_3 -A4.1

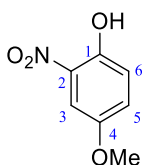


6 : 1,4-dimethoxy-2-nitrobenzene



To commercial 1,4-dimethoxybenzene **5** (2 g, 14.47 mmol) solution in CHCl_3 (37 mL) and AcOH (2.48 mL, 43.41 mmol) cooled in an ice-bath, was added nitric acid (1.37 mL, 21.7 mmol, 70% in water) dropwise. The reaction was stirred for 15 min and then poured onto an ice/water mixture (100 mL). The organic layer was washed with an aqueous NaHCO_3 solution (0.5N, 2 x 20 mL), water, and brine, dried over MgSO_4 , filtered, concentrate *in vacuo*. The crude product was purified by column chromatography on silica gel (PE/ AcOEt 9:1) affording the expected product **6** as a yellow solid (2.15g, 81% yield) R_f : 0.30 (EP/AcOEt) **m.p.** : 72°C $^1\text{H NMR}$: (400 MHz, CDCl_3 , 25 °C) δ : 7.39 (d, $^4J = 3.04$ Hz, 1H, H₃), 7.12 (dd, $^3J = 9.18$ Hz, $^4J = 3.04$ Hz, 1H, H₅), 7.03 (d, $^3J = 9.18$ Hz, 1H, H₆), 3.92 (s, 3H, $\text{OCH}_{3(1)}$), 3.81 (s, 3H, $\text{OCH}_{3(4)}$) $^{13}\text{C NMR}$: (100 MHz, CDCl_3 , 25 °C) δ : 153.1 (C₄), 147.5 (C₁), 139.8 (C₂), 121.0 (C₅), 115.4 (C₆), 110.2 (C₃), 57.3 ($\text{OCH}_{3(1)}$), 56.2 ($\text{OCH}_{3(4)}$) **HRMS** : (ES+) m/z calculated for $\text{C}_8\text{H}_{10}\text{NO}_4$ $[\text{M}+\text{H}]^+$, 184.0610; found 184.0601 **FT-IR** : $\nu(\text{CH}_{\text{Me}})$: 2950, 2848, $\nu_{\text{as}}(\text{NO}_2)$: 1522, $\nu_{\text{s}}(\text{NO}_2)$: 1351, $\nu(\text{CN}_{\text{NO}_2})$: 873.

7 : 4-methoxy-2-nitrophenol

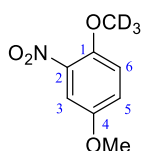


To a solution of 1,4-dimethoxy-2-nitrobenzene **6** (2.15g, 11.7 mmol) in CH_2Cl_2 (600mL) was added BBr_3 (25.8 mL, 1M in CH_2Cl_2 , 25.8 mmol) at -78°C under inert

atmosphere. The mixture was then stirred for 30 min and poured onto ice and aqueous saturated sodium bicarbonate solution. After being shaken vigorously, the mixture was extracted with CH₂Cl₂. The combined organic layers were then washed with water, brine, dried over MgSO₄, filtered and concentrated off. The crude product was purified by column chromatography on silica gel (PE/ CH₂Cl₂: 9/1) affording expected product **7** as an orange solid (1.85g, 94% yield).

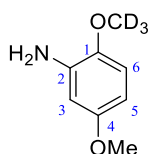
R_f: 0.55 (PE/ AcOEt : 9/1+1% acetic acid) **m.p.**: 81 °C **¹H NMR** : (400 MHz, CDCl₃, 25 °C) δ : 10.33 (s, 1H, OH), 7.51 (d, ⁴J = 3.12 Hz, 1H, H₃), 7.22 (dd, ³J = 9.24 Hz, ⁴J = 3 Hz, 1H, H₅), 7.09 (d, ³J = 9.24 Hz, 1H, H₆), 3.83 (s, 3H, OMe) **¹³C NMR** : (100 MHz, CDCl₃, 25 °C) δ : 152.8 (C₄), 150.2 (C₁), 133.2 (C₂), 127.4 (C₅), 121.0 (C₆), 105.9 (C₃), 56.2 (OMe) **HRMS** : (ES-) m/z calculated for C₇H₆NO₄ [M-H]⁻, 168.0297; found 168.0289 **FT-IR** : ν(OH) : 3222 ; ν(CH_{ar}) : 3052 ; ν(CH_{Me}) : 2844 ; ν_{as}(NO₂) : 1527 ; ν_s(NO₂) : 1305 ; ν(CN) : 862, 761.

d₃-8 : 4-methoxy-1-(methoxy-d₃)-2-nitrobenzene



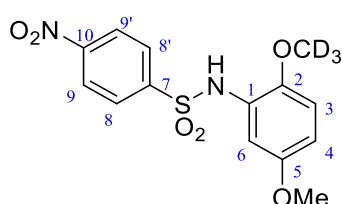
To a solution of 4-methoxy-2-nitrophenol **7** (860mg, 5.08 mmol) in DMF (7mL) was added K₂CO₃ (1.55g, 11.19 mmol) portionwise. After the solution became red, iodomethane (345 μL, 5.59 mmol) was added and was stirred overnight at rt and filtered. The filtrate was diluted with AcOEt (25mL) and washed with an aqueous saturated sodium bicarbonate solution (5 x 30 mL). The organic layer was dried over MgSO₄, filtered and concentrate. The expected product **d₃-8** was obtained without further purification needed as a yellow solid (815 mg, 86% yield). **R_f**: 0.32 in petroleum ether/ Ethyl acetate 9:1 **m.p.**: 74 °C **¹H NMR** : (400 MHz, CDCl₃, 25 °C) δ : 7.39 (d, ⁴J = 3.10 Hz, 1H, H₃), 7.11 (dd, ³J = 9.04 Hz, ⁴J = 3.10 Hz, 1H, H₅), 7.02 (d, ³J = 9.04 Hz, 1H, H₆), 3.81 (s, 3H, OMe) **¹³C NMR** : (100 MHz, CDCl₃, 25 °C) δ : 153.0 (C₄), 147.5 (C₁), 139.8 (C₂), 121.0 (C₅), 115.3 (C₆), 110.2 (C₃), 56.4 (OCD₃), 56.2 (OMe) **HRMS** : (ES+) m/z calculated for C₈H₇D₃NO₄ [M+H]⁺, 187.0798; found 187.0796 **FT-IR** : ν(CH_{Me}) : 2851 ; ν(CD_{CD3}) : 2077, ν_{as}(NO₂) : 1521 ; ν_s(NO₂) : 1351 ; ν(CN) : 873.

d₃-1 : 5-methoxy-2-(methoxy-d₃)aniline



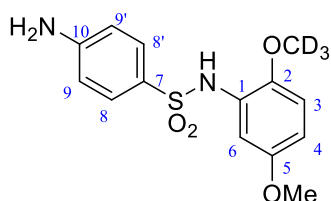
d3-1 was obtained following general procedure **B**, using 4-methoxy-1-(methoxy-*d3*)-2-nitrobenzene ***d3-8*** (0.6g, 3.22 mmol), iron (1.07g, 19.32 mmol) and NH₄Cl (1.7g in 15 mL of water, 32.2 mmol). No further purification needed to afford the expected compound ***d3-1*** as a green solid (0.48 g, 96%). **R_f**: 0.42 (PE/AcOEt : 9/1) **m.p.**: 81 °C **¹H NMR** : (400 MHz, CDCl₃, 25 °C) δ : 6.69 (d, ³J = 8.71 Hz, 1H, H₃), 6.33 (d, ⁴J = 2.86 Hz, 1H, H₆), 6.24 (dd, ³J = 8.71 Hz, ⁴J = 2.86 Hz, 1H, H₄), 3.73 (s, 3H, OMe₅). **¹³C NMR** : (100 MHz, CDCl₃, 25 °C) δ : 154.6 (C₅), 142.0 (C₂), 137.4 (C₁), 111.5 (C₃), 102.3 (C₆), 102.1 (C₄), 55.7 (OMe₅), 55.7 (m, ¹J ≈ 22 Hz, OCD₃). **HRMS** : (ES⁺) m/z calculated for C₈H₉D₃NO₂ [M+H]⁺, 157.1056; found 157.1053 **FT-IR** : ν(NH) : 3457, 3366 ; ν(CD_{CD3}) : 2071 ; ν(CN) : 1227.

***d3-2* : N-(5-methoxy-2-(methoxy-*d3*)phenyl)-4-nitrobenzenesulfonamide**



d3-2 was obtained following general procedure A, using 5-methoxy-2-(methoxy-*d3*)aniline ***d3-1*** (483 mg, 3,09 mmol), pyridine (432 μL, 5.37 mmol) and 4-nitrobenzenesulfonile chloride (0.85g, 3.84 mmol). After purification (PE/EtOAc: 7/3), it afford the expected compound ***d3-2*** as a yellow solid (0.95 g, 90%). **R_f**: 0.42 (PE/AcOEt : 7/3) **m.p.**: 160 °C **¹H NMR** : (300 MHz, CDCl₃, 25 °C) δ : 8.25-8.21 (m, ³J = 8.83 Hz, ⁴J = 2.38 Hz, ⁵J = 1.96 Hz, 2H, H₉ et H_{9'}), 7.96-7.91 (m, ³J = 8.83 Hz, ⁴J = 2.38 Hz, ⁵J = 1.96 Hz, 2H, H₈ et H_{8'}), 7.16 (d, ⁴J = 2.80 Hz, 1H, H₆), 7.12 (s, 1H, NH), 6.66 (d, ³J = 8.97 Hz, 1H, H₃), 6.59 (dd, ³J = 8.97 Hz, ⁴J = 2.80 Hz 1H, H₄), 3.75 (s, 3H, OMe) **¹³C NMR** : (75 MHz, CDCl₃, 25 °C) δ : 154.0, 150.3, 144.9, 144.0 (C^{IV}), 128.6 (2 C^{IV}), 125.4 (C^{IV}), 124.1 (2C^{IV}), 111.6 (C₃), 110.8 (C₄), 108.4 (C₆), 55.9 (OCH₃), 55.6 (m, J = 22.18 Hz, OCD₃) **HRMS** : (ES⁻) m/z calculated for C₁₄H₁₀D₃N₂O₆S [M-H]⁻, 340.0683; found 340.0683 **FT-IR** : ν(NH_{sulfonamide}) : 3311, ν(CH_{ar}) : 3107, ν(CD_{CD3}) : 2079, ν_{as}(NO₂) : 1533, ν_s(NO₂) : 1346, ν_s(SO) : 1173, ν(CN) : 855.

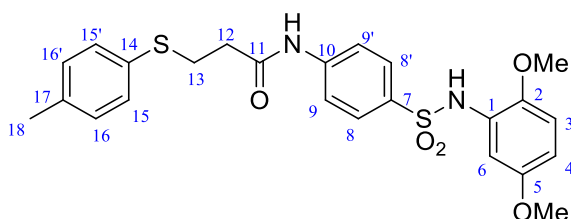
***d3-3* : 4-amino-N-(5-methoxy-2-(methoxy-*d3*)phenyl)benzenesulfonamide**



d3-3 was obtained following general procedure B, using 4-methoxy-1-(methoxy-*d3*)-2-nitrobenzenesulfonamide ***d3-2*** (1.08g, 3.16 mmol), iron (1.06g, 18.96 mmol) and NH₄Cl (1.67g in 15 mL of water, 31.6 mmol). No purification needed to afford the expected compound ***d3-3***

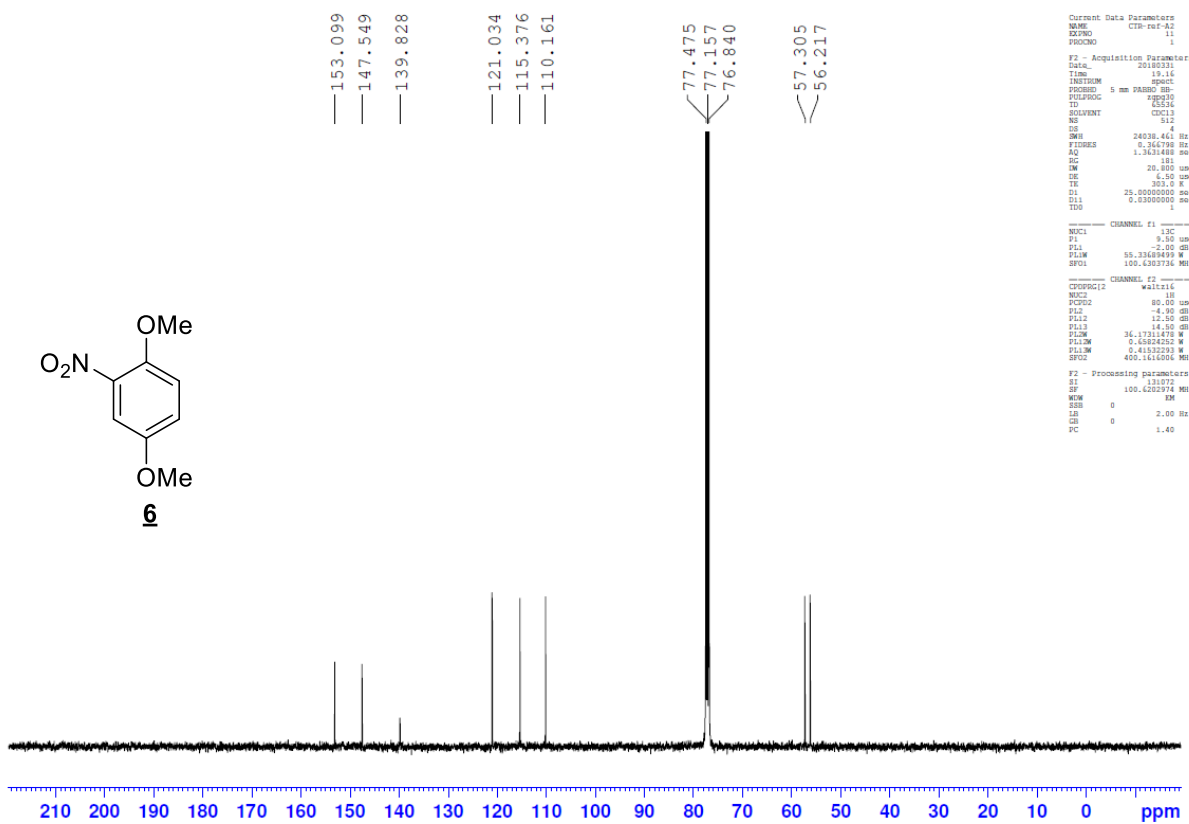
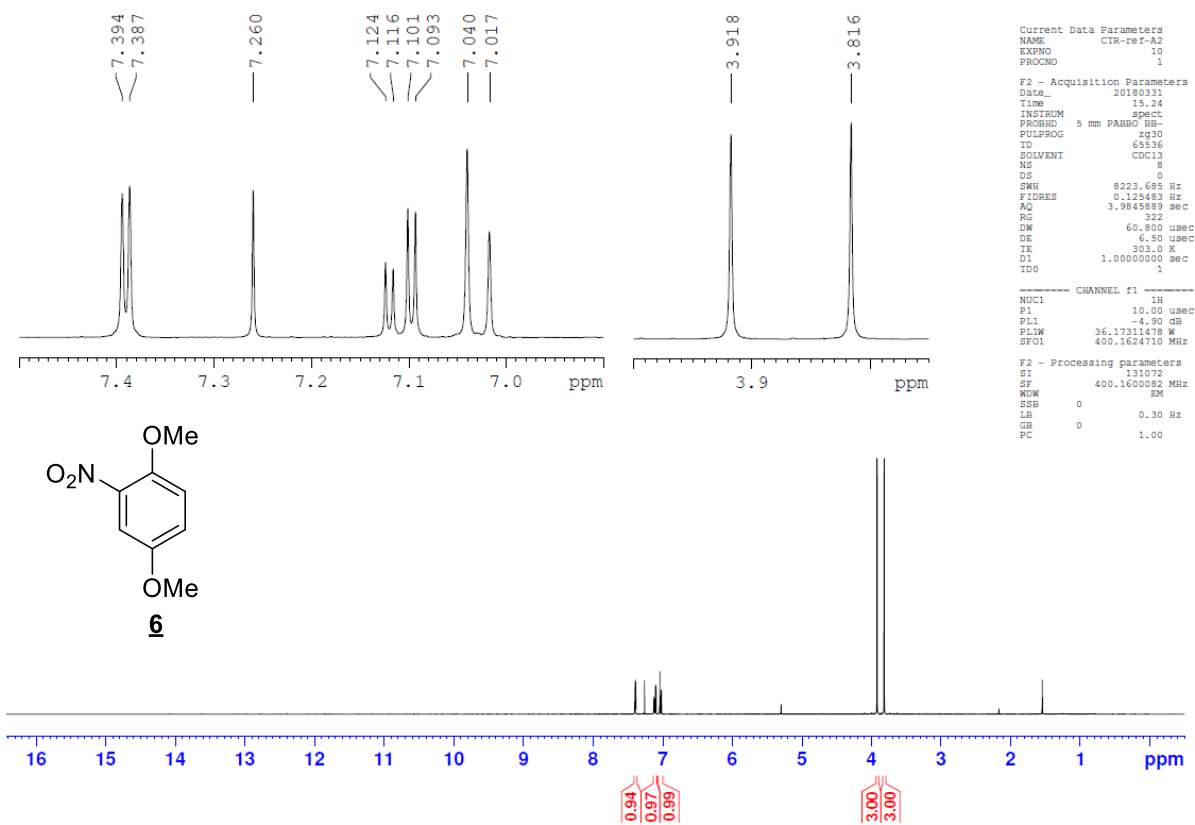
as a beige solid (910mg, 92%) R_f : 0.079 (PE/AcOEt : 7/3) **m.p.**: 120 °C $^1\text{H NMR}$: (300 MHz, CDCl_3 , 25 °C) δ : 7.57-7.54 (m, 2H, $\text{H}_9\text{-H}_{9'}$), 7.12 (d; 1H, H_6 , $^4J = 2.9$ Hz), 6.98 (s, 1H, NH), 6.65 (d, 1H, H_3 , $^3J = 8.9$ Hz), 6.59-6.54 (m, 2H, $\text{H}_8\text{-H}_{8'}$), 6.51 (dd, 1H, H_4 , $^3J = 8.8$ Hz, $^4J = 2.9$ Hz), 4.06 (s, 2H, NH_2), 3.73 (s, 3H, OMe_5) $^{13}\text{C NMR}$: (75 MHz, CDCl_3 , 25 °C) δ : 154.0 (C_5), 150.8 (C_{10}), 143.6 (C_2), 129.6 ($\text{C}_8\text{-C}_{8'}$), 127.6 (C_1), 127.4 (C_7), 113.9 ($\text{C}_9\text{-C}_{9'}$), 111.6 (C_3), 109.5 (C_4), 106.9 (C_6), 55.9 (OCH_3), 55.6 (m, $J = 22.18$ Hz, OCD_3) **HRMS** : (ES-) m/z calculated for $\text{C}_{14}\text{H}_{12}\text{D}_3\text{N}_2\text{O}_4\text{S}$ $[\text{M-H}]^-$, 310.0941; found 310.0939 **FT-IR** : $\nu(\text{NH}_{\text{amine}})$: 3483,3391 ; $\nu(\text{NH}_{\text{sulfonamide}})$: 3259 ; $\nu(\text{CH}_{\text{Me}})$: 2939 ; $\nu(\text{CD}_{\text{CD}_3})$: 2073 ; $\nu_{\text{as}}(\text{SO})$: 1308 ; $\nu(\text{CN})$: 1217 ; $\nu_{\text{s}}(\text{SO})$: 1152.

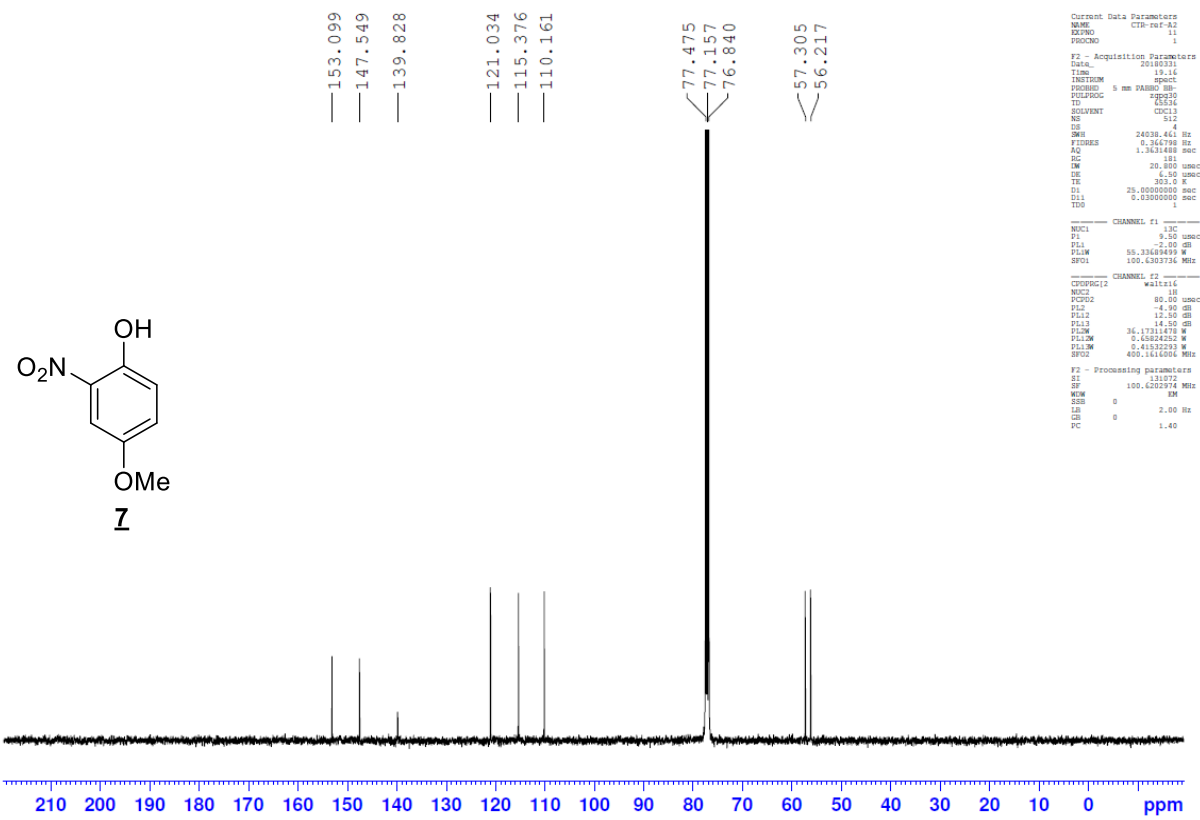
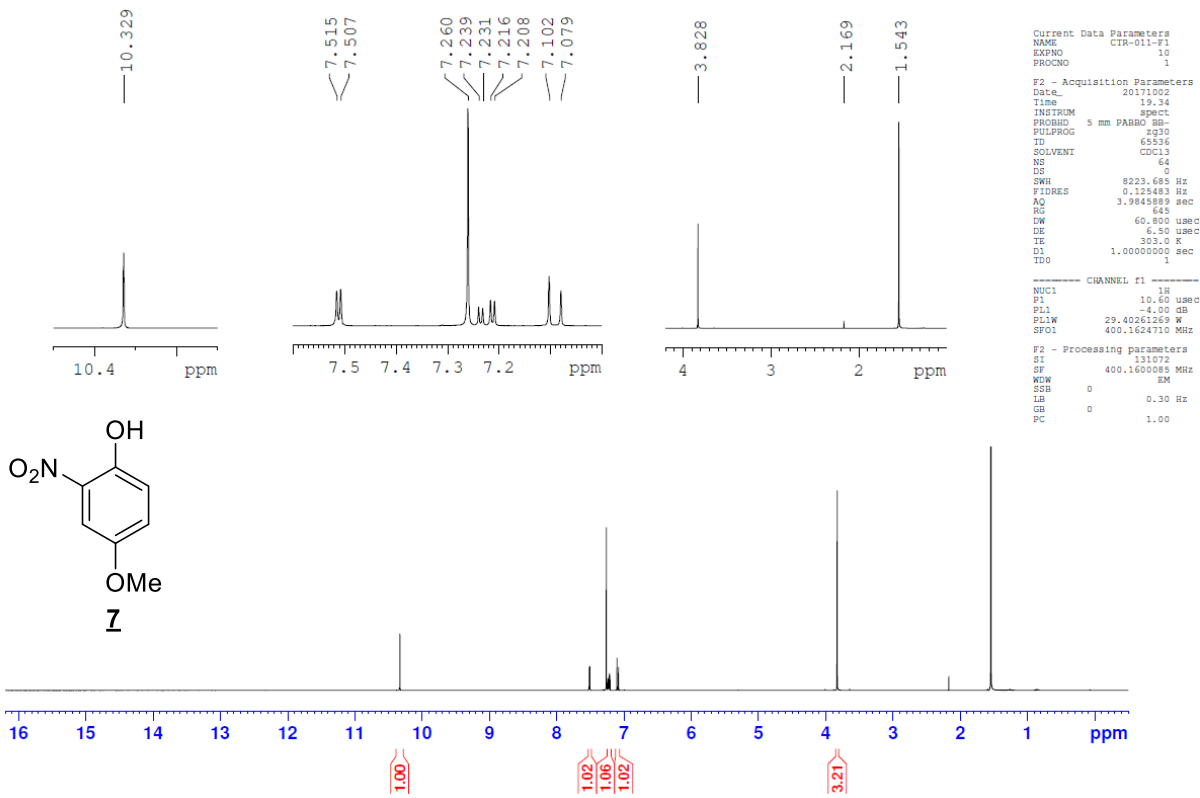
$d_3\text{-A4.1}$: N-(4-(N-(5-methoxy-2-(methoxy-d3)phenyl)sulfamoyl)phenyl)-3-(p-tolylthio)propanamide

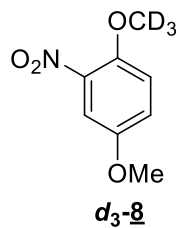
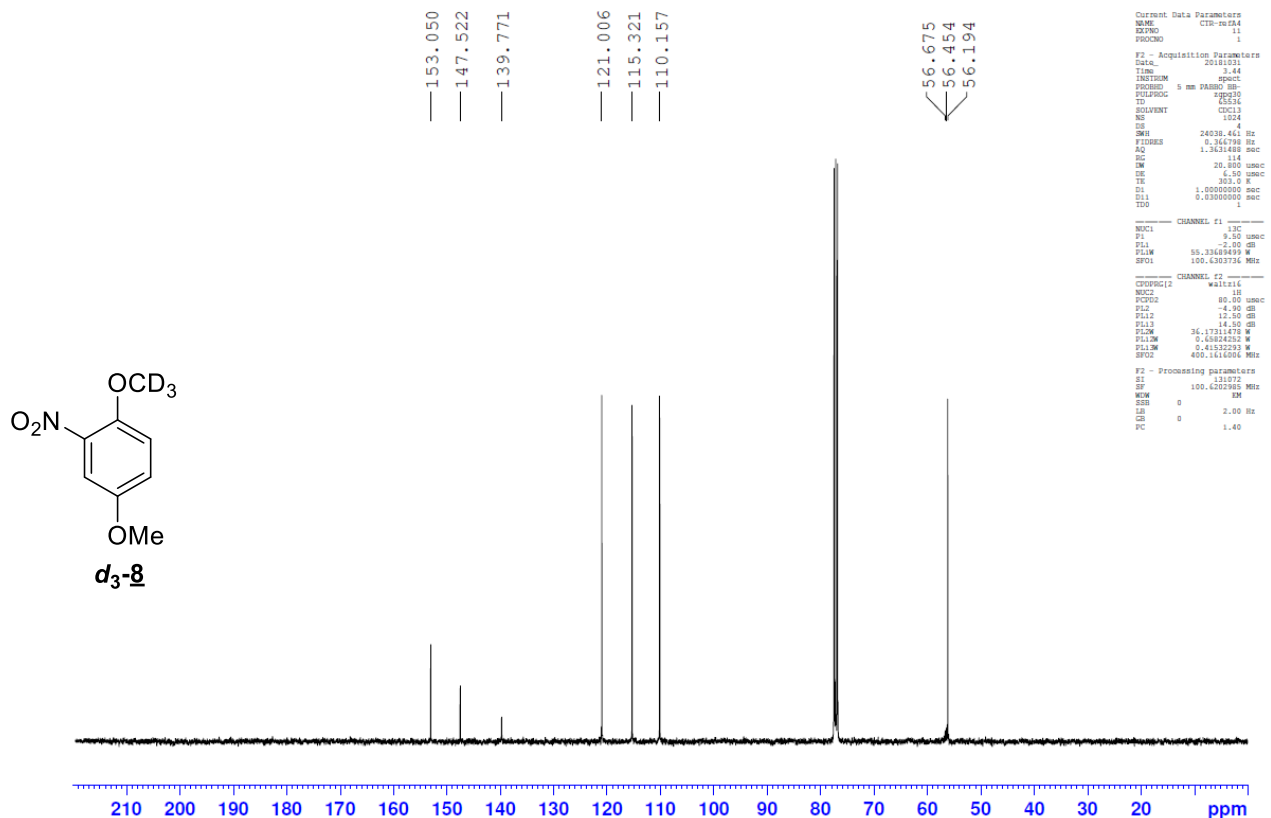
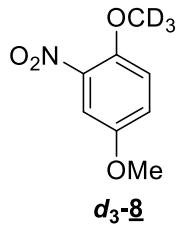
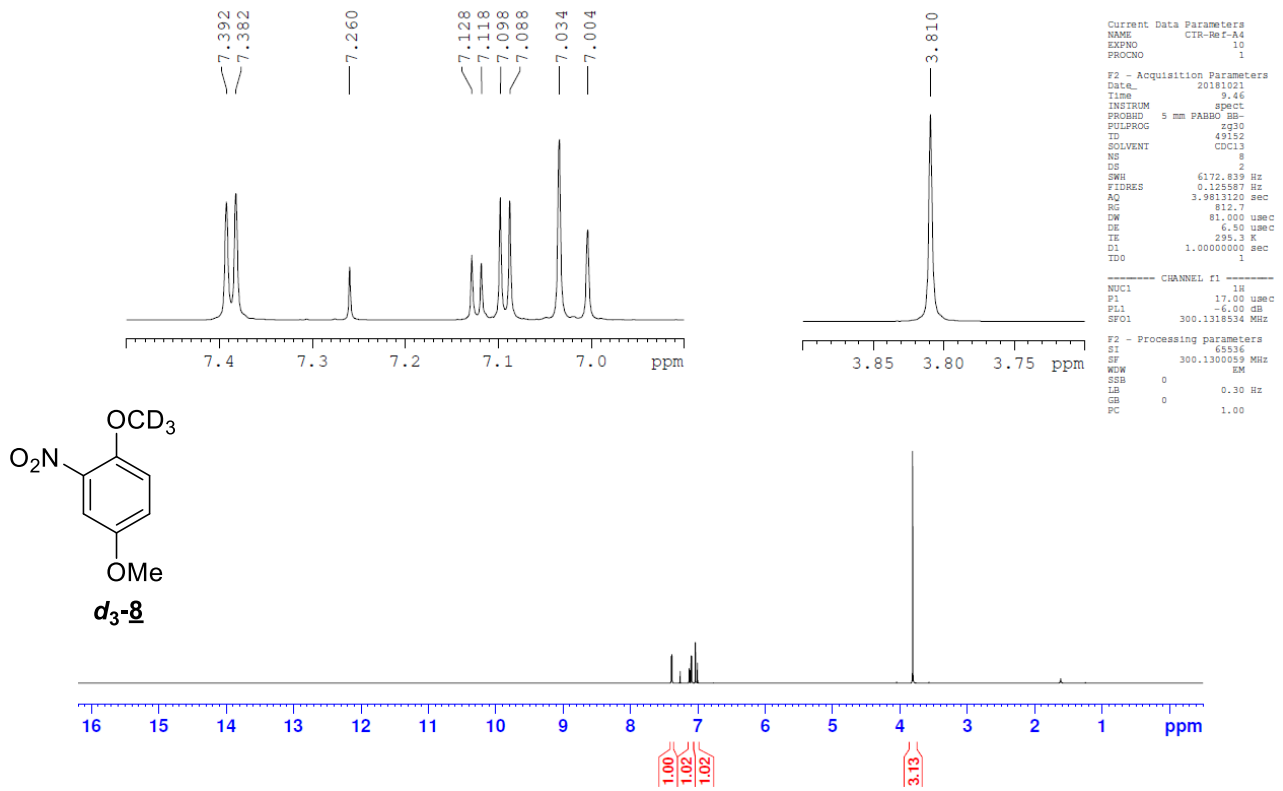


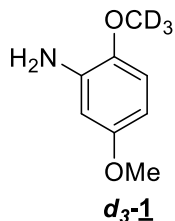
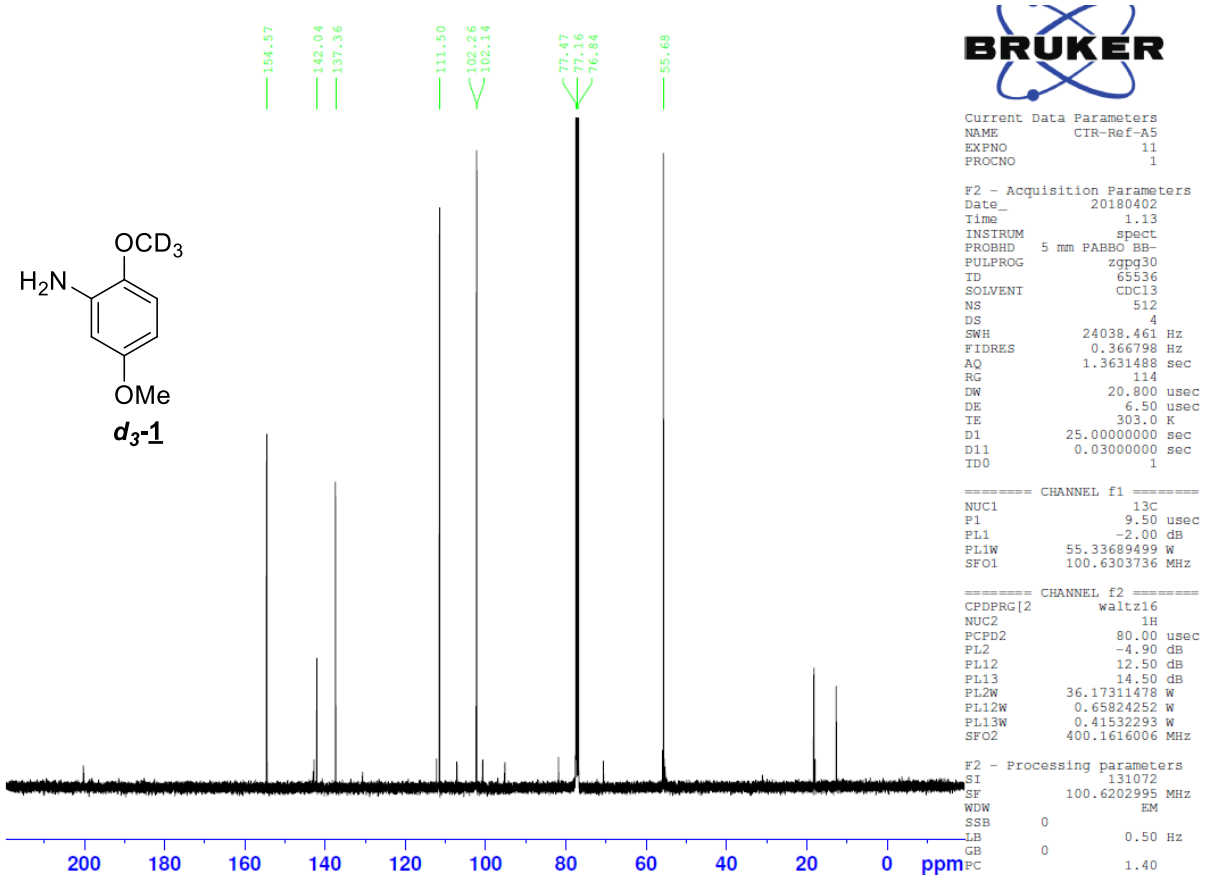
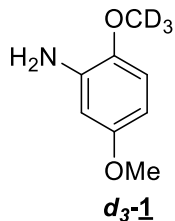
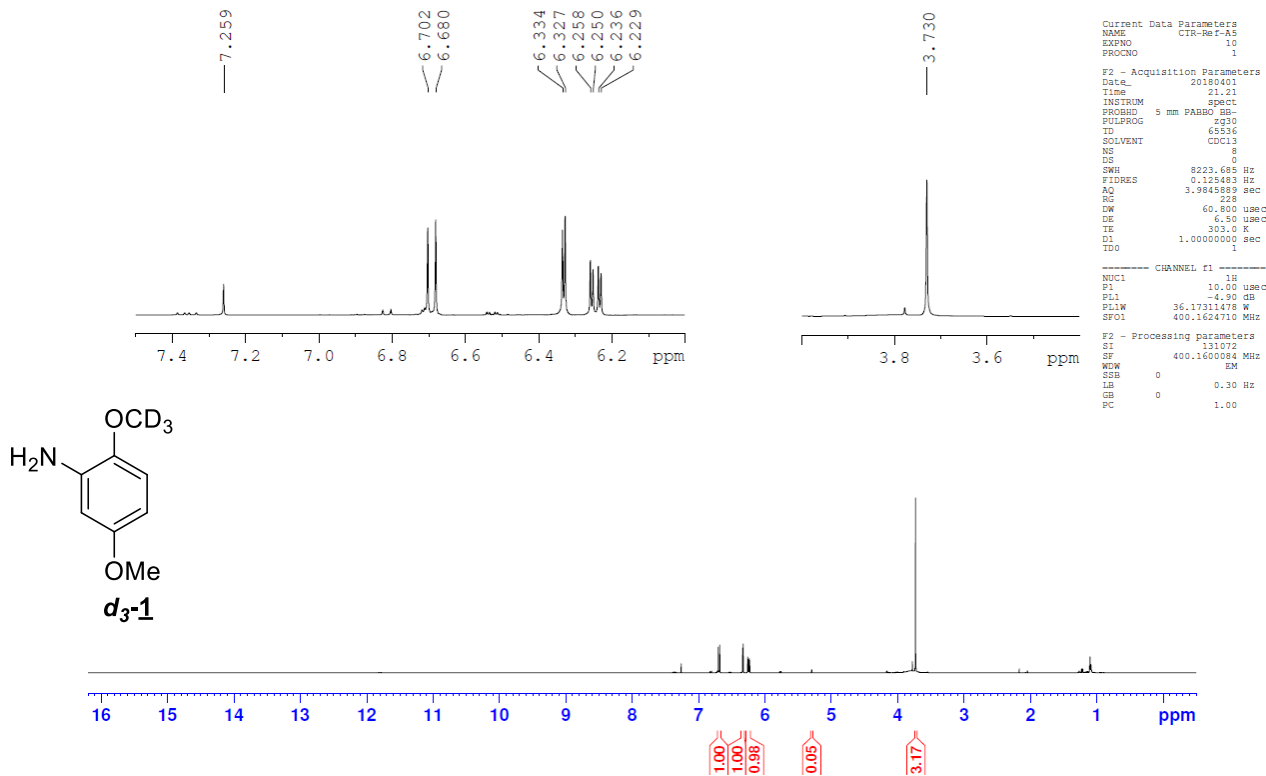
$d_3\text{-3}$ was obtained following general procedure C, using commercial 3-(p-tolylthio)propanoic acid (1.58 g, 2.75 mmol), oxalyl chloride (0.69 mL, 8.1 mmol), 4-amino-N-(5-methoxy-2-(methoxy-d3)phenyl)benzenesulfonamide **$d_3\text{-3}$** (0.5 g, 1.6 mmol) and Et_3N (0.24 mL, 1.76 mmol). After purification (PE/EtOAc/ CH_2Cl_2 : 6/2/2), it afford the expected compound **$d_3\text{-A4.1}$** as a white solid (0.59 g, 69%) R_f : 0.15 (PE/ AcOEt/ CH_2Cl_2 : 5/3/2) **m.p.** : 129°C $^1\text{H NMR}$: (300 MHz, CDCl_3 , 25 °C) δ ppm: 7.97 (s, 1H, CONH), 7.69-7.66 (m, 2H, $\text{H}_8\text{-H}_{8'}$), 7.56-7.55 (m, 2H, $\text{H}_9\text{-H}_{9'}$), 7.28-7.25 (m, 2H, $\text{H}_{14}\text{-H}_{14'}$), 7,13 (d, 1H, H_6 , $^4J = 2,8$ Hz), 7.11-7.08 (m, 3H, $\text{H}_{15}\text{-H}_{15'}$ and SO_2NH), 6,65 (d, 1H, H_3 , $^3J = 8,8$ Hz), 6.55 (dd, 1H, H_4 , $^3J = 8,9$ Hz, $^4J = 2,9$ Hz), 3.73 (s, 3H, OMe_5), 3.21 (t, 2H, H_{12} , $^3J = 6,9$ Hz), 2.64 (t, 2H, H_{13} , $^3J = 6,9$ Hz), 2,30 (s, 3H, H_{17}) $^{13}\text{C NMR}$: (100 MHz, CDCl_3 , 25 °C) δ : 169.9 (C_{11}), 153.9 (C_2), 143.72 (C_{10}), 142.18 (C_5), 137.1 (C_{17}), 133.7 (C_7), 131.2 ($\text{C}_{15}\text{-C}_{15'}$), 130.7 (C_{14}), 130.0 ($\text{C}_8\text{-C}_{8'}$), 128.6 ($\text{C}_{16}\text{-C}_{16'}$), 126.5 (C_1), 119.2 ($\text{C}_9\text{-C}_{9'}$), 111.6 (C_3), 109.8 (C_4), 107.5 (C_6), 55.8 (OCH_3), 55.6 (OCD_3), 37.3 (C_{12}), 29.9 (C_{13}), 21.0 (C_{18}) **HRMS** : (ES+) m/z calculated for $\text{C}_{24}\text{H}_{24}\text{D}_3\text{N}_2\text{O}_5\text{S}_2$ $[\text{M-H}]^+$, 490.1550; found 490.1545 **FT-IR** : $\nu(\text{NH}_{\text{amide}})$: 3325 ; $\nu(\text{NH}_{\text{sulfonamide}})$: 3270; $\nu(\text{CH}_{\text{Me}})$: 2924 ; $\nu(\text{CD}_{\text{CD}_3})$: 2071 ; $\nu(\text{C=O})$: 1695 ; $\nu_{\text{as}}(\text{SO})$: 1330; $\nu_{\text{s}}(\text{SO})$: 1153.

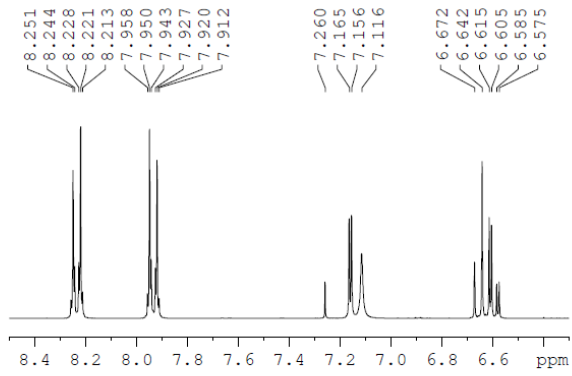
NMR spectra of the intermediates **6**, **7**, **d₃-8**, **d₃-1**, **d₃-2**, **d₃-3** and final compounds **d₃-A4.1**











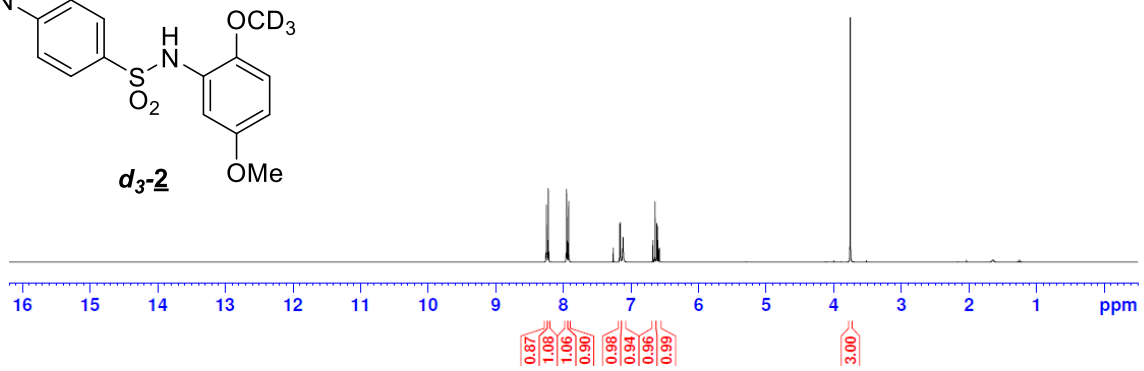
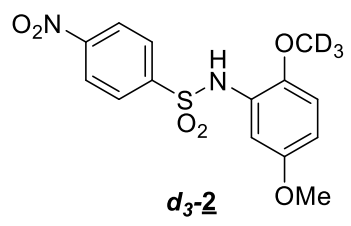
```

Current Data Parameters
NAME      CTR-076-ref
EXPNO    10
PROCNO   1

F2 - Acquisition Parameters
Date_    20180825
Time     11.10
INSTRUM spect
PROBHD   5 mm PABBO BB-
PULPROG zg30
ID       49152
SOLVENT  CDCl3
NS       8
DS       2
SWE      6172.839 Hz
FIDRES   0.135587 Hz
AQ       3.9813120 sec
RG       362
RW       81.000 usec
DE       6.50 usec
TE       300.2 K
D1       1.00000000 sec
TDO      1

----- CHANNEL f1 -----
NUC1     1H
P1       17.00 usec
PL1      -6.00 dB
SFO1    300.1318534 MHz

F2 - Processing parameters
SI       655.6
SF       300.1300057 MHz
WDW      EM
SSB      0
LB       0.30 Hz
GB       0
PC       1.00
  
```



```

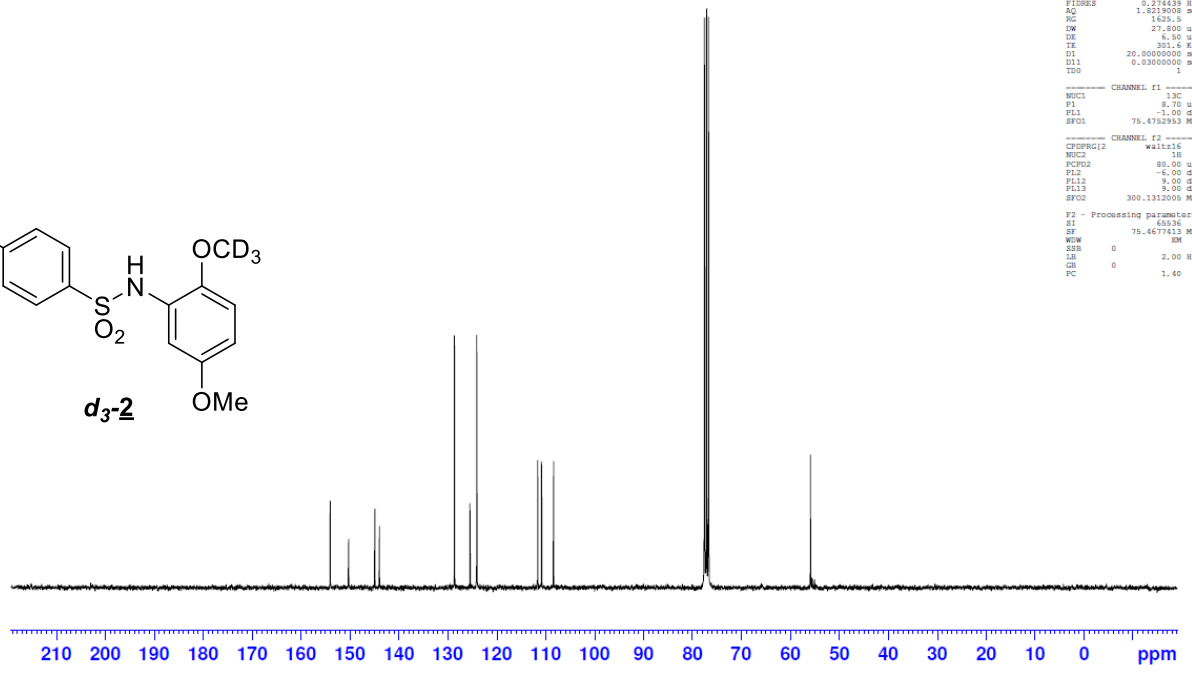
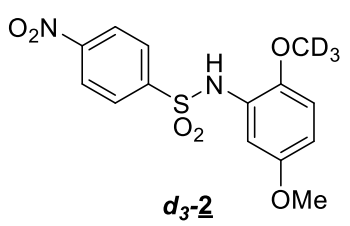
Current Data Parameters
NAME      CTR-076-ref
EXPNO    11
PROCNO   1

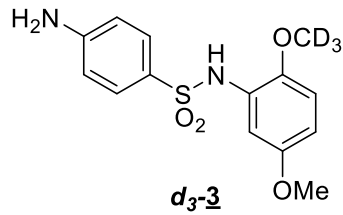
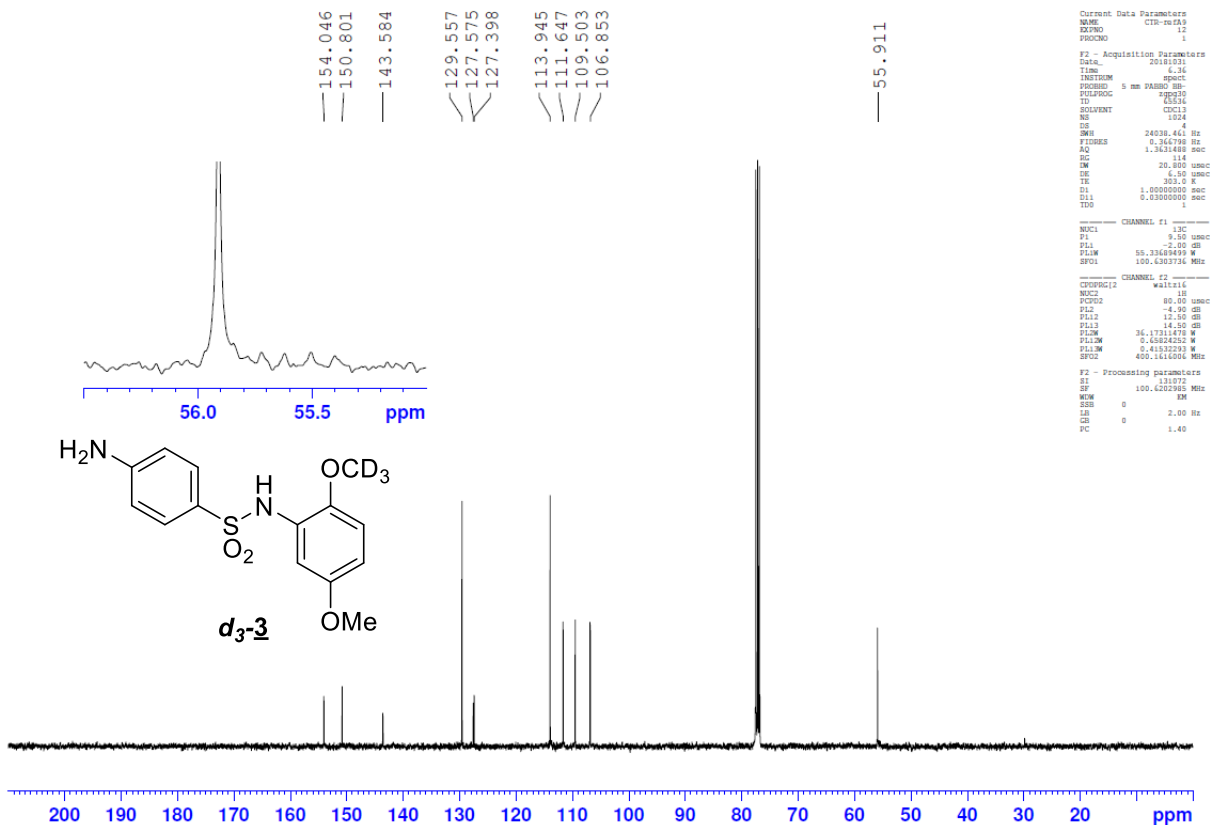
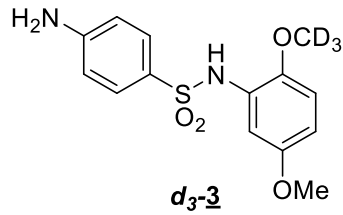
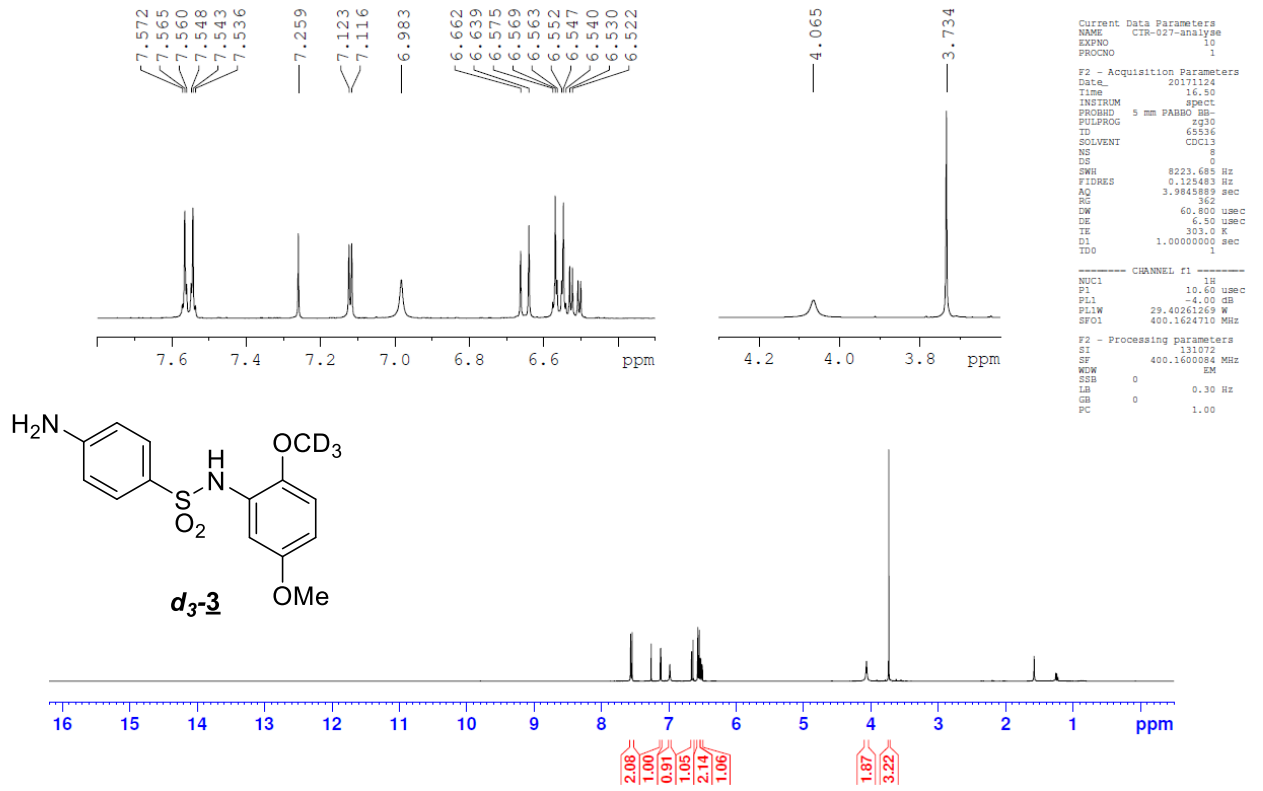
F2 - Acquisition Parameters
Date_    20180825
Time     14.23
INSTRUM spect
PROBHD   5 mm PABBO BB-
PULPROG zgpg30
ID       65136
SOLVENT  CDCl3
NS       4
DS       4
SWE      17985.611 Hz
FIDRES   0.274439 Hz
AQ       1.8219008 sec
RG       1625.5
RW       27.800 usec
DE       6.50 usec
TE       301.4 K
D1       20.00000000 sec
D11      0.03000000 sec
TDO      1

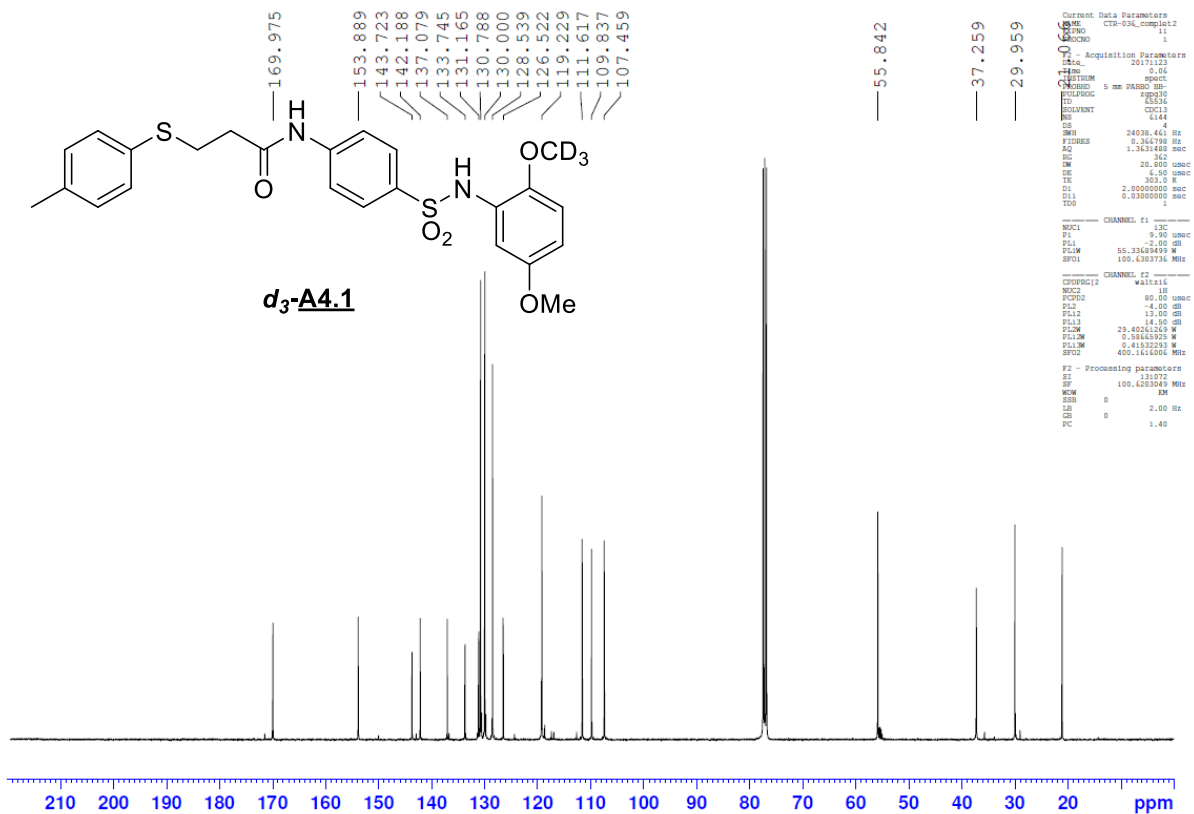
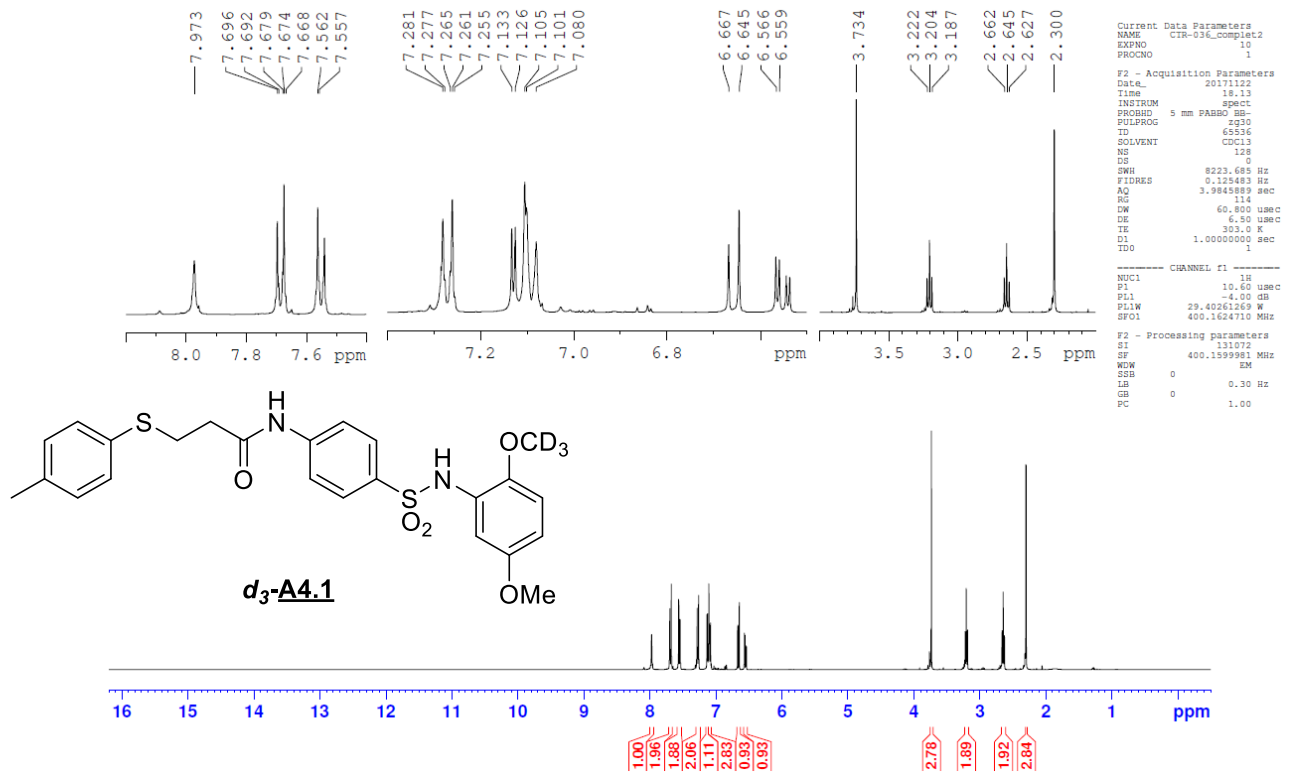
----- CHANNEL f1 -----
NUC1     13C
P1       8.70 usec
PL1      -1.00 dB
SFO1    75.4762953 MHz

----- CHANNEL f2 -----
CPDPRG2  waltz16
NUC2     1H
PCPD2    80.00 usec
PL2      -6.00 dB
PL12     9.00 dB
PL13     9.00 dB
SFO2    300.1312005 MHz

F2 - Processing parameters
SI       649.36
SF       75.4677413 MHz
WDW      RM
SSB      0
LB       2.00 Hz
GB       0
PC       1.40
  
```







HRMS spectra of the final compounds A4.1, A4.14, A4.15, A4.16, A4.20, d₃-A4.1

Elemental Composition Report

Single Mass Analysis

Tolerance = 5.0 PPM / DBE: min = -1.5, max = 100.0
 Element prediction: Off
 Number of isotope peaks used for i-FIT = 4

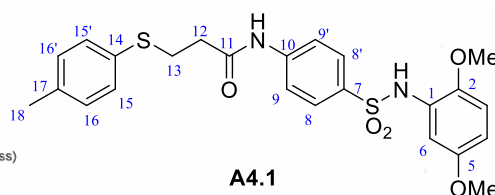
Monoisotopic Mass, Even Electron Ions
 135 formula(e) evaluated with 1 results within limits (up to 50 closest results for each mass)
 Elements Used:

C: 0-30 H: 0-120 N: 0-2 O: 0-5 Na: 0-1 S: 2-2

LCT

MJR-59p2c2 / CH₂Cl₂+MeOH / ESI+

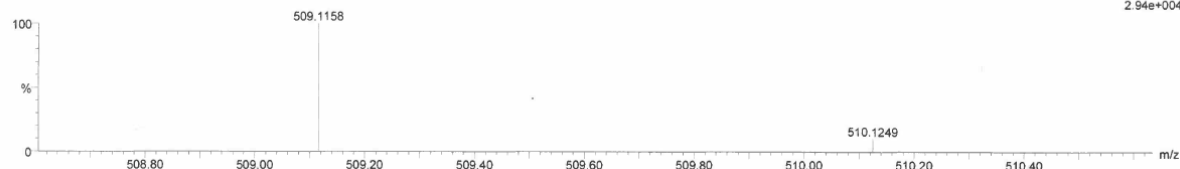
1: TOF MS ES+



A4.1

20150413_MJR-59p2c2 59 (1.186) AM (Cen,13, 80.00, Ar,4100.0,556.28,0.00,LS 10); Cm (47.63) 13-Apr-2015

Page 1



Minimum: 5.0 5.0 -1.5
 Maximum: 5.0 5.0 100.0

Mass	Calc. Mass	mDa	PPM	DBE	i-FIT	Formula
509.1158	509.1181	-2.3	-4.5	12.5	n/a	C24 H26 N2 O5 Na S2

2.94e+004

Elemental Composition Report

Single Mass Analysis

Tolerance = 5.0 PPM / DBE: min = -1.5, max = 100.0
 Element prediction: Off
 Number of isotope peaks used for i-FIT = 4

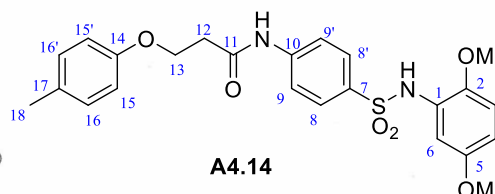
Monoisotopic Mass, Even Electron Ions
 105 formula(e) evaluated with 1 results within limits (up to 50 closest results for each mass)
 Elements Used:

C: 0-100 H: 5-100 N: 0-2 O: 0-6 Na: 1-1 S: 1-1

LCT

MJR-77 / CH₂Cl₂+MeOH / ESI+

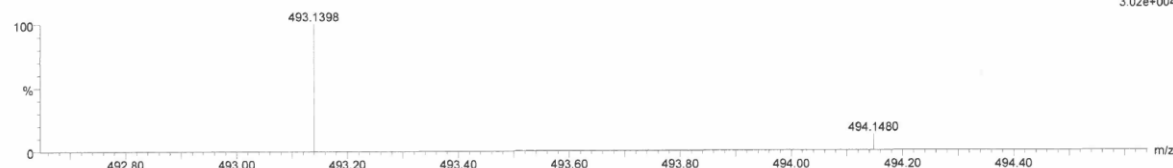
1: TOF MS ES+



A4.14

20150602_MJR-77 13 (0.269) AM (Cen,13, 80.00, Ar,4000.0,556.28,0.00,LS 10); Cm (3.14) 02-Jun-2015

Page 1



Minimum: 5.0 5.0 -1.5
 Maximum: 5.0 5.0 100.0

Mass	Calc. Mass	mDa	PPM	DBE	i-FIT	Formula
493.1398	493.1409	-1.1	-2.2	12.5	n/a	C24 H26 N2 O6 Na S

3.02e+004

Elemental Composition Report

Single Mass Analysis

Tolerance = 5.0 PPM / DBE: min = -1.5, max = 100.0
 Element prediction: Off
 Number of isotope peaks used for i-FIT = 4

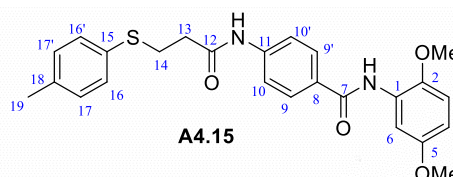
Monoisotopic Mass, Even Electron Ions
 622 formula(e) evaluated with 3 results within limits (up to 50 closest results for each mass)
 Elements Used:

C: 0-100 H: 0-100 N: 0-3 O: 0-16 S: 0-1

LCT

MJR-80p2 / CH₂Cl₂+MeOH / ESI-

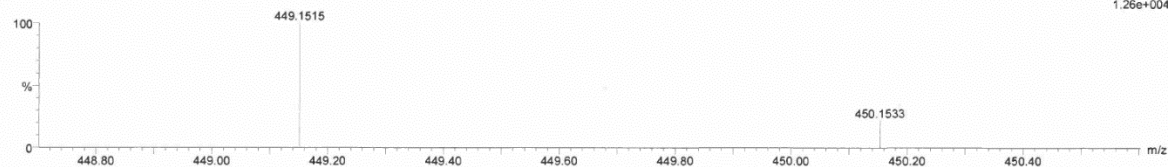
1: TOF MS ES-



A4.15

20150528_MJR-80p2 3 (0.069) AM (Cen,13, 80.00, Ar,3000.0,554.28,0.00,LS 10); Cm (2.10) 28-May-2015

Page 1



Minimum: 5.0 5.0 -1.5
 Maximum: 5.0 5.0 100.0

Mass	Calc. Mass	mDa	PPM	DBE	i-FIT	Formula
449.1515	449.1506	0.9	2.0	1.5	n/a	C15 H29 O15
	449.1501	1.4	3.1	19.5	n/a	C28 H21 N2 O4
	449.1535	-2.0	-4.5	14.5	n/a	C25 H25 N2 O4 S

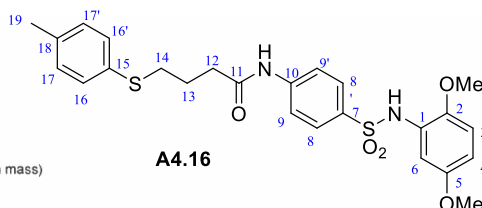
1.26e+004

Elemental Composition Report *A4.16*

Single Mass Analysis

Tolerance = 5.0 PPM / DBE: min = -1.5, max = 100.0
 Element prediction: Off
 Number of isotope peaks used for i-FIT = 4

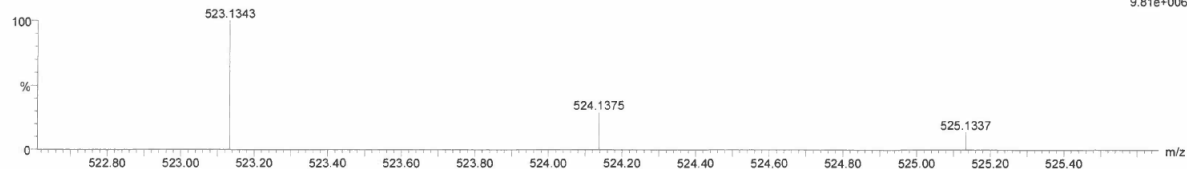
Monoisotopic Mass, Even Electron Ions
 700 formula(e) evaluated with 5 results within limits (up to 50 closest results for each mass)
 Elements Used:
 C: 0-100 H: 5-100 N: 0-6 O: 0-10 Na: 1-1 S: 1-2
 SYNAPT-G2#NotSet
 29-Jun-2015
 1: TOF MS ES+



A4.16

20150629_MJR-90 81 (0.442) AM2 (Ar,20000.0,0.00,0.00); Cm (69-96)
 MJR-90 / CH2Cl2+MeOH / ES+

9.81e+006



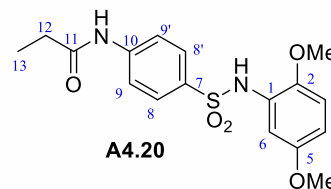
Mass	Calc. Mass	mDa	PPM	DBE	i-FIT	Formula
523.1343	523.1344	-0.1	-0.2	21.5	n/a	C33 H24 O3 Na S
523.1337	523.1337	0.6	1.1	12.5	n/a	C25 H28 N2 O5 Na S2
523.1351	523.1351	-0.8	-1.5	17.5	n/a	C26 H24 N6 O Na S2
523.1362	523.1362	-1.9	-3.6	8.5	n/a	C21 H28 N2 O10 Na S
523.1317	523.1317	2.6	5.0	22.5	n/a	C29 H20 N6 O Na S

Elemental Composition Report *A4.20*

Single Mass Analysis

Tolerance = 5.0 PPM / DBE: min = -1.5, max = 50.0
 Element prediction: Off
 Number of isotope peaks used for i-FIT = 4

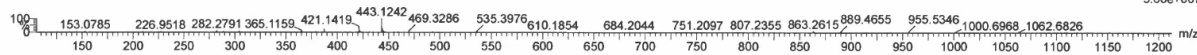
Monoisotopic Mass, Even Electron Ions
 3616 formula(e) evaluated with 20 results within limits (up to 50 closest results for each mass)
 Elements Used:
 C: 0-100 H: 0-100 N: 0-20 O: 0-20 Na: 0-1 S: 0-1
 MJR101 / DCM - eau/ACN/AF (90/10/0.1%) / ES+
 20170116_MJR101 18 (0.381) AM2 (Ar,22000.0,0.00,0.00); Cm (17:20)



A4.20

XEVO G2-XS QTOF

16-Jan-2017
 1: TOF MS ES+
 5.68e+007



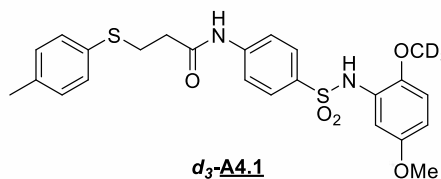
Mass	Calc. Mass	mDa	PPM	DBE	i-FIT	Norm	Conf(%)	Formula
387.0977	387.0975	0.2	0.5	0.5	990.7	16.659	0.00	C8 H20 N4 O12 Na
387.0975	387.0975	0.2	0.5	11.5	989.3	15.255	0.00	C6 H8 N18 O2 Na
387.0974	387.0974	0.3	0.8	7.5	975.3	1.223	29.44	C14 H19 N4 O7 S
387.0981	387.0981	-0.4	-1.0	16.5	989.7	15.605	0.00	C22 H15 N2 O5
387.0973	387.0973	0.4	1.0	4.5	990.8	16.699	0.00	C6 H15 N10 O10
387.0970	387.0970	0.7	1.9	18.5	990.4	16.273	0.00	C21 H12 N6 O Na
387.0986	387.0986	-0.9	-2.3	9.5	990.0	15.951	0.00	C7 H11 N14 O6
387.0986	387.0986	-0.9	-2.3	-1.5	990.8	16.693	0.00	C9 H23 O16
387.0988	387.0988	-1.1	-2.8	12.5	976.3	2.205	11.02	C15 H15 N8 O3 S
387.0989	387.0989	-1.2	-3.1	5.5	990.2	16.116	0.00	C9 H16 N8 O8 Na S
387.0964	387.0964	1.3	3.4	9.5	977.3	3.256	3.86	C13 H16 N8 O3 Na S
387.0991	387.0991	-1.4	-3.6	8.5	974.7	0.620	53.79	C17 H20 N2 O5 Na S
387.0962	387.0962	1.5	3.9	6.5	990.9	16.862	0.00	C5 H12 N14 O6 Na
387.0961	387.0961	1.6	4.1	13.5	978.8	4.716	0.90	C11 H11 N14 O S

Elemental Composition Report

Single Mass Analysis

Tolerance = 5.0 PPM / DBE: min = -50.0, max = 500.0
 Element prediction: Off
 Number of isotope peaks used for i-FIT = 4

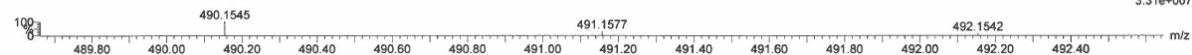
Monoisotopic Mass, Even Electron Ions
 1116 formula(e) evaluated with 6 results within limits (all results (up to 1000) for each mass)
 Elements Used:
 C: 0-100 H: 0-30 2H: 0-5 N: 0-5 O: 0-5 S: 2-2
 CTR-036-F1 (DCM) - MeOH (100%)
 20171114_CTR-036-F1 17 (0.364) AM2 (Ar,22000.0,0.00,0.00); ABS; Cm (17:18)



d₃-A4.1

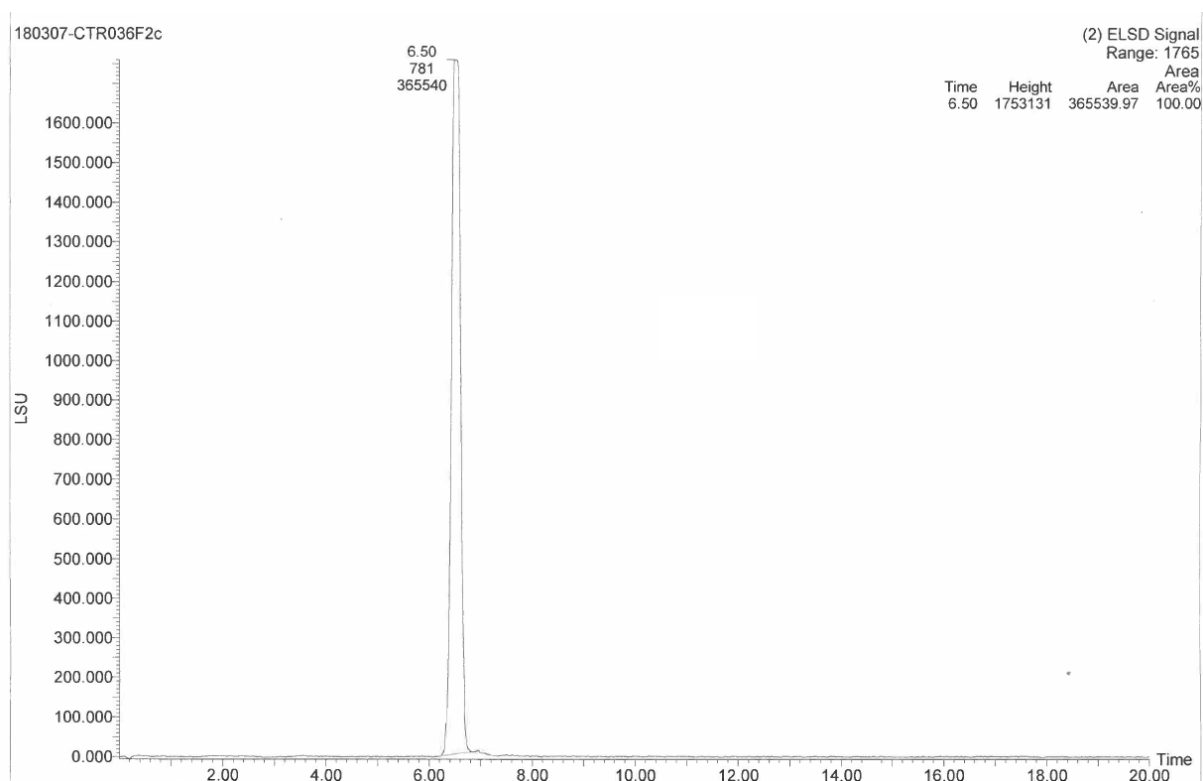
XEVO G2-XS QTOF

14-Nov-2017
 1: TOF MS ES+
 3.31e+007



Mass	Calc. Mass	mDa	PPM	DBE	i-FIT	Norm	Conf(%)	Formula
490.1545	490.1550	-0.5	-1.0	12.5	60.8	0.763	46.64	C24 H24 2H3 N2 O5 S2
490.1552	490.1552	-0.7	-1.4	12.5	61.4	1.385	25.02	C22 H24 2H2 N5 O4 S2
490.1559	490.1559	-1.4	-2.9	17.5	62.1	2.102	12.23	C29 H20 2H5 O3 S2
490.1561	490.1561	-1.6	-3.3	17.5	62.1	2.066	12.66	C27 H20 2H4 N3 O2 S2
490.1522	490.1522	2.3	4.7	20.5	63.7	3.728	2.40	C31 H24 2H N2 S2
490.1521	490.1521	2.4	4.9	13.5	64.6	4.564	1.04	C22 H20 2H4 N5 O4 S2

LCMS analysis of the final compound **d₃-A4.1** for pharmacokinetic studies



Analytical Conditions :

LC characterization was performed on a Waters Atlantis T3 (5 μ m, 4.6 x 150 mm; Waters) equipped with an ELSD detector. The chromatographic separation was carried out with the injection of 2 μ L of a sample solution (1mg/mL) followed by an isocratic elution (H₂O/Methanol: 25/75) at a flow rate of 0.8 mL/min.

Safety screen. The specificity of A4.1 activity was tested on 87 targets by Enzyme and Radioligand Binding Assays by Eurofins Panlabs Taiwan, Ltd. Methods employed in this study have been adapted from the scientific literature to maximize reliability and reproducibility.

Molecule toxicity. To assess the toxicity of A4.1, bacterial cytotoxicity, Ames fluctuation test and Micronucleus assays were performed by Eurofins Panlabs Taiwan, Ltd. The conditions of each test are detailed in the table below.

Assay	Source	Technique	Incubation	Detection Method
Toxicity				
Bacterial cytotoxicity (TA98 - S9)	Reverted Salmonella typhimurium (TA98)		96 hr 37°C	Photometry
Bacterial cytotoxicity (TA100 - S9)	Reverted Salmonella typhimurium (TA100)		96 hr 37°C	Photometry
Bacterial cytotoxicity (TA1535 - S9)	Reverted Salmonella typhimurium (TA1535)		96 hr 37°C	Photometry
Bacterial cytotoxicity (TA1537 - S9)	Reverted Salmonella typhimurium (TA1537)		96 hr 37°C	Photometry
Ames fluctuation test (TA98 - S9)	<i>Salmonella typhimurium</i> (TA98)	Fluctuation test	96 hr 37°C	Photometry
Ames fluctuation test (TA98 + S9)	<i>Salmonella typhimurium</i> (TA98) and rat liver S9	Fluctuation test	96 hr 37°C	Photometry
Ames fluctuation test (TA100 - S9)	<i>Salmonella typhimurium</i> (TA100)	Fluctuation test	96 hr 37°C	Photometry
Ames fluctuation test (TA100 + S9)	<i>Salmonella typhimurium</i> (TA100) and rat liver S9	Fluctuation test	96 hr 37°C	Photometry
Ames fluctuation test (TA1535 - S9)	<i>Salmonella typhimurium</i> (TA1535)	Fluctuation test	96 hr 37°C	Photometry
Ames fluctuation test (TA1535 + S9)	<i>Salmonella typhimurium</i> (TA1535) and rat liver S9	Fluctuation test	96 hr 37°C	Photometry
Ames fluctuation test (TA1537-S9)	<i>Salmonella typhimurium</i> (TA1537)	Fluctuation test	96 hr 37°C	Photometry
Ames fluctuation test (TA1537 + S9)	<i>Salmonella typhimurium</i> (TA1537)	Fluctuation test	96 hr 37°C	Photometry
Micronucleus (CHO + S9, HCA)	CHO-K1 cell line and rat liver S9	High content analysis (HCA)	4 hr 37°C	Fluorescent Image Analysis
Micronucleus (CHO - S9, HCA)	CHO-K1 cell line	High content analysis (HCA)	24 hr 37°C	Fluorescent Image Analysis

Bacterial Cytotoxicity

The results for cytotoxicity are expressed as percent of control growth (OD650). Compounds with growth of less than 60 % of control are flagged and considered cytotoxic.

Ames Tests

Wells that displayed bacteria growth due to the reversion of the histidine mutation (as judged by the ratio of OD430/OD570 being greater than 1.0) are counted and recorded as positive counts. The significance of the positive counts between the treatment (in the presence of test compound) and the control (in the absence of test compound) are calculated using the one-tailed Fisher's exact test. Three significance levels are reported as follows:

Weak positive, if $0.01 \leq p < 0.05$, denoted as "+" Strong positive, if $0.001 \leq p < 0.01$, denoted as "++" Very strong positive, if $p < 0.001$, denoted as "+++"

in vitro Micronucleus

The percent of micronucleated cells is calculated. A marginally-positive result ("-/+") is defined as a value significantly higher than controls (t-test, $p < 0.05$), and at least 2-fold higher than controls. A positive result ("+") is defined as a value significantly higher than controls (t-test,

p < 0.05) and at least 3-fold higher than controls. Cytotoxicity indexes are also provided to aid in the interpretation of the results.

A "scorable" cell is a bi-nucleated cell contained within the field boundary, in which both nuclei are of similar size (the maximum area ratio of the largest nucleus versus the smallest nucleus within a cell must be lower than 1.5).

Cytokinesis Block Proliferation Index (CBPI) % Cytotoxicity uses a modified version of the (CBPI). This method takes advantage of the fact that cytotoxicity very often induces cell cycle arrest, which is reflected in a decreased ratio of bi-nucleated to mononucleated cells when using cytochalasin B. A CBPI of 1 is equivalent to 100% cytotoxicity.

The % cytotoxicity based on the CBPI is calculated as follows:

$$Cytotoxicity(\%) = 100 - \left(\frac{CBPI_t - 1}{CBPI_c - 1} \times 100 \right)$$

where:

CBPI_t = CBPI of treated cells CBPI_c = CBPI of control cells CBPI is defined as:

$$\frac{(MoNC + 2 \times BiNC + 3 \times MuNC)}{Total\ number\ of\ cells}$$

Since most multinucleated cells are bi-nucleated, our approximation is:

$$CBPI = \frac{(MoNC + 2 \times MuNC)}{Total\ number\ of\ cells}$$

where

MoNC = number of mononucleated cells

BiNC = number of binucleated cells

MuNC = number of multinucleated cells

The Cell Number % Cytotoxicity is an index based on cell numbers, in which:

$$Cytotoxicity(\%) = 100 - \left(\frac{Number\ of\ treated\ cells \times 100}{Number\ of\ control\ cells} \right)$$

For both indexes, the control cell population is defined as the cells exposed to medium containing 1% DMSO. For the S9-treated cells, the control cell population is also exposed to medium containing 1% DMSO.

In most cases, the cell number index of cytotoxicity is more sensitive than the CBPI index. This is probably because the cell number index accounts for both cell proliferation and cell death, whereas the CBPI index is only based on cell proliferation. In addition, we find the cell number index especially useful in detecting aneugens, since aneugens can inhibit cytokinesis and they might not induce a drop in CBPI even at very cytotoxic concentrations.

The % Micronucleated Cells is the percentage of scorable cells that contain at least one micronucleus within their cytoplasmic domain. The largest allowed ratio of a micronucleus radius to the average nuclei radius within a scorable cell is 0.33.

Animals use. All experimental procedures and animal care were performed in accordance with the European Community Standards on the Care and Use of Laboratory Animals and approved by the local ethics committee (Comité d’Ethique en Expérimentation Animale des Pays de Loire). NMRI and NMRI Nude mice were purchased from Janvier Labs, C57Bl/6 mice from Charles River. In all experiments, A4.1 was dissolved in the vehicle DMSO/PEG300/water (ratio 10:40:50).

***In vivo* pharmacokinetics.** All reagents were provided from Sigma Aldrich (Saint-Quentin-Fallavier, France). A4.1 was administrated intraperitoneally (25 mg/kg, aqueous solution of A4.1 in 5% DMSO, 50% PEG) in 2 months old C57Bl/6 after 4h of fasting. After 5, 30, 60, 120 and 360 minutes following injection, mice ($n = 3$ *per* kinetic time) were sacrificed and tissues (blood, heart, lung, liver, kidney and brain) were collected. Control mice ($n = 5$) were used to get blank tissues for mass spectrometry analyses. Blood was collected by cardiac puncture into tubes containing 10% EDTA. Immediately after blood collection, plasma was separated by centrifugation for 5 min at 4 °C ($2,000 \times g$). Solid tissues were rapidly excised and

snap frozen in liquid nitrogen before to be disrupted and homogenized in PBS (1/10; wt/vol) using TissueLyser II (Quiagen). A4.1 concentrations were determined in mouse plasma and tissues by liquid chromatography-tandem mass spectrometry (LC-MS/MS). All solvents were LC-MS grade and purchased from Biosolve (Valkenswaard, Netherlands). A4.1 10× standard solutions were prepared and serially diluted in acetonitrile to obtain 8 standard solutions ranging 10-20,000 nmol/L. A4.1 10X standard solutions (5 μL or 20 μL) were added to blank plasma (45 μL) or blank tissue homogenates (180 μL), respectively, to get final concentrations ranging 1-2,000 nmol/L. Acetonitrile (5 μL or 20 μL) was added to plasma (45 μL) or tissue samples (180 μL). Tissue homogenates (standards and samples) were then centrifugated for 5 min at $5,000 \times g$ for 5 min at 10 °C and supernatants (100 μL) were collected. Proteins were precipitated by the addition of 150 μL or 300 μL of acetonitrile containing labeled D_3 -A4.1 as internal standard (200 nmol/L) in all plasma (50 μL) and tissue supernatants (100 μL), respectively. After centrifugation ($17,000 \times g$, 10 min, 10 °C), supernatants were collected and dried under a gentle stream of nitrogen. Dried samples were finally reconstituted with 25% acetonitrile containing 0.1% formic acid (100 μL), and injected into the LC-MS/MS system. Analyses were performed on a Xevo[®] TQD mass spectrometer with an electrospray (ESI) interface and an Acquity H-Class[®] UPLC[™] device (Waters Corporation, Milford, MA, USA). Samples (10 μL) were injected onto a BEH C₁₈ column (1.7 μm; 2.1 × 50 mm, Waters Corporation) held at 60 °C, and compounds were separated with a linear gradient of mobile phase B (acetonitrile, 0.1% formic acid) in mobile phase A (water, 0.1% formic acid) at a flow rate of 500 μL/min. Mobile phase B was kept constant for 0.5 min at 1%, linearly increased from 1% to 100% for 3 min, kept constant for 0.5 min, returned to the initial condition over 0.5 min, and kept constant for 0.5 min before the next injection. A4.1 and its internal standard D_3 -A4.1 were then detected by the mass spectrometer with the ESI interface operating in the positive ion mode (capillary voltage, 3 kV; desolvation gas (N₂) flow and temperature, 900

L/h and 450 °C; source temperature, 120 °C). The multiple reaction monitoring mode was applied for MS/MS detection at the following mass-to-charge (m/z) ratio transitions: 487.1 → 153.0 and 490.2 → 156.0 for A4.1 and D_3 -A4.1, respectively. Cone voltage and collision energy were set at 35 V and 20 eV, respectively. Data acquisition and processing were achieved using MassLynx[®] and TargetLynx[®] softwares (version 4.1, Waters Corporation). Chromatographic peak area ratios between A4.1 and its internal standard constituted the detector responses. Standard solutions were used to plot calibration curves for quantification and dilution factors related to biological matrix preparations were included in calculation. The linearity was expressed by the mean r^2 which was greater than 0.995 for all matrices (linear regression, 1/x weighting, origin excluded). AUC_{0-6h} was calculated as follow:

$$AUC_{0-6h} = \int_0^{6h} C_0 e^{-Kt} dt = C_0/K$$

Where K = constant of elimination, and C_0 = administrated dose.

Rac1 labeling by irradiation and photoaffinity. Solutions of Rac1 (2.1 mg/mL) in PBS containing EDTA (84 µg/mL) were irradiated with or without [N3]-A4.1 (500 µg/mL) at 302 nm for 6 min. A control solution of Rac1 (no irradiation and without [N3]-A4.1) was used to ascertain the stability of the protein throughout the experiment. Prior all experiments, both modified and unmodified Rac1 samples (~100 µL) were desalted and concentrated with 3 mL of 50 mM ammonium bicarbonate (Sigma Aldrich) buffer (pH 8) and a 5-kDa molecular weight cut-off filter. Resulting samples were stored at -20 °C until analysis.

Analysis of whole proteins. Samples were directly analyzed by liquid chromatography-high resolution mass spectrometry (LC-HRMS). LC-HRMS analyses were performed on a Synapt™ G2 HRMS Q-TOF mass spectrometer equipped with an ESI interface operating in the positive mode and an Acquity H-Class® UPLC™ device (Waters Corporation). Samples were injected (10 µL) onto a Acquity® CSH C18 (1.7 µm; 2.1 × 150 mm; 180 Å) reversed-phased LC column held at 60 °C. Proteins were then eluted over 20 min with a linear gradient of mobile phase B (100% acetonitrile) in mobile phase A (5% acetonitrile), each containing 0.1% formic acid, and at a flow rate of 250 µL/min. Mobile phase B was kept constant at 1% for 1 min, then linearly increased from 1% to 80% for 15 min, kept constant at 80% for 1 min, returned to the initial condition over 1 min, and kept constant for 2 min before the next injection. The full-HRMS mode was applied for protein detection (m/z range 100-4,000) at a mass resolution of 25,000 full-widths at half maximum. The ionization settings were as follows: capillary voltage, +3 kV; cone voltage, 30 V; desolvation gas (N₂) flow rate, 900 L/h; desolvation gas/source temperatures, 450/120 °C. Leucine enkephalin solution (2 µg/mL, 50% acetonitrile) was infused at a constant flow rate of 10 µL/min in the lockspray channel, allowing for correction of the measured m/z throughout the batch (theoretical m/z 556.2771 in positive mode). Data acquisition and processing were achieved using MassLynx® software (version 4.1, Waters Corporation). Complex mass spectra under chromatographic peaks were deconvoluted with the

MaxEnt₁ extension software to get the experimental molecular weights of proteins, which were then compared with those of the unmodified protein to estimate the number of added [N3]-A4.1 residues.

Peptide mapping after Rac1 tryptic digestion. The positive ESI mode is appropriate for proteins (ESI+) but leads to the formation of several adducts (H⁺, K⁺, Na⁺...) with multiple charge states ([M+nH]ⁿ⁺ ions) in addition to natural isotope signals (¹³C, ²H, ¹⁵N...). Protein samples were therefore subjected to proteolysis in order to form peptides that are more easily detected by mass spectrometry (lower charge states) and suitable for tandem mass spectrometry (MS/MS) analysis. The protein samples (50 µL) were reduced (addition of 120 µL ammonium bicarbonate 50 mM containing 7 mg/mL of RapidGest detergent [Waters Corporation], incubated 10 min at 80 °C; then addition of dithiothreitol, 70 mM, 20 µL, incubated 20 min at 60 °C), alkylated (addition of iodoacetamide, 142 mM, 30 µL, incubated 20 min at room temperature in the dark) and trypsin digested overnight (7 mg/mL in HCl 1 mM, 30 µL, 37 °C) using the ready-to-use solutions of the ProteinWorks™ eXpress kit (Waters Corporation) and according to the manufacturer's instructions. Enzymatic digestion was stopped with 20% trifluoroacetic acid (TFA; 5 µL). After 15 min at 45 °C, the precipitate was removed by centrifugation (15 min, 10°C, 10,000 × g), and supernatants were removed for LC-HRMS and LC-MS/MS analyses. Proteotypic peptides were separated and detected by the full-HRMS mode as described above. In parallel, protein sequence was *in-silico* digested using the free ExPASy software (https://web.expasy.org/peptide_mass). All tryptic peptides were looked for from their theoretical *m/z* ratios assuming several charged ions (from 1+ to 6+). Relevant peptides were then subjected to MS/MS fragmentations to ascertain their amino-acid sequences. Then, peptide sequences were compared with each other and between both modified and unmodified protein samples to establish the location of the labeled [N3]-A4.1 (+485.1 Da).

Finally, MS/MS fragmentation patterns allowed the identification of the modified amino-acid during the labeling experiment.

Orthotopic breast cancer model. Orthotopic cell xenograft was performed by injection of 4 million MDA-MB-468Luc cells in the fourth fat pad from 5-week-old NMRI nude mice. Primary tumour was allowed to develop during 5.5 weeks and tumour growth was assessed by tumour volume measurement using a calliper. Primary tumor was then removed by exeresis and weighed. Treatments began 1 day before exeresis. 25 mg/kg of A4.1 was administered intraperitoneally on a daily basis during 4 weeks. Mice were weighed 5 times a week and *in vivo* bioluminescence intensities (Photon Imager, Biospace Lab) were measured once a week. At the end of the protocol, mice were sacrificed and *ex vivo* bioluminescence intensities of indicated organs were measured.

Statistics. All data are expressed as the mean \pm SEM of sample size n. For multiple comparisons, the non-parametric Kruskal-Wallis test was used followed by Dunns' post-test. When the sample size was greater than 30, the one-way ANOVA test was used followed by Tukey's multiple comparisons test. For individual comparisons, statistical analysis was performed using non-parametric t-test (Mann-Whitney). Data analysis was performed using the GraphPad Prism software. The threshold for statistical significance was set at $P < 0.05$.

References

- Asif, P.J., Longobardi, C., Hahne, M., Medema, J.P. (2021). The Role of Cancer-Associated Fibroblasts in Cancer Invasion and Metastasis. *Cancers (Basel)*; 13(18): 4720
- Cherfils, J., and Zeghouf, M. (2011). Chronicles of the GTPase switch. *Nat Chem Biol* 7, 493-495.
- Crnogorac-Jurcevic, T., Efthimiou, E., Capelli, P., Blaveri, E., Baron, A., Terris, B., Jones, M., Tyson, K., Bassi, C., Scarpa, A., *et al.* (2001). Gene expression profiles of pancreatic cancer and stromal desmoplasia. *Oncogene* 20, 7437-7446.
- Durand-Onayli, V., Haslauer, T., Harzschel, A., and Hartmann, T.N. (2018). Rac GTPases in Hematological Malignancies. *Int J Mol Sci* 19.
- Ferrandez, Y., Zhang, W., Peurois, F., Akendengue, L., Blangy, A., Zeghouf, M., and Cherfils, J. (2017). Allosteric inhibition of the guanine nucleotide exchange factor DOCK5 by a small molecule. *Sci Rep* 7, 14409.
- Guilluy, C., Swaminathan, V., Garcia-Mata, R., O'Brien, E.T., Superfine, R., BurrIDGE, K. (2011). The Rho GEFs LARG and GEF-H1 regulate the mechanical response to force on integrins. *Nat Cell Biol.* 13(6):722-7.
- Hasan, M.K., Yu, J., Widhopf, G.F., 2nd, Rassenti, L.Z., Chen, L., Shen, Z., Briggs, S.P., Neuberg, D.S., and Kipps, T.J. (2018). Wnt5a induces ROR1 to recruit DOCK2 to activate Rac1/2 in chronic lymphocytic leukemia. *Blood* 132, 170-178.
- Jang, K., Kim, M., Seo, H. S. & Shin, I. (2010) PTEN sensitizes MDA-MB-468 cells to inhibition of MEK/Erk signaling for the blockade of cell proliferation. *Oncol Rep* 24, 787-793.
- Jansen, S., Gosens, R., Wieland, T., and Schmidt, M. (2018). Paving the Rho in cancer metastasis: Rho GTPases and beyond. *Pharmacol Ther* 183, 1-21.
- Kawasaki, Y., Sato, R., and Akiyama, T. (2003). Mutated APC and Asef are involved in the migration of colorectal tumour cells. *Nat Cell Biol* 5, 211-215.
- Kawazu, M., Ueno, T., Kontani, K., Ogita, Y., Ando, M., Fukumura, K., Yamato, A., Soda, M., Takeuchi, K., Miki, Y., *et al.* (2013). Transforming mutations of RAC guanosine triphosphatases in human cancers. *Proc Natl Acad Sci U S A* 110, 3029-3034.
- Kazanietz, M.G., and Caloca, M.J. (2017). The Rac GTPase in Cancer: From Old Concepts to New Paradigms. *Cancer Res* 77, 5445-5451.
- Krammer, A., Kichhoff, P.D., Jiang, X., Venkatachalam, C.M., Waldman, M. (2005). LigScore: a novel scoring function for predicting binding affinities. *J Mol Graph Model* 23(5):395-407.
- Ledford, H. (2015). Cancer: The Ras renaissance. *Nature* 520, 278-280.
- Lin, Y., and Zheng, Y. (2015). Approaches of targeting Rho GTPases in cancer drug discovery. *Expert Opin Drug Discov* 10, 991-1010.
- Loirand, G., Sauzeau, V., and Pacaud, P. (2013). Small G proteins in the cardiovascular system: physiological and pathological aspects. *Physiol Rev* 93, 1659-1720.
- McIver, S.C., Roman, S.D., Nixon, B., Loveland, K.L., and McLaughlin, E.A. (2013). The rise of testicular germ cell tumours: the search for causes, risk factors and novel therapeutic targets. *F1000Res* 2, 55.
- Ridley, A.J. (2015). Rho GTPase signalling in cell migration. *Curr Opin Cell Biol* 36, 103-112.
- Tarricone, C., Xiao, B., Justin, N., Walker, P.A., Rittinger, K., Gamblin, S.J., Smerdon, S.J. (2001). The structural basis of Arfaptin-mediated cross-talk between Rac and Arf signalling pathways. *Nature* 411(6834):215-9.

Tian, Y., Xu, L., He, Y., Xu, X., Li, K., Ma, Y., Gao, Y., Wei, D., and Wei, L. (2018). Knockdown of RAC1 and VASP gene expression inhibits breast cancer cell migration. *Oncol Lett* 16, 2151-2160.

Venkatachalam, CM., Jiang, X., Oldfield, T., Waldman, M. (2003) LigandFit: A Novel Method for the Shape-Directed Rapid Docking of Ligands to Protein Active Sites. *J Mol Graph Model*, 21 (4):289-307.

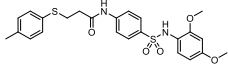
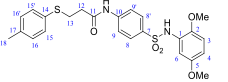
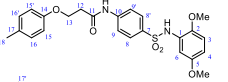
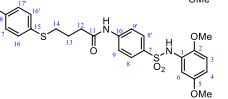
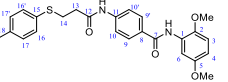
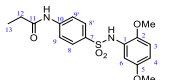
Wang, J., Rao, Q., Wang, M., Wei, H., Xing, H., Liu, H., Wang, Y., Tang, K., Peng, L., Tian, Z., *et al.* (2009). Overexpression of Rac1 in leukemia patients and its role in leukemia cell migration and growth. *Biochem Biophys Res Commun* 386, 769-774.

Welsch, M.E., Kaplan, A., Chambers, J.M., Stokes, M.E., Bos, P.H., Zask, A., Zhang, Y., Sanchez-Martin, M., Badgley, M.A., Huang, C.S., *et al.* (2017). Multivalent Small-Molecule Pan-RAS Inhibitors. *Cell* 168, 878-889 e829..

Yan, B., and Sun, Y. (1997). Glycine Residues Provide Flexibility for Enzyme Active Sites. *J Biol Chem* 272:3190-3194.

List of table

Table 1: Chemical library derived from A4 compound.

Name	Structure	Molecular Formula	Druglikeness				Docking score	IC ₅₀ (M)
			MW	logP	HBD	HBA		
A4		C ₂₄ H ₂₆ N ₂ O ₅ S ₂	486,60	4,197	2	6	-10.32	3.10 ⁻⁸
A4.1		C ₂₄ H ₂₆ N ₂ O ₅ S ₂	486,60	4,197	2	6	-11.12	0.67.10 ⁻⁹
A414		C ₂₄ H ₂₆ N ₂ O ₆ S	470,54	3,639	2	6	-11.62	0.56.10 ⁻⁹
A416		C ₂₅ H ₂₈ N ₂ O ₅ S ₂	500,63	4,518	2	6	-9.92	2.6 .10 ⁻⁶
A415		C ₂₅ H ₂₆ N ₂ O ₄ S	450,55	4,494	2	5	-7.53	-
A420		C ₁₇ H ₂₀ N ₂ O ₅ S	364,42	2,072	2	5	-13.80	-

For each molecule, druglikeness has been assessed according to Lipinski's rules: molecular weight (MW)<500; high lipophilicity (LogP<5); less than 5 hydrogen bond donors (HBD); less than 10 hydrogen bond acceptors (HBA). The docking score (kcal/mol) for the nucleotide binding site corresponds to the value of the binding free energy after in situ ligand minimization divided by the number of heavy atoms of each ligand. IC₅₀ was determined experimentally from the inhibition on RAC1-dependent ruffle formation.

List of figures

Figure 1

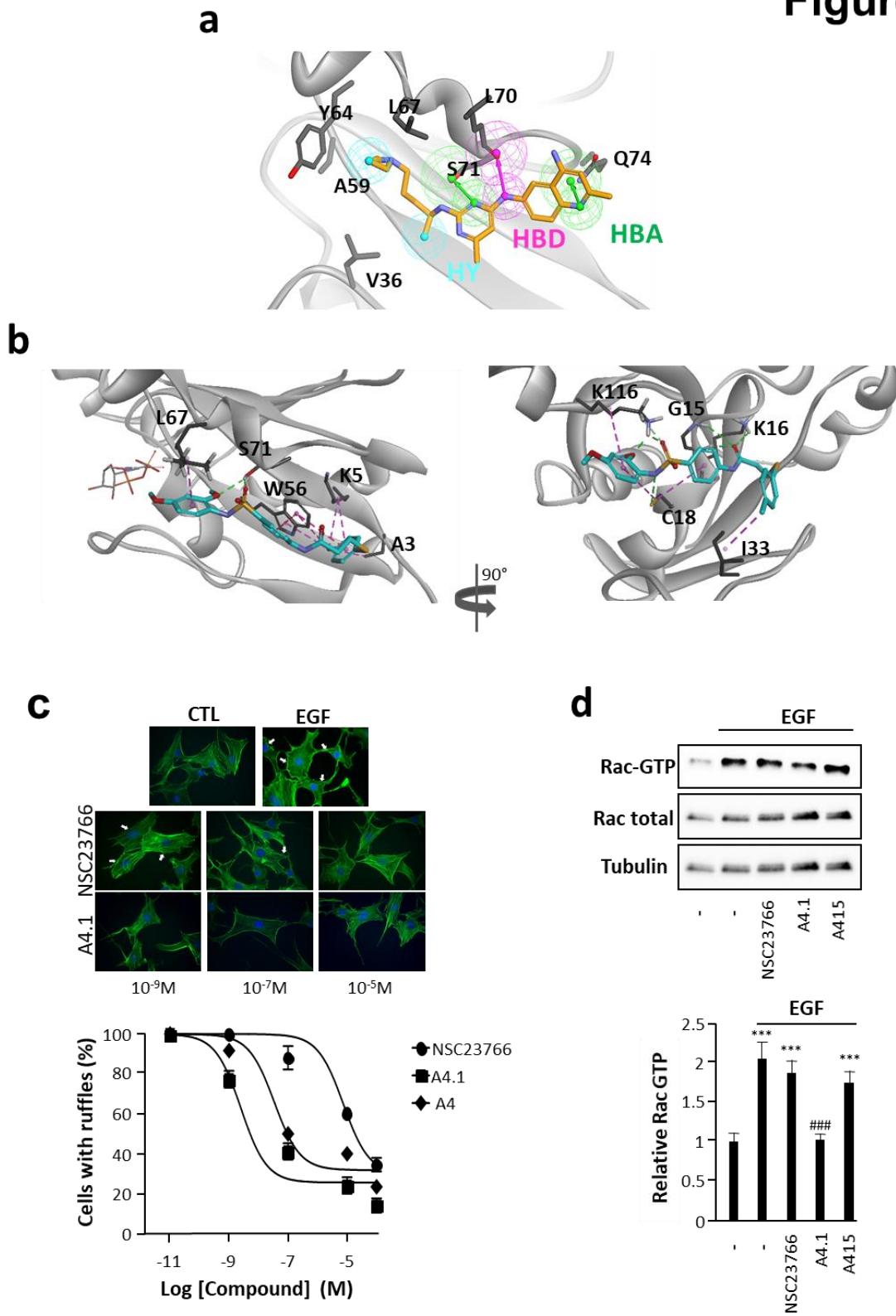


Figure 1: Identification of a new RAC1 inhibitor. (a) Predicted binding modes of NSC23766 on RAC1. **(b)** Predicted binding modes of A4 to the NSC23766 binding site or the GDP binding pocket of RAC1. In the NSC23766 binding site of RAC1 (left), the compound A4 (blue) makes 2 hydrogen bonds (green dotted line) with Ser71 (S71) and 8 hydrophobic interactions (pink dotted line) with Ala3 (A3), Lys5 (K5), Trp56 (W56) and Leu67 (L67) leading to a docking score of -6.03 kcal/mol. The GDP molecule is shown with fine line. In the GDP binding pocket (right), A4 is involved in 6 hydrogen bonds with Gly15 (G15), Lys16 (K16), Cys18 (C18) and Lys116 (K116), 1 carbon hydrogen bond with Lys116 and 4 hydrophobic interactions with Cys18, Ile33 (I33) and Lys116, resulting in a docking score of -10.32 kcal/mol. **(c)** NIH-3T3 cells were incubated in serum-free growth medium and stimulated by EGF (10 ng/mL) to induce ruffle formation. 1h before this stimulation, cell cultures were pre-incubated with A4.1 or NSC23766 at indicated concentration. Ruffles are indicated by arrows (top panel). Percentages of cells with ruffles were quantified (bottom panel). Results shown are representative of 3 independent experiments. **(d)** Immunoblot analysis and associated quantification of Rac-GTP levels and total Rac expression in fibroblasts (NIH3T3 cells) stimulated by EGF (10ng/mL, 5 min) and pre-incubated or not with NSC23766, A4.1 or A4.15 at 10^{-5} M for 1 h. ***P<0.001 vs controls without EGF stimulation, ### P<0.001 vs controls with EGF stimulation.

Figure 2

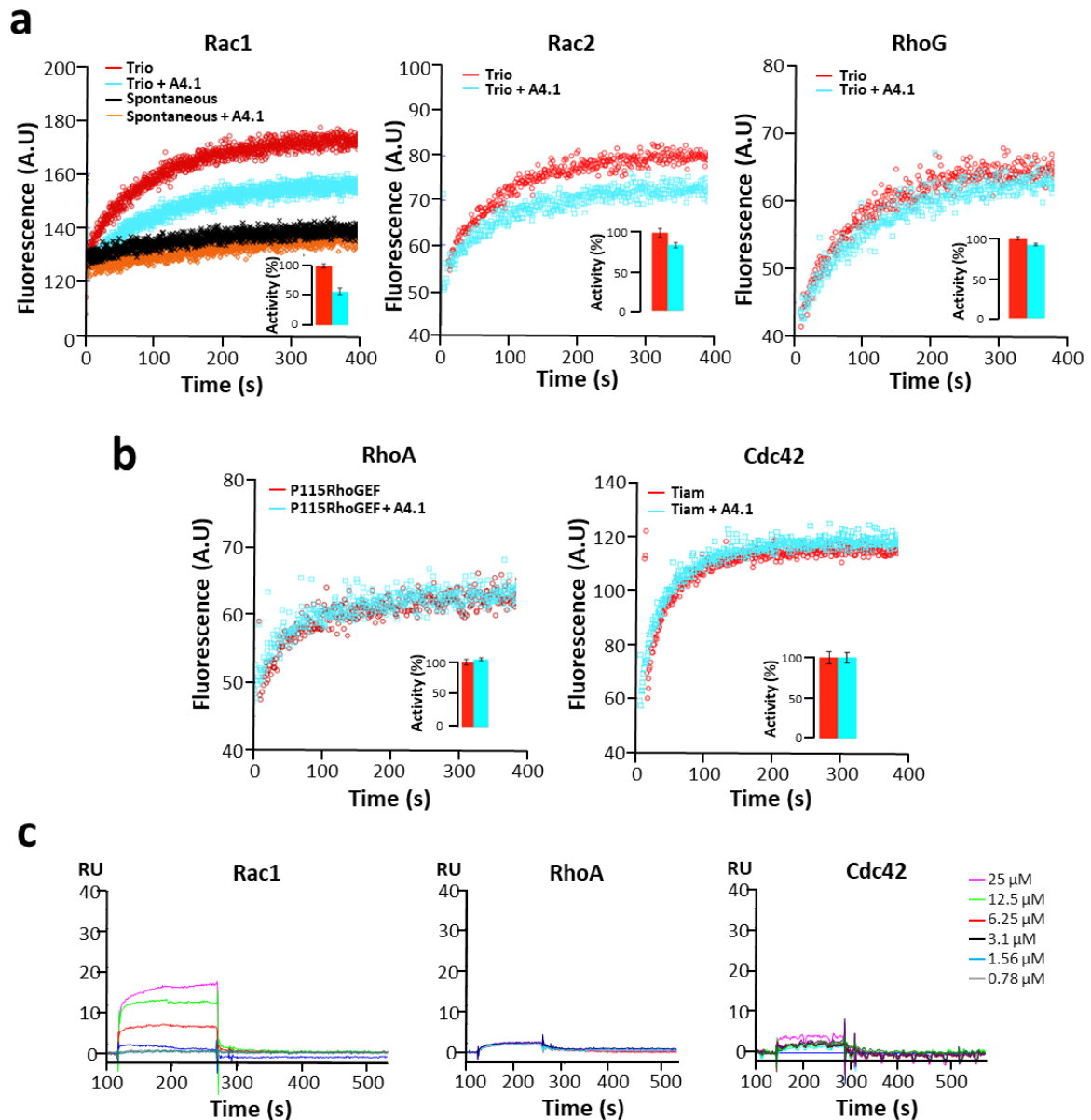


Figure 2: A4.1 selectively impairs Rac proteins activation. (a) Effect of A4.1 on GEF-stimulated Rac1, Rac2 and RhoG nucleotide exchange. Purified GTPases were pre-loaded with GDP, then nucleotide exchange was monitored as an increase in fluorescence following mant-GTP binding. (b) Effect of A4.1 on GEF-stimulated RhoA and Cdc42 nucleotide exchange. Experimental conditions are similar as described in (a). (c) Representative surface plasmon

resonance (SPR) sensograms of binding of immobilized Rac1, RhoA or Cdc42 small GTPase with increasing concentrations of A4.1. $n > 3$.

Figure 3

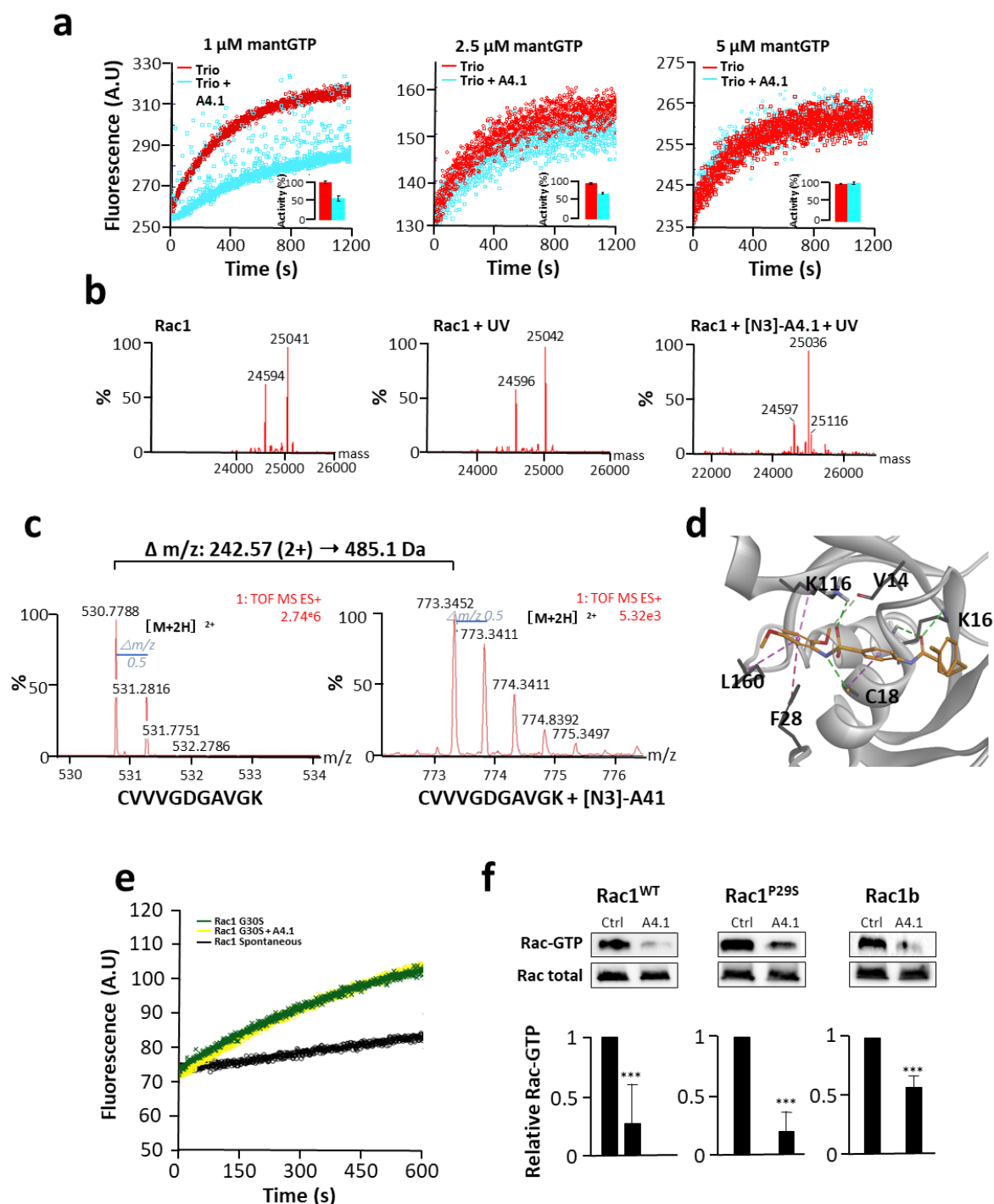


Figure 3: Inhibitory mechanism of A4.1. (a) Rac1 activation was monitored following mant-GTP binding. The protein complex Rac1/TRIO was incubated with mant-GTP at indicated

concentrations and A4.1 at fixed concentration 5 μ M. A.U.= arbitrary fluorescence units. **(b)** Deconvoluted mass spectra generated from crude mass spectrum analyses to evaluate Rac1 photolabeling with [N3]-A4.1 by LC-HRMS on native protein. **(c)** Representative mass spectra of both labeled and unlabeled CVVVG DGAVGK peptide during LC-HRMS analysis of Rac1 photolabeling with [N3]-A4.1 after trypsin digestion. **(d)** Predicted binding mode of A4.1 to the GDP binding pocket of RAC1. Compound A4.1 (orange) makes 4 hydrogen bonds (green dotted line) with Lys16 (K16), Cys18 (C18) and Lys116 (K116), 1 carbon hydrogen bond (light green dotted line) with Val14 (V14) and 4 hydrophobic interactions (pink dotted line) with Cys18, Phe28 (F28), Lys116 (K116) and Leu160 (L160). **(e)** Effect of A4.1 on Rac1^{G30S} activation. Rac1^{G30S} activation was monitored following mant-GTP binding. The GEFs TRIO and DHR2, or EDTA were used to induce nucleotide exchange. **(f)** Immunoblot analysis and associated quantification of Rac-GTP levels and total Rac expression in fibroblasts expressing Rac wild-type (Rac1^{WT}) or Rac1 oncomutants (Rac1^{P29S} and Rac1b). Data are presented as mean \pm SEM. ***P<0.001 vs controls.

Figure 4

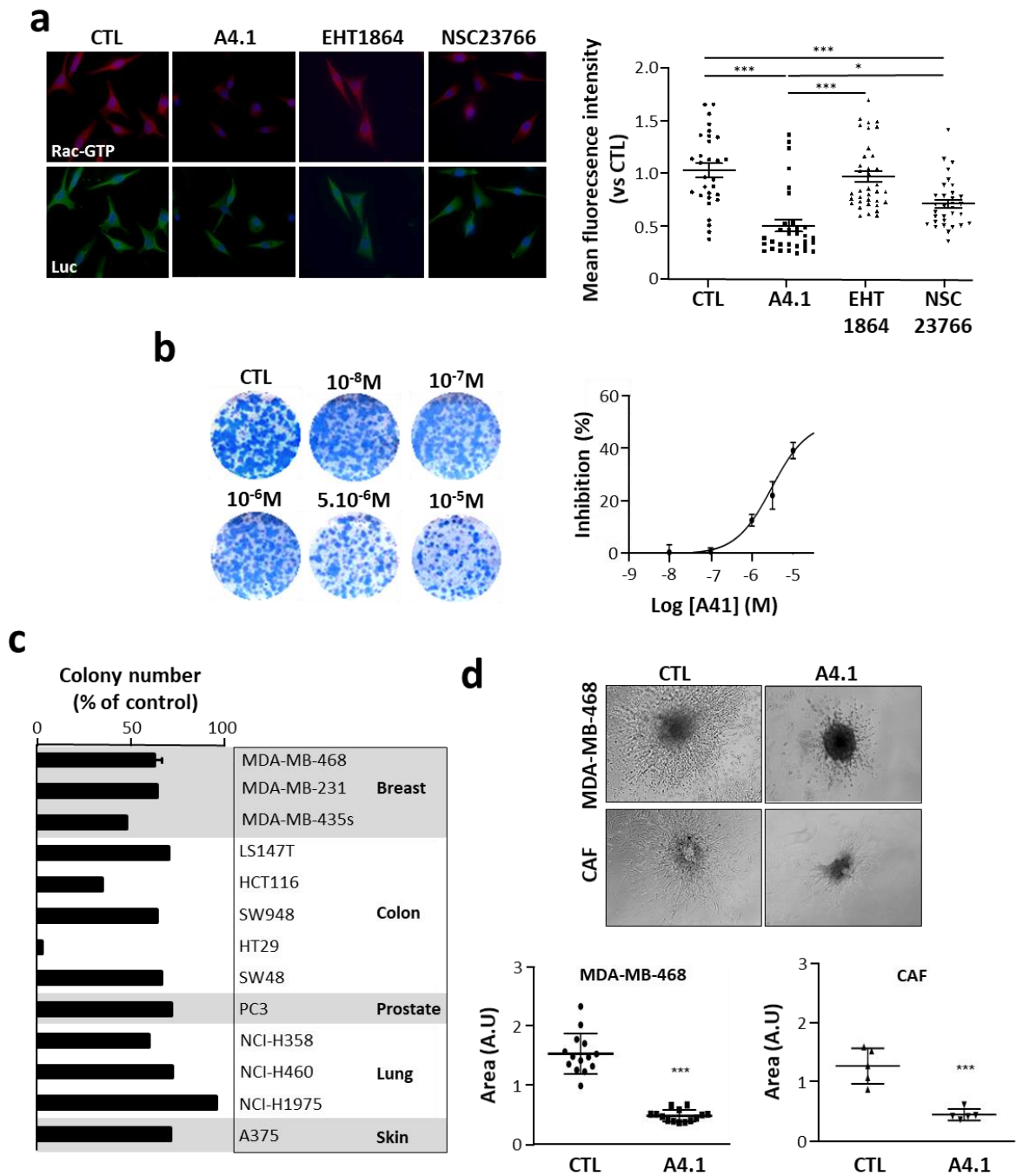


Figure 4: A4.1 decreases growth and invasiveness of triple negative breast cancer cells *in vitro*. (a) Representative images of Rac-GTP levels (Red) in MDA-MB-468Luc cells (Left panel). Luciferase (Luc, green) was used to detect the cells. When indicated, cells were treated with EHT1864, NSC23766 or A4.1 during 1h at 10^{-5} M. Rac-GTP mean fluorescence intensity

was quantified inside the cell area (Right panel). n=31-37 cells from 3 independent experiments. *P<0.05, ***P<0.001. **(b)** Focus formation assay of MDA-MB-468Luc cells (Left panel). When indicated, cells were treated with indicated concentrations of A4.1. Quantification of colony formation inhibition by A4.1 (Right panel). n=6 independent experiments. **(c)** A4.1 efficacy was tested on focus assays on various cancer cell lines. **(d)** 3D Invasion and associated quantification of MDA-MB-468Luc and cancer associated fibroblasts (CAFs). When indicated, Matrigel was polymerized with 10^{-5} M of A4.1. n=3 independent experiments. ***P<0.001 vs controls.

Figure 5

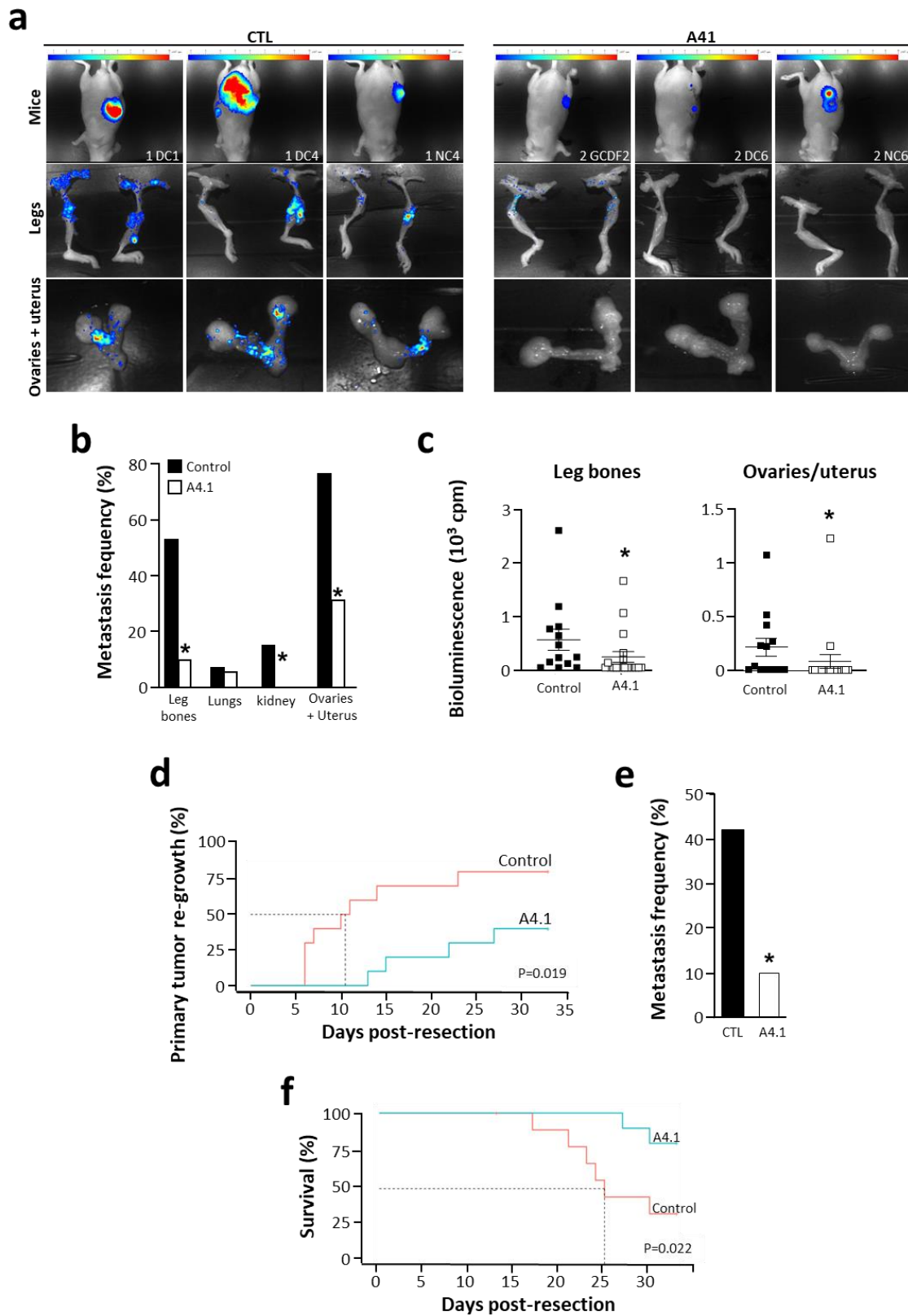


Figure 5: A4.1 decreases metastasis of triple negative breast cancer cells *in vivo*. (a) Representative images of luciferase bioluminescence intensities (BLI) in whole body or legs or

overies + uterus of NMRI nude mice 80 days post-xenograft. When indicated, mice were treated with A4.1. **(b)** Metastasis frequency quantification based on *ex vivo* BLI measurements in indicated organs (black bars). When indicated, mice were treated with A4.1 (white bars). n=10-15 mice. *P<0.05 vs controls. **(c)** BLI quantification in legs and ovaries/uterus from NMRI nude mice 80 days post-xenograft (black circles). When indicated, mice were treated with A4.1 (white squares). n=10-15 mice. *P<0.05 vs controls. **(d)** Tumor growth proportion in immunocompetent mice after primary tumor resection treated (blue line) or not (red line) with A4.1. **(e)** Metastasis frequency quantification based on *ex vivo* BLI measurements in indicated organs (grey bars) from immunocompetent mice. When indicated, mice were treated with A4.1 (white bars). n=10 mice. *P<0.05 vs control. **(f)** Survival curve of immunocompetent mice after primary tumor resection treated (blue line) or not (red line) with A4.1.

Figure 6

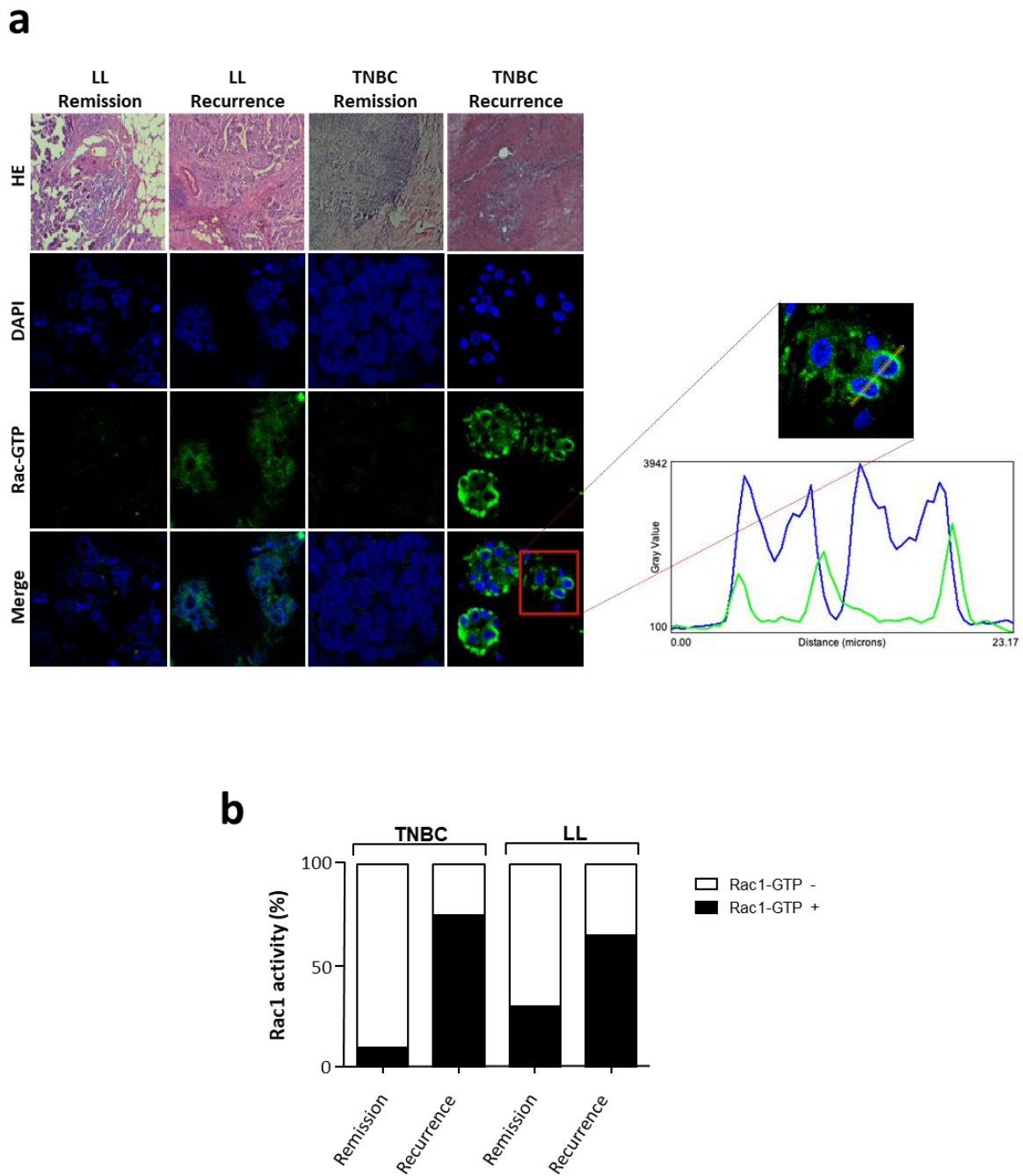


Figure 6: Analysis of Rac activity in breast cancer biopsies. (a) By immunofluorescence, Rac-GTP was detected in biopsies from patients with luminal B-like (LL) (n=20) or triple negative (TNBC) breast cancer (n=20). In each group, biopsies were divided in two sub-groups: patients who will develop metastases (Recurrence) or will be in remission (Remission). HE,

hematoxylin-eosin staining; DAPI, nucleus labelling; merge, fusion of DAPI and Rac-GTP images. **(b)** Proportion of Rac-GTP positive (P, in black) and negative (N, in white) biopsies in different patient groups.

List of supplemental tables

Supp. Table 1: Ranking of RAC inhibitor candidates retained from virtual screening and docking.

#Sample ID (10 ⁻⁵ M)	Adhesion (% inhib)	Migration (% inhib)	Proliferation (% ctrl)	Rac-GTP level (relative to EHT1864)
A4	58	34	100	0.38
D10	36	25	114	0.60
D9	42	10	110	0.77
B10	62	32	7	0.80
D6	37	35	94	0.82
A2	32	13	131	0.83
B3	51	22	51	0.95
EHT1864	32	35	101	1.00
G5	36	44	134	1.08
H7	40	14	144	1.41
A8	65	10	53	1.46
E6	48	27	101	2.44
E4	44	22	143	2.87
D11	37	40	88	3.79
NSC23766	34	0	131	<i>N.D</i>

Small molecules have been tested for their inhibitory effect on RAC-dependent processes (adhesion, migration and proliferation) and EGF-induced RAC activation assessed by pull-down assay in NIH-3T3 cells. EGF-induced RAC activity in the presence of EHT1864 has been set to 1. Molecules are ranked according to their efficacy compared to that of NSC23766 and EHT1864 and are displayed in the table the molecules better than the reference inhibitors.

Supp. Table 2: Known mutations of cancer cell lines from various organs and tissues used in clonogenic assays.

Tissue	Cell line	Mutation
Breast	MDA-MB-468	<i>P53</i>
	MDA-MB-231	<i>KRAS, BRAF</i>
	MDA-MB-435s	<i>BRAF</i>
Colon	LS147T	<i>KRAS, PI3K</i>
	HCT 116	<i>KRAS, PI3K</i>
	SW948	<i>PI3K</i>
	HT29	<i>BRAF</i>
	SW48	NA
Prostate	PC3	<i>PTEN</i>
Lung	NCI-H358	<i>KRAS</i>
	NCI-H460	<i>KRAS, PI3K</i>
	NCI-H1975	<i>PI3K</i>
Skin	A375	<i>BRAF</i>

A4.1 efficacy was tested on focus assays. For each cancer cell lines, mutations were indicated.

Supp. Table 3: A4.1 SafetyScreen.

Assay Name	Spec.	% inh.		
ATPase, Na ⁺ /K ⁺ , Heart, Pig	pig	-15	Glucocorticoid	hum 17
Cholinesterase, Acetyl, ACES	hum	64	Glutamate, AMPA	rat 9
Cyclooxygenase COX-1	hum	-11	Glutamate, Kainate	rat -8
Cyclooxygenase COX-2	hum	11	Glutamate, Metabotropic, mGlu5	hum -12
Monoamine Oxidase MAO-A	hum	10	Glutamate, NMDA, Agonism	rat 4
Monoamine Oxidase MAO-B	hum	17	Assay Name	Spec.
Peptidase, Angiotensin Converting Enzyme	rabbit	11	% inh.	
Peptidase, CTSG (Cathepsin G)	hum	-2	Glutamate, NMDA, Glycine	rat 7
Phosphodiesterase PDE3	hum	9	Glutamate, NMDA, Phencyclidine	rat -6
Phosphodiesterase PDE4	hum	4	Glutamate, NMDA, Polyamine	rat 19
Protein Serine/Threonine Kinase, PKC, Non-Selective	rat	48	Glycine, Strychnine-Sensitive	rat -17
Protein Tyrosine Kinase, Insulin Receptor	hum	-25	Histamine H1	hum 41
Protein Tyrosine Kinase, LCK	hum	14	Histamine H2	hum -14
Adenosine A1	hum	2	Leukotriene, Cysteinyl CysLT1	hum 14
Adenosine A2A	hum	16	Melanocortin MC1	hum 14
Adrenergic α1A	rat	34	Melanocortin MC4	hum 8
Adrenergic α1B	rat	41	Muscarinic M1	hum 11
Adrenergic α1D	hum	21	Muscarinic M2	hum 12
Adrenergic α2A	hum	29	Muscarinic M3	hum 4
Adrenergic α2B	hum	9	Muscarinic M4	hum -1
Adrenergic β1	hum	2	Neuropeptide Y Y1	hum -2
Adrenergic β2	hum	5	Nicotinic Acetylcholine	hum -3
Androgen (Testosterone)	hum	10	Nicotinic Acetylcholine α1, Bungarotoxin	hum 0
Angiotensin AT1	hum	17	Opiate δ1 (OP1, DOP)	hum 6
Bradykinin B2	hum	1	Opiate κ(OP2, KOP)	hum 10
Calcium Channel L-Type, Benzothiazepine	rat	46	Opiate μ(OP3, MOP)	hum 14
Calcium Channel L-Type, Dihydropyridine	rat	85	Platelet Activating Factor (PAF)	hum 78
Calcium Channel L-Type, Phenylalkylamine	rat	52	Potassium Channel [KATP]	ham 11
Calcium Channel N-Type	rat	3	Potassium Channel hERG	hum 22
Cannabinoid CB1	hum	81	PPARγ	hum -7
Cannabinoid CB2	hum	36	Progesterone PR-B	hum -16
Chemokine CCR1	hum	2	Serotonin (5-Hydroxytryptamine) 5-HT1A	hum 6
Chemokine CXCR2 (IL-8RB)	hum	1	Serotonin (5-Hydroxytryptamine) 5-HT1B	hum 15
Cholecystokinin CCK1 (CCKA)	hum	31	Serotonin (5-Hydroxytryptamine) 5-HT2A	hum 84
Cholecystokinin CCK2 (CCKB)	hum	0	Serotonin (5-Hydroxytryptamine) 5-HT2B	hum 90
Dopamine D1	hum	17	Serotonin (5-Hydroxytryptamine) 5-HT2C	hum 56
Dopamine D2L	hum	9	Serotonin (5-Hydroxytryptamine) 5-HT3	hum -2
Dopamine D2S	hum	35	Sodium Channel, Site 2	rat 57
Endothelin ETA	hum	-8	Tachykinin NK1	hum 41
Estrogen ERα	hum	10	Transporter, Adenosine	gp 37
GABAA, Chloride Channel, TBOB	rat	45	Transporter, Dopamine (DAT)	hum 30
GABAA, Flunitrazepam, Central	rat	15	Transporter, GABA	rat -4
GABAA, Ro-15-1788, Hippocampus	rat	-12	Transporter, Norepinephrine (NET)	hum 36
GABAB1A	hum	-6	Transporter, Serotonin (5-Hydroxytryptamine) (SERT)	hum -3
			Vasopressin V1A	hum 1

The activity of A4.1 in 87 radioligands binding assays against other targets than small GTPases was measured at a concentration of 10 μ M A4.1. The degree of radioligand inhibition is indicated in each case.

Supp. Table 4: Bacterial cytotoxicity effects of A4.1.

Test Concentration	%Effect			Mean %Effect	Cytotoxicity (% of control)
	1 st	2 nd	3 rd		
Bacterial cytotoxicity (TA98 - S9)					
6.0E-07 M	92.4	82.4	82.4	85.7	86
1.2E-06 M	89.7	74.1	55.8	73.2	73
2.5E-06 M	80.5	83.3	82.4	82.0	82
5.0E-06 M	88.8	84.2	81.4	84.8	85
1.0E-05 M	82.4	76.9	77.8	79.0	79
2.5E-05 M	95.2	92.4	83.3	90.3	90
5.0E-05 M	88.8	83.3	75.9	82.7	83
1.0E-04 M	154.6	177.5	143.7	158.6	159
Bacterial cytotoxicity (TA100 - S9)					
6.0E-07 M	104.7	104.7	98.2	102.5	103
1.2E-06 M	103.4	99.5	92.9	98.6	99
2.5E-06 M	106.0	103.4	92.9	100.8	101
5.0E-06 M	116.5	116.5	91.6	108.2	108
1.0E-05 M	116.5	108.6	92.9	106.0	106
2.5E-05 M	113.9	111.3	100.8	108.6	109
5.0E-05 M	112.6	153.1	102.1	107.3	107
1.0E-04 M	222.5	205.5	199.0	209.0	209
Bacterial cytotoxicity (TA1535 - S9)					
6.0E-07 M	89.4	96.4	94.0	93.3	93
1.2E-06 M	91.7	97.5	88.2	92.5	92
2.5E-06 M	92.9	91.7	97.5	94.0	94
5.0E-06 M	96.4	95.2	99.8	97.1	97
1.0E-05 M	96.4	98.7	108.0	101.0	101
2.5E-05 M	116.1	99.8	98.7	104.9	105
5.0E-05 M	175.3	168.3	163.7	169.1	169
1.0E-04 M	219.4	233.3	215.9	222.9	223
Bacterial cytotoxicity (TA1537 - S9)					
6.0E-07 M	107.2	107.2	115.3	109.9	110
1.2E-06 M	109.9	108.6	101.9	106.8	107
2.5E-06 M	111.2	104.5	99.2	105.0	105
5.0E-06 M	116.6	111.2	100.5	109.4	109
1.0E-05 M	109.9	108.6	111.2	109.9	110
2.5E-05 M	128.7	115.3	112.6	118.8	119
5.0E-05 M	162.2	150.1	148.8	153.7	154
1.0E-04 M	222.5	214.4	229.2	222.0	222

Supp. Table 5: Ames-fluctuation assay of A4.1.

Test Concentration	Count (# of wells)	Positive Significance (- to +++)
5.0E-06 M	0	-
1.0E-05 M	2	-
5.0E-05 M	0	-
1.0E-04 M	1	-
5.0E-06 M	3	-
1.0E-05 M	1	-
5.0E-05 M	0	-
1.0E-04 M	0	-
5.0E-06 M	8	-
1.0E-05 M	5	-
5.0E-05 M	5	-
1.0E-04 M	3	-
Ames fluctuation test (TA100 + S9)		
5.0E-06 M	6	-
1.0E-05 M	10	-
5.0E-05 M	9	-
1.0E-04 M	7	-
Ames fluctuation test (TA1535 - S9)		
5.0E-06 M	0	-
1.0E-05 M	2	-
5.0E-05 M	0	-
1.0E-04 M	0	-
Ames fluctuation test (TA1535 + S9)		
5.0E-06 M	1	-
1.0E-05 M	0	-
5.0E-05 M	0	-
1.0E-04 M	1	-
5.0E-06 M	1	-
1.0E-05 M	0	-
5.0E-05 M	0	-
1.0E-04 M	1	-
Ames fluctuation test (TA1537 + S9)		
5.0E-06 M	4	-
1.0E-05 M	5	-
5.0E-05 M	2	-
1.0E-04 M	1	-

Supp Table 6: Micronucleus assay of A4.1 on CHO cells.

Test Concentration	Scored Cells	% Cytotoxicity CBPI Index	% Cytotoxicity Cell Numbers
Micronucleus (CHO + S9, HCA)			
6.3E-05 M	2143	-0.4	54.3
1.3E-04 M	2168	3.0	63.7
2.5E-04 M	2114	3.3	71.5
5.0E-04 M	2130	46.8	72.1
1.0E-03 M	486	82.3	77.9
Micronucleus (CHO - S9, HCA)			
7.8E-06 M	2034	-21.4	14.3
1.6E-05 M	2287	-23.9	26.4
3.1E-05 M	2155	8.1	42.0
6.3E-05 M	1868	65.8	52.5
1.3E-04 M	1018	72.8	64.6
2.5E-04 M	751	73.8	73.6

Supp Table 7: Pharmacokinetic parameters calculated of A4.1 in mice after a single intraperitoneal injection at 25 mg/kg.

	Plasma
$t_{1/2}$ (min)	97.764
C_0 ($\mu\text{g/ml}$)	4.335
AUC_{0-6h} ($\mu\text{g}\cdot\text{h/ml}$)	14.3
Vd (ml)	5.767
Cl (ml/h)	1.748
C_{max} ($\mu\text{g/ml}$)	15.056 \pm 0.5
T_{max} (min)	5

Supp Table 8: White blood cell counts in control and A4.1-treated mice (25mg/kg/d; 33d)

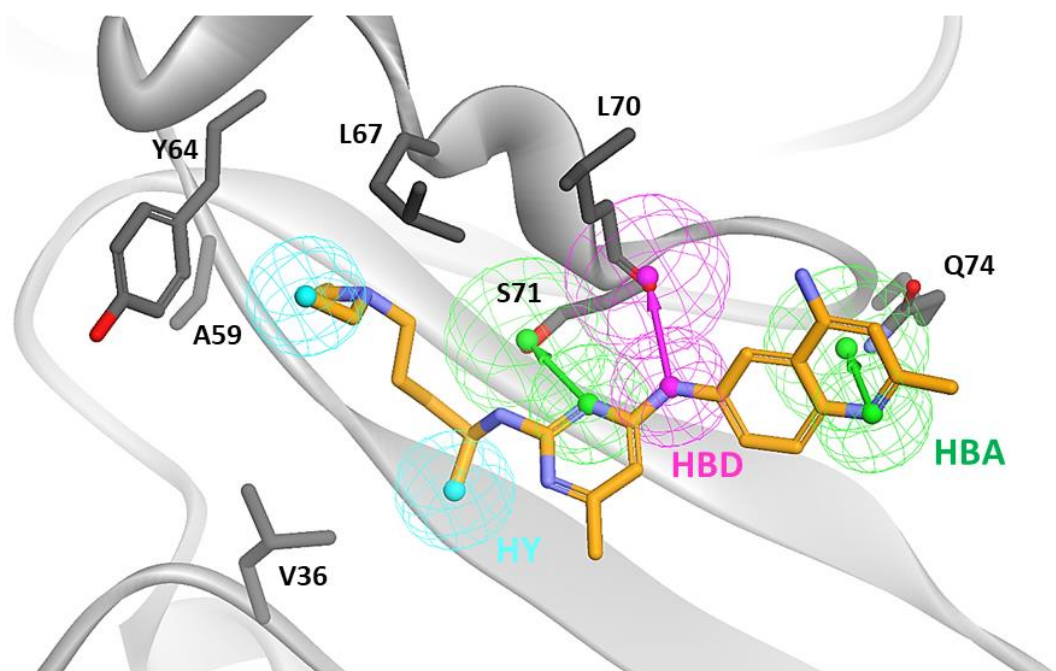
	Control (N=5)	A41 (N=5)	p value
Mix1.Leucocytes			0.33
Mean (SD)	99.30 (0.62)	92.75 (11.92)	
N	5	4	
Mix1.Bcells			0.14
Mean (SD)	14.11 (2.69)	11.62 (1.58)	
N	5	4	
Mix1.Tcells			0.22
Mean (SD)	44.72 (8.28)	52.20 (2.11)	
N	5	4	
Mix1.TCD4+			0.46
Mean (SD)	88.80 (3.82)	90.33 (1.27)	
N	5	4	
Mix1.CD8+			0.46
Mean (SD)	9.54 (3.44)	8.35 (1.42)	
N	5	4	
Mix1.ImmNKCell			0.81
Mean (SD)	0.09 (0.03)	0.10 (0.05)	
N	5	4	
Mix1.NKCell			0.81
Mean (SD)	0.44 (0.14)	0.40 (0.22)	
N	5	4	
Mix2.Leucocytes			0.77
Mean (SD)	99.93 (0.04)	99.85 (0.15)	
N	4	4	
Mix2.Macrophage			0.77
Mean (SD)	2.74 (1.85)	2.46 (2.34)	
N	4	4	
Mix2.Monocytes			1.00
Mean (SD)	0.72 (0.15)	0.86 (0.57)	
N	4	4	
Mix2.Neutrophiles			1.00
Mean (SD)	4.88 (5.16)	4.19 (6.24)	
N	4	4	

Supp Table 9: Clinicopathologic data of TNBC and Luminal B-like patients included in the analyze of Rac1 activity.

	TNBC (N=18)	LL (N=20)		TNBC (N=18)	LL (N=20)
Histologic.subtype			Radiotherapy.Breast.ChestWall		
Poorly differentiated	16/18	16/20	NO	2/18	0/20
Micropapillary	0/18	1/20	YES	16/18	20/20
Colloidal 20%	0/18	1/20	Radiotherapy.LymphNodes.area		
Non specified	2/18	2/20	NO	15/18	9/20
Status			YES	3/18	11/20
Remission	10/18	10/20	Chemotherapy.Type		
Recurrence	8/18	10/20	NO	3/18	3/20
Age.Dg (years)			ANTHRACYCLINE	2/18	6/20
Median	63.000	60.500	TAXANE	1/18	0/20
Q1, Q3	52.0, 72.2	47.7, 65.5	ANTHRACYCLINE + TAXANE	11/18	11/20
Laterality			ANTHRACYCLINE + TAXANE + BEVACIZUMAB	1/18	0/20
Left	12/18	9/20	Hormonotherapy.Adjuvant		
Right	6/18	11/20	NO	17/18	0/20
Neoadjuvant.Chemotherapy			YES	1/18	20/20
NO	17/18	20/20	Tumoral emboli		
YES	1/18	0/20	NO	13/18	6/20
Breast.Surgery			YES	5/18	14/20
Conservative	13/18	15/20			
Mastectomy	5/18	5/20			
LymphNode.Surgery					
GAS	13/18	4/20			
CURAGE	5/18	16/20			
Stade.UICC					
I	10/18	5/20			
IIA	3/18	6/20			
IIB	1/18	2/20			
IIIA	2/18	5/20			
IIIB	1/18	1/20			
IIIC	1/18	1/20			
Histologic.Grade					
-1	1/18	2/20			
-2	5/18	5/20			
-3	12/18	13/20			
CIS					
NO	8/18	8/20			
YES	10/18	12/20			
Embols					
NO	13/18	6/20			
YES	5/18	14/20			
Lymphocytic.infiltration					
NO	14/18	20/20			
YES	4/18	0/20			
RE.H					
Negative	17/18	0/20			
Positive	1/18	20/20			
RP.H					
Negative	18/18	1/20			
Positive	0/18	19/20			

List of supplemental figures

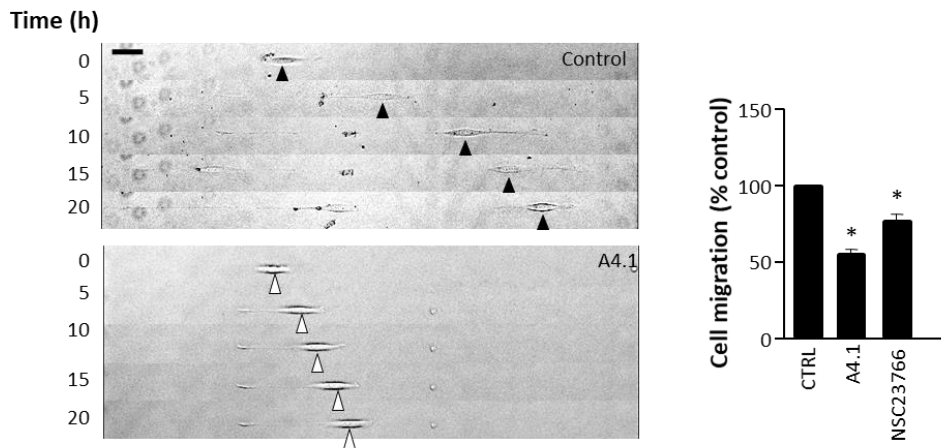
Supp Figure 1



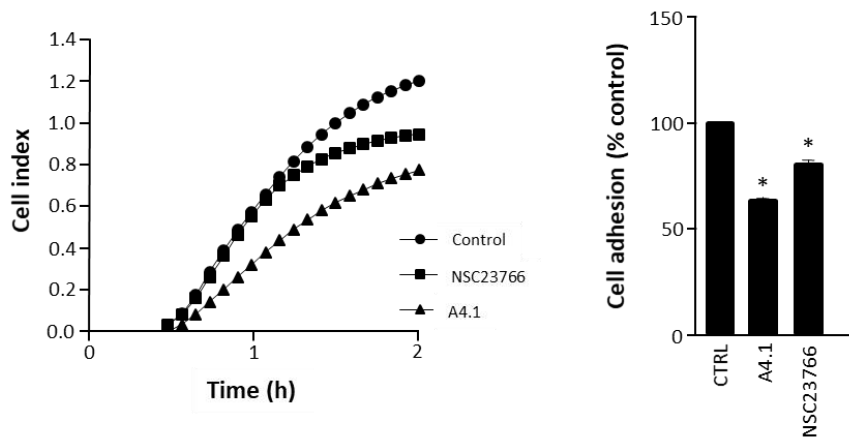
Supp. Figure 1: Example of one pharmacophore model used for virtual screening. The pharmacophore model shown was created based on RAC1 (grey) and NSC23766 (orange) interaction. The pharmacophore model is formed by two hydrogen bond acceptor (HBA) features, one oriented towards the hydroxyl group of Ser71 (S71) and the other towards the amine group of Gln74 (Q74), one hydrogen bond donor (HBD) feature pointed to the oxygen atom of Leu70 (L70) and two hydrophobic features (HY) located on certain carbon atoms of NSC23766 and facing residues Val36 (V36), Ala59 (A59), Tyr64 (Y64) and Leu67 (L67). The spheres correspond to location constraint. The pharmacophore model was completed by thirteen exclusion sphere centered on the main residues of RAC1 defining the binding site (not shown).

Supp. Figure 2

a

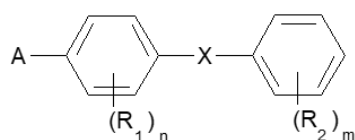


b



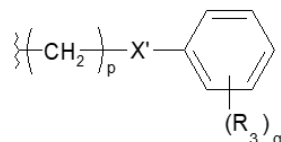
Supp. Figure 2: A4.1 inhibits RAC-dependent cell functions. (a) Representative records with arrows indicating NIH-3T3 cells location at different times. Cells were incubated or not with A4.1 or NSC23766 at 10^{-5} M (Left panel). Quantification of cell speed in each experimental condition (Right panel). Results shown are representative of 3 independent experiments. * $P < 0.05$ vs controls (b) Representative kinetics of fibroblast adhesion pre-treated or not with $10 \mu\text{M}$ A4.1 or NSC23766 (left panel). Quantification of cell adhesion (Right panel). Results shown are representative of 3 independent experiments. * $P < 0.05$ vs control.

Supp. Figure 3



Wherein :

- A is in particular $-N(R'_a)-C(=O)-R$, R'_a being H or a (C_1-C_6) alkyl group, and R being preferably a group having the following formula :



- X is in particular chosen from the group consisting of: $-SO_2-N(R'_b)-$, R'_b being H or a (C_1-C_6) alkyl group, $-N(R''_b)-SO_2-$, R''_b being H or a (C_1-C_6) alkyl group, $-CO-NH-$, and $-NH-CO-$

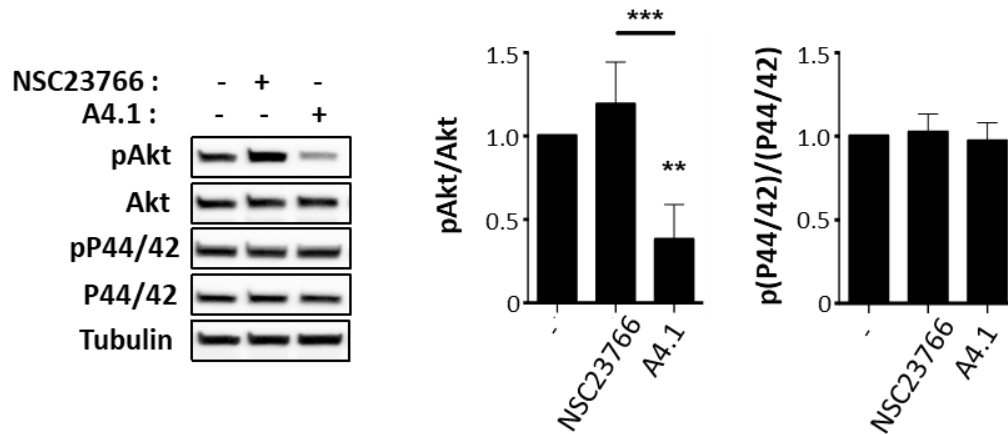
Supp. Figure 3: Rac inhibitor chemical skeleton model.

Supp. Figure 4

	16		30	
	*****		* * * *	
Rac1	MQAIKCVVVG	DGAVGK	TCLLISYT	TNAFPGEYIPTVFDNY 40
Rac2	MQAIKCVVVG	DGAVGK	TCLLISYT	TNAFPGEYIPTVFDNY 40
CdC42	MQTIKCVVVG	DGAVGK	TCLLISYT	TNKFPSEYVPTVFDNY 40
RhoG	MQSIKCVVVG	DGAVGK	TCLLICYT	TNAFPKEYIPTVFDNY 40
RhoA	AIRKKLVI	VG	DGACGK	TCLLIVFSKDQFPEVYVPTVFENY 42
	P-loop		Switch I	

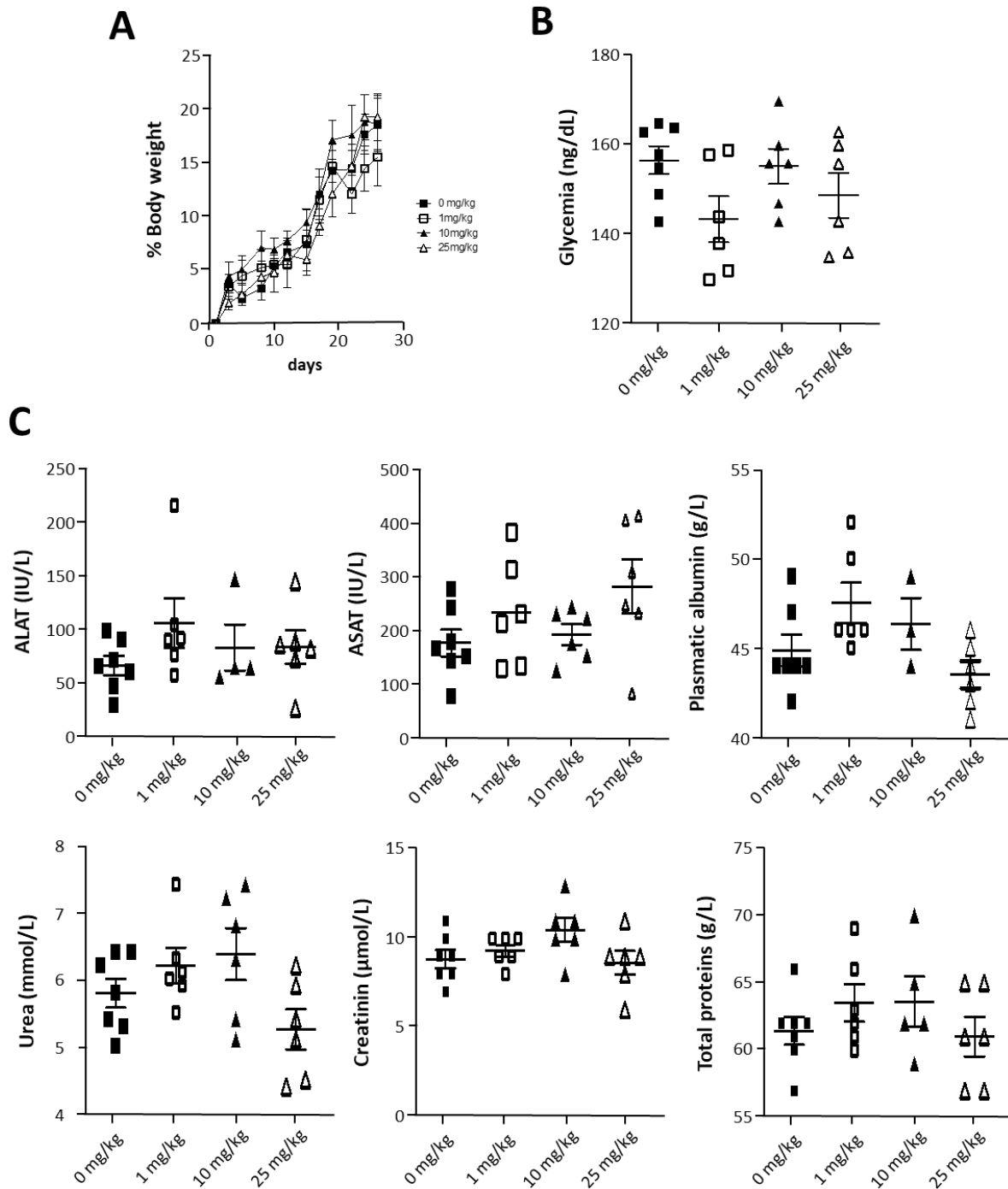
Supp. Figure 4: Sequence alignment of Rho GTPases focus on P-loop and Switch I domain

Supp. Figure 5



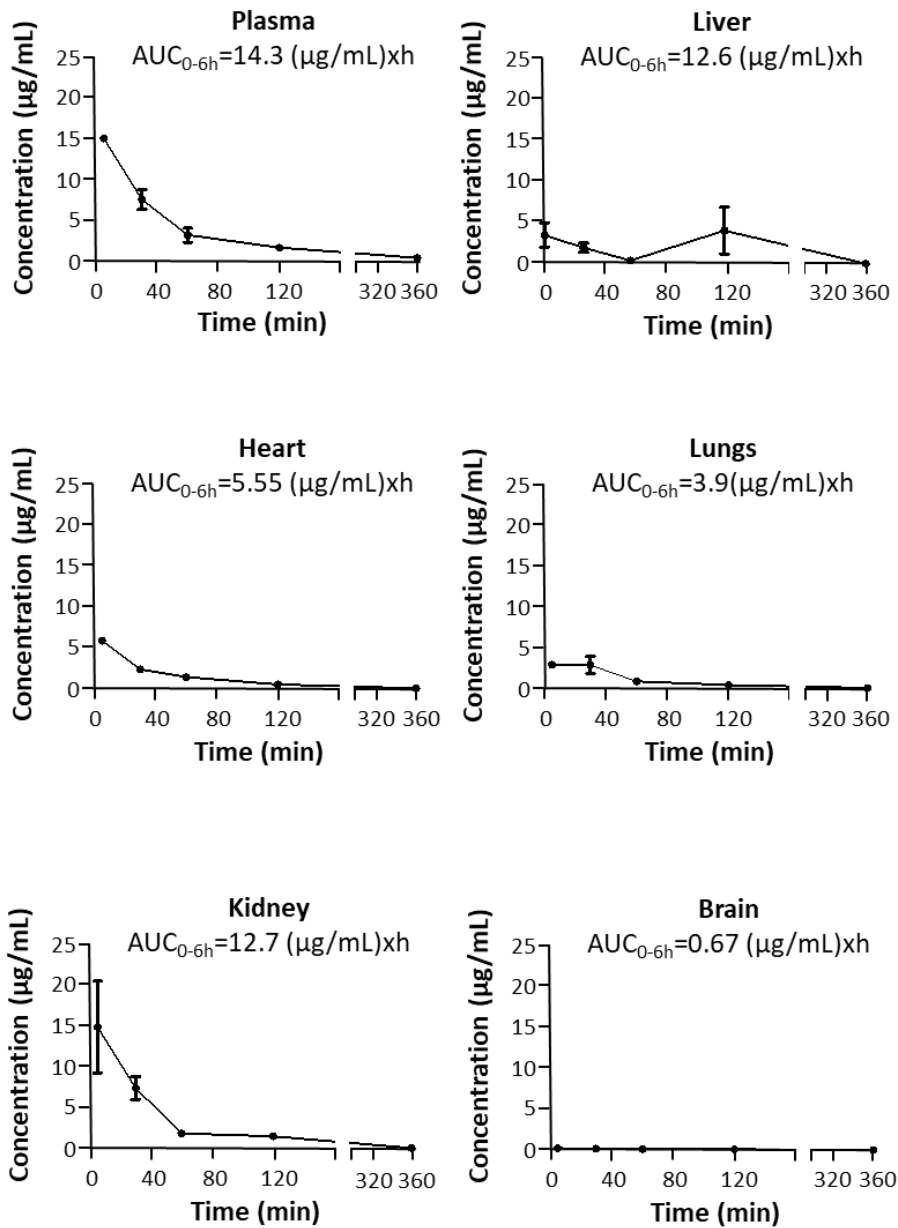
Supp. Figure 5: Effect of A4.1 on Akt-dependent signalling pathway in triple negative breast cancer cells *in vitro*. Immunoblot analysis and corresponding quantification of Akt and P44/42 expression and phosphorylation in MDA-MB-468Luc cells treated with NSC23766 or A4.1 during 1h at 10^{-5} M. Results shown are representative of 3 independent experiments. **P<0.01 vs untreated cells, ***P<0.001 vs NSC23766 treated cells.

Supp. Figure 6



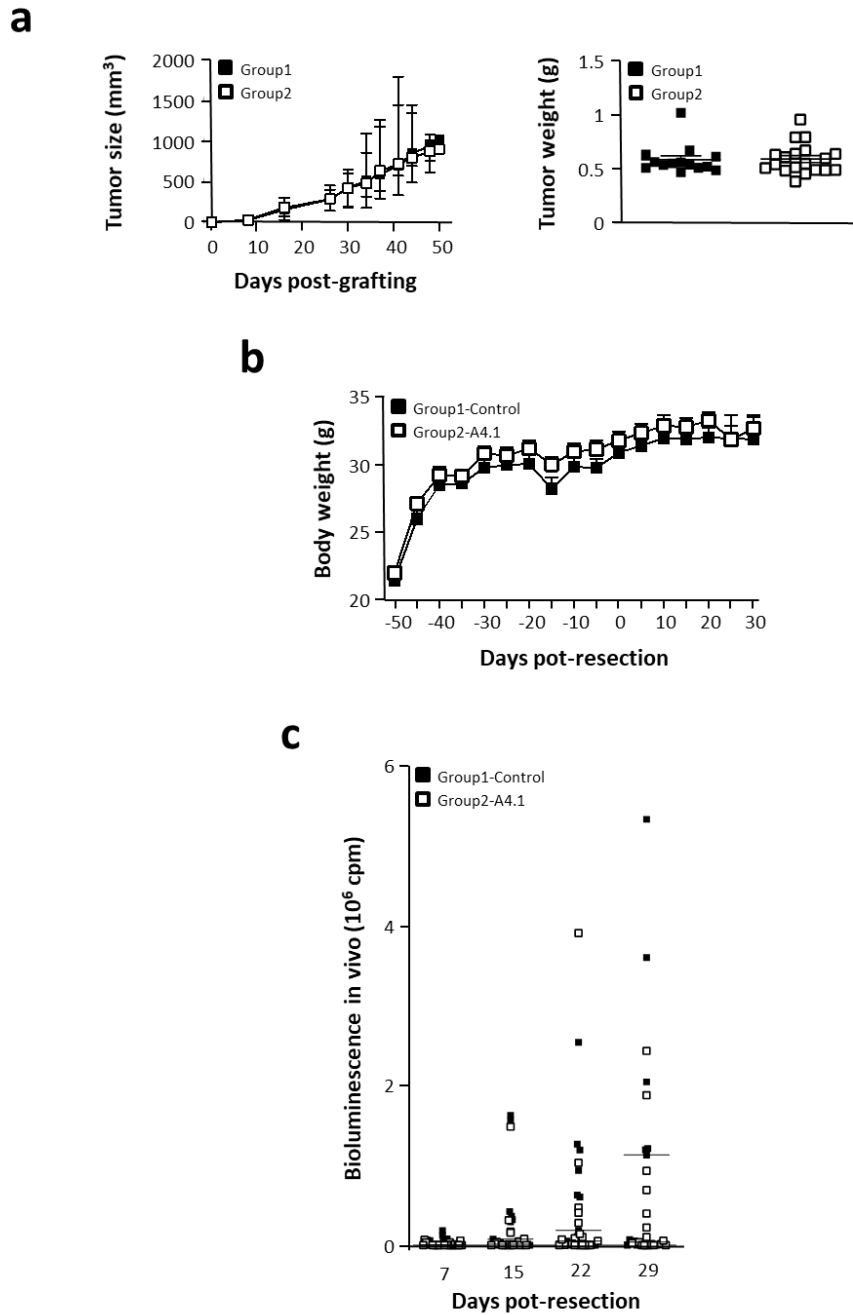
Supp. Figure 6: A4.1 toxicity in vivo. Effect of A4.1 chronic intraperitoneal administration at the indicated concentrations by intraperitoneal injections was analyzed in mice on weight gain (a), glycemia (b) and indicated plasmatic constants (c). n=6-7 mice.

Supp. Figure 7



Supp. Figure 7: A4.1 pharmacokinetics. Molecule distribution in indicated organs after intraperitoneal injection of A4.1 (25 mg/kg). AUC = Area Under the Concentration-time curve. n=3 mice.

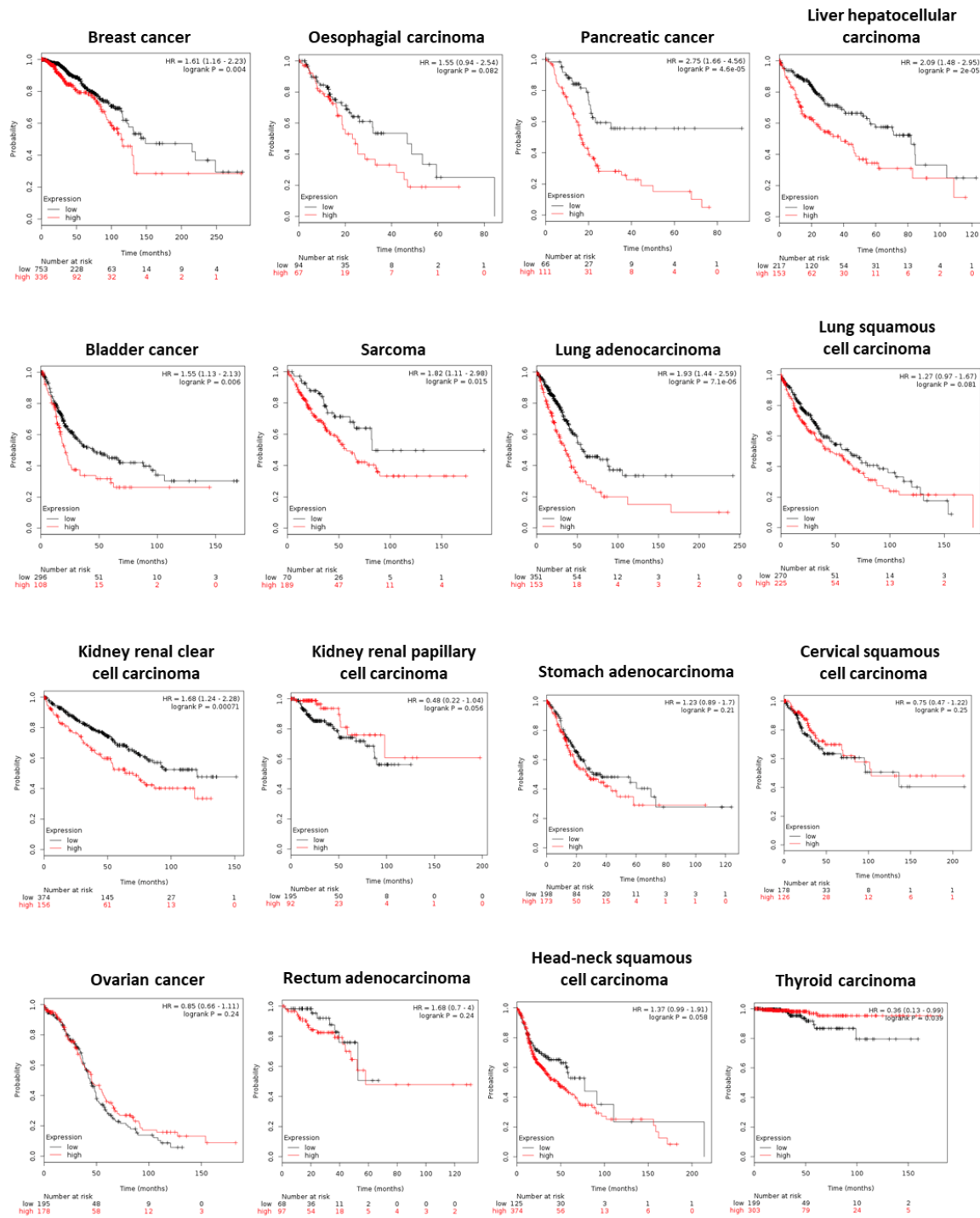
Supp. Figure 8



Supp. Figure 8: Effect of A4.1 on the experimental model of triple negative breast cancer.

(a) Time course of tumor growth in the two experimental groups after transplantation of MDA-MB-468Luc cells. (b) Monitoring of the body weight of mice in the different groups after after primary tumor resection. (c) In vivo quantification of bioluminescence in mice after primary tumor resection.

Supp. Figure 9



Supp. Figure 9: Rac1 activity as poor prognostic factor of aggressive cancer.

Survival analysis of patients with low (black line) or high (red line) Rac mRNA in the indicated cancer types.

DISCUSSION

L'objectif de ma thèse était d'élucider le rôle de la GTPase Rac1 dans les CMLb au cours de l'asthme allergique sévère et de développer et caractériser un nouvel inhibiteur spécifique de cette protéine qui puisse être utilisé en clinique.

Dans la première partie de ma thèse, nous nous sommes intéressés au rôle de Rac1 dans les CMLb dans le contexte de l'asthme allergique sévère. Pour cela, nous avons utilisé un modèle murin d'asthme allergique chronique reposant sur une sensibilisation et des challenges aux acariens. Dans ce modèle, les souris développent une HRB, une inflammation pulmonaire mixte Th2/Th17 persistante ainsi qu'un remodelage des voies respiratoires caractérisé par une hypertrophie de l'épithélium, une inflammation péri-bronchique et une hyperplasie du muscle lisse bronchique. De plus, la sensibilité de ces souris aux corticoïdes est fortement altérée. L'ensemble de ces modifications fonctionnelles et histologiques se rapprochent du tableau clinique observé chez les patients souffrant d'asthme allergique sévère. D'autres modèles murins d'asthme existent, notamment ceux reposant sur l'utilisation de l'ovalbumine comme allergène. Ces modèles se caractérisent par une inflammation de type Th2 avec un infiltrat majoritairement éosinophilique (Daubeuf et Frossard 2013), une HRB et un remodelage des voies aériennes uniquement pour les modèles chroniques (McMillan et Lloyd 2004; Nials et Uddin 2008). Bien que l'ovalbumine induise une inflammation des voies aériennes chez la souris ce n'est pas le cas chez l'Homme contrairement aux acariens (Aun et al. 2017). De plus, il a été mis en évidence que l'utilisation de l'ovalbumine à forte dose ou durant une longue période diminue l'inflammation chez les souris probablement à cause d'un phénomène de tolérance (Hove et al. 2012).

Notre étude a permis de mettre en évidence le rôle clé de Rac1 dans le remodelage des voies aériennes associé à l'asthme sévère. Par immunofluorescence, nous avons observé dans les biopsies bronchiques une augmentation de l'activité de Rac1 localisée principalement dans les CMLb chez les patients souffrants d'asthme sévères en comparaison aux patients contrôles. Cette augmentation de l'activité de Rac1 est associée à une prolifération accrue des CMLb. Nous avons constaté *in vitro* que la stimulation de Rac1 dans les CMLb active la voie de signalisation dépendante de STAT3 permettant la prolifération et l'hyperplasie du muscle lisse bronchique. Ces cellules chez les patients souffrants d'asthme sévère présentent effectivement une hausse de leur capacité proliférative en comparaison aux patients souffrants d'asthme modéré, léger ou non asthmatiques (Johnson et al. 2001). Il existe de nombreux facteurs

mitogènes induisant la prolifération des CMLb et nombre d'entre eux, dont le facteur de croissance dérivé des plaquettes BB (PDGF-BB) et le facteur de croissance basique des fibroblastes (bFGF), sont décrits pour être exprimés et sécrétés de façon plus importante chez les patients asthmatiques (ZOU et al. 2014). Nous avons observé une hausse de la prolifération des CMLb en réponse à ces deux facteurs de croissance. Cette prolifération cellulaire est dépendante de l'activité de Rac1 et de l'activation la voie de signalisation de STAT3.

Le niveau d'activité de Rac1 est donc un élément clé dans la prolifération des CMLb et l'hyperplasie du muscle lisse bronchique. La suractivation de Rac1 peut être due à une augmentation de l'activité de l'un de ses GEFs. Dans le contexte de l'asthme, il a récemment été observé une augmentation de l'expression de P-Rex1 dans les CMLb. Ce GEF est décrit pour participer à la prolifération de ces cellules et donc à l'hyperplasie du muscle lisse bronchique (Huang et al. 2019). Le niveau d'activité de P-Rex1 pourrait être évalué dans les biopsies bronchiques ainsi que dans les CMLb provenant de patients souffrant d'asthme sévère. Cette hypothèse pourrait également être étudiée *in vivo* dans notre modèle murin d'asthme allergique sévère grâce à l'utilisation d'un inhibiteur du complexe Rac/P-rex1 comme l'1A-116.

Mes résultats démontrent que la protéine Rac1 joue un rôle essentiel dans les CMLb et que l'augmentation de son activation participe au développement de l'HRB et au remodelage des voies aériennes. Rac1 apparait donc aujourd'hui comme une cible thérapeutique d'intérêt dont l'inhibition permettrait d'induire une bronchodilatation tout en limitant l'augmentation de la masse des cellules musculaires lisses. Afin de valider cette hypothèse, nous avons traité des souris asthmatiques sévères avec un inhibiteur de Rac1, le NSC23766, par nébulisation. Nous avons établi que l'inhibition pharmacologique de Rac1 réduit le remodelage des voies aériennes, notamment l'hyperplasie du muscle lisse bronchique, l'HRB ainsi que l'infiltration éosinophilique. De ce fait l'inhibition de Rac1 permet de moduler les trois composantes principales de l'asthme sévère et est aujourd'hui la seule stratégie thérapeutique capable de d'affecter ces trois composantes.

Rac1 est une protéine ubiquitaire, c'est pourquoi l'utilisation d'un inhibiteur pourrait induire de nombreux effets secondaires. Cependant, l'administration d'un inhibiteur par voie inhalée permet de limiter l'exposition pharmacologique à la sphère pulmonaire et ainsi restreindre les potentiels effets systémiques. Dans notre modèle, nous n'avons pas observé d'effets secondaires induits par la nébulisation du NSC23766 bien que cet inhibiteur soit décrit pour pouvoir affecter l'agrégation plaquettaire (Dütting et al. 2015). L'absence d'effets secondaires du NSC23766 dans notre étude peut s'expliquer également par la dose administrée

(40 µg/kg). De plus, le NSC23766 est un inhibiteur ayant une faible efficacité ($IC_{50} \sim 50 \mu M$) (Gao et al. 2004) ce qui peut induire une inhibition partielle de Rac1 localisée au niveau de la sphère pulmonaire et limiter l'apparition d'effets secondaires. Bien que l'inhibition de Rac1 puisse être partielle, elle est cependant suffisante pour observer des effets thérapeutiques bénéfiques. Dans notre étude, nous avons administré le NSC23766 avant chaque challenge ce qui permet de prévenir le développement de la pathologie. Il serait maintenant pertinent d'évaluer le potentiel curatif de l'inhibition de Rac1 dans le développement de l'asthme sévère. Toutefois, la persistance du phénotype asthmatique chez la souris pourrait être une des limites à cette étude. Effectivement, il a été démontré dans certains modèles que suite à l'arrêt des challenges il y a regression ou disparition des symptômes caractéristiques de la pathologie tels que l'HRB, le remodelage des voies aériennes et l'inflammation au cours du temps (McMillan et Lloyd 2004; Lloyd 2007; Nials et Uddin 2008). Il sera donc nécessaire d'évaluer la réversibilité de notre modèle expérimental pour étudier les effets curatifs de la nébulisation d'un inhibiteur de Rac1.

Dans la seconde partie de ma thèse, nous avons identifié et caractérisé un nouvel inhibiteur spécifique de la GTPase Rac1. Comme décrit dans l'introduction de nombreuses stratégies thérapeutiques visant à réguler l'activité de Rac1 ont été développées mais aucune n'est aujourd'hui utilisable en clinique à cause notamment d'un défaut de spécificité et/ou d'efficacité.

Grâce à une approche de criblage virtuel et de docking nous avons identifié la structure d'un pharmacophore. Nous avons basé ce screening sur la structure cristallographique de Rac1 lié à un de ses inhibiteurs le NSC23766 et non sur la structure cristallographique de Rac1 seule ou liée au nucléotide comme cela a été fait dans d'autres études (V- Stratégies thérapeutiques régulant l'activité de la GTPase Rac1). Le docking de la molécule identifiée sur Rac1 a permis de prédire que cette molécule se fixe préférentiellement au niveau de la poche nucléotidique de Rac1 selon deux poses possibles. La première montrant des interactions possibles avec les acides aminés Leu67, Ser71, Trp56, Lys5 et Ala3 mettant en jeu majoritairement des interactions de type hydrophobes et deux liaisons hydrogènes avec la Ser71. La seconde pose quant à elle permet des interactions avec la Lys116, Gly15, Cys18, Lys16 et Ile33 grâce majoritairement à des liaisons hydrogènes et quelques interactions de type hydrophobes. L'énergie libre de liaison obtenue pour ces deux poses est en faveur de la seconde puisqu'elle met en jeu un plus grand nombre de liaisons hydrogènes entraînant des interactions plus fortes entre la molécule et la protéine.

A partir de la structure de cette première molécule identifiée, l'A4, une première librairie chimique a été synthétisée afin de pouvoir évaluer l'effet de ces molécules sur des fonctions dépendantes de Rac1. La molécule A4.1 présente une énergie libre de liaison plus faible que l'A4 ce qui devrait favoriser sa fixation sur Rac1. Ce nouvel inhibiteur de Rac, A4.1, présente un mécanisme d'action unique car il agit comme un compétiteur réversible du nucléotide en se liant à la poche nucléotidique et en limitant l'incorporation du GTP. Cependant l'affinité de notre molécule pour Rac1 étant plus faible que celle du GTP, nous observons une inhibition partielle de la GTPase. Une inhibition partielle de Rac1 est préférable au vu de son rôle dans des fonctions cellulaires essentielles et son expression ubiquitaire.

La validation du site de fixation d'un ligand sur une protéine est une étape indispensable suite à sa prédiction par le docking. La stratégie couramment employée est la cristallisation du complexe ligand-protéine. Nous avons tenté d'obtenir la structure cristallographique de Rac1 complexée à l'A4.1 sans succès. C'est pourquoi nous avons utilisé une stratégie de photomarquage par affinité afin d'identifier le ou les acides aminés impliqués dans la liaison entre Rac1 et l'A4.1. Nous avons mis en évidence que l'acide aminé impliqué dans cette liaison est la Lys16. Cet acide aminé est présent dans la poche nucléotidique de Rac1 au niveau de la boucle G1 et a été prédit pour établir une liaison hydrogène avec notre inhibiteur par docking. Cependant la Lys16 est un acide aminé conservé entre les GTPases Rac1, Cdc42 et RhoA, ainsi la fixation de l'A4.1 sur cet acide aminé ne permet pas d'expliquer la spécificité de la molécule pour Rac. En effet notre étude montre que l'A4.1 inhibe spécifiquement Rac1, son isoforme Rac1b et également sa forme mutée Rac1^{P29S} mais n'a pas d'effet sur RhoA et Cdc42 contrairement aux autres inhibiteurs de Rac1 (Tableau I). En réalisant des mutagenèses dirigées des autres acides aminés identifiés comme pouvant interagir avec Rac1 (Lys116, Gly15, Cys18 et Ile33), nous pourrions identifier l'ensemble des acides aminés impliqués dans l'interaction entre Rac1 et l'A4.1 et expliquer la spécificité d'action de cet inhibiteur. L'obtention de ces résultats pourrait permettre la création d'une nouvelle série chimique dérivée de l'A4.1 ayant des propriétés physico-chimiques optimisées.

Différents tests de toxicité ont permis d'établir l'innocuité de notre molécule et une étude pharmacocinétique par injection intrapéritonéale (25 mg/kg) a permis d'étudier ses différents paramètres pharmacocinétiques. Les petites molécules inhibant Rac1 présentent des demi-vie relativement courtes 1.65h pour l'EHT1864 (Hampsch et al. 2017), 2.17h pour le MBQ-167 (Maldonado et al. 2019), environ 5h pour EHop-16 (Humphries-Bickley et al. 2015) et 1.6h pour notre inhibiteur. L'ensemble des paramètres pharmacocinétiques de l'A4.1 que nous avons pu déterminer sont compatibles avec une utilisation de la molécule *in vivo*. Il serait

intéressant maintenant d'identifier les métabolites de l'A4.1. Cela permettrait d'étudier la biotransformation de la molécule et de savoir si elle subit un métabolisme de phase I avec des réactions de fonctionnalisation ou de phase II avec des réactions de conjugaison ; ou les deux.

Il a été observé dans différents types de cancer, une hausse de l'expression et/ou de l'activation de Rac1 qui est corrélée au stade de la maladie (Ji et al. 2015; Tian et al. 2018; Liang et al. 2021). De plus, les multiples rôles de Rac1 aux différents stades de la tumorigenèse comme décrit précédemment (III.2- Rac1 en oncologie) en font une cible thérapeutique d'intérêt en oncologie. Notre analyse de l'activité de Rac1 dans des biopsies de tumeurs primaires de patientes souffrant de cancer du sein montre pour la première fois que l'activité de Rac1 pourrait être un facteur prédictif d'une rechute métastatique. Cet élément montre qu'évaluer le niveau d'activité de Rac1 dans la tumeur primaire d'un patient pourrait permettre de modifier sa prise en charge thérapeutique ainsi que son suivi clinique.

Au vu du rôle de Rac1 en oncologie, nous avons étudié l'effet de l'A4.1 *in vitro* et *in vivo* dans ce contexte pathologique. *In vitro*, nous avons évalué l'effet de l'A4.1 sur la capacité des cellules cancéreuses à former des clones. Ces études de clonogénicité ont établi que l'A4.1 est capable de diminuer l'activité de Rac1 dans différentes lignées de cellules cancéreuses et réduit leur capacité à former des clones de façon dose-dépendante quelque soit l'origine de ces cellules cancéreuses ou leurs mutations. Le cancer du sein triple négatif étant hautement métastatique nous avons centré notre étude sur ce type de cancer. L'A4.1 réduit la migration et l'invasion des cellules MDA-MB-468. D'autres inhibiteurs de Rac1 sont décrits pour réduire la migration des cellules cancéreuses sans que leur effet sur l'invasion n'ait été évalué, c'est notamment le cas pour le MBQ-167 (Humphries-Bickley et al. 2017), le GYS32661 (Goka et al. 2019; 2020; Goka, Mesa Lopez, et Lippman 2021) et EHOp-016 (Montalvo-Ortiz et al. 2012). Ces éléments suggèrent un effet potentiel de l'A4.1 sur la formation de métastases.

Nous avons donc évalué l'effet de l'A4.1 *in vivo* dans un modèle murin immunodéficient de xéno greffe de cancer du sein triple négatif induit par injection orthotopique de cellules MDA-MB-468 Luc. Ces cellules expriment la luciférine ce qui permet par imagerie bioluminescente de pouvoir les localiser. Nous avons notamment utilisé cette capacité de bioluminescence afin d'analyser la repousse tumorale et la présence de métastases chez les souris. Le traitement chronique à l'A4.1 a réduit la repousse tumorale et limité l'apparition des métastases. Ces résultats sont concordants avec ceux obtenus dans une étude utilisant le GYS32661 dans un modèle murin de xéno greffe de cancer du côlon (Goka et al. 2019). La diminution de la repousse tumorale et de la formation de métastases par l'A4.1 suggèrent un effet de notre inhibiteur sur le cycle cellulaire. Une étude de la prolifération et du cycle cellulaire

des cellules cancéreuses en réponse à l'A4.1 a mis en évidence que cet inhibiteur n'a pas d'effet direct sur le cycle cellulaire. Il est tout de même possible que l'A4.1 module la prolifération de ces cellules de façon indirecte notamment via le microenvironnement tumoral et les cellules immunitaires qui le composent.

Afin de prendre en compte ce facteur dans notre étude, nous avons utilisé un modèle murin d'allogreffe de cancer du sein par injection orthotopique de cellules 4T1 Luc. L'inhibition de l'activité de Rac1 par l'A4.1 après résection de la tumeur primaire a limité la repousse tumorale ainsi que la fréquence d'apparition des métastases tout en améliorant la survie des souris. Concernant l'effet de l'utilisation de l'A4.1 sur le système immunitaire nous n'avons pas observé de modification de la formulation leucocytaire bien que Rac1 soit active dans les lymphocytes infiltrants la tumeur.

L'utilisation de l'A4.1 dans ces deux modèles murins de cancer du sein n'a pas entraîné de perte de poids chez les animaux, de modifications comportementales et aucun effet secondaire n'a été observé. Ainsi l'inhibition de Rac1 par l'A4.1 permet de réduire la repousse tumorale, limiter l'apparition des métastases et améliorer la survie sans effet délétère sur le système immunitaire ou autres effets secondaires. Nous avons étudié l'effet de l'A4.1 sur la repousse tumorale et la formation de métastases suite à une résection tumorale. Il serait pertinent d'étudier également son effet sur la pousse de la tumeur primaire à partir d'une taille détectable afin de déterminer si l'utilisation d'un inhibiteur de Rac1 lors de la détection précoce de la tumeur aurait un effet bénéfique sur le développement de la pathologie et ainsi limiter sa progression. Il serait également intéressant d'élucider le rôle de Rac1 dans les lymphocytes infiltrants la tumeur afin de savoir si ces cellules ont un impact sur la prolifération des cellules cancéreuses et donc la pousse tumorale.

L'ensemble de mes travaux de thèse mettent en évidence le rôle clé de Rac1 dans plusieurs contextes pathologiques ainsi que l'intérêt thérapeutique de limiter l'activité de cette GTPase. En effet mes résultats montrent que la protéine Rac1 dans les CMLb régulent leur contraction ainsi que leur prolifération via l'activation de voie de signalisation dépendante de STAT3. Ainsi dans le contexte de l'asthme sévère, la suractivation de Rac1 participe à l'HRB et à l'hyperplasie du muscle lisses caractéristique du remodelage des voies aériennes. La nébulisation d'un inhibiteur de Rac1 permet de limiter le développement de cette pathologie en influant sur l'HRB, le remodelage des voies aériennes mais également l'inflammation. Ce qui met en lumière l'intérêt thérapeutique de développer de nouveaux inhibiteurs de Rac1 pouvant être utilisés en clinique.

Mes travaux de thèse ont également permis l'identification *in silico* et la caractérisation *ex vivo*, *in vitro* et *in vivo* d'un nouvel inhibiteur spécifique de Rac, l'A4.1, ayant un mécanisme d'action innovant. Dans le contexte oncologique, l'A4.1 est aujourd'hui la première molécule à potentiel anti-métastatique et ayant une spécificité pour Rac ainsi qu'une efficacité permettant d'envisager son utilisation en clinique.

BIBLIOGRAPHIE

- Aghazadeh, Behzad, William E Lowry, Xin-Yun Huang, et Michael K Rosen. 2000. « Structural Basis for Relief of Autoinhibition of the Dbl Homology Domain of Proto-Oncogene Vav by Tyrosine Phosphorylation ». *Cell* 102 (5): 625-33. [https://doi.org/10.1016/S0092-8674\(00\)00085-4](https://doi.org/10.1016/S0092-8674(00)00085-4).
- Aktories, Klaus, Alexander E. Lang, Carsten Schwan, et Hans G. Mannherz. 2011. « Actin as Target for Modification by Bacterial Protein Toxins ». *The FEBS Journal* 278 (23): 4526-43. <https://doi.org/10.1111/j.1742-4658.2011.08113.x>.
- Amberg, Gregory C., et Manuel F. Navedo. 2013. « Calcium dynamics in vascular smooth muscle ». *Microcirculation (New York, N.Y. : 1994)* 20 (4): 281-89. <https://doi.org/10.1111/micc.12046>.
- André, Gwennan, Juan E. Sandoval, Kevin Retailleau, Laurent Loufrani, Gilles Toumaniantz, Stefan Offermanns, Malvyne Rolli-Derkinderen, Gervaise Loirand, et Vincent Sauzeau. 2014. « Smooth Muscle Specific Rac1 Deficiency Induces Hypertension by Preventing P116^{RIP3}-Dependent RhoA Inhibition ». *Journal of the American Heart Association* 3 (3): e000852. <https://doi.org/10.1161/JAHA.114.000852>.
- André-Grégoire, Gwennan, Florian Dilasser, Julie Chesné, Faouzi Braza, Antoine Magnan, Gervaise Loirand, et Vincent Sauzeau. 2017. « Targeting of Rac1 Prevents Bronchoconstriction and Airway Hyperresponsiveness ». *Journal of Allergy and Clinical Immunology* 0 (0). <https://doi.org/10.1016/j.jaci.2017.09.049>.
- . 2018. « Targeting of Rac1 prevents bronchoconstriction and airway hyperresponsiveness ». *Journal of Allergy and Clinical Immunology* 142 (3): 824-833.e3. <https://doi.org/10.1016/j.jaci.2017.09.049>.
- Arias-Romero, Luis E., Olga Villamar-Cruz, Min Huang, Klaus P. Hoeflich, et Jonathan Chernoff. 2013. « Pak1 kinase links ErbB2 to β -catenin in transformation of breast epithelial cells ». *Cancer research* 73 (12): 3671-82. <https://doi.org/10.1158/0008-5472.CAN-12-4453>.
- Arnst, Jamie L., Ashley L. Hein, Margaret A. Taylor, Nick Y. Palermo, Jacob I. Contreras, Yogesh A. Sonawane, Andrew O. Wahl, Michel M. Ouellette, Amarnath Natarajan, et Ying Yan. 2017. « Discovery and characterization of small molecule Rac1 inhibitors ». *Oncotarget* 8 (21): 34586-600. <https://doi.org/10.18632/oncotarget.16656>.
- Aun, Marcelo Vivolo, Rafael Bonamichi-Santos, Fernanda Magalhães Arantes-Costa, Jorge Kalil, et Pedro Giavina-Bianchi. 2017. « Animal models of asthma: utility and limitations ». *Journal of Asthma and Allergy* 10 (novembre): 293-301. <https://doi.org/10.2147/JAA.S121092>.
- Azoitei, Mihai L., Jungsik Noh, Daniel J. Marston, Philippe Roudot, Christopher B. Marshall, Timothy A. Daugird, Sidney L. Lisanza, et al. 2019. « Spatiotemporal Dynamics of GEF-H1 Activation Controlled by Microtubule- and Src-Mediated Pathways ». *Journal of Cell Biology* 218 (9): 3077-97. <https://doi.org/10.1083/jcb.201812073>.
- Bedard, Karen, et Karl-Heinz Krause. 2007. « The NOX Family of ROS-Generating NADPH Oxidases: Physiology and Pathophysiology ». *Physiological Reviews* 87 (1): 245-313. <https://doi.org/10.1152/physrev.00044.2005>.
- Birchmeier, W., et J Behrens. 1994. « Cadherin Expression in Carcinomas: Role in the Formation of Cell Junctions and the Prevention of Invasiveness ». *Biochimica et Biophysica Acta (BBA) - Reviews on Cancer* 1198 (1): 11-26. [https://doi.org/10.1016/0304-419X\(94\)90003-5](https://doi.org/10.1016/0304-419X(94)90003-5).
- Bond, Mark, Yih-Jer Wu, Graciela B. Sala-Newby, et Andrew C. Newby. 2008. « Rho GTPase, Rac1, regulates Skp2 levels, vascular smooth muscle cell proliferation, and intima

- formation in vitro and in vivo ». *Cardiovascular Research* 80 (2): 290-98. <https://doi.org/10.1093/cvr/cvn188>.
- Bos, Johannes L., Holger Rehmann, et Alfred Wittinghofer. 2007. « GEFs and GAPs: Critical Elements in the Control of Small G Proteins ». *Cell* 129 (5): 865-77. <https://doi.org/10.1016/j.cell.2007.05.018>.
- Cabrera, Maia, Emiliana Echeverria, Federico Remes Lenicov, Georgina Cardama, Nazareno Gonzalez, Carlos Davio, Natalia Fernández, et Pablo Lorenzано Menna. 2017. « Pharmacological Rac1 inhibitors with selective apoptotic activity in human acute leukemic cell lines ». *Oncotarget* 8 (58): 98509-23. <https://doi.org/10.18632/oncotarget.21533>.
- Cardama, Georgina A, Maria J Comin, Leandro Hornos, Nazareno Gonzalez, Lucas Defelipe, Adrian G Turjanski, Daniel F Alonso, Daniel E Gomez, et Pablo Lorenzано Menna. 2014. « Preclinical Development of Novel Rac1-GEF Signaling Inhibitors using a Rational Design Approach in Highly Aggressive Breast Cancer Cell Lines ». *Anti-Cancer Agents in Medicinal Chemistry* 14 (6): 840-51. <https://doi.org/10.2174/18715206113136660334>.
- Cardama, Georgina A, Nazareno Gonzalez, Matias Ciarlantini, Lucia Gandolfi Donadío, María Julieta Comin, Daniel F Alonso, Pablo Lorenzано Menna, et Daniel E Gomez. 2014. « Proapoptotic and antiinvasive activity of Rac1 small molecule inhibitors on malignant glioma cells ». *Oncotargets and therapy* 7 (octobre): 2021-33. <https://doi.org/10.2147/OTT.S67998>.
- Carr, Tara F., Amir A. Zeki, et Monica Kraft. 2018. « Eosinophilic and Noneosinophilic Asthma ». *American Journal of Respiratory and Critical Care Medicine* 197 (1): 22-37. <https://doi.org/10.1164/rccm.201611-2232PP>.
- Castillo-Pichardo, Linette, Tessa Humphries-Bickley, Columba De La Parra, Ingrid Forestier-Roman, Magaly Martinez-Ferrer, Eliud Hernandez, Cornelis Vlaar, et al. 2014. « The Rac Inhibitor EHop-016 Inhibits Mammary Tumor Growth and Metastasis in a Nude Mouse Model ». *Translational Oncology* 7 (5): 546-55. <https://doi.org/10.1016/j.tranon.2014.07.004>.
- Castoria, Gabriella, Loredana D'Amato, Alessandra Ciociola, Pia Giovannelli, Tiziana Giraldi, Leandra Sepe, Giovanni Paoletta, Maria Vittoria Barone, Antimo Migliaccio, et Ferdinando Auricchio. 2011. « Androgen-Induced Cell Migration: Role of Androgen Receptor/Filamin A Association ». *PLoS ONE* 6 (2): e17218. <https://doi.org/10.1371/journal.pone.0017218>.
- Chen, Liang, Shuning Bi, Jiuzhou Hou, Zhijun Zhao, Chaojie Wang, et Songqiang Xie. 2019. « Targeting p21-activated kinase 1 inhibits growth and metastasis via Raf1/MEK1/ERK signaling in esophageal squamous cell carcinoma cells ». *Cell Communication and Signaling* 17 (1): 31. <https://doi.org/10.1186/s12964-019-0343-5>.
- Chen, Qing-Yong, Li-Qun Xu, De-Min Jiao, Qing-Hua Yao, Yan-Yi Wang, Hui-Zhen Hu, Yu-Quan Wu, Jia Song, Jie Yan, et Li-Jun Wu. 2011. « Silencing of Rac1 modifies lung cancer cell migration, invasion and actin cytoskeleton rearrangements and enhances chemosensitivity to antitumor drugs ». *International Journal of Molecular Medicine* 28 (5): 769-76. <https://doi.org/10.3892/ijmm.2011.775>.
- Chen, Zhe, Liang Guo, Jana Hadas, Stephen Gutowski, Stephen R. Sprang, et Paul C. Sternweis. 2012. « Activation of P115-RhoGEF Requires Direct Association of Gα13 and the Dbl Homology Domain* ». *Journal of Biological Chemistry* 287 (30): 25490-500. <https://doi.org/10.1074/jbc.M111.333716>.
- Cherfils, Jacqueline, et Mahel Zeghouf. 2013. « Regulation of Small GTPases by GEFs, GAPs, and GDIs ». *Physiological Reviews* 93 (1): 269-309. <https://doi.org/10.1152/physrev.00003.2012>.

- Chung, Kian Fan, Sally E. Wenzel, Jan L. Brozek, Andrew Bush, Mario Castro, Peter J. Sterk, Ian M. Adcock, et al. 2014. « International ERS/ATS Guidelines on Definition, Evaluation and Treatment of Severe Asthma ». *European Respiratory Journal* 43 (2): 343-73. <https://doi.org/10.1183/09031936.00202013>.
- Cooper, Geoffrey M. 2000. « Structure and Organization of Actin Filaments ». *The Cell: A Molecular Approach. 2nd Edition*. <http://www.ncbi.nlm.nih.gov/books/NBK9908/>.
- Courjal, Frank, Paul Chuchana, Charles Theillet, et Philippe Fort. 1997. « Structure and Chromosomal Assignment to 22q12 and 17qter of the Ras-Related Rac2 and Rac3 Human Genes ». *Genomics* 44 (2): 242-46. <https://doi.org/10.1006/geno.1997.4871>.
- Crompton, Anne M., Louise H. Foley, Alexander Wood, William Roscoe, David Stokoe, Frank McCormick, Marc Symons, et Gideon Bollag. 2000. « Regulation of Tiam1 Nucleotide Exchange Activity by Pleckstrin Domain Binding Ligands * ». *Journal of Biological Chemistry* 275 (33): 25751-59. <https://doi.org/10.1074/jbc.M002050200>.
- Cruz-Collazo, Ailed, Jean F. Ruiz-Calderon, Hector Picon, Luis D. Borrero-Garcia, Irmaris Lopez, Linette Castillo-Pichardo, Maria del Mar Maldonado, et al. 2021. « Efficacy of Rac and Cdc42 Inhibitor MBQ-167 in Triple-negative Breast Cancer ». *Molecular Cancer Therapeutics* 20 (12): 2420-32. <https://doi.org/10.1158/1535-7163.MCT-21-0348>.
- D'Amato, Gennaro, Carolina Vitale, Antonio Molino, Anna Stanziola, Alessandro Sanduzzi, Alessandro Vatrella, Mauro Mormile, et al. 2016. « Asthma-related deaths ». *Multidisciplinary Respiratory Medicine* 11 (octobre): 37. <https://doi.org/10.1186/s40248-016-0073-0>.
- Daubeuf, François, et Nelly Frossard. 2013. « Acute Asthma Models to Ovalbumin in the Mouse ». *Current Protocols in Mouse Biology* 3 (1): 31-37. <https://doi.org/10.1002/9780470942390.mo120202>.
- Davis, Matthew J., Byung Hak Ha, Edna C. Holman, Ruth Halaban, Joseph Schlessinger, et Titus J. Boggon. 2013. « RAC1P29S is a spontaneously activating cancer-associated GTPase ». *Proceedings of the National Academy of Sciences* 110 (3): 912-17. <https://doi.org/10.1073/pnas.1220895110>.
- Derksen, Patrick W. B., Xiaoling Liu, Francis Saridin, Hanneke van der Gulden, John Zevenhoven, Bastiaan Evers, Judy R. van Beijnum, et al. 2006. « Somatic Inactivation of E-Cadherin and P53 in Mice Leads to Metastatic Lobular Mammary Carcinoma through Induction of Anoikis Resistance and Angiogenesis ». *Cancer Cell* 10 (5): 437-49. <https://doi.org/10.1016/j.ccr.2006.09.013>.
- DerMardirossian, Céline, et Gary M. Bokoch. 2005. « GDIs: Central Regulatory Molecules in Rho GTPase Activation ». *Trends in Cell Biology* 15 (7): 356-63. <https://doi.org/10.1016/j.tcb.2005.05.001>.
- Dovas, Athanassios, et John R. Couchman. 2005. « RhoGDI: multiple functions in the regulation of Rho family GTPase activities ». *Biochemical Journal* 390 (1): 1-9. <https://doi.org/10.1042/BJ20050104>.
- Dütting, S., J. Heidenreich, D. Cherpokova, E. Amin, S.-C. Zhang, M. R. Ahmadian, C. Brakebusch, et B. Nieswandt. 2015. « Critical Off-Target Effects of the Widely Used Rac1 Inhibitors NSC23766 and EHT1864 in Mouse Platelets ». *Journal of Thrombosis and Haemostasis* 13 (5): 827-38. <https://doi.org/10.1111/jth.12861>.
- Eitel, Julia, Karolin Meixenberger, Claudia van Laak, Christine Orlovski, Andreas Hocke, Bernd Schmeck, Stefan Hippenstiel, Philippe Dje N'Guessan, Norbert Suttrop, et Bastian Opitz. 2012. « Rac1 Regulates the NLRP3 Inflammasome Which Mediates IL-1beta Production in Chlamydomyces pneumoniae Infected Human Mononuclear Cells ». *PLoS ONE* 7 (1): e30379. <https://doi.org/10.1371/journal.pone.0030379>.

- Etienne-Manneville, Sandrine, et Alan Hall. 2002. « Rho GTPases in Cell Biology ». *Nature* 420 (6916): 629-35. <https://doi.org/10.1038/nature01148>.
- Fabbiano, Salvatore, Mauricio Menacho-Márquez, María A. Sevilla, Julián Albarrán-Juárez, Yi Zheng, Stefan Offermanns, María J. Montero, et Xosé R. Bustelo. 2014. « Genetic Dissection of the Vav2-Rac1 Signaling Axis in Vascular Smooth Muscle Cells ». *Molecular and Cellular Biology* 34 (24): 4404-19. <https://doi.org/10.1128/MCB.01066-14>.
- Fehrenbach, Heinz, Christina Wagner, et Michael Wegmann. 2017. « Airway Remodeling in Asthma: What Really Matters ». *Cell and Tissue Research* 367 (3): 551-69. <https://doi.org/10.1007/s00441-016-2566-8>.
- Feng, Jianhua, Masaaki Ito, Kazuhito Ichikawa, Naoki Isaka, Masakatsu Nishikawa, David J. Hartshorne, et Takeshi Nakano. 1999. « Inhibitory Phosphorylation Site for Rho-Associated Kinase on Smooth Muscle Myosin Phosphatase* ». *Journal of Biological Chemistry* 274 (52): 37385-90. <https://doi.org/10.1074/jbc.274.52.37385>.
- Fleming, Ian N., Ian H. Batty, Alan R. Prescott, Alex Gray, Gursant S. Kular, Hazel Stewart, et C. Peter Downes. 2004. « Inositol phospholipids regulate the guanine-nucleotide-exchange factor Tiam1 by facilitating its binding to the plasma membrane and regulating GDP/GTP exchange on Rac1 ». *Biochemical Journal* 382 (Pt 3): 857-65. <https://doi.org/10.1042/BJ20040916>.
- Fort, Philippe, et Anne Blangy. 2017. « The Evolutionary Landscape of Dbl-Like RhoGEF Families: Adapting Eukaryotic Cells to Environmental Signals ». *Genome Biology and Evolution* 9 (6): 1471-86. <https://doi.org/10.1093/gbe/evx100>.
- Frank, Scott R., et Steen H. Hansen. 2008. « The PIX-GIT complex: a G protein signaling cassette in control of cell shape ». *Seminars in cell & developmental biology* 19 (3): 234-44. <https://doi.org/10.1016/j.semcdb.2008.01.002>.
- Friedland, Julie C., Johnathon N. Lakins, Marcelo G. Kazanietz, Jonathan Chernoff, David Boettiger, et Valerie M. Weaver. 2007. « $\alpha\beta 4$ integrin activates Rac-dependent p21-activated kinase 1 to drive NF- κ B-dependent resistance to apoptosis in 3D mammary acini ». *Journal of Cell Science* 120 (20): 3700-3712. <https://doi.org/10.1242/jcs.03484>.
- Fu, Yixin, et Jorge E. Galán. 1999. « A Salmonella Protein Antagonizes Rac-1 and Cdc42 to Mediate Host-Cell Recovery after Bacterial Invasion ». *Nature* 401 (6750): 293-97. <https://doi.org/10.1038/45829>.
- Gao, Yuan, J. Bradley Dickerson, Fukun Guo, Jie Zheng, et Yi Zheng. 2004. « Rational design and characterization of a Rac GTPase-specific small molecule inhibitor ». *Proceedings of the National Academy of Sciences* 101 (20): 7618-23. <https://doi.org/10.1073/pnas.0307512101>.
- Garcia-Mata, Rafael, Etienne Boulter, et Keith Burridge. 2011. « The invisible hand: regulation of RHO GTPases by RHOGDIs ». *Nature Reviews. Molecular Cell Biology* 12 (8): 493-504. <https://doi.org/10.1038/nrm3153>.
- Gerthoffer, William T. 2007. « Mechanisms of Vascular Smooth Muscle Cell Migration ». *Circulation Research* 100 (5): 607-21. <https://doi.org/10.1161/01.RES.0000258492.96097.47>.
- Goehring, Udo-Michael, Gudula Schmidt, Kristin J. Pederson, Klaus Aktories, et Joseph T. Barbieri. 1999. « The N-Terminal Domain of Pseudomonas Aeruginosa Exoenzyme S Is a GTPase-Activating Protein for Rho GTPases* ». *Journal of Biological Chemistry* 274 (51): 36369-72. <https://doi.org/10.1074/jbc.274.51.36369>.
- Goka, Erik T., Pallavi Chaturvedi, Dayrelis T. Mesa Lopez, Adriana De La Garza, et Marc E. Lippman. 2019. « RAC1b Overexpression Confers Resistance to Chemotherapy Treatment in Colorectal Cancer ». *Molecular Cancer Therapeutics* 18 (5): 957-68. <https://doi.org/10.1158/1535-7163.MCT-18-0955>.

- Goka, Erik T., Pallavi Chaturvedi, Dayrelis T. Mesa Lopez, et Marc E. Lippman. 2020. « Rac Signaling Drives Clear Cell Renal Carcinoma Tumor Growth by Priming the Tumor Microenvironment for an Angiogenic Switch ». *Molecular Cancer Therapeutics* 19 (7): 1462-73. <https://doi.org/10.1158/1535-7163.MCT-19-0762>.
- Goka, Erik T., Dayrelis T. Mesa Lopez, et Marc E. Lippman. 2021. « Hormone-Dependent Prostate Cancers are Dependent on Rac Signaling for Growth and Survival ». *Molecular Cancer Therapeutics* 20 (6): 1052-61. <https://doi.org/10.1158/1535-7163.MCT-20-0695>.
- Gorin, Yves, Jill M. Ricono, Brent Wagner, Nam-Ho Kim, Basant Bhandari, Goutam Ghosh Choudhury, et Hanna E. Abboud. 2004. « Angiotensin II-induced ERK1/ERK2 activation and protein synthesis are redox-dependent in glomerular mesangial cells ». *Biochemical Journal* 381 (Pt 1): 231-39. <https://doi.org/10.1042/BJ20031614>.
- Guo, Yuna, Shelby Ray Kenney, Carolyn Y. Muller, Sarah Adams, Teresa Rutledge, Elsa Romero, Cristina Murray-Krezan, et al. 2015. « R-ketorolac Targets Cdc42 and Rac1 and Alters Ovarian Cancer Cell Behaviors Critical for Invasion and Metastasis ». *Molecular cancer therapeutics* 14 (10): 2215-27. <https://doi.org/10.1158/1535-7163.MCT-15-0419>.
- Haga, Raquel B., et Anne J. Ridley. 2016. « Rho GTPases: Regulation and roles in cancer cell biology ». *Small GTPases* 7 (4): 207-21. <https://doi.org/10.1080/21541248.2016.1232583>.
- Hage, Beatrix, Katrin Meinel, Iris Baum, Klaudia Giehl, et Andre Menke. 2009. « Rac1 activation inhibits E-cadherin-mediated adherens junctions via binding to IQGAP1 in pancreatic carcinoma cells ». *Cell Communication and Signaling* 7 (1): 23. <https://doi.org/10.1186/1478-811X-7-23>.
- Hakoshima, T. 2003. « Structural Basis of the Rho GTPase Signaling ». *Journal of Biochemistry* 134 (3): 327-31. <https://doi.org/10.1093/jb/mvg149>.
- Hall, Alan. 2012. « Rho family GTPases ». *Biochemical Society Transactions* 40 (6): 1378-82. <https://doi.org/10.1042/BST20120103>.
- Hampsch, Riley A., Kevin Shee, Darcy Bates, Lionel D. Lewis, Laurent Désiré, Bertrand Leblond, Eugene Demidenko, Kurtis Stefan, Yina H. Huang, et Todd W. Miller. 2017. « Therapeutic sensitivity to Rac GTPase inhibition requires consequential suppression of mTORC1, AKT, and MEK signaling in breast cancer ». *Oncotarget* 8 (13): 21806-17. <https://doi.org/10.18632/oncotarget.15586>.
- Hill-Eubanks, David C., Matthias E. Werner, Thomas J. Heppner, et Mark T. Nelson. 2011. « Calcium Signaling in Smooth Muscle ». *Cold Spring Harbor Perspectives in Biology* 3 (9): a004549. <https://doi.org/10.1101/cshperspect.a004549>.
- Hodge, Richard G., et Anne J. Ridley. 2016. « Regulating Rho GTPases and Their Regulators ». *Nature Reviews Molecular Cell Biology* 17 (8): 496-510. <https://doi.org/10.1038/nrm.2016.67>.
- Hoffman, Gregory R, et Richard A Cerione. 2002. « Signaling to the Rho GTPases: Networking with the DH Domain ». *FEBS Letters, Protein Domains*, 513 (1): 85-91. [https://doi.org/10.1016/S0014-5793\(01\)03310-5](https://doi.org/10.1016/S0014-5793(01)03310-5).
- Hove, Chris L. Van, Tania Maes, Guy F. Joos, et Kurt G. Tournoy. 2012. « Prolonged Inhaled Allergen Exposure Can Induce Persistent Tolerance ». *American Journal of Respiratory Cell and Molecular Biology*, décembre. <https://doi.org/10.1165/rcmb.2006-0385OC>.
- Huang, Yapei, Yan Xie, Haihong Jiang, Peter W. Abel, Reynold A. Panettieri, Thomas B. Casale, et Yaping Tu. 2019. « Upregulated P-Rex1 exacerbates human airway smooth muscle hyperplasia in asthma ». *Journal of Allergy and Clinical Immunology* 143 (2): 778-781.e5. <https://doi.org/10.1016/j.jaci.2018.09.020>.

- Humphries-Bickley, Tessa, Linette Castillo-Pichardo, Francheska Corujo-Carro, Jorge Duconge, Eliud Hernandez-O’Farrill, Cornelis Vlaar, Jose F. Rodriguez-Orengo, Luis Cubano, et Suranganie Dharmawardhane. 2015. « Pharmacokinetics of Rac Inhibitor EHOp-016 in Mice by Ultra-Performance Liquid Chromatography Tandem Mass Spectrometry ». *Journal of chromatography. B, Analytical technologies in the biomedical and life sciences* 0 (février): 19-26. <https://doi.org/10.1016/j.jchromb.2014.12.021>.
- Humphries-Bickley, Tessa, Linette Castillo-Pichardo, Eliud Hernandez-O’Farrill, Luis D. Borrero-Garcia, Ingrid Forestier-Roman, Yamil Gerena, Manuel Blanco, et al. 2017. « Characterization of a Dual Rac/Cdc42 Inhibitor MBQ-167 in Metastatic Cancer ». *Molecular cancer therapeutics* 16 (5): 805-18. <https://doi.org/10.1158/1535-7163.MCT-16-0442>.
- Itzen, Aymelt, et Roger S. Goody. 2011. « GTPases Involved in Vesicular Trafficking: Structures and Mechanisms ». *Seminars in Cell & Developmental Biology*, GTPases in Intracellular Trafficking, 22 (1): 48-56. <https://doi.org/10.1016/j.semcdb.2010.10.003>.
- Jaffe, Aron B., et Alan Hall. 2005. « RHO GTPASES: Biochemistry and Biology ». *Annual Review of Cell and Developmental Biology* 21 (1): 247-69. <https://doi.org/10.1146/annurev.cellbio.21.020604.150721>.
- Ji, Jun, Xiaojing Feng, Min Shi, Qu Cai, Yingyan Yu, Zhenggang Zhu, et Jun Zhang. 2015. « Rac1 is correlated with aggressiveness and a potential therapeutic target for gastric cancer ». *International Journal of Oncology* 46 (3): 1343-53. <https://doi.org/10.3892/ijo.2015.2836>.
- Johnson, Peter R. A., Michael Roth, Michael Tamm, Margaret Hughes, Qi Ge, Greg King, Janette K. Burgess, et Judith L. Black. 2001. « Airway Smooth Muscle Cell Proliferation Is Increased in Asthma ». *American Journal of Respiratory and Critical Care Medicine* 164 (3): 474-77. <https://doi.org/10.1164/ajrccm.164.3.2010109>.
- Jordan, Peter, Raquel Brazão, Maria Guida Boavida, Christian Gespach, et Eric Chastre. 1999. « Cloning of a Novel Human Rac1b Splice Variant with Increased Expression in Colorectal Tumors ». *Oncogene* 18 (48): 6835-39. <https://doi.org/10.1038/sj.onc.1203233>.
- Joyce, David, Boumediene Bouzahzah, Maofu Fu, Chris Albanese, Mark D’Amico, Jay Steer, Joshua U. Klein, et al. 1999. « Integration of Rac-Dependent Regulation of Cyclin D1 Transcription through a Nuclear Factor-KB-Dependent Pathway* ». *Journal of Biological Chemistry* 274 (36): 25245-49. <https://doi.org/10.1074/jbc.274.36.25245>.
- Kao, Yu-Ya, Davide Gianni, Benjamin Bohl, Ross M. Taylor, et Gary M. Bokoch. 2008. « Identification of a Conserved Rac-binding Site on NADPH Oxidases Supports a Direct GTPase Regulatory Mechanism ». *The Journal of Biological Chemistry* 283 (19): 12736-46. <https://doi.org/10.1074/jbc.M801010200>.
- Kawazu, Masahito, Toshihide Ueno, Kenji Kontani, Yoshitaka Ogita, Mizuo Ando, Kazutaka Fukumura, Azusa Yamato, et al. 2013. « Transforming mutations of RAC guanosine triphosphatases in human cancers ». *Proceedings of the National Academy of Sciences of the United States of America* 110 (8): 3029-34. <https://doi.org/10.1073/pnas.1216141110>.
- Kazanietz, Marcelo G., et Maria J. Caloca. 2017. « THE RAC GTPase IN CANCER: FROM OLD CONCEPTS TO NEW PARADIGMS ». *Cancer research* 77 (20): 5445-51. <https://doi.org/10.1158/0008-5472.CAN-17-1456>.
- Klein, Eric A., Chengfeng Yang, Marcelo G. Kazanietz, et Richard K. Assoian. 2007. « NFκB-Independent Signaling to the Cyclin D1 Gene by Rac ». *Cell Cycle* 6 (9): 1115-21. <https://doi.org/10.4161/cc.6.9.4147>.

- Koyama, Mutsumi, Masaaki Ito, Jianhua Feng, Tetsuya Seko, Katsuya Shiraki, Koujiro Takase, David J. Hartshorne, et Takeshi Nakano. 2000. « Phosphorylation of CPI-17, an Inhibitory Phosphoprotein of Smooth Muscle Myosin Phosphatase, by Rho-Kinase ». *FEBS Letters* 475 (3): 197-200. [https://doi.org/10.1016/S0014-5793\(00\)01654-9](https://doi.org/10.1016/S0014-5793(00)01654-9).
- Lam, B. Daniel, et Peter L. Hordijk. 2013. « The Rac1 hypervariable region in targeting and signaling ». *Small GTPases* 4 (2): 78-89. <https://doi.org/10.4161/sgtp.23310>.
- Laurin, Mélanie, et Jean-François Côté. 2014. « Insights into the biological functions of Dock family guanine nucleotide exchange factors ». *Genes & Development* 28 (6): 533-47. <https://doi.org/10.1101/gad.236349.113>.
- Lawson, Campbell D., et Anne J. Ridley. 2018. « Rho GTPase Signaling Complexes in Cell Migration and Invasion ». *The Journal of Cell Biology* 217 (2): 447-57. <https://doi.org/10.1083/jcb.201612069>.
- Laxmanan, Balaji, et D Kyle Hogarth. 2015. « Bronchial thermoplasty in asthma: current perspectives ». *Journal of Asthma and Allergy* 8 (mai): 39-49. <https://doi.org/10.2147/JAA.S49306>.
- Lerm, Maria, Gudula Schmidt, et Klaus Aktories. 2000. « Bacterial protein toxins targeting Rho GTPases ». *FEMS Microbiology Letters* 188 (1): 1-6. <https://doi.org/10.1111/j.1574-6968.2000.tb09159.x>.
- Li, Chaohong, Yanhua Hu, Gertraud Sturm, Georg Wick, et Qingbo Xu. 2000. « Ras/Rac-Dependent Activation of p38 Mitogen-Activated Protein Kinases in Smooth Muscle Cells Stimulated by Cyclic Strain Stress ». *Arteriosclerosis, Thrombosis, and Vascular Biology* 20 (3): e1-9. <https://doi.org/10.1161/01.ATV.20.3.e1>.
- Li, Qingjian, Tao Qin, Zhuofei Bi, Huangming Hong, Lin Ding, Jiewen Chen, Wei Wu, et al. 2020. « Rac1 Activates Non-Oxidative Pentose Phosphate Pathway to Induce Chemoresistance of Breast Cancer ». *Nature Communications* 11 (1): 1-18. <https://doi.org/10.1038/s41467-020-15308-7>.
- Liang, Jiabin, Linda Oyang, Shan Rao, Yaqian Han, Xia Luo, Pin Yi, Jinguan Lin, et al. 2021. « Rac1, A Potential Target for Tumor Therapy ». *Frontiers in Oncology* 11. <https://www.frontiersin.org/article/10.3389/fonc.2021.674426>.
- Ligeti, Erzsébet, Stefan Welti, et Klaus Scheffzek. 2012. « Inhibition and Termination of Physiological Responses by GTPase Activating Proteins ». *Physiological Reviews* 92 (1): 237-72. <https://doi.org/10.1152/physrev.00045.2010>.
- Liu, Linna, Hongmei Zhang, Lei Shi, Wenjuan Zhang, Juanli Yuan, Xiang Chen, Juanjuan Liu, Yan Zhang, et Zhipeng Wang. 2014. « Inhibition of Rac1 activity induces G1/S phase arrest through the GSK3/cyclin D1 pathway in human cancer cells ». *Oncology Reports* 32 (4): 1395-1400. <https://doi.org/10.3892/or.2014.3388>.
- Liu, Zheng, Sicai Zhang, Peng Chen, Songhai Tian, Ji Zeng, Kay Perry, Min Dong, et Rongsheng Jin. 2021. « Structural basis for selective modification of Rho and Ras GTPases by Clostridioides difficile toxin B ». *Science Advances* 7 (43): eabi4582. <https://doi.org/10.1126/sciadv.abi4582>.
- Lloyd, Clare M. 2007. « Building Better Mouse Models of Asthma ». *Current allergy and asthma reports* 7 (3): 231-36.
- Loirand, Gervaise, Vincent Sauzeau, et Pierre Pacaud. 2013. « Small G Proteins in the Cardiovascular System: Physiological and Pathological Aspects ». *Physiological Reviews* 93 (4): 1659-1720. <https://doi.org/10.1152/physrev.00021.2012>.
- López-Lago, Miguel, Hyunmi Lee, Cristina Cruz, Nieves Movilla, et Xosé R. Bustelo. 2000. « Tyrosine Phosphorylation Mediates Both Activation and Downmodulation of the Biological Activity of Vav ». *Molecular and Cellular Biology* 20 (5): 1678-91. <https://doi.org/10.1128/MCB.20.5.1678-1691.2000>.

- Lou, Shu, Penglai Wang, Jianrong Yang, Junqing Ma, Chao Liu, et Meng Zhou. 2018. « Prognostic and Clinicopathological Value of Rac1 in Cancer Survival: Evidence from a Meta-Analysis ». *Journal of Cancer* 9 (14): 2571-79. <https://doi.org/10.7150/jca.24824>.
- Lu, Jie, Lai Chan, Hannah D. G. Fiji, Russell Dahl, Ohyun Kwon, et Fuyuhiko Tamanoi. 2009. « In vivo antitumor effect of a novel inhibitor of protein geranylgeranyltransferase I ». *Molecular cancer therapeutics* 8 (5): 1218-26. <https://doi.org/10.1158/1535-7163.MCT-08-1122>.
- Ma, Le, Rajat Rohatgi, et Marc W. Kirschner. 1998. « The Arp2/3 complex mediates actin polymerization induced by the small GTP-binding protein Cdc42 ». *Proceedings of the National Academy of Sciences of the United States of America* 95 (26): 15362-67.
- Ma, Xuefei, Zhaoqin Cheng, Hong Kong, Ying Wang, Helmut Unruh, Newman L. Stephens, et Michel Laviolette. 2002. « Changes in Biophysical and Biochemical Properties of Single Bronchial Smooth Muscle Cells from Asthmatic Subjects ». *American Journal of Physiology. Lung Cellular and Molecular Physiology* 283 (6): L1181-1189. <https://doi.org/10.1152/ajplung.00389.2001>.
- Maldonado, María del Mar, Gabriela Rosado-González, Joseph Bloom, Jorge Duconge, Jean F. Ruiz-Calderón, Eliud Hernández-O’Farrill, Cornelis Vlaar, José F. Rodríguez-Orengo, et Suranganie Dharmawardhane. 2019. « Pharmacokinetics of the Rac/Cdc42 Inhibitor MBQ-167 in Mice by Supercritical Fluid Chromatography–Tandem Mass Spectrometry ». *ACS Omega* 4 (19): 17981-89. <https://doi.org/10.1021/acsomega.9b01641>.
- Marei, Hadir, et Angeliki Malliri. 2017. « Rac1 in Human Diseases: The Therapeutic Potential of Targeting Rac1 Signaling Regulatory Mechanisms ». *Small GTPases* 8 (3): 139-63. <https://doi.org/10.1080/21541248.2016.1211398>.
- Matos, Paulo, Jennifer Skaug, Bárbara Marques, Sebastian Beck, Fátima Veríssimo, Christian Gespach, Maria Guida Boavida, Stephen W. Scherer, et Peter Jordan. 2000. « Small GTPase Rac1: Structure, Localization, and Expression of the Human Gene ». *Biochemical and Biophysical Research Communications* 277 (3): 741-51. <https://doi.org/10.1006/bbrc.2000.3743>.
- Matsumoto, Hisako, Lyn M Moir, Brian G G Oliver, Janette K Burgess, Michael Roth, Judith L Black, et Brent E McParland. 2007. « Comparison of gel contraction mediated by airway smooth muscle cells from patients with and without asthma ». *Thorax* 62 (10): 848-54. <https://doi.org/10.1136/thx.2006.070474>.
- McMillan, S. J., et C. M. Lloyd. 2004. « Prolonged allergen challenge in mice leads to persistent airway remodelling ». *Clinical and experimental allergy : journal of the British Society for Allergy and Clinical Immunology* 34 (3): 497-507.
- Melzer, Catharina, Ralf Hass, Hendrik Lehnert, et Hendrik Ungefroren. 2019. « RAC1B: A Rho GTPase with Versatile Functions in Malignant Transformation and Tumor Progression ». *Cells* 8 (1): 21. <https://doi.org/10.3390/cells8010021>.
- Mettouchi, Amel, Sharon Klein, Wenjun Guo, Miguel Lopez-Lago, Emmanuel Lemichez, John K. Westwick, et Filippo G. Giancotti. 2001. « Integrin-Specific Activation of Rac Controls Progression through the G1 Phase of the Cell Cycle ». *Molecular Cell* 8 (1): 115-27. [https://doi.org/10.1016/S1097-2765\(01\)00285-4](https://doi.org/10.1016/S1097-2765(01)00285-4).
- Mierke, Claudia Tanja, Stefanie Puder, Christian Aermes, Tony Fischer, et Tom Kunschmann. 2020. « Effect of PAK Inhibition on Cell Mechanics Depends on Rac1 ». *Frontiers in Cell and Developmental Biology* 8. <https://www.frontiersin.org/articles/10.3389/fcell.2020.00013>.

- Miki, Hiroaki, Hideki Yamaguchi, Shiro Suetsugu, et Tadaomi Takenawa. 2000. « IRSp53 Is an Essential Intermediate between Rac and WAVE in the Regulation of Membrane Ruffling ». *Nature* 408 (6813): 732-35. <https://doi.org/10.1038/35047107>.
- Millard, Thomas H, Stewart J Sharp, et Laura M Machesky. 2004. « Signalling to actin assembly via the WASP (Wiskott-Aldrich syndrome protein)-family proteins and the Arp2/3 complex. » *Biochemical Journal* 380 (Pt 1): 1-17. <https://doi.org/10.1042/BJ20040176>.
- Molnár, Judit, Csilla Fazakas, János Haskó, Orsolya Sipos, Krisztina Nagy, Ádám Nyúl-Tóth, Attila E. Farkas, et al. 2015. « Transmigration characteristics of breast cancer and melanoma cells through the brain endothelium: Role of Rac and PI3K ». *Cell Adhesion & Migration* 10 (3): 269-81. <https://doi.org/10.1080/19336918.2015.1122156>.
- Montalvo-Ortiz, Brenda L., Linette Castillo-Pichardo, Eliud Hernández, Tessa Humphries-Bickley, Alina De La Mota-Peynado, Luis A. Cubano, Cornelis P. Vlaar, et Suranganie Dharmawardhane. 2012. « Characterization of EHop-016, Novel Small Molecule Inhibitor of Rac GTPase ». *The Journal of Biological Chemistry* 287 (16): 13228-38. <https://doi.org/10.1074/jbc.M111.334524>.
- Morishita, Yuji, Koji Tsutsumi, et Yasutaka Ohta. 2015. « Phosphorylation of Serine 402 Regulates RacGAP Protein Activity of FilGAP Protein* ». *Journal of Biological Chemistry* 290 (43): 26328-38. <https://doi.org/10.1074/jbc.M115.666875>.
- Mosaddeghzadeh, Niloufar, et Mohammad Reza Ahmadian. 2021. « The RHO Family GTPases: Mechanisms of Regulation and Signaling ». *Cells* 10 (7): 1831. <https://doi.org/10.3390/cells10071831>.
- Mubarak, Bushra, Huma Shakoor, et Fozia Masood. 2019. *Eosinophilic Asthma. Asthma - Biological Evidences*. IntechOpen. <https://doi.org/10.5772/intechopen.84297>.
- Nials, Anthony T., et Sorif Uddin. 2008. « Mouse models of allergic asthma: acute and chronic allergen challenge ». *Disease Models & Mechanisms* 1 (4-5): 213-20. <https://doi.org/10.1242/dmm.000323>.
- Onesto, Cercina, Adam Shutes, Virginie Picard, Fabien Schweighoffer, et Channing J. Der. 2008. « Characterization of EHT 1864, a Novel Small Molecule Inhibitor of Rac Family Small GTPases ». In *Methods in Enzymology*, 439:111-29. Small GTPases in Disease, Part B. Academic Press. [https://doi.org/10.1016/S0076-6879\(07\)00409-0](https://doi.org/10.1016/S0076-6879(07)00409-0).
- Oprea, Tudor I., Larry A. Sklar, Jacob O. Agola, Yuna Guo, Melina Silberberg, Joshua Roxby, Anna Vestling, et al. 2015. « Novel Activities of Select NSAID R-Enantiomers against Rac1 and Cdc42 GTPases ». *PLoS ONE* 10 (11): e0142182. <https://doi.org/10.1371/journal.pone.0142182>.
- Pagiatakis, Christina, Joseph W. Gordon, Saviz Ehyai, et John C. McDermott. 2012. « A Novel RhoA/ROCK-CPI-17-MEF2C Signaling Pathway Regulates Vascular Smooth Muscle Cell Gene Expression ». *The Journal of Biological Chemistry* 287 (11): 8361-70. <https://doi.org/10.1074/jbc.M111.286203>.
- Panday, Arvind, Malaya K Sahoo, Diana Osorio, et Sanjay Batra. 2015. « NADPH oxidases: an overview from structure to innate immunity-associated pathologies ». *Cellular and Molecular Immunology* 12 (1): 5-23. <https://doi.org/10.1038/cmi.2014.89>.
- Papi, Alberto, Christopher Brightling, Søren E. Pedersen, et Helen K. Reddel. 2018. « Asthma ». *The Lancet* 391 (10122): 783-800. [https://doi.org/10.1016/S0140-6736\(17\)33311-1](https://doi.org/10.1016/S0140-6736(17)33311-1).
- Peretti, Amanda S., Dayna Dominguez, Martha M. Grimes, Helen J. Hathaway, Eric R. Prossnitz, Melanie R. Rivera, Angela Wandinger-Ness, Donna F. Kusewitt, et Laurie G. Hudson. 2018. « The R-Enantiomer of Ketorolac Delays Mammary Tumor Development in Mouse Mammary Tumor Virus-Polyoma Middle T Antigen (MMTV-

- PyMT) Mice ». *The American Journal of Pathology* 188 (2): 515-24. <https://doi.org/10.1016/j.ajpath.2017.10.018>.
- Radu, Maria, Galina Semenova, Rachele Kosoff, et Jonathan Chernoff. 2014. « PAK Signalling during the Development and Progression of Cancer ». *Nature Reviews Cancer* 14 (1): 13-25. <https://doi.org/10.1038/nrc3645>.
- Rathinam, Rajamani, Allison Berrier, et Suresh K. Alahari. 2011. « Role of Rho GTPases and their regulators in cancer progression ». *Frontiers in Bioscience-Landmark* 16 (7): 2561-71. <https://doi.org/10.2741/3872>.
- Ravi, Laxmi Iyer, Timothy J. Tan, Boon Huan Tan, et Richard J. Sugrue. 2021. « Virus-Induced Activation of the Rac1 Protein at the Site of Respiratory Syncytial Virus Assembly Is a Requirement for Virus Particle Assembly on Infected Cells ». *Virology* 557 (mai): 86-99. <https://doi.org/10.1016/j.virol.2021.02.008>.
- Reddel, Helen K., Eric D. Bateman, Allan Becker, Louis-Philippe Boulet, Alvaro A. Cruz, Jeffrey M. Drazen, Tari Haahtela, et al. 2015. « A summary of the new GINA strategy: a roadmap to asthma control ». *The European Respiratory Journal* 46 (3): 622-39. <https://doi.org/10.1183/13993003.00853-2015>.
- Ridley, Anne J. 2001. « Cyclin' Round the Cell with Rac ». *Developmental Cell* 1 (2): 160-61. [https://doi.org/10.1016/S1534-5807\(01\)00029-6](https://doi.org/10.1016/S1534-5807(01)00029-6).
- . 2006. « Rho GTPases and Actin Dynamics in Membrane Protrusions and Vesicle Trafficking ». *Trends in Cell Biology, Membrane Dynamics*, 16 (10): 522-29. <https://doi.org/10.1016/j.tcb.2006.08.006>.
- Rossman, Kent L., Channing J. Der, et John Sondek. 2005. « GEF Means Go: Turning on RHO GTPases with Guanine Nucleotide-Exchange Factors ». *Nature Reviews Molecular Cell Biology* 6 (2): 167-80. <https://doi.org/10.1038/nrm1587>.
- Sauzeau, Vincent, María A. Sevilla, María J. Montero, et Xosé R. Bustelo. 2010. « The Rho/Rac exchange factor Vav2 controls nitric oxide-dependent responses in mouse vascular smooth muscle cells ». *The Journal of Clinical Investigation* 120 (1): 315-30. <https://doi.org/10.1172/JCI38356>.
- Sawada, Naoki, Yuxin Li, et James K. Liao. 2010. « Novel aspects of the roles of Rac1 GTPase in the cardiovascular system ». *Current opinion in pharmacology* 10 (2): 116-21. <https://doi.org/10.1016/j.coph.2009.11.004>.
- Schaefer, Antje, Nathalie R Reinhard, et Peter L Hordijk. 2014. « Toward understanding RhoGTPase specificity: structure, function and local activation ». *Small GTPases* 5 (2): e968004. <https://doi.org/10.4161/21541248.2014.968004>.
- Schnelzer, A., D. Prechtel, U. Knaus, K. Dehne, M. Gerhard, H. Graeff, N. Harbeck, M. Schmitt, et E. Lengyel. 2000. « Rac1 in Human Breast Cancer: Overexpression, Mutation Analysis, and Characterization of a New Isoform, Rac1b ». *Oncogene* 19 (26): 3013-20. <https://doi.org/10.1038/sj.onc.1203621>.
- Schürmann, A., A. F. Mooney, L. C. Sanders, M. A. Sells, H. G. Wang, J. C. Reed, et G. M. Bokoch. 2000. « p21-Activated Kinase 1 Phosphorylates the Death Agonist Bad and Protects Cells from Apoptosis ». *Molecular and Cellular Biology* 20 (2): 453-61.
- Shifren, Adrian, Chad Witt, Chandrika Christie, et Mario Castro. 2012. « Mechanisms of Remodeling in Asthmatic Airways ». *Journal of Allergy*. <https://doi.org/10.1155/2012/316049>.
- Shutes, Adam, Cercina Onesto, Virginie Picard, Bertrand Leblond, Fabien Schweighoffer, et Channing J. Der. 2007. « Specificity and Mechanism of Action of EHT 1864, a Novel Small Molecule Inhibitor of Rac Family Small GTPases* ». *Journal of Biological Chemistry* 282 (49): 35666-78. <https://doi.org/10.1074/jbc.M703571200>.
- Snyder, Jason T., David K. Worthylake, Kent L. Rossman, Laurie Betts, Wendy M. Pruitt, David P. Siderovski, Channing J. Der, et John Sondek. 2002. « Structural Basis for the

- Selective Activation of Rho GTPases by Dbl Exchange Factors ». *Nature Structural Biology* 9 (6): 468-75. <https://doi.org/10.1038/nsb796>.
- Sprang, Stephen R. 1997. « G PROTEIN MECHANISMS: Insights from Structural Analysis ». *Annual Review of Biochemistry* 66 (1): 639-78. <https://doi.org/10.1146/annurev.biochem.66.1.639>.
- Stallings-Mann, Melody L., Jens Waldmann, Ying Zhang, Erin Miller, Mona L. Gauthier, Daniel W. Visscher, Gregory P. Downey, Evette S. Radisky, Alan P. Fields, et Derek C. Radisky. 2012. « Matrix Metalloproteinase Induction of Rac1b, a Key Effector of Lung Cancer Progression ». *Science translational medicine* 4 (142): 142ra95. <https://doi.org/10.1126/scitranslmed.3004062>.
- Sumi, Yuki, et Qutayba Hamid. 2007. « Airway Remodeling in Asthma ». *Allergology International* 56 (4): 341-48. <https://doi.org/10.2332/allergolint.R-07-153>.
- Sung, Hyuna, Jacques Ferlay, Rebecca L. Siegel, Mathieu Laversanne, Isabelle Soerjomataram, Ahmedin Jemal, et Freddie Bray. 2021. « Global Cancer Statistics 2020: GLOBOCAN Estimates of Incidence and Mortality Worldwide for 36 Cancers in 185 Countries ». *CA: A Cancer Journal for Clinicians* 71 (3): 209-49. <https://doi.org/10.3322/caac.21660>.
- Surviladze, Zurab, Anna Waller, Yang Wu, Elsa Romero, Bruce S. Edwards, Angela Wandinger-Ness, et Larry A. Sklar. 2010. « Identification of a Small GTPase Inhibitor Using a High-Throughput Flow Cytometry Bead-Based Multiplex Assay ». *Journal of Biomolecular Screening* 15 (1): 10-20. <https://doi.org/10.1177/1087057109352240>.
- Swärd, Karl, Mitsuo Mita, David P. Wilson, Jing Ti Deng, Marija Susnjar, et Michael P. Walsh. 2003. « The Role of RhoA and Rho-Associated Kinase in Vascular Smooth Muscle Contraction ». *Current Hypertension Reports* 5 (1): 66-72. <https://doi.org/10.1007/s11906-003-0013-1>.
- Takahashi, Kazuhide, et Katsuo Suzuki. 2009. « Membrane Transport of WAVE2 and Lamellipodia Formation Require Pak1 That Mediates Phosphorylation and Recruitment of Stathmin/Op18 to Pak1–WAVE2–Kinesin Complex ». *Cellular Signalling* 21 (5): 695-703. <https://doi.org/10.1016/j.cellsig.2009.01.007>.
- Taya, Shinichiro, Naoyuki Inagaki, Hiroaki Sengiku, Hiroshi Makino, Akihiro Iwamatsu, Itaru Urakawa, Kenji Nagao, Shiro Kataoka, et Kozo Kaibuchi. 2001. « Direct interaction of insulin-like growth factor-1 receptor with leukemia-associated RhoGEF ». *The Journal of Cell Biology* 155 (5): 809-20. <https://doi.org/10.1083/jcb.200106139>.
- Thomas, Emily K., Jose A. Cancelas, Hee-Don Chae, Adrienne D. Cox, Patricia J. Keller, Danilo Perrotti, Paolo Neviani, et al. 2007. « Rac Guanosine Triphosphatases Represent Integrating Molecular Therapeutic Targets for BCR-ABL-Induced Myeloproliferative Disease ». *Cancer Cell* 12 (5): 467-78. <https://doi.org/10.1016/j.ccr.2007.10.015>.
- Thompson, Andrew P., Christina Bitsina, Janine L. Gray, Frank von Delft, et Paul E. Brennan. 2021. « RHO to the DOCK for GDP Disembarking: Structural Insights into the DOCK GTPase Nucleotide Exchange Factors ». *Journal of Biological Chemistry* 296 (janvier): 100521. <https://doi.org/10.1016/j.jbc.2021.100521>.
- Tian, Yihao, Liu Xu, Yanqi He, Xiaolong Xu, Kai Li, Yanbin Ma, Yang Gao, Defei Wei, et Lei Wei. 2018. « Knockdown of RAC1 and VASP gene expression inhibits breast cancer cell migration ». *Oncology Letters* 16 (2): 2151-60. <https://doi.org/10.3892/ol.2018.8930>.
- Toma-Fukai, Sachiko, et Toshiyuki Shimizu. 2019. « Structural Insights into the Regulation Mechanism of Small GTPases by GEFs ». *Molecules* 24 (18): 3308. <https://doi.org/10.3390/molecules24183308>.
- Vadlamudi, Ratna K., Liana Adam, Rui-An Wang, Mahitosh Mandal, Diep Nguyen, Aysegul Sahin, Jonathan Chernoff, Mien-Chie Hung, et Rakesh Kumar. 2000. « Regulatable

- Expression of P21-Activated Kinase-1 Promotes Anchorage-Independent Growth and Abnormal Organization of Mitotic Spindles in Human Epithelial Breast Cancer Cells* ». *Journal of Biological Chemistry* 275 (46): 36238-44. <https://doi.org/10.1074/jbc.M002138200>.
- Vetter, Ingrid R., et Alfred Wittinghofer. 2001. « The Guanine Nucleotide-Binding Switch in Three Dimensions ». *Science* 294 (5545): 1299-1304. <https://doi.org/10.1126/science.1062023>.
- Viaud, Julien, et Jeffrey R. Peterson. 2009. « An allosteric kinase inhibitor binds the p21-activated kinase (Pak) autoregulatory domain covalently ». *Molecular cancer therapeutics* 8 (9): 2559-65. <https://doi.org/10.1158/1535-7163.MCT-09-0102>.
- Vincent, Sylvie, Philippe Jeanteur, et Philippe Fort. 1992. « Growth-Regulated Expression of RhoG, a New Member of the Ras Homolog Gene Family ». *MOL. CELL. BIOL.* 12: 11.
- Von Pawel-Rammingen, Ulrich, Maxim V. Telepnev, Gudula Schmidt, Klaus Aktories, Hans Wolf-Watz, et Roland Rosqvist. 2000. « GAP Activity of the Yersinia YopE Cytotoxin Specifically Targets the Rho Pathway: A Mechanism for Disruption of Actin Microfilament Structure ». *Molecular Microbiology* 36 (3): 737-48. <https://doi.org/10.1046/j.1365-2958.2000.01898.x>.
- Watanabe, Masaru, Hannah D. G. Fiji, Lea Guo, Lai Chan, Sape S. Kinderman, Dennis J. Slamon, Ohyun Kwon, et Fuyuhiko Tamanoi. 2008. « Inhibitors of Protein Geranylgeranyltransferase I and Rab Geranylgeranyltransferase Identified from a Library of Allenoate-Derived Compounds* ». *Journal of Biological Chemistry* 283 (15): 9571-79. <https://doi.org/10.1074/jbc.M706229200>.
- Wertheimer, Eva, Alvaro Gutierrez-Uzquiza, Cinthia Roseblit, Cynthia Lopez-Haber, Maria Soledad Sosa, et Marcelo G. Kazanietz. 2012. « Rac Signaling in Breast Cancer: A Tale of GEFs and GAPs ». *Cellular Signalling* 24 (2): 353-62. <https://doi.org/10.1016/j.cellsig.2011.08.011>.
- Whalley, Helen J., Andrew P. Porter, Zoi Diamantopoulou, Gavin R. M. White, Eduardo Castañeda-Saucedo, et Angeliki Malliri. 2015. « Cdk1 Phosphorylates the Rac Activator Tiam1 to Activate Centrosomal Pak and Promote Mitotic Spindle Formation ». *Nature Communications* 6 (1): 7437. <https://doi.org/10.1038/ncomms8437>.
- Winge, Mårten C.G., Bungo Ohyama, Clara N. Dey, Lisa M. Boxer, Wei Li, Nazanin Ehsani-Chimeh, Allison K. Truong, et al. 2016. « RAC1 activation drives pathologic interactions between the epidermis and immune cells ». *The Journal of Clinical Investigation* 126 (7): 2661-77. <https://doi.org/10.1172/JCI85738>.
- Wong, Leo Lap-Yan, Ian Pak-Yan Lam, Tracy Yuk-Nar Wong, Wai-Lung Lai, Heong-Fai Liu, Lam-Lung Yeung, et Yick-Pang Ching. 2013. « IPA-3 Inhibits the Growth of Liver Cancer Cells By Suppressing PAK1 and NF-KB Activation ». *PLOS ONE* 8 (7): e68843. <https://doi.org/10.1371/journal.pone.0068843>.
- Worthylake, David K., Kent L. Rossman, et John Sondek. 2000. « Crystal Structure of Rac1 in Complex with the Guanine Nucleotide Exchange Region of Tiam1 ». *Nature* 408 (6813): 682-88. <https://doi.org/10.1038/35047014>.
- Yoshida, Tatsushi, Yaqin Zhang, Leslie A. Rivera Rosado, Junjie Chen, Tahira Khan, Sun Young Moon, et Baolin Zhang. 2010. « Blockade of Rac1 Activity Induces G1 Cell Cycle Arrest or Apoptosis in Breast Cancer Cells through Downregulation of Cyclin D1, Survivin, and X-Linked Inhibitor of Apoptosis Protein ». *Molecular Cancer Therapeutics* 9 (6): 1657-68. <https://doi.org/10.1158/1535-7163.MCT-09-0906>.
- Zeng, Rui-Jie, Chun-Wen Zheng, Jing-E Gu, Hai-Xia Zhang, Lei Xie, Li-Yan Xu, et En-Min Li. 2019. « RAC1 inhibition reverses cisplatin resistance in esophageal squamous cell

- carcinoma and induces downregulation of glycolytic enzymes ». *Molecular Oncology* 13 (9): 2010-30. <https://doi.org/10.1002/1878-0261.12548>.
- Zheng, Yi. 2001. « Dbl Family Guanine Nucleotide Exchange Factors ». *Trends in Biochemical Sciences* 26 (12): 724-32. [https://doi.org/10.1016/S0968-0004\(01\)01973-9](https://doi.org/10.1016/S0968-0004(01)01973-9).
- ZOU, HUI, QIU-HONG FANG, YING-MIN MA, et XUE-YAN WANG. 2014. « Analysis of growth factors in serum and induced sputum from patients with asthma ». *Experimental and Therapeutic Medicine* 8 (2): 573-78. <https://doi.org/10.3892/etm.2014.1759>.

ANNEXES

Au cours de ma thèse j'ai également participé à d'autres études menées au laboratoire et notamment une étude portant sur le rôle de la GTPase Rac1 dans les CMLs vasculaires au cours de l'hypertension artérielle pulmonaire.

Annexe 1: Smooth muscle Rac1 contributes to pulmonary hypertension

Article publié dans le journal *British Journal of Pharmacology*

Smooth muscle Rac1 contributes to pulmonary hypertension

Florian Dilasser¹ | Marc Rio¹ | Lindsay Rose¹ | Angela Tesse¹ |
 Christophe Guignabert^{2,3}  | Gervaise Loirand¹ | Vincent Sauzeau¹ 

¹Université de Nantes, CHU Nantes, CNRS, INSERM, l'institut du thorax, Nantes, France

²Inserm UMR_S 999 "Pulmonary Hypertension: Pathophysiology and Novel Therapies", Hôpital Marie Lannelongue, Le Plessis-Robinson, France

³Faculté de Médecine, Université Paris-Saclay, Le Kremlin-Bicêtre, France

Correspondence

Vincent Sauzeau, UMR Inserm 1087/CNRS 6291, IRS-UN, 8 quai Moncoussu, 44007 Nantes cedex 1, France.
 Email: vincent.sauzeau@univ-nantes.fr

Background and Purpose: Pulmonary hypertension (PH) is a multifactorial chronic disease characterized by an increase in pulmonary artery (PA) resistance leading to right ventricle (RV) failure. Endothelial dysfunction and alteration of NO/cGMP signalling in PA plays a major role in PH. We recently described the involvement of the Rho protein Rac1 in the control of systemic blood pressure through its involvement in NO-mediated relaxation of arterial smooth muscle cell (SMC). The aim of this study was to analyse the role of SMC Rac1 in PH.

Experimental Approach: PH is induced by exposure of control and SMC Rac1-deficient (SM-Rac1-KO) mice to chronic hypoxia (10% O₂, 4 weeks). PH is assessed by the measurement of RV systolic pressure and hypertrophy. PA reactivity is analysed by isometric tension measurements. PA remodelling is quantified by immunofluorescence in lung sections and ROS are detected using the dihydroethidium probe and electronic paramagnetic resonance analysis. Rac1 activity is determined by immunofluorescence.

Key Results: Rac1 activation in PA of hypoxic mice and patients with idiopathic PH. Hypoxia-induced rise in RV systolic pressure, RV hypertrophy and loss of endothelium-dependent relaxation were significantly decreased in SM-Rac1-KO mice compared to control mice. SMC Rac1 deletion also limited hypoxia-induced PA remodelling and ROS production in pulmonary artery smooth muscle cells (PASMCS).

Conclusion and Implications: Our results provide evidence for a protective effect of SM Rac1 deletion against hypoxic PH. Rac1 activity in PASMCS plays a causal role in PH by favouring ROS-dependent PA remodelling and endothelial dysfunction induced by chronic hypoxia.

KEYWORDS

pulmonary hypertension, Rac1, smooth muscle

1 | INTRODUCTION

Abbreviations: iPAH, idiopathic pulmonary arterial hypertension; LVSP, left ventricular systolic pressure; PA, pulmonary artery; PASMCS, pulmonary artery smooth muscle cell; PH, pulmonary hypertension; RV, right ventricle; RVSP, right ventricular systolic pressure; SMC, smooth muscle cell.

Pulmonary arterial hypertension (PH) is a multifactorial and chronic disease characterized by a progressive increase in pulmonary vascular resistance and pulmonary arterial pressure that leads to right ventricle

This is an open access article under the terms of the [Creative Commons Attribution-NonCommercial-NoDerivs](https://creativecommons.org/licenses/by-nc-nd/4.0/) License, which permits use and distribution in any medium, provided the original work is properly cited, the use is non-commercial and no modifications or adaptations are made.

© 2022 The Authors. *British Journal of Pharmacology* published by John Wiley & Sons Ltd on behalf of British Pharmacological Society.

(RV) failure and death (Simonneau et al., 2019; Thenappan et al., 2018). The increase in pulmonary vascular resistance results from both excessive vasoconstriction and vascular wall remodelling, which together lead to a narrowing of pulmonary arterial lumen. Pulmonary artery (PA) wall remodelling is a hallmark of PH and is characterized by structural changes including intimal cell proliferation, medial hypertrophy and hyperplasia, enhanced muscularity of small PA, adventitial thickening, fibrosis and complex and/or thrombotic lesions over time (Humbert et al., 2004, 2019). Current treatments such as **phosphodiesterase 5** inhibitors, **soluble guanylate cyclase** stimulators, **endothelin receptor** antagonists and activators of the **prostacyclin** pathway aim at promoting vasodilation of PA (Sitbon et al., 2019; Thenappan et al., 2018). Although these treatments improve the 6-min-walk distance, haemodynamic parameters and the quality of life of PH patients, with the exception of prostacyclin, they do not prolong survival. This suggests that targeting only vasoconstriction is not sufficient to stop disease progression (Galiè et al., 2008, 2009; McLaughlin et al., 2002, 2015; Sitbon et al., 2002, 2019).

Vascular SMCs are strongly involved in PH through their role in PA vasoconstriction but also in remodelling (Humbert et al., 2019; Lyle et al., 2017) (Thenappan et al., 2018). Small G proteins of the Rho family (**RhoA**, **Rac1** and **CDC42**) are recognized as major regulators of vascular smooth muscle cell (SMC) functions such as contraction, proliferation and migration, thus participating in the physiological regulation of blood pressure and remodelling. Accordingly, dysregulation or overactivation of Rho proteins plays a causal role in cardiovascular diseases (Loirand et al., 2013). In this way, we have shown that vascular SMC Rac1 is a regulator of systemic blood pressure through its involvement in **nitric oxide (NO)**-mediated relaxation of systemic arterial SMCs and that alteration of Rac1 signalling pathway can lead to high blood pressure (Andre et al., 2014; Sauzeau et al., 2010). Since abnormalities in **NO** production and metabolism, and NO-induced vasodilation contribute to the pathophysiology of PH (Humbert et al., 2019; Watanabe, 2018), the aim of the present study was to assess the role of Rac1 in the SMCs of PA and its involvement in PH development. Our data show that Rac1 is activated in pulmonary artery smooth muscle cell (PASM) in a mouse model of PH induced by chronic hypoxia and in lung samples from PH patients. By using mice harbouring specific deletion of Rac1 in SMCs, we provide evidence that this activation has a causal role in the development of hypoxia-induced PH. Deletion of Rac1 in PSMCs limits hypoxia-induced PH in mice by impeding reactive oxygen species (ROS)-dependent PASM proliferation and PA remodelling, and endothelium dysfunction.

2 | METHODS

2.1 | Mice

All experimental procedures and animal care were performed in accordance with the Regional Ethical Committee for Animal Experiments of

What is already known

- Pulmonary hypertension (PH) is characterized by an increase in pulmonary artery resistance and endothelial dysfunction.
- Rac1 regulates the systemic blood pressure through its involvement in NO-mediated relaxation of smooth muscle cell.

What this study adds

- Rac1 activation is observed in pulmonary arteries of hypoxic mice and patients with idiopathic PH.
- Smooth muscle Rac1 deletion limited hypoxia-induced pulmonary artery remodelling and ROS production.

What is the clinical significance

- Our results provide evidence for a protective effect of Rac1 inhibition against hypoxic PH.

the Pays de la Loire (Authorization number 00909.01). Animal studies are reported in compliance with the ARRIVE guidelines (Percie du Sert et al., 2020) and with the recommendations made by the *British Journal of Pharmacology* (Lilley et al., 2020). Mice were housed in transparent open-top cages (29.5 × 16 × 13 cm; five mice per cage) under a 12-h light/dark cycle in a temperature-controlled and humidity-controlled room with food and water available *ad libitum*. All *in vivo* studies were carried out during the light phase of the cycle. Animal experiments were designed to have groups of equal size using randomized and blinded analysis. In some instance, however, group sizes were unequal due to unexpected loss of animals while conducting the procedures.

C57Bl/6 Rac1^{lox/lox} (Rac1^{lox/lox}, RRID:IMSR_NM-CKO-200212) and SMMHC-Cre (RRID:IMSR_JAX:019079) mice were crossed to produce SMMHC-Rac1^{lox/lox} mice as previously described (Andre et al., 2014). Considering that the SMMHC-Cre construct is carried on the Y chromosome, only male mice were analysed in this study. Eight-week-old SMMHC-Rac1^{lox/lox} males were treated with **tamoxifen** (intraperitoneally, 1 mg d⁻¹ in sunflower oil) for five consecutive days during 2 weeks to induce Rac1 deletion in smooth muscle cells (SM-Rac1-KO). Tamoxifen-treated Rac1^{lox/lox} mice were used as control (SM-Rac1^{lox/lox}).

2.2 | Hypoxia-induced pulmonary hypertensive (PH) mice

To induce PH, mice were exposed to chronic hypoxia in a gaseous hypoxic chamber providing nitrogen injection to obtain 10% O₂ for

28 days (five mice per cage). Mice exposed to normoxia (21% O₂) for 28 days were used as normoxic controls (five mice per cage).

2.3 | Right and left ventricular systolic pressure (RVSP and LVSP)

As previously described (Dumas de la Roque et al., 2017), RVSP and LVSP were measured in non-ventilated mice under isoflurane anaesthesia. To maintain the body temperature, mice were maintained on a heated blanket. At the end of the experiment, mice were killed by exsanguination. Mice were thoracotomized and a heparin-filled hypodermic needle coupled to a polyethylene catheter was inserted in subdiaphragmatic directly into the right or the left ventricle. RVSP and LVSP were measured with a fluid-filled pressure sensor connected to the PowerLab recording unit (AD Instruments, RRID:SCR_018833) and recorded with the LabChart software (AD Instruments, RRID:SCR_001620).

2.4 | Right ventricular (RV) hypertrophy measurements

After exsanguination, the right ventricle (RV) was separated from the left ventricle plus septum (LV + S). The RV/(LV + S) ratio (Fulton index) was then determined from the tissue weight.

2.5 | Ex vivo pulmonary artery (PA) reactivity

Murine PA were cleaned, cut in rings and mounted on a multichannel isometric myograph (Danish Myo Technology, Aarhus, Denmark) in Krebs-Henseleit physiological solution (in mol·L⁻¹: 118.4 NaCl, 4.7 KCl, 2 CaCl₂, 1.2 MgSO₄, 1.2 KH₂PO₄, 25 NaHCO₃, and 11 glucose) bubbled with carbogen (5% CO₂-95% O₂ at 37°C. A pretension of 10 mN was applied. The wire myograph was connected to a digital data recorder (MacLab/4e, AD Instruments, RRID:SCR_018833), and recordings were analysed using LabChart software (AD Instruments, RRID:SCR_0017551, version #7). Concentration-response curves to KCl and **endothelin-1 (ET-1)** were obtained by measuring the amplitude of the contractile responses to increasing concentration of KCl (30 mmol·L⁻¹ to 110 mol·L⁻¹), ET-1 (10⁻⁹ mol·L⁻¹ to 10⁻⁶ mol·L⁻¹) or **5-HT** (10⁻⁸ mol·L⁻¹ to 10⁻⁴ mol·L⁻¹). Endothelium/NO-dependent and independent relaxations were tested by adding increasing concentrations of **acetylcholine (ACh)** (10⁻⁸ mol·L⁻¹ to 10⁻⁴ mol·L⁻¹) or **S-nitroso-N-acetyl-D,L-penicillamine (SNAP)** (10⁻⁸ mol·L⁻¹ to 10⁻⁴ mol·L⁻¹) to rings pre-contracted by **phenylephrine (PhE)** (1 μmol·L⁻¹) and were quantified as the percentage of the maximal PhE-induced contraction.

2.6 | Lung tissue preparation

Mice lungs were fixed in 4% paraformaldehyde (PFA) for 48 h and embedded into paraffin. These samples were then sliced in 7-μm-thick

sections. For immunofluorescence analyses and ROS detection assay, mice lungs were placed into Tissue-Tek O.C.T. Compound (Sakura Finetek) and snap-frozen in liquid nitrogen before the realization of 10-μm-thick sections. Human lung biopsies were fixed in 4% PFA and embedded in paraffin. The Immuno-related procedures used comply with the recommendations made by the *British Journal of Pharmacology* (Alexander et al., 2018).

2.7 | Measurement of PA remodelling

Lung sections were stained by immunohistochemistry with anti-SM22α antibody (Abcam, RRID:AB_443021) on haematoxylin and eosin-stained sections for visualization of SMC. Sections were then observed (fluorescence microscope, Nikon) and analysed (Fiji/ImageJ software, RRID:SCR_002285 and RRID:SCR_003070). PA muscularization was then quantified as the percentage of SM22α positive distal PA (intra-alveolar vessels <100 μm) within the section. Five-μm-thick sections were analysed to calculate a mean value in each animal. The percentage of medial thickness of muscularized PA was determined as [(2 × medial wall thickness/external diameter) × 100].

2.8 | Human lung specimens

Human lung specimens were obtained during lung transplantation in patients with idiopathic pulmonary arterial hypertension (iPAH) and during lobectomy or pneumonectomy for localized lung cancer in control subjects. Preoperative echocardiological evaluation, including echocardiography, was performed in the control subjects to rule out PH, and the lung specimens from the control subjects were collected at a distance from the tumour foci. The absence of tumoral infiltration was retrospectively established in all tissue sections by the histopathological analysis. This study was approved by the local ethics committee (CPP Ile-de-France VII, Le Kremlin-Bicêtre, France). All enrolled patients gave written approval. As these biopsies are not easy to obtain and in order to maintain homogeneous groups, we included three samples in each group. Thus, no statistical analysis was performed on this study.

2.9 | Analysis of Rac1 activity

Human pulmonary biopsies and lungs paraffin-embedded sections were deparaffinized and permeabilized (PBS + 0.1% Triton-X100) before incubation with anti-Rac-GTP antibody (NewEast Biosciences, RRID:AB_1961793) (1/1000) overnight at room temperature. After three washes in PBS, sections were incubated for 1 h at room temperature with the secondary Alexa568-labelled anti-rabbit antibody (RRID:AB_10563566) (1/1000). Anti-SM22α antibody (Abcam) (1/500, overnight at room temperature) with a secondary Alexa488-labelled anti-mouse antibody (RRID:AB_138404) (1/1000,

1 h at room temperature) were used to localize smooth muscle. To quantify Rac-GTP levels within SMC, Rac-GTP fluorescence intensities were measured with Fiji (Fiji, RRID:SCR_002285) inside a mask delimited by SM22 α positive cell areas and normalized to the control condition. To emphasize the specificity of Rac-GTP signal within SMC, an intensity profile was realized on Fiji along the designated line. To allow the comparison between them, each channel intensities was normalized individually as follow: - lowest intensity level = 0 A.U. and highest intensity level = 1 A.U.

2.10 | Cell culture

Pulmonary artery smooth muscle cells (PASMCs) were isolated from PA of SM-Rac1^{lox/lox} mice. Tissues were cleaned manually and digested for 1 h with collagenase II (1 mg·ml⁻¹, Worthington Biochemical) at 37°C under agitation. Cells were cultured in Dulbecco modified Eagle medium (Gibco) containing 10% FBS, 1 g·L⁻¹ glucose, 100 units·ml⁻¹ penicillin, and 100 μ g·ml⁻¹ streptomycin at 37°C and 5% CO₂. All experiments were performed between passages 1 and 3.

2.11 | ROS detection assay

For tissue ROS detection, cryosection (10 μ m) of unfixed snap-frozen lungs were incubated in 10- μ M dihydroethidium (DHE, Invitrogen) for 30 min incubation at 37°C. Sections were then mounted with Prolong™ Gold antifade reagent containing DAPI (Invitrogen). For *in vitro* ROS detection, 6000 PASMCs per well were seeded into 8-well ibidi μ -Slide (Ibidi) and allowed to adhere during 6 h and then serum starved during 24 h. When indicated, cells were pre-incubated with 10⁻⁵ M of EHT1864 (Tocris Bioscience) or 1.5 mmol·L⁻¹ of tempol (Sigma-Aldrich) during 30 min. Cells were placed in normoxic or hypoxic (1% O₂) conditions in a Heracell 150 incubator (Kendro) during 6 h. Then cells were incubated with 10 μ mol·L⁻¹ at 37°C for 15 min and fixed with 4% PFA for 10 min. After fixation, cells were incubated with Hoescht to stain nuclei. Images were captured with an inverted microscope (Nikon) in epifluorescence. DAPI and Hoescht staining were detected at 405 nm, and oxidized DHE was detected at 555 nm. A threshold mask removing the background signal was applied to allow the detection of dihydroethidium positive cells.

2.12 | Superoxide ion measurement by electronic paramagnetic resonance (EPR)

Mice lungs were incubated in a Krebs–Hepes solution with 500 μ M of 1-hydroxy-3-methoxycarbonyl-2,2,5,5-tetramethylpyrrolidin (CMH; Noxygen), 25- μ M deferoxamine (Sigma-Aldrich) and 5- μ M DETC (Sigma-Aldrich) and frozen in liquid nitrogen. The samples were analysed using a table-top x-band spectrometer Miniscope (Magnetech, MS5000). The instrument settings and the modality of signal quantification were previously described (Tesse et al., 2021).

2.13 | Xanthine oxidase activity assay

Mice lungs were homogenized in 100-mM Tris-HCl, pH 7.5, containing 1 \times protease inhibitors (Sigma-Aldrich). Xanthine oxidase activity was measured in the lungs with a fluorometric assay kit (Cayman Chemical) according to manufacturer's instructions.

2.14 | RNA extraction and real-time PCR

Total RNA was extracted from the pulmonary arteries with TRIZOL reagent (Life Technologies) according to the manufacturer's instructions. One microgram of RNA was used for reverse transcription with High-Capacity cDNA Reverse Transcription Kit (Life Technologies). Real-time PCR using TaqMan probes was performed in 7900HT Fast Real-Time PCR System (Applied Biosystems). The expression of Hif1a (item number Mm00468869_m1, ThermoFisher), NOS3 (eNOS) (item number Mm00435217_m1, ThermoFisher), Nox1 (item number Mm00549170_m1, ThermoFisher), Cybb (Nox2) (item number Mm01287743_m1, ThermoFisher), GAPDH (item number Mm99999915_g1, ThermoFisher) and HPRT (item number Mm03024075_m1, ThermoFisher) was analysed. Natural product studies are reported in compliance with the recommendations made by the British Journal of Pharmacology (Izzo et al., 2020).

2.15 | Pulmonary artery smooth muscle cells (PASMCs) proliferation

Ten thousand PASMCs per well were seeded in 24-well plate and allowed to adhere during 6 h and then serum-starved during 24 h. When indicated, cells were pre-incubated with 10⁻⁵ mol·L⁻¹ of EHT1864 (Tocris Bioscience) or 1.5 mmol·L⁻¹ of tempol (Sigma-Aldrich) during 30 min. Cells were placed in normoxia or hypoxia (1% O₂) in a Heracell 150 incubator (Kendro) during 96 h, and time-lapse images were captured for 96 h (1 image/15 min) on a JuliStage microscope (NanoEntek, Seoul, Korea). The number of dividing cells during this time was then counted.

2.16 | Statistics

Data and statistical analysis complied with the recommendations of the *British Journal of Pharmacology* on experimental design and analysis (Curtis et al., 2018). Data analysis was performed in a blinded manner wherever possible. For multiple comparisons, the one-way ANOVA test was used followed by Tukey's post-test to specifically compare indicated groups. For multiple comparison of contractility studies, the two-way ANOVA test was used followed by a Bonferroni post-test. For two group comparisons, the Mann–Whitney test was performed. Post hoc tests were conducted only if *F* in ANOVA achieved *P* < 0.05. Sample size subjected to statistical analysis was at least five animals per group (*n* = 5, where *n* is the number of independent values). Data analysis was performed using the GraphPad Prism software (GraphPad Prism, RRID:SCR_002798). The threshold for statistical significance was set at *P* < 0.05.

2.17 | Materials

5-HT, ACh, phenylephrine, 1-hydroxy-3-methoxycarbonyl-2,2,5,5-tetramethylpyrrolidin (CMH) deferoxamine, DETC from Sigma Aldrich Chimie S.a.r. 80 Rue de Luzais L' Isle St. Quentin Fallavier Cedex 38297 France.

Tissue Tek from Sakura Finetek, 18 rue Hergé Parc Scientifique de la Haute Borne 59650 Villeneuve d'Ascq. SM22a antibody from Abcam, 24 rue Louis Blanc 75010 PARIS FRANCE. Rac-GTP antibody from NewEast Biosciences, 1150 First Avenue, Suite 501A King of Prussia, PA 19406 USA. Collagenase from Worthington, Worthington Biochemical Corporation, 730 Vassar Ave., Lakewood, NJ 08701, USA. Cell culture medium, Tirol, DHE and DAPI from Thermo Fisher,

Life Technologies SAS16 Avenue du Québec BP 30210, F - 91941 Courtaboeuf Cedex (Villebon-sur-Yvette). EHT1864 from Tocris, 19 Rue Louis Delourmel 35230 Noyal Châillon sur Seiche France. CMH from Noxygen, Lindenmatte 42,79215 Elzach, Germany.

2.18 | Nomenclature of targets and ligands

Key protein targets and ligands in this article are hyperlinked to corresponding entries in the IUPHAR/BPS Guide to PHARMACOLOGY <http://www.guidetopharmacology.org> and are permanently archived in the Concise Guide to PHARMACOLOGY 2021/22 (Alexander, Christopoulos, et al., 2021; Alexander, Fabbro, et al., 2021).

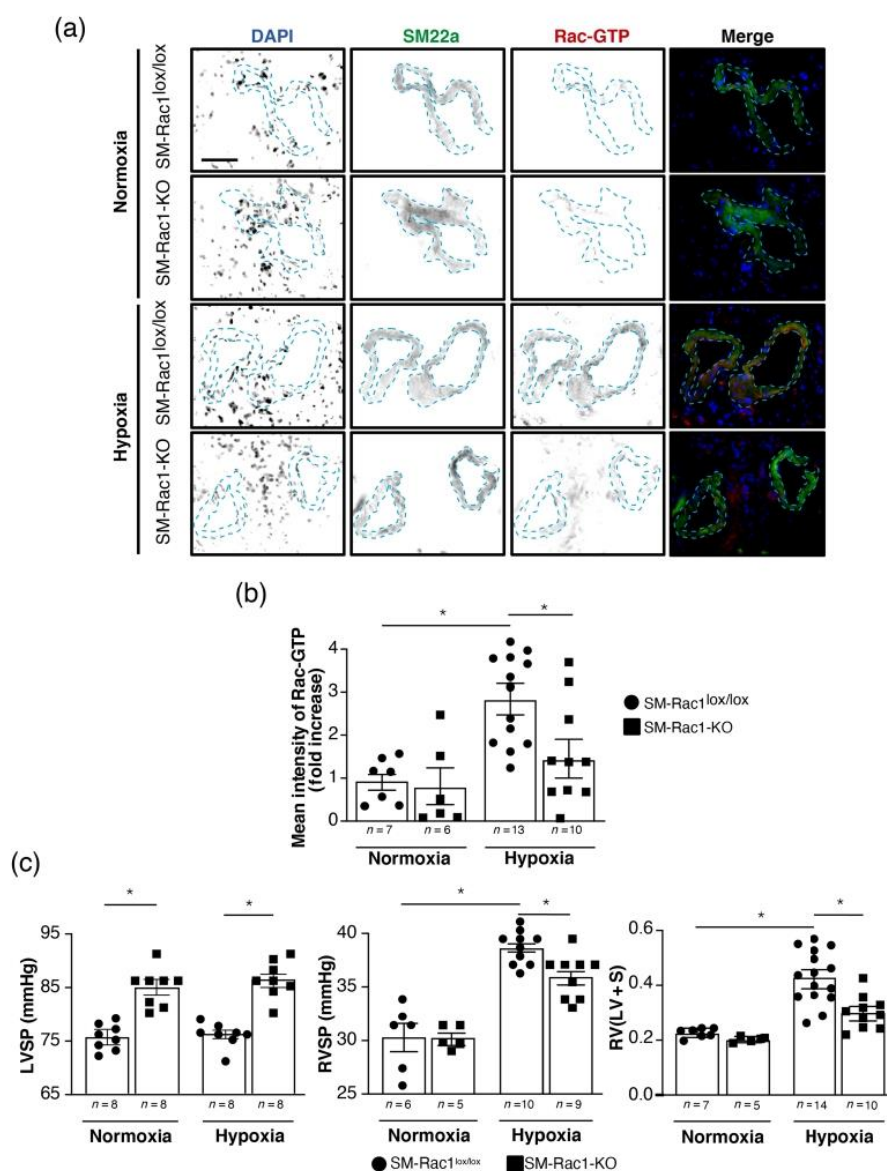


FIGURE 1 Smooth muscle (SM) Rac1 deletion prevents chronic hypoxia-induced increase in right ventricular systolic pressure and right ventricular remodelling. (a) Representative images of Rac-GTP immunofluorescence (red) in cryosections of lung from SM-Rac1^{lox/lox} and SM-Rac1-KO mice exposed for 4 weeks to normoxia or hypoxia. Nuclei are detected by DAPI staining (blue) and smooth muscle by SM22 α immunofluorescence labelling (green). Scale bar = 80 μ m. (b) Quantification of Rac-GTP labelling fluorescence intensity in SMCs. (c) Right ventricular systolic pressure (RVSP, left panel), left ventricular systolic pressure (LVSP, middle panel) and Fulton index (RV/(LV + S); right panel) in SM-Rac1^{lox/lox} and SM-Rac1-KO mice exposed for 4 weeks to normoxia or hypoxia. Data are expressed as mean \pm SEM. * P < 0.05

3 | RESULTS

3.1 | Rac1 contributes to pulmonary hypertension (PH) development

We first assessed the level of Rac1 activation by immunofluorescence with a conformational sensitive anti-Rac1-GTP antibody in lung sections from normoxic and hypoxic mice. Rac1-GTP staining was significantly increased in PA walls of hypoxic SM-Rac1^{lox/lox} mice compared to normoxic SM-Rac1^{lox/lox} mice, while in contrast, Rac1-GTP fluorescence remained as weak as that of normoxic SM-Rac1-KO mice in hypoxic SM-Rac1-KO mice (Figure 1a,b). Rac1-GTP labelling co-localized with SM22 α staining indicating that the increased Rac1 activity observed in PA of hypoxic SM-Rac1^{lox/lox} mice occurred in PASMOC (Figure 1a).

As expected, SM-Rac1^{lox/lox} mice exposed to hypoxic condition developed PH characterized by a strong elevation of RVSP and a right ventricular remodelling attested by the increase in the Fulton index (Figure 1c). Deletion of Rac1 in SMC reduced PH as shown by the 30% decrease in RVSP and the 60% decrease in right ventricular

hypertrophy in hypoxic SM-Rac1-KO mice compared to hypoxic SM-Rac1^{lox/lox} mice (Figure 1c). As previously described, SM-Rac1-KO mice develop a systemic hypertension associated with an increase of LVSP (Andre et al., 2014). Under hypoxic condition, the deletion of Rac1 in SMC has no effect on LVSP. These results show that Rac1 is activated in PASMOC of hypoxic mice and contributes to the pathogenesis of PH.

3.2 | SM-Rac1 deletion has no effect on the contractile properties of PA

To determine whether the involvement of Rac1 in PH was due to its role in the modulation of the vascular tone (Andre et al., 2014), we measured *ex vivo* contractile properties of PA from normoxic and hypoxic SM-Rac1^{lox/lox} and SM-Rac1-KO mice. Contractile responses of PA to KCl and ET-1 were similar in SM-Rac1^{lox/lox} and SM-Rac1-KO mice both in normoxic and hypoxic conditions (Figure 2). Contractile responses to 5-HT were increased in hypoxic conditions compared to normoxia but were similar in SM-Rac1^{lox/lox} and SM-Rac1-KO mice (Figure 2). Regarding vasodilation,

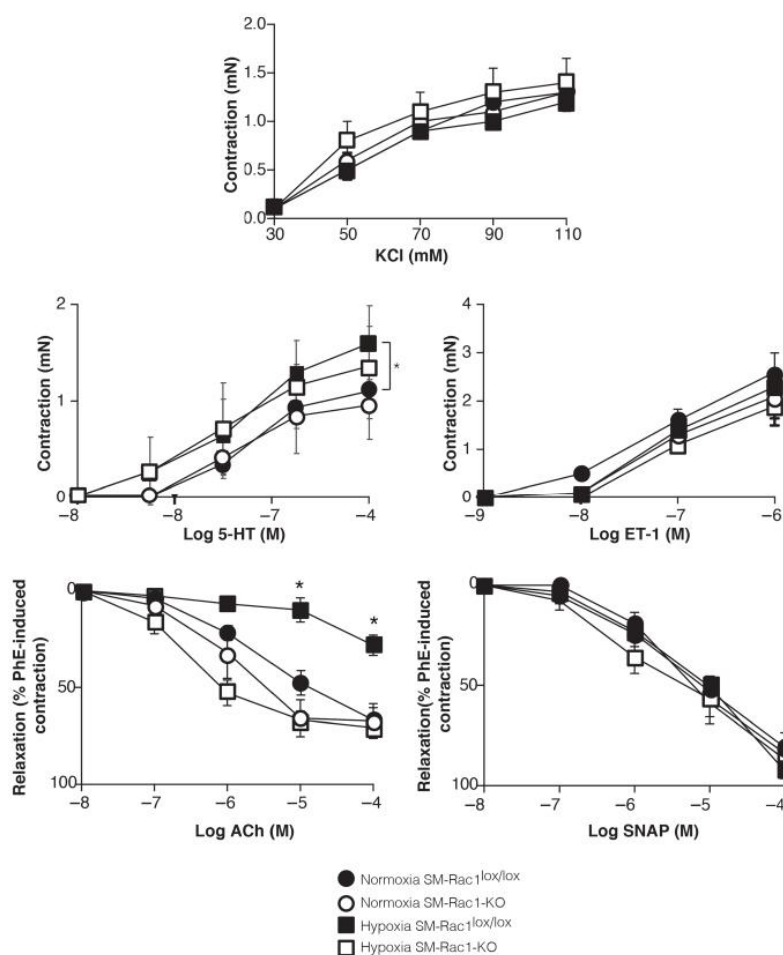


FIGURE 2 Smooth muscle Rac1 deletion prevents hypoxia-induced reduction of endothelium-dependent relaxation. Contractile responses to potassium chloride (KCl), 5-HT and endothelin-1 (ET-1), and relaxation of phenylephrine (PhE)-induced tension (1 μ M) by acetylcholine (ACh) and S-nitroso-N-acetyl-D,L-penicillamine (SNAP) in pulmonary artery (PA) from SM-Rac1^{lox/lox} and SM-Rac1-KO mice exposed for 4 weeks in normoxia or hypoxia (Normoxia SM-Rac1^{Lox/Lox} $n = 9$ mice; Normoxia SM-Rac1-KO $n = 7$ mice; hypoxia SM-Rac1^{Lox/Lox} $n = 11$ mice; hypoxia SM-Rac1-KO $n = 5$ mice). Data are expressed as mean \pm SEM. * $P < 0.05$

ACh-induced NO-dependent relaxation was similar in PA from normoxic SM-Rac1^{lox/lox} and SM-Rac1-KO mice, suggesting that Rac1 is not involved in NO-mediated relaxation of PASM in basal conditions (Figure 2). Chronic exposure of SM-Rac1^{lox/lox} mice to hypoxia decreased ACh-mediated relaxation of PA, attesting the endothelium dysfunction known to be associated with hypoxic PH. This defect in endothelium-derived NO-dependent relaxation is not observed in PA from hypoxic SM-Rac1-KO mice, suggesting that Rac1 in PASM is involved in hypoxia-induced loss of NO-induced PA dilation (Figure 2). To directly assess the role of Rac1 in NO-signalling pathway in PASM, we then used the NO donor SNAP, which directly triggers guanylate cyclase activation, cyclic GMP (cGMP) production and relaxation, independently of the endothelium (Figure 2). Concentration-relaxation response curves to SNAP were similar in PA from normoxic SM-Rac1^{lox/lox} and SM-Rac1-KO mice, confirming that Rac1 is not involved in cGMP signalling-mediated relaxation of PASM in basal conditions. Chronic exposure to hypoxia did not modify the endothelium-independent vasodilator effect of SNAP, both in SM-Rac1^{lox/lox} and SM-Rac1-KO mice (Figure 2). These results indicate that Rac1 in PASM is neither involved neither in intracellular signalling mechanisms inducing contraction nor in cGMP signalling mediating NO-dependent relaxation. However, they show that PASM Rac1 deletion prevents hypoxia-induced defect in endothelium/NO-

dependent relaxation suggesting a role of PASM Rac1 upstream in the effect of NO on PASM.

3.3 | Rac1 is required for hypoxia-induced PA remodelling

To assess the role of Rac1 in hypoxia-induced PA remodelling, muscularization of small PA has been analysed on lung sections by immunohistochemical labelling with an antibody that recognizes the SMC phenotypic marker SM22 α . SM22 α staining was weak in lung sections from normoxic SM-Rac1^{lox/lox} and SM-Rac1-KO mice (Figure 3). Exposure to chronic hypoxia increased the number and the thickness of muscularized distal PA in SM-Rac1^{lox/lox} mice but only had very limited effect on PA wall structure in SM-Rac1-KO mice (Figure 3). These observations suggest an essential role of SM Rac1 in PA remodelling associated with hypoxia-induced PH.

3.4 | Rac1 is essential for hypoxia-induced ROS production in the lung

Rac1 is well known for its essential role in ROS production through the regulation of NADPH oxidase activity (Hordijk, 2006) and ROS

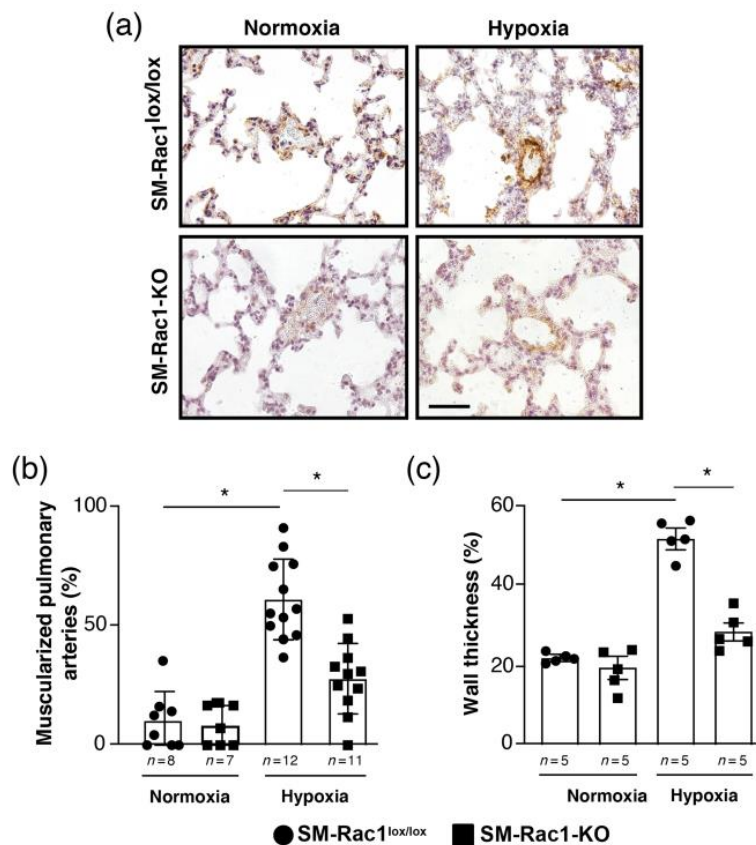


FIGURE 3 Smooth muscle Rac1 deletion prevents pulmonary artery (PA) remodelling induced by hypoxia. (a) Representative images of SM22 α labelling on haematoxylin and eosin-stained sections of lung from SM-Rac1^{lox/lox} and SM-Rac1-KO mice exposed for 4 weeks to normoxia or hypoxia. Scale bar = 80 μ m. (b and c) quantification of the number of muscularized PA (b) and wall thickness (c). Data are expressed as mean \pm SEM. *P < 0.05

stimulate SMC proliferation (Li et al., 2014; Wang et al., 2014; Wang & Sun, 2010). In addition, lung ROS levels are increased in chronically hypoxic mice (Fresquet et al., 2006; Liu et al., 2006). We thus hypothesize that the role of Rac1 in PA remodelling in hypoxic PH can be related to ROS production. To address this hypothesis, we measured ROS production by dihydroethidium staining in lung cryosections from normoxic and hypoxic SM-Rac1^{lox/lox} and SM-Rac1-KO mice. Dihydroethidium labelling was similarly weak in both normoxic SM-Rac1^{lox/lox} and SM-Rac1-KO mice indicating a low ROS production (Figure 4). The strong rise in dihydroethidium staining in hypoxic SM-Rac1^{lox/lox} mice demonstrated an increase in ROS production detection in both PA and lung parenchyma (Figure 4a,b). This hypoxia-induced stimulation of ROS production was significantly reduced in PA and marginally decreased in the lung parenchyma of hypoxic SM-Rac1-KO mice (Figure 4a,b). These observations were confirmed by electronic paramagnetic resonance, demonstrating that Rac1

deletion in SMC prevents hypoxia-induced superoxide ion (O₂⁻) overproduction in lungs (Figure 4c). This result is not related to a significant modification in xanthine oxidase activity (Figure 4c) or expression of major drivers of ROS production such as NOX1, NOX2, eNOS (NOS3) and HIF1a (Figure 4d). These results suggest that PASMCM Rac1 plays a critical and a direct role in hypoxia-induced ROS production in the lungs.

3.5 | Rac1 is required for hypoxia induced PASMCM proliferation

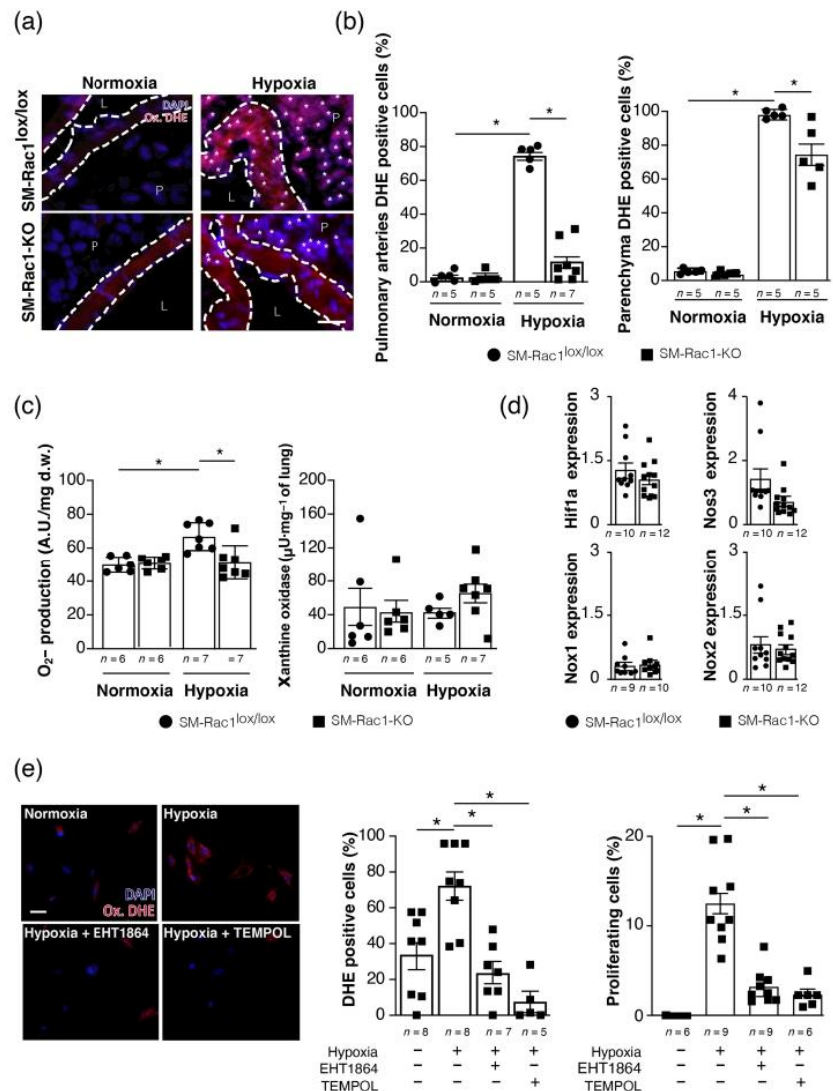
We next wanted to investigate the role of Rac1 in ROS production and PASMCM proliferation by a pharmacological approach *in vitro*. As shown in Figure 4e, hypoxia induced increased ROS production and PASMCM proliferation, both of which were suppressed by Rac1

FIGURE 4 Smooth muscle Rac1 deletion prevents hypoxia-induced ROS production in pulmonary artery (PA) and pulmonary artery smooth muscle cell (PASMCM) proliferation. (a) Representative images of dihydroethidium (DHE) staining of lung sections from SM-Rac1^{lox/lox} and SM-Rac1-KO mice exposed for 4 weeks to normoxia or hypoxia. Scale bar = 20 μm. L, lumen; P, parenchyma; * indicates DHE positive cell.

(b) Quantification of DHE positive cells in PA (left panel) and in lung parenchyma (right panel). Data are expressed as mean ± SEM. *P < 0.05. (c) Detection of O₂⁻ by electronic paramagnetic resonance (right panel) and xanthine oxidase activity in lungs from SM-Rac1^{lox/lox} and SM-Rac1-KO mice exposed for 4 weeks to normoxia or hypoxia (left panel). Data are expressed as mean ± SEM. *P < 0.05.

(d) Analysis by real-time PCR of the relative expression of HIF1a, eNOS (NOS3), NOX1 and NOX2 in pulmonary arteries from SM-Rac1^{lox/lox} and SM-Rac1-KO mice exposed for 4 weeks to hypoxia compared to SM-Rac1^{lox/lox} exposed for 4 weeks to normoxia. Data are expressed as mean ± SEM.

(e) Representative images of DHE (red) and DAPI (blue) staining of PASMCMs cultured in normoxic or hypoxic condition, and quantification of DHE positive cells and PASMCMs proliferation. When indicated, cells were treated with EHT1864 (10⁻⁵ M) or 1.5-mM tempol. Scale bar = 10 μm. Data are expressed as mean ± SEM. *P < 0.05



inhibition of by EHT1864 or the antioxidant tempol. These results revealed that hypoxia-induced ROS production and the resulting ROS-mediated PASMCM proliferation depend on Rac1.

3.6 | Rac1 is overactivated in PA of idiopathic pulmonary arterial hypertension (iPAH) patients

In order to assess whether SMC Rac1 may play a role similar to that observed in mice in the pathogenesis of PH in humans, we performed Rac1-GTP immunostaining in lungs specimens from PH patients (Figure 5). As expected, immunostaining of PASMCM by the anti-SM22 α antibody shows the thickening of the medial layers of the PA in explanted lungs from iPAH patients compared to control samples (Figure 5a). The weak Rac1-GTP immunostaining in control lung samples indicated a low level of active Rac1 in these subjects. In contrast, the strong fluorescence intensity of Rac1-GTP observed in iPAH patient samples showed that PH is associated with a strong Rac1 activity in the PA (Figure 5a,b). Analysis of the spatial profile of fluorescence intensities revealed that active Rac1 is specifically localized in PASMCM, in agreement with our observation in the experimental model of PH in mice (Figure 5c).

4 | DISCUSSION

Our study demonstrates an increase in Rac1 activity in human and murine PASMCMs during PH. The specific deletion of Rac1 in SMC limits the rise in RSVPM and PA remodelling induced by chronic hypoxia, suggesting a causal role of SM Rac1 activity in the development of PH. Our results thus show that, in contrast to systemic circulation (Andre et al., 2014; Sauzeau et al., 2010), SM Rac1 is not involved in the contraction or the relaxation of PASMCMs, but that its role in PH is mediated by an increase in ROS production and proliferation of PASMCMs.

Studies on the identification of the role of Rac1 in SMCs have produced conflicting results (Loirand & Pacaud, 2014). Indeed, in the vascular system, Rac1 is described to promote relaxation by regulating cGMP level in SMCs (Andre et al., 2014; Sauzeau et al., 2010) while it is involved in the contraction of visceral and bronchial SMCs (Andre-Gregoire et al., 2018; Rahman et al., 2014). These discrepancies suggest that the role of Rac1 depends on the type or tissue/organ location of SMCs and cannot be generalized to all SMCs. In the same line, we show in the present study that the role of Rac1 in PASMCM is different from that in systemic arteries. In PA, SM Rac1 deletion has no direct effect on vasoconstriction or vasodilation. However, SM

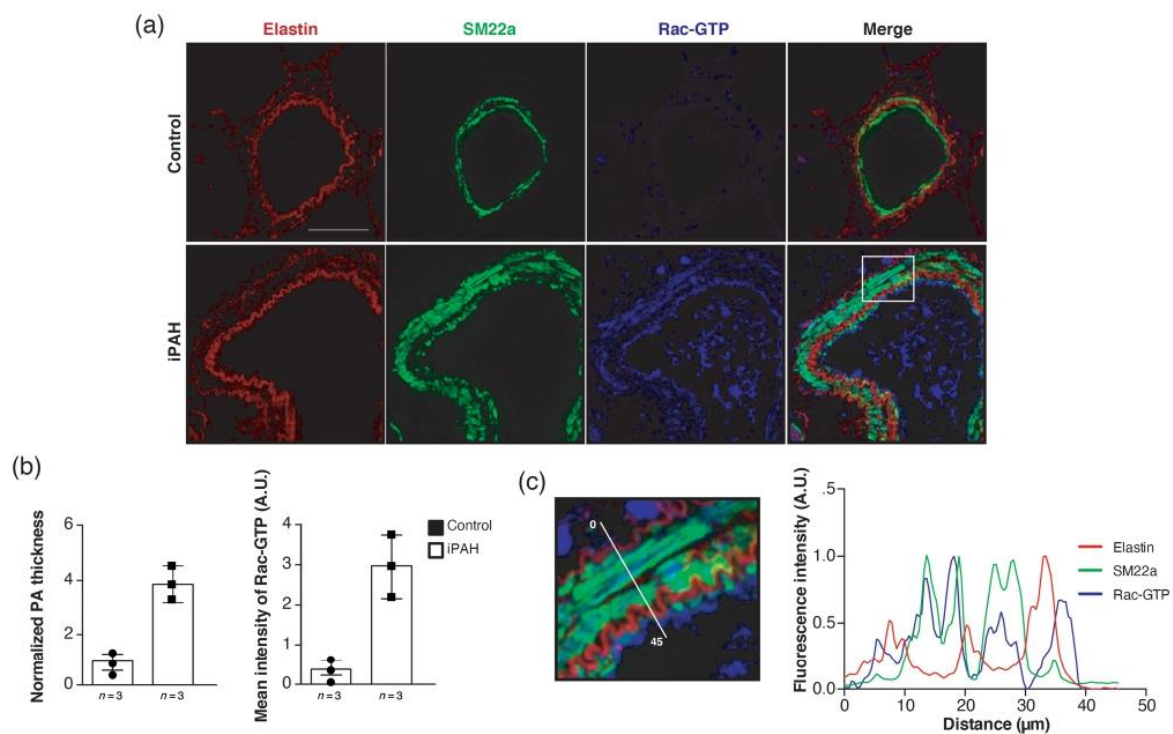


FIGURE 5 Rac1 is overactivated in pulmonary artery (PA) of idiopathic pulmonary arterial hypertension (iPAH) patients. (a) Representative confocal images of Rac-GTP immunofluorescence (blue) in cryosections of lung from control and iPAH patients. Arteries were detected by elastin autofluorescence (red), smooth muscle by SM22 α immunofluorescence (green), and Rac1 activity by Rac-GTP immunofluorescence (blue). Scale bar = 80 μ m. (b) Quantification of smooth muscle (SM) layer thickness and Rac1 activity (Rac-GTP labelling fluorescence intensity) in lung sections from control and iPAH patients. (c) Magnification corresponding to the white square in (a) and spatial profile of fluorescence intensity for indicated fluorescence channels for the white line positioned on the image. Data are expressed as mean \pm SEM

Rac1 deletion improves endothelial-dependent PA vasodilation in mice exposed to chronic hypoxia, without having an effect on the dilation induced by a NO-donor (SNAP), suggesting a role of PSMC Rac1 upstream to the effect of endothelial NO on PSMC. Endothelial dysfunction in PA, characterized by impaired synthesis and/or bioactivity of endothelium-derived NO and a decrease in endothelium-dependent relaxation is recognized as a key event and a common feature of all types of PH, including hypoxic PH (Budhiraja et al., 2004; Hampl & Herget, 2000). This endothelial dysfunction has been ascribed, at least in part, to elevated level of NOX-derived ROS in experimental model of PH (Fresquet et al., 2006; Knock, 2019), in agreement with the increase in plasma oxidative stress biomarkers in PH patients (Reis et al., 2013). High levels of superoxide anion (O_2^-) favour its interaction with NO to produce peroxynitrite ($ONOO^-$), thus decreasing NO (Boota et al., 1996; Fresquet et al., 2006). Oxidative stress has become recognized as a central player in the underlying pathophysiology of PH and antioxidants or drugs that target specific sources of ROS, such as NOX, have been suggested as potential therapies for PH (Knock, 2019).

NOX1 and NOX2 are both expressed in PA, and NOX1- and NOX2-derived ROS have been shown to participate to PH in experimental animal models and in humans (Yan et al., 2020). NOX1 or NOX2 knockout in mice suppresses the increased right ventricular systolic pressure and prevents the right ventricular hypertrophy and vascular remodelling induced by chronic hypoxia (Hanna et al., 2004; Liu et al., 2006; Nisbet et al., 2009). Full activation of NOX1 or NOX2 allowing sustained long-lasting increase in ROS production is dependent on the recruitment of active Rac1 (or Rac2) that completes the assembly of the holoenzyme (Knock, 2019). Our results showing that chronic hypoxia-induced ROS production in the lungs is prevented in SM-Rac1-KO mice. This supports a major role of PSMC NOX1 and NOX2 in the generation of deleterious ROS in PH and demonstrate *in vivo* the essential role of Rac1 in the production of ROS by NOX1 and NOX2 without modification of their expression. They also prove the SMC origin of the ROS responsible for endothelial dysfunction, PSMCs proliferation and PA wall remodelling in hypoxic PH. As previously demonstrated *in vitro* (Diebold et al., 2008, 2010; Patil et al., 2004), Rac1-dependent ROS production in PSMCs is directly stimulated by hypoxia suggesting that chronic hypoxia in mice may be the trigger for Rac1 activation and Rac1-mediated stimulation of NOX involved *in vivo* in pulmonary vascular remodelling associated to hypoxic PH. However, besides hypoxia, vasoconstrictors and other receptor ligands such as 5-HT, ET-1 or EGF involved in PH and known to activate NOXs (Knock, 2019) are also described as Rac1 activators. This suggests that the involvement of Rac1 in NOX/ROS signalling in the pathogenesis of PH may not be limited to hypoxic PH but can be common to all types of PH. This is supported by the increase in Rac1 activity observed in PA of iPAH patients.

In conclusion, our study provides evidence that Rac1 activation in PSMC participates in the pathophysiology of PH by causing endothelial dysfunction and PSMC proliferation through increased production of ROS. In addition, it has been demonstrated that Rac1 in endothelial cells (Sun et al., 2020; Taraseviciene-Stewart et al., 2006;

Yu et al., 2012), or in pulmonary artery fibroblasts (Zhang et al., 2020) plays a role in the development of pulmonary hypertension, supporting the idea that pharmacological inhibition of Rac1 may restrict disease progression and improve clinical outcomes of PH patients. To validate the therapeutic interest to inhibit Rac1 activity in PH, it will be necessary to develop specific and potent Rac1inhibitors suitable for *in vivo* analyses.

ACKNOWLEDGEMENTS

The authors thank Morgane Roussele (l'institut du thorax) for expert technical assistance. We also value the support provided by the animal facility units of the University of Nantes. We thank Therassay, Micropicell and Cytocell core facilities (SFR François Bonamy, University of Nantes) for the functional and cellular explorations.

This work was supported by grants from the Institut de Recherche en Santé Respiratoire des Pays de la Loire (STARac and NARACAS projects) and the Institut National de la Santé et de la Recherche Médicale (INSERM). LR was supported by a grant from MRES. FD was supported by a grant from Fondation pour la Recherche Médicale.

AUTHOR CONTRIBUTIONS

C.G., G.L. and V.S. were responsible for the conception and design. F.D., M.R., L.R., A.T. and V.S. were responsible for the experimentation. G.L. and V.S. were responsible for the analysis and interpretation. F.D., G.L. and V.S. were responsible for drafting the manuscript.

CONFLICT OF INTEREST

The authors have reported that they have no relationships with industry relevant to the contents of this paper to disclose.

DECLARATION OF TRANSPARENCY AND SCIENTIFIC RIGOUR

This Declaration acknowledges that this paper adheres to the principles for transparent reporting and scientific rigour of preclinical research as stated in the *British Journal of Pharmacology* guidelines for [Design and Analysis](#), [Immunoblotting and Immunochemistry](#) and [Animal Experimentation](#), and as recommended by funding agencies, publishers and other organizations engaged with supporting research.

DATA AVAILABILITY STATEMENT

The data that support the findings of this study are available from the corresponding author upon reasonable request. Some data may not be made available because of privacy or ethical restrictions.

ORCID

Christophe Guignabert  <https://orcid.org/0000-0002-8545-4452>

Vincent Sauzeau  <https://orcid.org/0000-0002-6187-0312>

REFERENCES

- Alexander, S. P., Christopoulos, A., Davenport, A. P., Kelly, E., Mathie, A., Peters, J. A., Veale, E. L., Armstrong, J. F., Faccenda, E., Harding, S. D., Pawson, A. J., Southan, C., Davies, J. A., Abbracchio, M. P., Alexander, W., Al-hosaini, K., Bäck, M., Barnes, N. M., Bathgate, R., ...

- Ye, R. D. (2021). The Concise Guide to PHARMACOLOGY 2021/22: G protein-coupled receptors. *British Journal of Pharmacology*, 178(S1), S27–S156. <https://doi.org/10.1111/bph.15538>
- Alexander, S. P., Fabbro, D., Kelly, E., Mathie, A., Peters, J. A., Veale, E. L., Armstrong, J. F., Faccenda, E., Harding, S. D., Pawson, A. J., Southan, C., Davies, J. A., Boison, D., Burns, K. E., Dessauer, C., Gertsch, J., Helsby, N. A., Izzo, A. A., Koesling, D., ... Wong, S. S. (2021). The Concise Guide to PHARMACOLOGY 2021/22: Enzymes. *British Journal of Pharmacology*, 178(S1), S313–S411. <https://doi.org/10.1111/bph.15542>
- Alexander, S. P. H., Roberts, R. E., Broughton, B. R. S., Sobey, C. G., George, C. H., Stanford, S. C., Cirino, G., Docherty, J. R., Giembycz, M. A., Hoyer, D., Insel, P. A., Izzo, A. A., Ji, Y., MacEwan, D. J., Mangum, J., Wonnacott, S., & Ahluwalia, A. (2018). Goals and practicalities of immunoblotting and immunohistochemistry: A guide for submission to the *British Journal of Pharmacology*. *British Journal of Pharmacology*, 175, 407–411. <https://doi.org/10.1111/bph.14112>
- Andre, G., Sandoval, J. E., Retailleau, K., Loufrani, L., Toumaniantz, G., Offermanns, S., Rolli-Derkinderen, M., Loirand, G., & Sauzeau, V. (2014). Smooth muscle specific Rac1 deficiency induces hypertension by preventing p116RIP3-dependent RhoA inhibition. *Journal of the American Heart Association*, 3, e000852.
- Andre-Gregoire, G., Dilasser, F., Chesne, J., Braza, F., Magnan, A., Loirand, G., & Sauzeau, V. (2018). Targeting of Rac1 prevents bronchoconstriction and airway hyperresponsiveness. *The Journal of Allergy and Clinical Immunology*, 142(824–833), e823.
- Boota, A., Zar, H., Kim, Y. M., Johnson, B., Pitt, B., & Davies, P. (1996). IL-1 beta stimulates superoxide and delayed peroxynitrite production by pulmonary vascular smooth muscle cells. *The American Journal of Physiology*, 271, L932–L938.
- Budhiraja, R., Tuder, R. M., & Hassoun, P. M. (2004). Endothelial dysfunction in pulmonary hypertension. *Circulation*, 109(2), 159–165. <https://doi.org/10.1161/01.CIR.0000102381.57477.50>
- Curtis, M. J., Alexander, S., Cirino, G., Docherty, J. R., George, C. H., Giembycz, M. A., Hoyer, D., Insel, P. A., Izzo, A. A., Ji, Y., MacEwan, D. J., Sobey, C. G., Stanford, S. C., Teixeira, M. M., Wonnacott, S., & Ahluwalia, A. (2018). Experimental design and analysis and their reporting II: Updated and simplified guidance for authors and peer reviewers. *British Journal of Pharmacology*, 175(7), 987–993. <https://doi.org/10.1111/bph.14153>
- Diebold, I., Djordjevic, T., Hess, J., & Gørlach, A. (2008). Rac-1 promotes pulmonary artery smooth muscle cell proliferation by upregulation of plasminogen activator inhibitor-1: Role of NFkappaB-dependent hypoxia-inducible factor-1alpha transcription. *Thrombosis and Haemostasis*, 100, 1021–1028. <https://doi.org/10.1160/TH08-07-0473>
- Diebold, I., Petry, A., Djordjevic, T., Belaiba, R. S., Fineman, J., Black, S., Schreiber, C., Fratz, S., Hess, J., Kietzmann, T., & Gørlach, A. (2010). Reciprocal regulation of Rac1 and PAK-1 by HIF-1alpha: A positive-feedback loop promoting pulmonary vascular remodeling. *Antioxidants & Redox Signaling*, 13, 399–412. <https://doi.org/10.1089/ars.2009.3013>
- Dumas de la Roque, E., Smeralda, G., Quignard, J. F., Freund-Michel, V., Courtois, A., Marthan, R., Muller, B., Guibert, C., & Dubois, M. (2017). Altered vasoreactivity in neonatal rats with pulmonary hypertension associated with bronchopulmonary dysplasia: Implication of both eNOS phosphorylation and calcium signaling. *PLoS ONE*, 12, e0173044. <https://doi.org/10.1371/journal.pone.0173044>
- Fresquet, F., Pourageaud, F., Leblais, V., Brandes, R. P., Savineau, J. P., Marthan, R., & Muller, B. (2006). Role of reactive oxygen species and gp91phox in endothelial dysfunction of pulmonary arteries induced by chronic hypoxia. *British Journal of Pharmacology*, 148, 714–723. <https://doi.org/10.1038/sj.bjp.0706779>
- Galiè, N., Brundage, B. H., Ghofrani, H. A., Oudiz, R. J., Simonneau, G., Safdar, Z., Shapiro, S., White, R. J., Chan, M., Beardsworth, A., Frumkin, L., & Barst, R. J. (2009). Tadalafil therapy for pulmonary arterial hypertension. *Circulation*, 119, 2894–2903. <https://doi.org/10.1161/CIRCULATIONAHA.108.839274>
- Galiè, N., Rubin, L., Hoeper, M., Jansa, P., al-Hiti, H., Meyer, G., Chiassi, E., Kusic-Pajic, A., & Simonneau, G. (2008). Treatment of patients with mildly symptomatic pulmonary arterial hypertension with bosentan (EARLY study): A double-blind, randomised controlled trial. *Lancet*, 371, 2093–2100. [https://doi.org/10.1016/S0140-6736\(08\)60919-8](https://doi.org/10.1016/S0140-6736(08)60919-8)
- Hampfl, V., & Herget, J. (2000). Role of nitric oxide in the pathogenesis of chronic pulmonary hypertension. *Physiological Reviews*, 80(4), 1337–1372. <https://doi.org/10.1152/physrev.2000.80.4.1337>
- Hanna, I. R., Hilenski, L. L., Dikalova, A., Taniyama, Y., Dikalov, S., Lyle, A., Quinn, M. T., Lassègue, B., & Griendling, K. K. (2004). Functional association of nox1 with p22phox in vascular smooth muscle cells. *Free Radical Biology & Medicine*, 37, 1542–1549. <https://doi.org/10.1016/j.freeradbiomed.2004.08.011>
- Hordijk, P. L. (2006). Regulation of NADPH oxidases: The role of Rac proteins. *Circulation Research*, 98, 453–462. <https://doi.org/10.1161/01.RES.0000204727.46710.5e>
- Humbert, M., Guignabert, C., Bonnet, S., Dorfmueller, P., Klinger, J. R., Nicolls, M. R., Olschewski, A. J., Pullamsetti, S. S., Schermuly, R. T., Stenmark, K. R., & Rabinovitch, M. (2019). Pathology and pathobiology of pulmonary hypertension: State of the art and research perspectives. *The European Respiratory Journal*, 53, 1801887. <https://doi.org/10.1183/13993003.01887-2018>
- Humbert, M., Morrell, N. W., Archer, S. L., Stenmark, K. R., MacLean, M. R., Lang, I. M., Christman, B. W., Weir, E. K., Eickelberg, O., Voelkel, N. F., & Rabinovitch, M. (2004). Cellular and molecular pathobiology of pulmonary arterial hypertension. *Journal of the American College of Cardiology*, 43, S13–S24. <https://doi.org/10.1016/j.jacc.2004.02.029>
- Izzo, A. A., Teixeira, M., Alexander, S. P., Cirino, G., Docherty, J. R., George, C. H., Insel, P. A., Ji, Y., Kendall, D. A., Panattieri, R. A., Sobey, C. G., Stanford, S. C., Stefanska, B., Stephens, G., & Ahluwalia, A. (2020). A practical guide for transparent reporting of research on natural products in the *British Journal of Pharmacology*: Reproducibility of natural product research. *British Journal of Pharmacology*, 177(10), 2169–2178. <https://doi.org/10.1111/bph.15054>
- Knock, G. A. (2019). NADPH oxidase in the vasculature: Expression, regulation and signalling pathways; role in normal cardiovascular physiology and its dysregulation in hypertension. *Free Radical Biology & Medicine*, 145, 385–427. <https://doi.org/10.1016/j.freeradbiomed.2019.09.029>
- Li, Q., Qiu, Y., Mao, M., Lv, J., Zhang, L., Li, S., Li, X., & Zheng, X. (2014). Antioxidant mechanism of Rutin on hypoxia-induced pulmonary arterial cell proliferation. *Molecules*, 19, 19036–19049. <https://doi.org/10.3390/molecules191119036>
- Lilley, E., Stanford, S. C., Kendall, D. E., Alexander, S. P., Cirino, G., Docherty, J. R., George, C. H., Insel, P. A., Izzo, A. A., Ji, Y., Panattieri, R. A., Sobey, C. G., Stefanska, B., Stephens, G., Teixeira, M., & Ahluwalia, A. (2020). ARRIVE 2.0 and the *British Journal of Pharmacology*: Updated guidance for 2020. *British Journal of Pharmacology*, 177(16), 3611–3616. <https://doi.org/10.1111/bph.15178>
- Liu, J. Q., Zelko, I. N., Erbynn, E. M., Sham, J. S., & Folz, R. J. (2006). Hypoxic pulmonary hypertension: Role of superoxide and NADPH oxidase (gp91phox). *American Journal of Physiology. Lung Cellular and Molecular Physiology*, 290, L2–L10. <https://doi.org/10.1152/ajplung.00135.2005>
- Loirand, G., & Pacaud, P. (2014). Involvement of Rho GTPases and their regulators in the pathogenesis of hypertension. *Small GTPases*, 5, 1–10. <https://doi.org/10.4161/sgtp.28846>
- Loirand, G., Sauzeau, V., & Pacaud, P. (2013). Small G proteins in the cardiovascular system: Physiological and pathological aspects. *Physiological Reviews*, 93, 1659–1720. <https://doi.org/10.1152/physrev.00021.2012>

- Lyle, M. A., Davis, J. P., & Brozovich, F. V. (2017). Regulation of pulmonary vascular smooth muscle contractility in pulmonary arterial hypertension: Implications for therapy. *Frontiers in Physiology*, 8, 614. <https://doi.org/10.3389/fphys.2017.00614>
- McLaughlin, V. V., Shah, S. J., Souza, R., & Humbert, M. (2015). Management of pulmonary arterial hypertension. *Journal of the American College of Cardiology*, 65, 1976–1997. <https://doi.org/10.1016/j.jacc.2015.03.540>
- McLaughlin, V. V., Shillington, A., & Rich, S. (2002). Survival in primary pulmonary hypertension: The impact of epoprostenol therapy. *Circulation*, 106, 1477–1482. <https://doi.org/10.1161/01.CIR.0000029100.82385.58>
- Nisbet, R. E., Graves, A. S., Kleinhenz, D. J., Rupnow, H. L., Reed, A. L., Fan, T. H., Mitchell, P. O., Sutliff, R. L., & Hart, C. M. (2009). The role of NADPH oxidase in chronic intermittent hypoxia-induced pulmonary hypertension in mice. *American Journal of Respiratory Cell and Molecular Biology*, 40, 601–609. <https://doi.org/10.1165/2008-0145OC>
- Patil, S., Bunderson, M., Wilham, J., & Black, S. M. (2004). Important role for Rac1 in regulating reactive oxygen species generation and pulmonary arterial smooth muscle cell growth. *American Journal of Physiology. Lung Cellular and Molecular Physiology*, 287, L1314–L1322. <https://doi.org/10.1152/ajplung.00383.2003>
- Percie du Sert, N., Hurst, V., Ahluwalia, A., Alam, S., Avey, M. T., Baker, M., Browne, W. J., Clark, A., Cuthill, I. C., Dimagl, U., Emerson, M., Garner, P., Holgate, S. T., Howells, D. W., Karp, N. A., Lazic, S. E., Lidster, K., MacCallum, C. J., Macleod, M., ... Würbel, H. (2020). The ARRIVE guidelines 2.0: updated guidelines for reporting animal research. *PLoS Biology*, 18(7), e3000410. <https://doi.org/10.1371/journal.pbio.3000410>
- Rahman, A., Davis, B., Lövdahl, C., Hanumaiah, V. T., Feil, R., Brakebusch, C., & Amer, A. (2014). The small GTPase Rac1 is required for smooth muscle contraction. *The Journal of Physiology*, 592, 915–926. <https://doi.org/10.1113/jphysiol.2013.262998>
- Reis, G. S., Augusto, V. S., Silveira, A. P., Jordão, A. A. Jr., Baddini-Martinez, J., Neto, O. P., Rodrigues, A. J., & Evora, P. R. B. (2013). Oxidative-stress biomarkers in patients with pulmonary hypertension. *Pulmonary Circulation*, 3, 856–861. <https://doi.org/10.1086/674764>
- Sauzeau, V., Sevilla, M. A., Montero, M. J., & Bustelo, X. R. (2010). The Rho/Rac exchange factor Vav2 controls nitric oxide-dependent responses in mouse vascular smooth muscle cells. *The Journal of Clinical Investigation*, 120, 315–330. <https://doi.org/10.1172/JCI38356>
- Simonneau, G., Montani, D., Celermajer, D. S., Denton, C. P., Gatzoulis, M. A., Krowka, M., Williams, P. G., & Souza, R. (2019). Haemodynamic definitions and updated clinical classification of pulmonary hypertension. *The European Respiratory Journal*, 53, 1801913. <https://doi.org/10.1183/13993003.01913-2018>
- Sitbon, O., Gomberg-Maitland, M., Granton, J., Lewis, M. I., Mathai, S. C., Rainisio, M., Stockbridge, N. L., Wilkins, M. R., Zamanian, R. T., & Rubin, L. J. (2019). Clinical trial design and new therapies for pulmonary arterial hypertension. *The European Respiratory Journal*, 53, 1801908. <https://doi.org/10.1183/13993003.01908-2018>
- Sitbon, O., Humbert, M., & Simonneau, G. (2002). Primary pulmonary hypertension: Current therapy. *Progress in Cardiovascular Diseases*, 45, 115–128. <https://doi.org/10.1053/pcad.2002.128449>
- Sun, X., Lu, Q., Yegambaram, M., Kumar, S., Qu, N., Srivastava, A., Wang, T., Fineman, J. R., & Black, S. M. (2020). TGF-beta1 attenuates mitochondrial bioenergetics in pulmonary arterial endothelial cells via the disruption of carnitine homeostasis. *Redox Biology*, 36, 101593. <https://doi.org/10.1016/j.redox.2020.101593>
- Taraseviciene-Stewart, L., Scerbavicius, R., Choe, K. H., Cool, C., Wood, K., Tuder, R. M., Burns, N., Kasper, M., & Voelkel, N. F. (2006). Simvastatin causes endothelial cell apoptosis and attenuates severe pulmonary hypertension. *American Journal of Physiology. Lung Cellular and Molecular Physiology*, 291, L668–L676. <https://doi.org/10.1152/ajplung.00491.2005>
- Tesse, A., Gena, P., Rützler, M., & Calamita, G. (2021). Ablation of aquaporin-9 ameliorates the systemic inflammatory response of LPS-induced endotoxemic shock in mouse. *Cell*, 10(2), 435. <https://doi.org/10.3390/cells10020435>
- Thenappan, T., Ormiston, M. L., Ryan, J. J., & Archer, S. L. (2018). Pulmonary arterial hypertension: Pathogenesis and clinical management. *BMJ*, 360, j5492.
- Wang, X., & Sun, Z. (2010). Thyroid hormone induces artery smooth muscle cell proliferation: Discovery of a new TRalpha1-Nox1 pathway. *Journal of Cellular and Molecular Medicine*, 14, 368–380. <https://doi.org/10.1111/j.1582-4934.2008.00489.x>
- Wang, Y., Ji, L., Jiang, R., Zheng, L., & Liu, D. (2014). Oxidized high-density lipoprotein induces the proliferation and migration of vascular smooth muscle cells by promoting the production of ROS. *Journal of Atherosclerosis and Thrombosis*, 21, 204–216. <https://doi.org/10.5551/jat.19448>
- Watanabe, H. (2018). Treatment selection in pulmonary arterial hypertension: Phosphodiesterase type 5 inhibitors versus soluble guanylate cyclase stimulator. *European Cardiology*, 13, 35–37. <https://doi.org/10.15420/ecr.2017.22.2>
- Yan, S., Resta, T. C., & Jernigan, N. L. (2020). Vasoconstrictor mechanisms in chronic hypoxia-induced pulmonary hypertension: Role of oxidant signaling. *Antioxidants (Basel, Switzerland)*, 9(10), 999. <https://doi.org/10.3390/antiox9100999>
- Yu, M., Gong, D., Lim, M., Arutyunyan, A., Groffen, J., & Heisterkamp, N. (2012). Lack of bcr and abr promotes hypoxia-induced pulmonary hypertension in mice. *PLoS ONE*, 7, e49756. <https://doi.org/10.1371/journal.pone.0049756>
- Zhang, S., Yin, Z., Qin, W., Ma, X., Zhang, Y., Liu, E., & Chu, Y. (2020). Pirfenidone inhibits hypoxic pulmonary hypertension through the NADPH/ROS/p38 pathway in adventitial fibroblasts in the pulmonary artery. *Mediators of Inflammation*, 2020, 2604967.

How to cite this article: Dilasser, F., Rio, M., Rose, L., Tesse, A., Guignabert, C., Loirand, G., & Sauzeau, V. (2022). Smooth muscle Rac1 contributes to pulmonary hypertension. *British Journal of Pharmacology*, 179(13), 3418–3429. <https://doi.org/10.1111/bph.15805>

Titre : Identification et caractérisation d'un nouvel inhibiteur de Rac1 à visée thérapeutique : implication en physiopathologies bronchiques et oncologie

Mots clés : Rac1, cellules musculaires lisses, asthme, cancer du sein, métastases, inhibiteur

Résumé : La GTPase Rac1 régule de nombreux processus cellulaires essentiels tels que la migration, la contraction et la prolifération. Une modification de son expression et/ou de son activité est associée à de nombreuses pathologies notamment cardiovasculaires. La première partie de ma thèse a consisté à déterminer le rôle de Rac1 dans les cellules musculaires lisses bronchiques (CMLb) au cours de l'asthme sévère. Par différentes approches *in vivo* et *in vitro*, j'ai mis en évidence le rôle clé de Rac1 dans la contraction et la prolifération des CMLb. Mes résultats montrent une suractivation de Rac1 dans un modèle murin d'asthme allergique sévère. Cette hyperactivité de Rac1 contribue à l'hyperréactivité bronchique et au remodelage des voies aériennes. Ces résultats démontrent le rôle de Rac1 dans l'asthme sévère.

La seconde partie de ma thèse a consisté à développer et à caractériser un nouvel inhibiteur de Rac1. L'analyse de la structure dynamique de Rac1 a permis de définir un pharmacophore original. Une approche de screening *in silico*, de tests *in vitro* et *ex vivo* ont permis d'identifier un nouvel inhibiteur de Rac1, l'A41. La caractérisation de cette molécule a démontré que l'A41 est le premier inhibiteur spécifique de Rac, réversible et compétitif du GTP. Rac1 étant un acteur majeur dans la tumorigenèse, l'intérêt thérapeutique de l'A41 a été évalué dans un modèle de cancer du sein triple négatif. Mes résultats montrent qu'un traitement chronique à l'A41 permet de réduire la formation de métastases et d'améliorer la survie des animaux. Ces résultats démontrent l'efficacité thérapeutique de ce nouvel inhibiteur de Rac1.

Title : Identification and characterization of a new Rac1 inhibitor for therapeutic purposes: implication in bronchial physiopathologies and oncology

Keywords : Rac1, smooth muscle cells, asthma, breast cancer, metastases, inhibitor

Abstract : The Rac1 GTPase regulates many essential cellular processes such as migration, contraction and proliferation. Modification of its expression and/or activity is associated with many pathologies notably cardiovascular. The first part of my thesis consisted in determining the role of Rac1 in bronchial smooth muscle cells (bSMC) during severe asthma. Using different *in vivo* and *in vitro* approaches, I demonstrated the key role of Rac1 in the contraction and proliferation of bSMCs. My results show an overactivation of Rac1 in a mouse model of severe allergic asthma. This Rac1 hyperactivity contributes to bronchial hyperreactivity and airway remodelling. These results demonstrate the role of Rac1 in severe asthma.

The second part of my thesis consisted in developing and characterising a new Rac1 inhibitor. The analysis of the dynamic structure of Rac1 allowed to define an original pharmacophore. An *in silico* screening approach, *in vitro* and *ex vivo* tests allowed the identification of a new Rac1 inhibitor, A41. The characterisation of this molecule demonstrated that A41 is the first Rac-specific, reversible and competitive GTP inhibitor. As Rac1 is a major player in tumorigenesis, the therapeutic value of A41 was evaluated in a triple negative breast cancer model. My results show that chronic treatment with A41 reduces metastasis and improves survival in mice. These results demonstrate the therapeutic efficacy of this novel Rac1 inhibitor.